FU JEN STUDIES

SCIENCE AND ENGINEERING

NO. 29 1995

目 次 CONTENTS

續 (Continued)

Fu Jen Catholic University
Taipei, Taiwan, Republic of China

目 次（續） CONTENTS (Continued)

核區別分析及 Hausdorff 距離區別分析之比較

廖建通
輔仁大學數學系

許玉生
中央大學數學系

摘　要

區別分析（discriminant analysis）是多變量分析（multivariate analysis）之一重要子域。區別分析大致可分爲母數（parametric）區別分析及無母數（nonparametric）區別分析，本文主要在討論後者。無母數區別分析最重要之二種方法爲核（kernel）方法及距離方法。評量一個區別方法之好壞的標準有很多，本文將用區別失誤率（rate of misclassification）以電腦模擬來比較核區別方法及 Hausdorff 距離區別方法在事前機率相等損失相等之模型下之表現。

一、簡　介

區別分析（discriminant analysis）是多變量分析（multivariate analysis）之一重要子域。區別分析大致可分爲母數（parametric）區別分析及無母數（nonparametric）區別分析，本文主要在討論後者。無母數區別分析最重之二種方法爲核（kernel）方法及距離方法。本文將分別於第二節介紹核方法，第三節介紹距離方法中的 Hausdorff 距離方法。

區別分析所探討之問題簡介如下。假設隨機變數 X_0 的樣本空間爲一維實數空間 R 之某一子集 Ω，其觀察值 x_0 來自兩母體 Π_1、Π_2 之機率分別爲 q_1、q_2，所以 $q_1+q_2=1$。本文假設 $q_1=q_2=\frac{1}{2}$，其它情況可用類似方法討論。同時假設誤判 x_0 屬於 Π_1 或 Π_2 之損失相等，其它情況可用類似方法討論。區別分析之目的在於根據分別得自 Π_1、Π_2 之二組樣本 $\{X_1, \cdots, X_m\}$ 及 $\{Y_1, \cdots, Y_n\}$ 來區別 x_0 屬於 Π_1 或 Π_2。簡單地說一個區別方法就是把 Ω 分爲不相交且聯集爲 Ω 的集合 D_1、D_2，如果 $x_0 \in D_1$ 則判斷 x_0 來自 Π_1，否則判斷 x_0 來自 Π_2。

首先簡介母數區別分析。在母數區別分析中，最重要的應屬常態分佈之區別分析。假使 Π_1 和 Π_2 之分布有相同的變異數 σ^2 及相異的期望值 μ_1、μ_2。當參數均爲已知時，則使區別失誤率（rate of misclassification）爲最小的最佳區別方法是 Fisher[6] 所提出的 LDF (linear discriminant function)，即：若

$$\frac{1}{\sigma^2}\left[x_0-\frac{1}{2}(\mu_1+\mu_2)\right][\mu_1-\mu_2]\geq 0$$

則推斷 x_0 來自 Π_1。若

$$\frac{1}{\sigma^2}\left[x_0-\frac{1}{2}(\mu_1+\mu_2)\right][\mu_1-\mu_2]<0$$

則推斷 x_0 來自 Π_2。當參數均爲未知時，則一常用之估計式爲：若

$$\frac{1}{S^2}\left[x_0-\frac{1}{2}(\bar{X}+\bar{Y})\right][\bar{X}-\bar{Y}]\geq 0$$

則推斷 x_0 來自 Π_1；若

$$\frac{1}{S^2}\left[x_0-\frac{1}{2}(\bar{X}+\bar{Y})\right][\bar{X}-\bar{Y}]<0$$

則推斷 x_0 來自 Π_2，其中 $\bar{X}=\frac{\Sigma X_i}{m}$，$\bar{Y}=\frac{\Sigma Y_i}{n}$，$S^2=\frac{1}{m+n-2}\left[\sum_{i=1}^{m}(X_i-\bar{X})^2+\sum_{j=1}^{n}(Y_i-\bar{Y})^2\right]$。

若 Π_1 和 Π_2 之變異數不同，分別爲 σ_1^2、σ_2^2，當參數均爲已知時，則使區別失誤率爲最小的最佳區別方法爲 QDF (quadratic discriminant function)，即；若

$$\frac{(x_0-\mu_2)^2}{\sigma_2^2}\geq\frac{(x_0-\mu_1)^2}{\sigma_1^2}+2\log\frac{\sigma_1}{\sigma_2}$$

則推斷 x_0 來自 Π_1。若

$$\frac{(x_0-\mu_2)^2}{\sigma_2^2}<\frac{(x_0-\mu_1)^2}{\sigma_1^2}+2\log\frac{\sigma_1}{\sigma_2}$$

則推斷 x_0 來自 Π_2。當參數均爲未知時，則一常用之估計式爲：若

$$\frac{(x_0-\bar{Y})^2}{S_2^2}\geq\frac{(x_0-\bar{X})^2}{S_1^2}+2\log\frac{S_1}{S_2}$$

則推斷 x_0 來自 Π_1；若

$$\frac{(x_0-\bar{Y})^2}{S_2^2}<\frac{(x_0-\bar{X})^2}{S_1^2}+2\log\frac{S_1}{S_2}$$

則推斷 x_0 來自 Π_2，其中 $S_1^2=\frac{1}{m-1}\sum_{i=1}^{m}(X_i-\bar{X})^2$，$S_2^2=\frac{1}{n-1}\sum_{i=1}^{n}(Y_i-\bar{Y})^2$。

現在我們討論無母數區別分析。令 F_1、F_2 分別表示 Π_1、Π_2 的累積分配函數 (cumulative ditribution function) 存在且絕對連續，所以它們的機率密度函數 (probability density function) 存在，分別以 f_1、f_2 表示。假設不知 F_1、F_2 是何種分配，所以無法使用母數區別分析法來區別 $X_0=x_0$ 是來自 Π_1 或 Π_2。若 f_1、f_2 均已知且事件 $\{x|f_1(x)=f_2(x)\}$ 發生的機率等於 0，則最佳的區別方法是 $D_1=\{x|f_1(x)\geq f_2(x)\}$ 且 $D_2=\{x|f_1(x)<f_2(x)\}$ (詳見 Anderson[1] 之第六章)。若 f_1、f_2 均未知，則 f_1、f_2 可以核方法估計得核估計值 $\hat{f}_1(x)$ 及 $f_2(x)$，進而得核區別法 $D_{k_1}=\{x|\hat{f}_1(x)\geq\hat{f}_2(x)\}$ 及 $D_{k_2}=\{x|\hat{f}_1(x)<\hat{f}(x)\}$。Hausdorff 距離法只和二樣本點的距離有關和 f_1、f_2 無關，令 D_{d_1}、D_{d_2} 表示 Hausdorff 之區別法。

評量一個區別方法之好壞的標準有很多，本文將用區別失誤率以電腦模擬來比較。

核方法之區別失誤率爲：

$$\int_{D_{k_2}} f_1(x)dx+\int_{D_{k_1}} f_2(x)dx$$

Hausdorff 距離方法之區別失誤率爲：

$$\int_{D_{d_2}} f_1(x)dx+\int_{D_{d_1}} f_2(x)dx$$

上述二方法在區別二左偏、右偏及對稱母體之表現爲第四節之主要內容。附錄則包括所有模擬結果及程式以供參考。

二、核 (kernel) 區別分析

核區別分析最重要之部份在機率密度函數的核估計，令 X_1，…，X_n 表示得自機率密度函數 (p.d.f.) 爲 $f(x)$ 之一組樣本，則 $f(x)$ 之核估計值定義如下：

$$f_n(x)=\frac{1}{nh_n}\sum_{i=1}^{n}K\left(\frac{x-X_i}{h_n}\right)$$

其中 $\{h_n\}$ 表示一極限爲 0 之正數列、K 爲一對稱之機率密度函數。此估計值最早由 Fix 及 Hodges[7] 提出，Rosenblatt (1951) 則發表第一篇有關核估計值之論文，此估計值在密度函數估計論及區別分析上均有很重大之貢獻應用，詳細內容可參閱 Silverman[25]、Prakasa Rao[23]、Revroy and Györfi (1985) 及 Hand[13]。

核估計值之優點爲：(1) 此估計值爲一機率密度函數 (p.d.f.) 且不像直方圖 (histogram) 只在某一閉區間內不爲 0 僅適用較少分佈，(2) 無直方圖相近點值不同相遠點值卻相同之缺點，(3) 無直方圖因維度之增加而增加估計困難度之缺點 (Bellman's[2] curse of dimensionality)，(4) 函數值之變化較平滑不像直方圖的跳點 (jump point) 多，(5) 受 outlier 之影響較直方圖小，(6) 適用於許多分佈，(7) 有許多好的數學及統計性質，如在一些正規假設下此估計值有一致性及中央極限定理：

$$\hat{f}_n(x) \xrightarrow{n\to\infty} f(x)$$

且

$$\mathcal{L}\{\sqrt{nh_n}[\hat{f}_n(x)-f(x)]\} \xrightarrow{n\to\infty} N\left[0, f(x)\int_{-\infty}^{\infty} K^2(y)dy\right]$$

(參考 Prakasa Rao[23])。

顯然決定核估計值的二大因素是核函數 K 及窗距 (bandwidth) h_n，通常 K 之選法有二種即定義於 R 或一區間，如常態 (normal) 或均勻 (uniform) 分佈，前者不致產生估計值爲 0 的情況但計算量較大，後者恰相反。窗距 h_n 較大時，估計值較平滑，但變異數 (variance) 較小偏差 (bias) 較大，適用於資料較稀疏之情形。窗距 h_n 較小時，估計值較不規則，但變異數較大偏差較小，適用於資料較密集之情形。核估計值的缺點爲計算時間較長，較佔記憶空間及邊界點函數值較不好估計等。

在理論上，最好能够在某一標準之下同時選出最佳的 K 及 h_n。

定　義

$$\text{MISE}=E[\hat{f}_n(x)-f(x)]^2dx$$

則當 n 大時上式近似：

$$\frac{1}{nh}\int K^2(y)dy+\frac{h^4}{4}\int[f''(x)]^2dx$$

此時最佳之 h_n 爲 $\left\{\dfrac{\int K^2(y)dy}{n\int[f''(x)]^2dx}\right\}^{1/5}$ 且最佳之 K 爲：

$$K(x)=\begin{cases}\dfrac{3}{4\sqrt{5}}-\dfrac{3x^2}{20\sqrt{5}}, & |x|\le\sqrt{5}\\ 0, & |x|>\sqrt{5}\end{cases}$$

詳細內容參閱 Parzen[22] 及 Epanechnikov[5]。

核 (kernel) 區別分析和母數區別分析法如 LDF 及 QDF 之比較結果大致如下：核區別法和其它方法各有優劣（參考 Gessaman 和 Gessaman[9]，Goldstein[10]，Van Ness 和 Simpson[28]），在高維度時核區別分析法最佳（參考 Van Ness[27]），在區別 lognormal 及 normal mixture 分佈時核區別分析法最佳（參考 Habbema、Hermans 和 Remme[12]）。

三、距離區別分析

Wolfowitz[29,30] 及 Matusita[17~19] 在 1950 年代便提出用距離概念來處理統計推論上的問題。在區別分析上 Matusita 在 1956 年提出距離區別分析法，Goldstein 和 Dillon 在 1978 年也提出另外一種距離區別分析法。Krzanowski 在 1987 年比較此二種距離區別分析法。

本文主要討論 Chatterjee 和 Narayanan 在 1992 年所提出的 Hausdorff 距離區別分析法，此法之優點爲簡單好用且適用任何分佈（甚至 p.d.f. 不存在亦可應用），應用此法於下列七組數據之結果較 LDF 爲佳或一樣好：(1) Stewart[26] 之同軸數據，(2) Seber[24] 之跳蚤甲蟲數據，(3) Flury 及 Riedwyl[8] 之電極棒數據，(4) Johnson 及 Wiohern[14] 之破產或未破產數據，(5) Flury 及Riedwyl[8] 之眞鈔或僞鈔數據，(6) Johnson 及 Wichern[14] 之原油數據，(7) Kendall 及 Stewart[15] 之 Fisher's 鳶尾科植物數據。

介紹 Hausdorff 距離區別分析法如下。Hausdorff 距離之定義如下：

定 義

假設集合 A 與集合 B 裏的元素皆爲有限個，則：

$$d_H(A, B)=\max_{x\in A}\{\min_{y\in B}\{d_E(x, y)\}\}+\max_{y\in B}\{\min_{x\in A}\{d_E(x, y)\}\}$$

叫做 A 和 B 之間的 Hausdorff distance。

在本文中，我們討論 $d_E(x, y)=|x-y|$ 之情形。令 $A=\{x_i, i=1, 2, \cdots, m\}$ 與 $B=\{y_i, i=1, 2, \cdots, n\}$ 代表二樣本分別得自 Π_1、Π_2，令 x_0 表示欲區別之觀察值，$A^*=A\cup\{x_0\}$，$B^*=B\cup\{x_0\}$。

定 義

函數 $\delta_A(x_0)=|d_H(A^*, B)-d_H(A, B)|$、$\delta_B(x_0)=|d_H(A, B^*)-d_H(A, B)|$，則 Hausdorff 區別方法如下：

若 $x_0\in D_{d_i}$ 則判斷 $x_0\in\Pi_i$；$i=1,2$。其中 $D_{d_1}=\{x_0|\delta_A(x_0)-\delta_B(x_0)\leq 0\}$ 且 $D_{d_2}=\{x_0|\delta_A(x_0)-\delta_B(x_0)>0\}$。

爲增進瞭解我們證明函數 $\delta_A(x_0)$ 與函數 $\delta_B(x_0)$ 皆爲片斷折線 (piecewise linear) 連續函數。

定理 3.1

令 $w_1=\max\limits_{x\in A}\{\min\limits_{y\in B}\{d_E(x,y)\}\}$ 且 $w_1^*(x_0)=\max\limits_{x\in A^*}\{\min\limits_{y\in B}\{d_E(x,y)\}\}$

令 $y_{(i)}$ 表示 B 中第 i 小之觀察值；$i=1,2,\cdots,n$，則：

$$w_1^*(x_0)=\begin{cases}-x_0+y_{(1)}, & \text{若 } x_0\in[-\infty,\ y_{(1)}-w_1]\\ x_0-y_{(i)}, & \text{若 } x_0\in\left[-y_{(i)}+w_1,\ \dfrac{y_{(i)}+y_{(i+1)}}{2}\right] \text{ 且 } y_{(i+1)}-y_{(i)}\geq 2w_1;\ i=1,2,\cdots,n-1\\ -x_0+y_{(i+1)}, & \text{若 } x_0\in\left[\dfrac{y_{(i)}+y_{(i+1)}}{2},\ y_{(i+1)}-w_1\right] \text{ 且 } y_{(i+1)}-y_{(i)}\geq 2w_1;\ i=1,2,\cdots,n-1\\ x_0-y_{(n)}, & \text{若 } x_0\in[y_{(n)}+w_1,\ +\infty]\\ w_1, & \text{其它情形}\end{cases}$$

證 明

首先按照定義

$$\begin{aligned}w_1^*(x_0)&=\max_{x\in A^*}\{\min_{y\in B}\{d_E(x,y\}\}\\&=\max\{\min_{y\in B}\{d_E(x,y)\},\max_{x\in A}\{\min_{y\in B}\{d_E(x,y\}\}\}\\&=\max\{\min_{y\in B}\{d_E(x_0,y)\},w_1\}\end{aligned}$$

所以若 $\min\limits_{y\in B}\{d_E(x_0,y)\}>w_1$，則 $w_1^*(x_0)=\min\limits_{y\in B}\{d_E(x_0,y)\}$，否則 $w_1^*(x_0)=w_1$。考慮下列三種情況：

(1) $x_0\leq y_{(1)}$ 時，因爲：

$$\min_{y\in B}\{d_E(x_0,y)\}=y_{(1)}-x_0>w_1\ \Leftrightarrow\ x_0<y_{(1)}-w_1$$

所以若 $x_0\in(-\infty,y_{(1)}-w_1]$，則 $\min\limits_{y\in B}\{d_E(x_0,y)\}\geq w_1$，故 $w_1^*(x_0)=y_{(1)}-x_0$。若 $x_0\in[y_{(1)}-w_1,y_{(1)})$，則 $y_{(1)}-x_0\leq w_1$。故 $w_1^*(x_0)=w_1$。

(2) $y_{(i)} \leq x_0 \leq y_{(i+1)}$，$i=1, 2, \cdots, n-1$，時

$$\min_{y \in B} \{d_E(x_0, y)\} = \min \{x_0 - y_{(i)}, y_{(i+1)} - x_0\}$$

若 $y_{(i+1)} - y_{(i)} \leq 2w_1$，則：

$$\min_{y \in B} \{d_E(x_0, y)\} \leq \frac{y_{(i+1)} - y_{(i)}}{2} \leq w_1$$

即 $w_1^*(x_0) = w_1$。若 $y_{(i+1)} - y_{(i)} \geq 2w_1$，則分下列四種情況討論：

(a) 若 $\min_{y \in B} \{d_E(x_0, y)\} = x_0 - y_{(i)}$ 且 $x_0 - y_{(i)} \geq w_1$，則：

$$w_1 \leq x_0 - y_{(i)} \leq y_{(i+1)} - x_0$$

即：

$$y_{(i)} + w_1 \leq x_0 \leq \frac{y_{(i+1)} + y_{(i)}}{2}$$

此時

$$w_1^*(x_0) = x_0 - y_{(i)}$$

(b) 若 $\min_{y \in B} \{d_E(x_0, y)\} = y_{(i+1)} - x_0$ 且 $y_{(i+1)} - x_0 \geq w_1$，則：

$$w_1 \leq y_{(i+1)} - x_0 \leq x_0 - y_{(i)}$$

即：

$$\frac{y_{(i)} + y_{(i+1)}}{2} \leq x_0 \leq y_{(i+1)} - w_1$$

此時

$$w_1^*(x_0) = y_{(i+1)} - x_0$$

(c) 若 $\min_{y \in B} \{d_E(x_0, y)\} = x_0 - y_{(i)}$ 且 $x_0 - y_{(i)} \leq w_1$，則：

$$y_{(i)} \leq x_0 \leq y_{(i)} + w_1$$

此時

$$w_1^*(x_0) = w_1$$

(d) 若 $\min_{y \in B} \{d_E(x_0, y)\} = y_{(i+1)} - x_0$ 且 $y_{(i+1)} - x_0 \leq w_1$，則：

$$y_{(i+1)} - w_1 \leq x_0 \leq y_{(i+1)}$$

此時

$$w_1^*(x_0) = w_1$$

(3) $x_0 \geq y_{(n)}$ 時，因爲：

$$\min_{y\in B}\{d_E(x_0, y)\} = x_0 - y_{(n)} \geq w_1 \Leftrightarrow x_0 \geq w_1 + y_{(n)}$$

所以若 $x_0 \in [w_1+y_{(n)}, +\infty)$，則 $\min_{y\in B}\{d_E(x_0, y)\} \geq w_1$，故 $w_1^*(x_0) = x_0 - y_{(n)}$。若 $x_0 \in [y_{(n)}, y_{(n)}+w_1]$，則 $x_0 - y_{(n)} \leq w_1$，故 $w_1^*(x_0) = w_1$。

□

定理 3.2

令 $w_2^*(x_0) = \max_{y\in B}\{\min_{x\in A^*}\{d_E(x, y)\}\}$，則 w_2^* 爲一片斷折線（piecewise linear）連續函數。

證 明

令 $x^{(i)}$ 表示 A 中離 y_i 最近之點且

$$d_i = |y_i - x^{(x)}| = \min_{x\in A}\{d_E(x, y_i)\}; \qquad i = 1, 2, \cdots, n$$

令 $d_{(j)}$ 表示 $d_1, d_2, \cdots, d_n$ 中第 j 小之數；$j = 1, 2, \cdots, n$。設

$$|y_k - x^{(k)}| = d_{(n)}$$

若 $x_0 \in [y_k + d_{(n)}, +\infty)$，則 $x_0 - y_k \geq d_{(n)}$，故

$$\min\{d_E(x_0, y_k), \min_{x\in A}\{d_E(x, y_k)\}\}$$
$$= \min\{x_0 - y_k, |y_k - x^{(k)}|\} = \min\{x_0 - y_k, d_{(n)}\} = d_{(n)}$$

若 $j \neq k$，則：

$$\min\{d_E(x_0, y_j), \min_{x\in A}\{d_E(x, y_j)\}\} \leq \min_{x\in A}\{d_E(x, y_j)\} \leq d_{(n)}$$

所以

$$w_2^*(x_0) = \max_{y\in B}\{\min_{x\in A^*}\{d_E(x, y)\}\} = \max_{y\in B}\{\min\{d_E(x_0, y), \min_{x\in A}\{d_E(x, y)\}\}\}$$
$$= d_{(n)}$$

同理若 $x_0 \in (-\infty, y_k - d_{(n)}]$，則：

$$w_2^*(x_0) = \max_{y\in B}\{\min_{x\in A^*}\{d_E(x, y)\}\} = d_{(n)}$$

設 $y_\ell - x^{(\ell)} = d_{(n-1)}$，若 $[y_k - d_{(n)}, y_k + d_{(n)}] \cap [y_\ell - d_{(n-1)}, y_\ell + d_{(n-1)}] = \phi$，則 $[y_\ell - d_{(n-1)}, y_\ell + d_{(n-1)}]$ 必在 $[y_k - d_{(n)}, y_k + d_{(n)}]$ 之外。

(1) 若 $x_0\in[y_k+d_{(n-1)}, y_k+d_{(n)}]$，則 $d_{(n-1)}\leq x_0-y_k\leq d_{(n)}$，故

$$\min\{d_E(x_0, y_k), \min_{x\in A}\{d_E(x, y_k)\}\}$$
$$=\min\{x_0-y_k, d_{(n)}\}=x_0-y_k=d_E(x_0, y_k)\geq d_{(n-1)}$$

若 $j\neq k$ 則：

$$\min\{d_E(x_0, y_j), \min_{x\in A}\{d_E(x, y_j)\}\}\leq d_{(n-1)}$$

所以

$$w_2^*(x_0)=\max_{y\in B}\{\min_{x\in A^*}\{d_E(x, y)\}\}=d_E(x_0, y_k)=x_0-y_k$$

(2) 同理若 $x_0\in[y_k-d_{(n)}, y_k-d_{(n-1)}]$，則：

$$w_2^*(x_0)=\max_{y\in B}\{\min_{x\in A^*}\{d_E(x, y)\}\}=d_E(x_0, y_k)=y_k-x_0$$

(3) 若 $x_0\in[y_k-d_{(n-1)}, y_k+d_{(n-1)}]$，則 $d_E(x_0, y_k)=|x_0-y_k|\leq d_{(n-1)}\leq d_{(n)}=\min_{x\in A}\{d_E(x, y_k)\}$，故

$$\min\{d_E(x_0, y_k), \min_{x\in A}\{d_E(x, y_k)\}\}=d_E(x_0, y_k)\leq d_{(n-1)}$$

且

$$\min\{d_E(x_0, y_\ell), \min_{x\in A}\{d_E(x, y_\ell)\}\}=\min_{x\in A}\{d_E(x, y_\ell)\}=d_{(n-1)},$$

(因爲 $|x_0-y_\ell|\geq|y_\ell-x^{(\ell)}|$)

若 $j\neq k, \ell$，則：

$$\min\{d_E(x_0, y_j), \min_{x\in A}\{d_E(x, y_j)\}\}\leq\min_{x\in A}\{d_E(x, y_j)\}\leq d_{(n-1)}$$

所以

$$w_2^*(x_0)=\max_{y\in B}\{\min_{x\in A^*}\{d_E(x, y)\}\}=d_{(n-1)}$$

若 $[y_k-d_{(n)}, y_k+d_{(n)}]\cap[y_\ell-d_{(n-1)}, y_\ell+d_{(n-1)}]\neq\phi$。

假設其交集爲 $[y_\ell-d_{(n-1)}, y_k+d_{(n)}]$ 如圖 1（其它情形討論方法類似），則：

(1) 若 $x_0\in[y_k-d_{(n)}, y_k-d_{(n-1)}]$，則 $d_{(n-1)}\leq|x_{(0)}-y_k|\leq d_{(n)}$，根據和前面相同的討論可得：

$$w_2^*(x_0)=\max_{y\in B}\{\min_{x\in A^*}\{d_E(x, y)\}\}=|x_0-y_k|$$

同理在 $x_0\in[y_k+d_{(n-1)}, y_k+d_{(n)}]$ 時

$$w_2^*(x_0)=\max_{y\in B}\{\min_{x\in A^*}\{d_E(x, y)\}\}=|x_0-y_k|$$

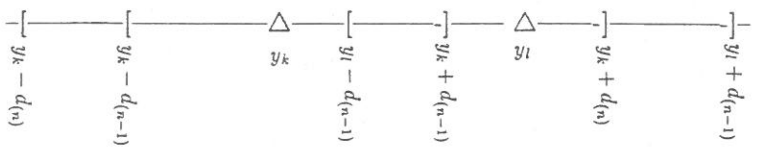

圖 1

(2) 若 $x_0 \in [y_k - d_{(n-1)}, y_\ell - d_{(n-1)}]$，則 $|x_0 - y_k| \leq d_{(n-1)} \leq |x_0 - y_\ell|$，故

$$w_2^*(x_0) = \max_{y \in B} \{\min_{x \in A^*} \{d_E(x, y)\}\} = d_{(n-1)}$$

(3) 若 $x_0 \in [y_\ell - d_{(n-1)}, y_k + d_{(n-1)}]$，則 $|x_0 - y_\ell| \leq d_{(n-1)}$ 且 $|x_0 - y_k| \leq d_{(n-1)}$，此時可分下列四種情形討論：

(a) $d_{(n-2)} \leq |x_0 - y_k| \leq d_{(n-1)}$，　$d_{(n-2)} \leq |x_0 - y_\ell| \leq d_{(n-1)}$

(b) $d_{(n-2)} \leq |x_0 - y_k| \leq d_{(n-1)}$，　$|x_0 - y_\ell| \leq d_{(n-2)}$

(c) $|x_0 - y_k| \leq d_{(n-2)}$，　$d_{(n-2)} \leq |x_0 - y_\ell| \leq d_{(n-1)}$

(d) $|x_0 - y_k| \leq d_{(n-2)}$，　$|x_0 - y_\ell| \leq d_{(n-2)}$

無論那種情形均可以類似上述之討論可得到片斷連續之性質。

□

由定理 3.1 及定理 3.2 可得下列定理：

定理 3.3

函數 $\delta_A(x_0)$ 和 $\delta_B(x_0)$ 均爲片斷折線 (piecewise linear) 連續函數。

例 1

令集合 $A=\{3, 4, 5\}$、$B=\{2, 9, 13\}$，求出 $\delta_A(x_0)$ 與 $\delta_B(x_0)$。

解

因爲

$$\min_{y \in B} \{d_E(3, y)\} = 1, \qquad \min_{x \in A} \{d_E(x, 2)\} = 1$$

$$\min_{y \in B} \{d_E(4, y)\} = 2, \qquad \min_{x \in A} \{d_E(x, 9)\} = 4$$

$$\min_{y \in B} \{d_E(5, y)\} = 3, \qquad \min_{x \in A} \{d_E(x, 13)\} = 8$$

所以

$$\max_{x\in A}\{\min_{y\in B}\{d_E(x,y)\}\}=3, \qquad \max_{y\in B}\{\min_{x\in A}\{d_E(x,y)\}\}=8$$

利用定理 3.1 與 3.2 求得：

$$\max_{x\in A^*}\{\min_{y\in B}\{d_E(x,y)\}\}=\begin{cases}-x_0+2, & \text{若 } x_0\in(-\infty,-1)\\ x_0-2, & \text{若 } x_0\in(5,5.5]\\ -x_0+9, & \text{若 } x_0\in(5.5,6)\\ x_0-13, & \text{若 } x_0\in(16,+\infty)\\ 3, & \text{其它情形}\end{cases}$$

(參考圖 2)。

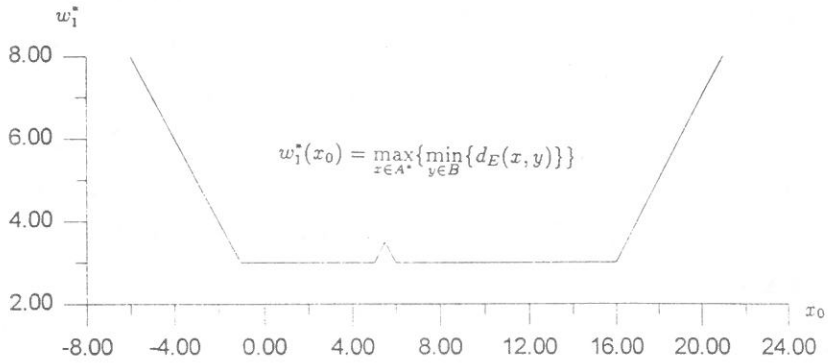

圖 2

$$\max_{y\in B}\{\min_{x\in A^*}\{d_E(x,y)\}\}=\begin{cases}-x_0+13, & \text{若 } x_0\in(5,11]\\ x_0-9, & \text{若 } x_0\in(11,13)\\ 4, & \text{若 } x_0\in[13,17]\\ x_0-13, & \text{若 } x_0\in(17,21)\\ 8, & \text{其它情形}\end{cases}$$

(參考圖 3)。所以

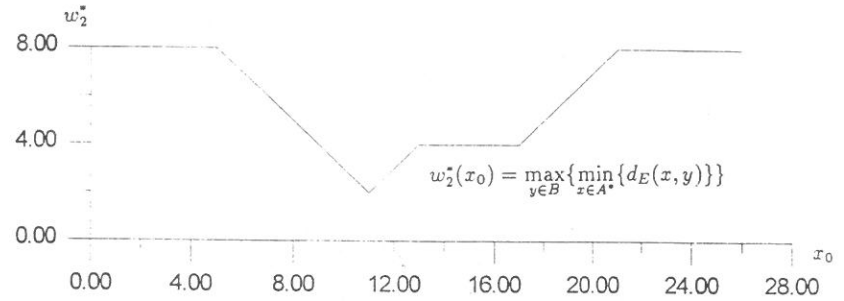

圖 3

$$\delta_A(x_0)=|d_H(A^*,B)-d_H(A,B)|=\begin{cases}-x_0-1, & \text{若 } x_0\in(-\infty,-1)\\ 0, & \text{若 } x_0\in[-1,5.5]\\ 2x_0-11, & \text{若 } x_0\in(5.5,6)\\ x_0-5, & \text{若 } x_0\in[6,11]\\ -x_0+17, & \text{若 } x_0\in(11,13)\\ 4, & \text{若 } x_0\in[13,16]\\ -x_0+20, & \text{若 } x_0(16,17]\\ -2x_0+37, & \text{若 } x_0\in(17,18.5]\\ 2x_0-37, & \text{若 } x_0\in(18.5,21)\\ x_0-16, & \text{若 } x_0\in[21,+\infty)\end{cases}$$

(參考圖 4)。

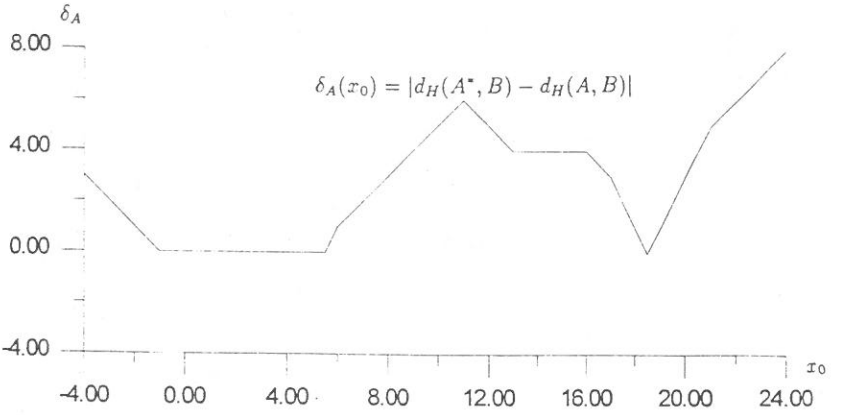

圖 4

同理

$$\max_{x\in A}\{\min_{y\in B^*}\{d_E(x,y)\}\}=\begin{cases}-x_0+5, & \text{若 } x_0\in(2,4)\\ 1, & \text{若 } x_0\in[4,5]\\ x_0-4, & \text{若 } x_0\in(5,6)\\ 2, & \text{若 } x_0\in[6,7]\\ x_0-5, & \text{若 } x_0\in(7,8)\\ 3, & \text{其它情形}\end{cases}$$

(參考圖 6)

$$\max_{y\in B^*}\{\min_{x\in A}\{d_E(x,y)\}\}=\begin{cases}-x_0+3, & \text{若 } x_0\in(-\infty,-5)\\ x_0-5, & \text{若 } x_0\in(13,+\infty)\\ 8, & \text{其它情形}\end{cases}$$

(參考圖 5)。所以

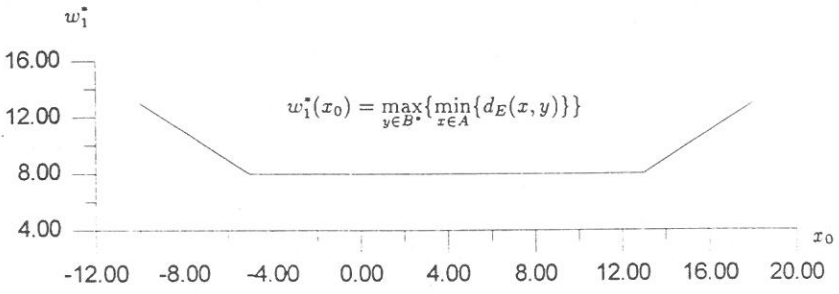

圖 5

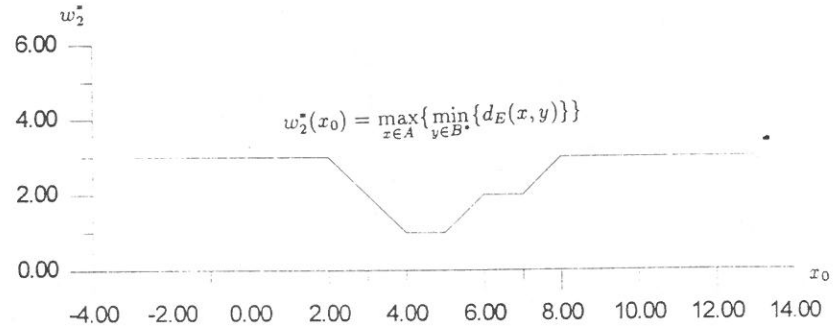

圖 6

$$\delta_B(x_0)=|d_H(A,B^*)-d_H(A,B)|=\begin{cases}-x_0-5, & \text{若 } x_0\in(-\infty,-5)\\ 0, & \text{若 } x_0\in[-5,2]\\ x_0-2, & \text{若 } x_0\in(2,4)\\ 2, & \text{若 } x_0\in[4,5]\\ -x_0+7, & \text{若 } x_0\in(5,6)\\ 1, & \text{若 } x_0\in[6,7]\\ -x_0+8, & \text{若 } x_0\in(7,8)\\ 0, & \text{若 } x_0\in[8,13]\\ x_0-13, & \text{若 } x_0\in(13,+\infty)\end{cases}$$

(參考圖 7)。所以

$$\delta_A(x_0)-\delta_B(x_0)=\begin{cases}4, & \text{若 } x_0\in(-\infty,-5)\\ -x_0-1, & \text{若 } x_0\in[-5,-1)\\ 0, & \text{若 } x_0\in[-1,2]\\ -x_0+2, & \text{若 } x_0\in(2,4)\\ -2, & \text{若 } x_0\in[4,5]\\ x_0-7, & \text{若 } x_0\in(5,5.5]\\ 3x_0-18, & \text{若 } x_0\in(5.5,6)\\ x_0-6, & \text{若 } x_0\in[6,7]\\ 2x_0-13, & \text{若 } x_0\in(7,8)\\ x_0-5, & \text{若 } x_0\in[8,11]\\ -x_0+17, & \text{若 } x_0\in(11,16]\\ -2x_0+33, & \text{若 } x_0\in(16,17]\\ -3x_0+50, & \text{若 } x_0\in(17,18.5]\\ x_0-24, & \text{若 } x_0\in(18.5,21)\\ -3, & \text{若 } x_0\in[21,+18)\end{cases}$$

(參考圖 9)。

因此我們能得到二集合 D_{d_1} 及 D_{d_2} 如下：

$D_{d_1}=[-1,6]\cup[16.5,+\infty)$　　$D_{d_2}=(-\infty,-1)\cup(6,16.5)$

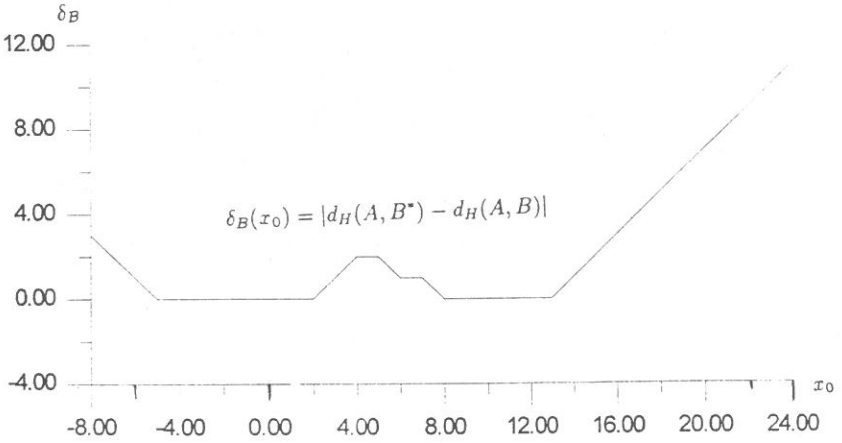
δ_B
12.00
8.00
4.00
0.00
-4.00
$\delta_B(x_0) = |d_H(A, B^*) - d_H(A, B)|$
x_0
-8.00
-4.00
0.00
4.00
8.00
12.00
16.00
20.00
24.00

圖 7

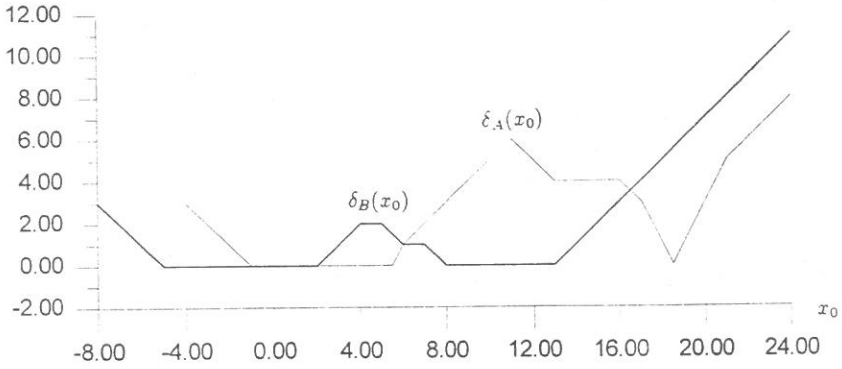
12.00
10.00
8.00
6.00
4.00
2.00
0.00
-2.00
$\delta_A(x_0)$
$\delta_B(x_0)$
x_0
-8.00
-4.00
0.00
4.00
8.00
12.00
16.00
20.00
24.00

圖 8

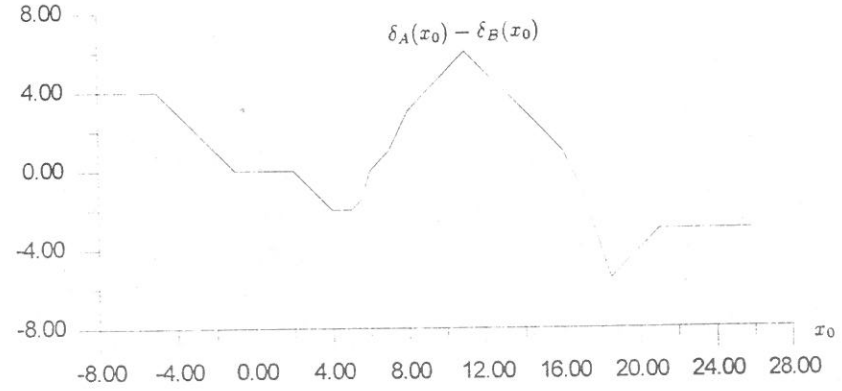
8.00
4.00
0.00
-4.00
-8.00
$\delta_A(x_0) - \delta_B(x_0)$
x_0
-8.00
-4.00
0.00
4.00
8.00
12.00
16.00
20.00
24.00
28.00

圖 9

四、核 (kernel) 區別分析及 Hausdorff 距離區別分析之比較

本章主要是以電腦模擬來比較 Hausdorff 距離區別方法與核 (kernel) 區別方法的失誤率。本章核 (kernel) 區別方法的 K 與 h_n 如下：

$$K(u)=\begin{cases}\dfrac{3}{4\sqrt{5}}-\dfrac{3}{20\sqrt{5}}u^2, & |u|\leq\sqrt{5}\\ 0, & |u|>\sqrt{5}\end{cases}$$

$$h_n=\left\{\frac{\int K^2(u)du}{n\int[\hat{f}''(x)]^2dx}\right\}^{1/5}$$

在這裏

$$\int_{-\sqrt{5}}^{\sqrt{5}}K^2(u)du=\frac{3\sqrt{5}}{25}$$

且

$$\begin{aligned}\int[\hat{f}''(x)]^2dx&=\int\left[\frac{1}{n\cdot n^{-1/5}}\left(\frac{1}{n^{-1/5}}\right)^2\sum_{i=1}^{n}K''\left(\frac{x-X_i}{n^{-1/5}}\right)\right]^2dx\\&=\frac{9n^{-4/5}}{500}\int\left[\sum_{i=1}^{n}I_{[X_i-n^{-1/5}\sqrt{5}\,,\,X_i+n^{-1/5}\sqrt{5}\,]}(x)\right]^2dx\end{aligned}$$

所以

$$h_n=\left\{\frac{20n^{-1/5}\sqrt{5}}{3\int\left[\sum_{i=1}^{n}I_{[X_i-\sqrt{5}\,n^{-1/5}\,,\,X_i+\sqrt{5}\,n^{-1/5}]}(x)\right]^2dx}\right\}^{1/5}$$

在二母體爲對稱分佈且變異相同，(1) 如果樣本數大小固定，則二母體期望值距離大到某程度以上時，Hausdorff 距離區別方法較核 (kernel) 區別方法佳 (參考附錄圖 10 至圖 14)，(2) 如果二母體期望值距離固定，不管樣本數大小，則當期望值距離很小時，核 (kernel) 區別方法總是比 Hausdorff 距離區別方佳，當期望值距離不小時，則樣本數大到某程度，核 (kernel) 區別方法比 Hausdorff 距離區別方法好，否則 Hausdorff 距離區別方法較好 (參考附錄圖 15 至圖 17)。

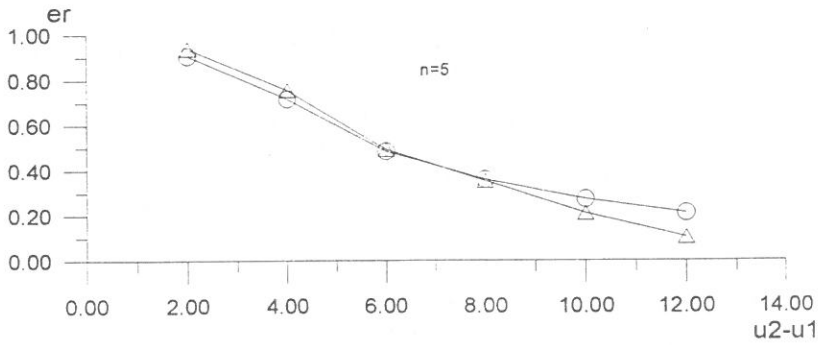

圖10 二母體分佈偏態爲對稱且變異相同。
註：△: Hausdorff 距離區別方法 *u2-u1*: 二母體期望值差
○: 核 (kernel) 區別方法 *n*: 樣本數 er: 失誤率

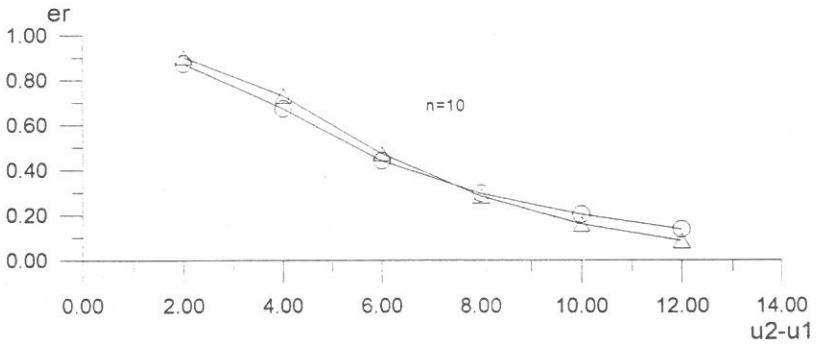

圖11 二母體分佈偏態爲對稱且變異相同。
註：△: Hausdorff 距離區別方法 *u2-u1*: 二母體期望值差
○: 核 (kernel) 區別方法 *n*: 樣本數 er: 失誤率

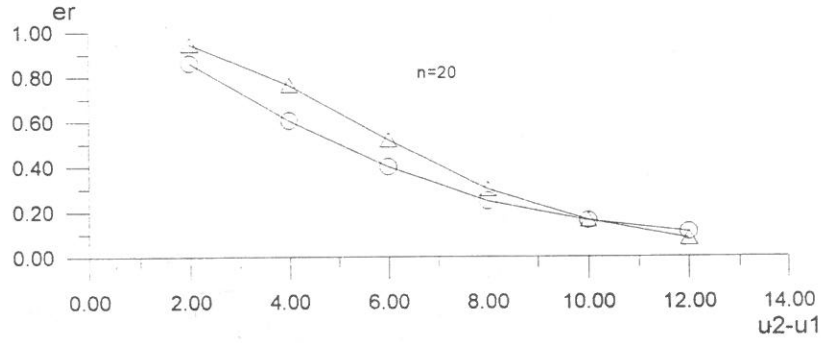

圖12 二母體分佈偏態爲對稱且變異相同。
註：△: Hausdorff 距離區別方法 *u2-u1*: 二母體期望值差
○: 核 (kernel) 區別方法 *n*: 樣本數 er: 失誤率

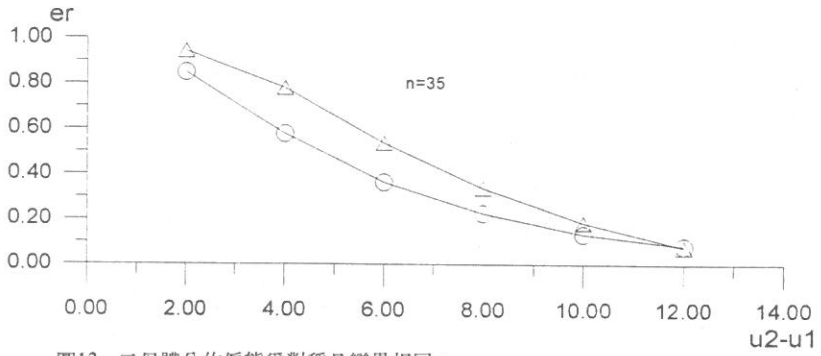

圖13 二母體分佈偏態爲對稱且變異相同。
註：△: Hausdorff 距離區別方法 *u2-u1*: 二母體期望值差
○: 核 (kernel) 區別方法 *n*: 樣本數 er: 失誤率

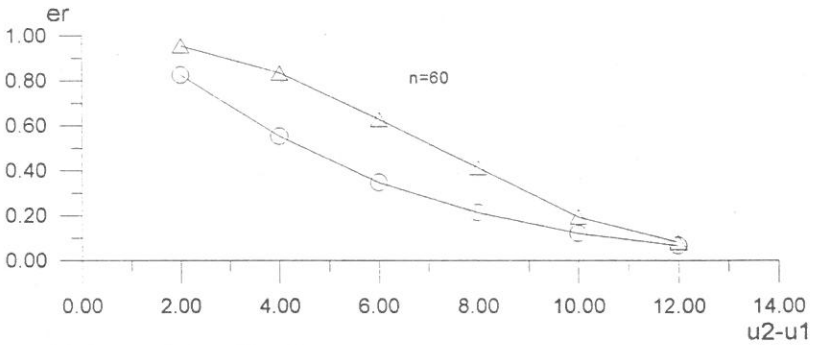

圖14 二母體分佈偏態爲對稱且變異相同。
註：△: Hausdorff 距離區別方法 *u2-u1*: 二母體期望值差
○: 核 (kernel) 區別方法 *n*: 樣本數 er: 失誤率

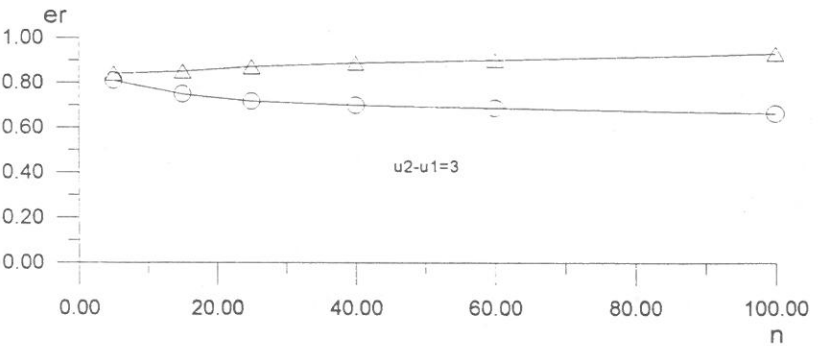

圖15 二母體分佈偏態爲對稱且變異相同。
註：△: Hausdorff 距離區別方法 *u2-u1*: 二母體期望值差
○: 核 (kernel) 區別方法 *n*: 樣本數 er: 失誤率

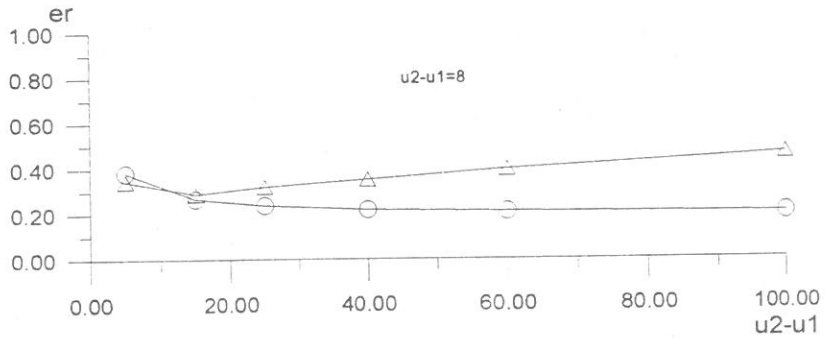

圖16 二母體分佈偏態爲對稱且變異相同。

註：△: Hausdorff 距離區別方法 $u2$-$u1$: 二母體期望值差
○: 核 (kernel) 區別方法 n: 樣本數 er: 失誤率

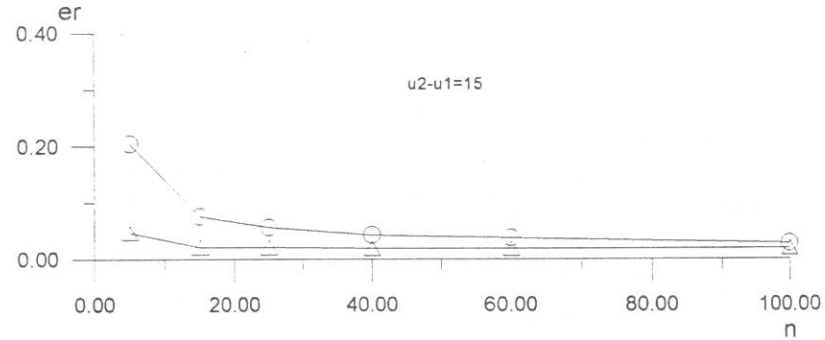

圖17 二母體分佈偏態爲對稱且變異相同。

註：△: Hausdorff 距離區別方法 $u2$-$u1$: 二母體期望值差
○: 核 (kernel) 區別方法 n: 樣本數 er: 失誤率

在二母體爲右偏分佈且變異相同，(1) 如果樣本數大小固定，則二母體期望值距離大到某程度以上時，Hausdorff 距離區別方法較核 (kernel) 區別方法佳或一樣好 (參考附錄圖 18 至圖 22)，(2) 如果二母體期望值距離固定，不管樣本數大小，則當期望值距離很小時，核 (kernel) 區別方法總是比 Hausdorff 距離區別方佳，當期望值距離不小時，則樣本數大到某程度，核 (kernel) 區別方法比 Hausdorff 距離區別方法好或一樣好，否則 Hausdorff 距離區別方法較好 (參考附錄圖 23 至圖 25)。

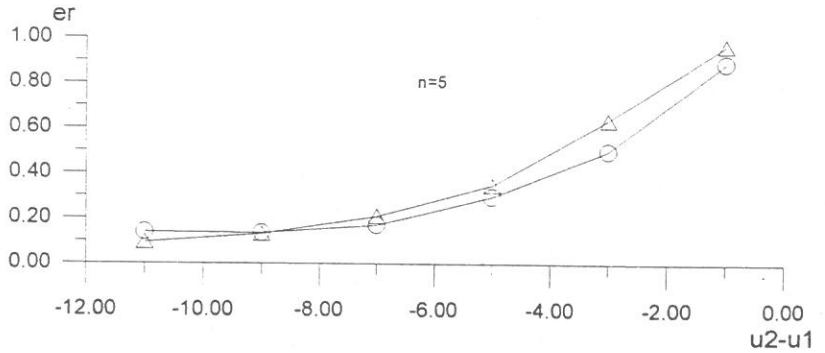

圖18 二母體分佈偏態爲右偏且變異相同。
註：△: Hausdorff 距離區別方法 $u2$-$u1$: 二母體期望值差
○: 核 (kernel) 區別方法 n: 樣本數 er: 失誤率

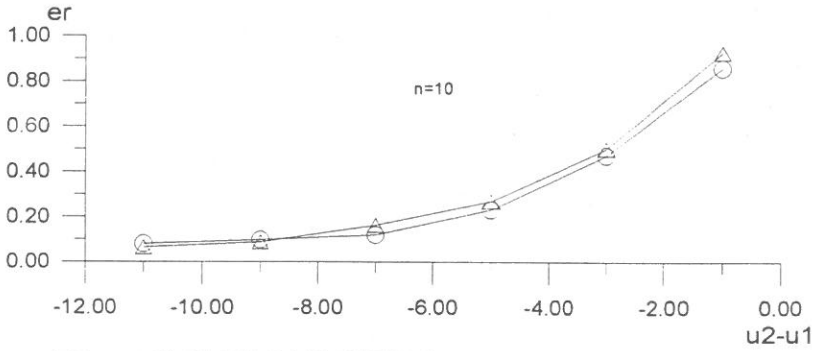

圖19 二母體分佈偏態爲右偏且變異相同。
註：△: Hausodrff 距離區別方法 $u2$-$u1$: 二母體期望值差
○: 核 (kernel) 區別方法 n: 樣本數 er: 失誤率

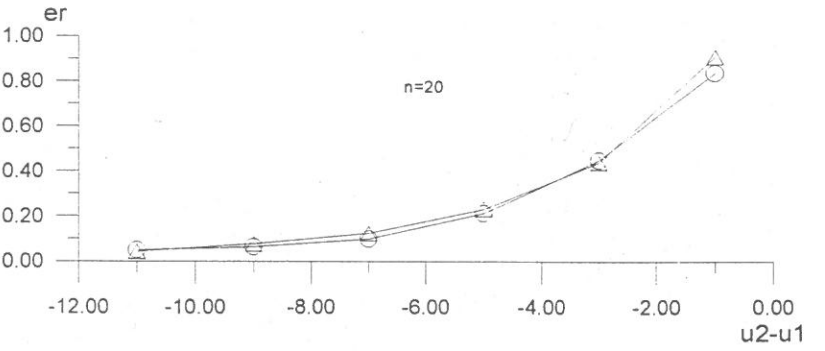

圖20 二母體分佈偏態爲右偏且變異相同。
註：△: Hausdorff 距離區別方法 $u2$-$u1$: 二母體期望值差
○: 核 (kernel) 區別方法 n: 樣本數 er: 失誤率

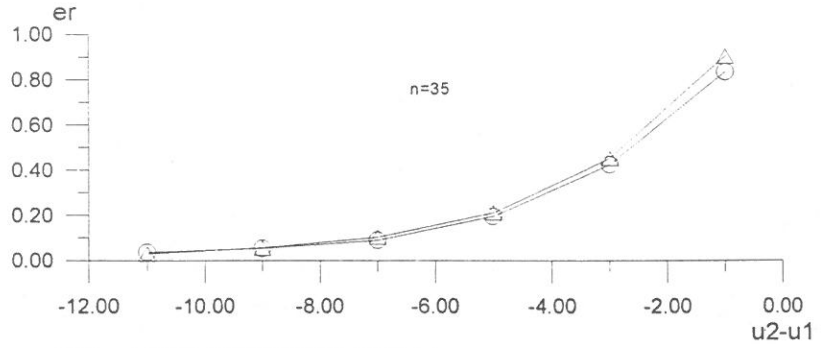

圖21 二母體分佈偏態爲右偏且變異相同。
註：△：Hausdorff 距離區別方法 *u2-u1*：二母體期望值差
○：核 (kernel) 區別方法 *n*：樣本數 er：失誤率

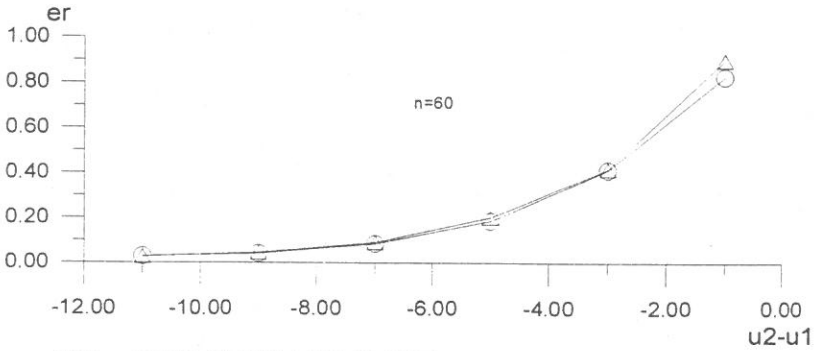

圖22 二母體分佈偏態爲右偏且變異相同。
註：△：Hausdorff 距離區別方法 *u2-u1*：二母體期望值差
○：核 (kernel) 區別方法 *n*：樣本數 er：失誤率

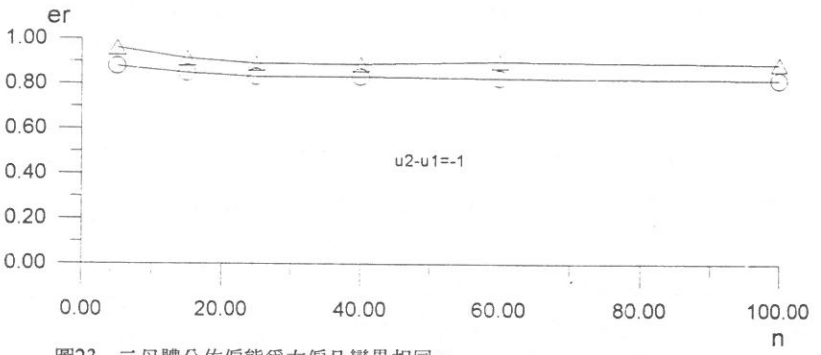

圖23 二母體分佈偏態爲右偏且變異相同。
註：△：Hausdorff 距離區別方法 *u2-u1*：二母體期望值差
○：核 (kernel) 區別方法 *n*：樣本數 er：失誤率

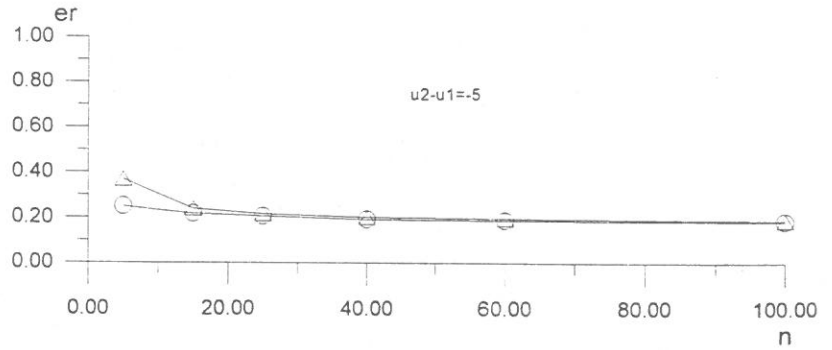

圖24 二母體分佈偏態爲右偏且變異相同。

註：△：Hausdorff 距離區別方法　　$u2-u1$：二母體期望值差

○：核 (kernel) 區別方法　　n：樣本數　　er：失誤率

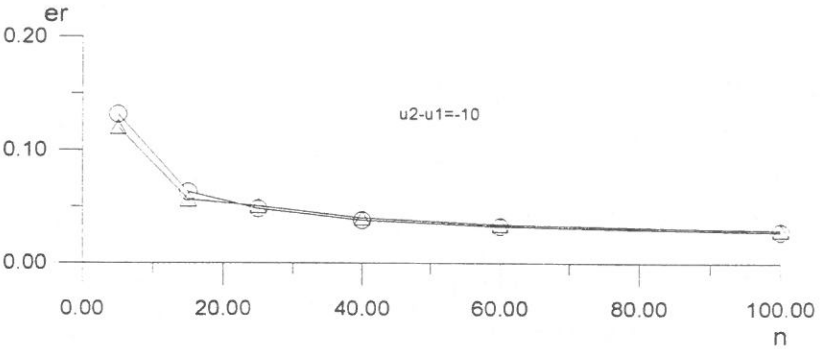

圖25 二母體分佈偏態爲右偏且變異相同。

註：△：Hausdorff 距離區別方法　　$u2-u1$：二母體期望值差

○：核 (kernel) 區別方法　　n：樣本數　　er：失誤率

在二母體爲左偏分佈且變異相同，(1) 如果樣本數大小固定，則二母體期望值距離大到某程度以上時，Hausdorff 距離區別方法較核 (kernel) 區別方法佳或一樣好 (參考附錄圖 26 至圖 30)，(2) 如果二母體期望值距離固定，不管樣本數大小，則當期望值距離很小時，核 (kernel) 區別方法總是比 Hausdorff 距離區別方佳，當期望值距離不小時，則樣本數大到某程度，核 (kernel) 區別方法比 Hausdorff 距離區別方法好或一樣好，否則 Hausdorff 距離區別方法較好 (參考附錄圖 31 至圖 33)。

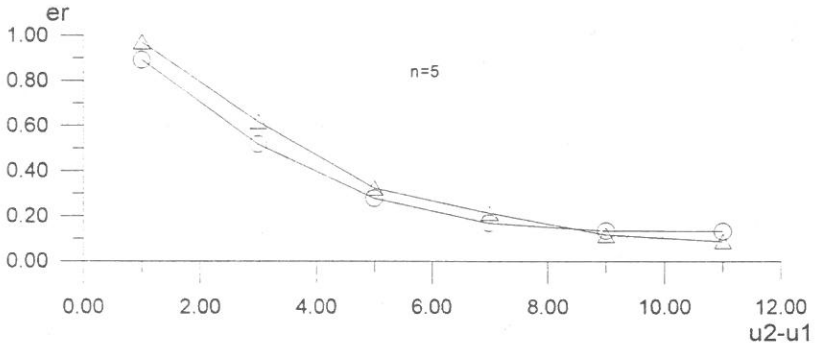

圖26 二母體分佈偏態爲左偏且變異相同。
註：△：Hausdorff 距離區別方法 *u*2-*u*1：二母體期望值差
○：核 (kernel) 區別方法 *n*：樣本數 er：失誤率

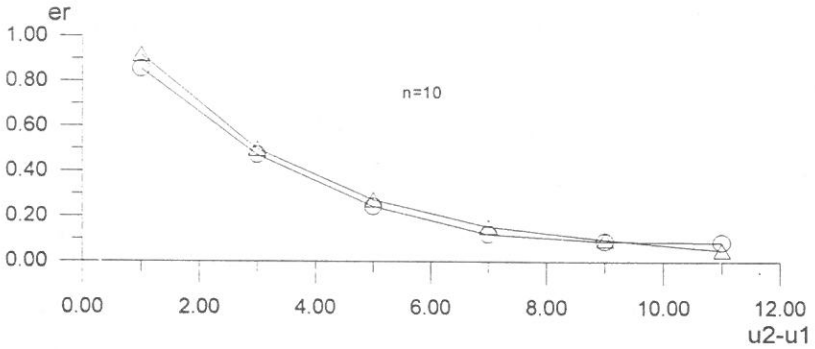

圖27 二母體分佈偏態爲左偏且變異相同。
註：△：Hausdorff 距離區別方法 *u*2-*u*1：二母體期望值差
○：核 (kerner) 區別方法 *n*：樣本數 er：失誤率

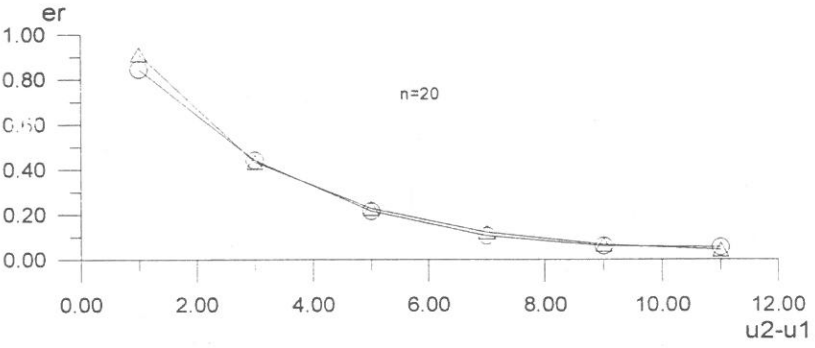

圖28 二母體分佈偏態爲左偏且變異相同。
註：△：Hausdorff 距離區別方法 *u*2-*u*1：二母體期望值差
○：核 (kernel) 區別方法 *n*：樣本數 er：失誤率

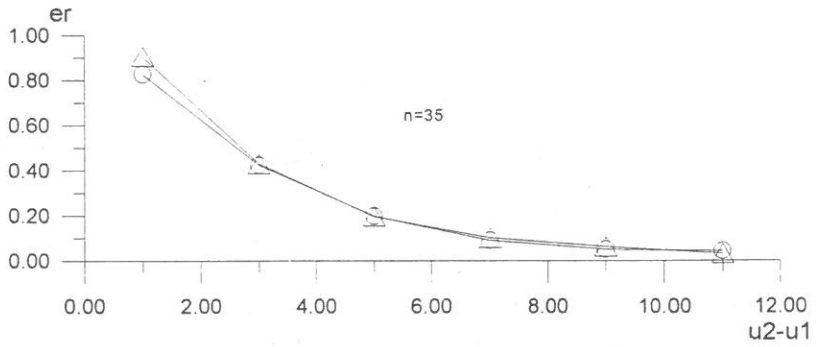

圖29 二母體分佈偏態爲左偏且變異相同。
註：△：Hausdorff 距離區別方法 *u2-u1*：二母體期望值差
○：核 (kernel) 區別方法 *n*：樣本數 er：失誤率

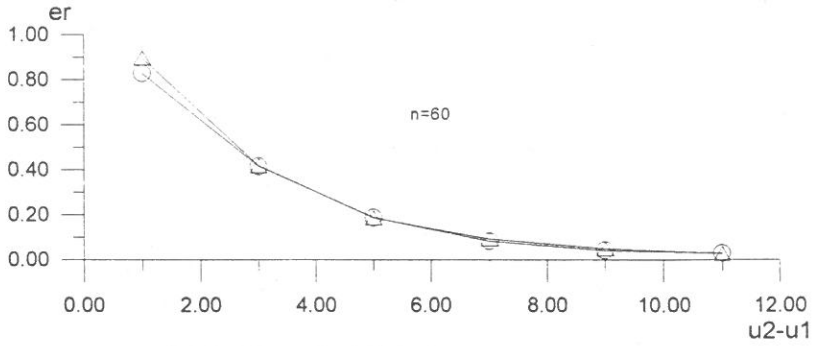

圖30 二母體分佈偏態爲左偏且變異相同。
註：△：Hausdorff 距離區別方法 *u2-u1*：二母體期望值差
○：核 (kernel) 區別方法 *n*：樣本數 er：失誤率

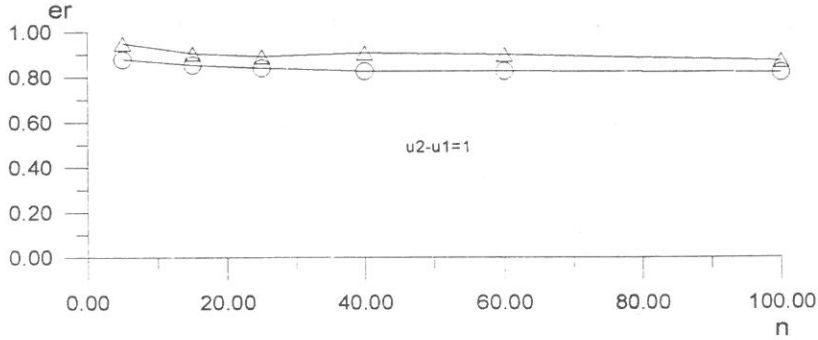

圖31 二母體分佈偏態爲左偏且變異相同。
註：△：Hausdorff 距離區別方法 *u2-u1*：二母體期望值差
○：核 (kernel) 區別方法 *n*：樣本數 er：失誤率

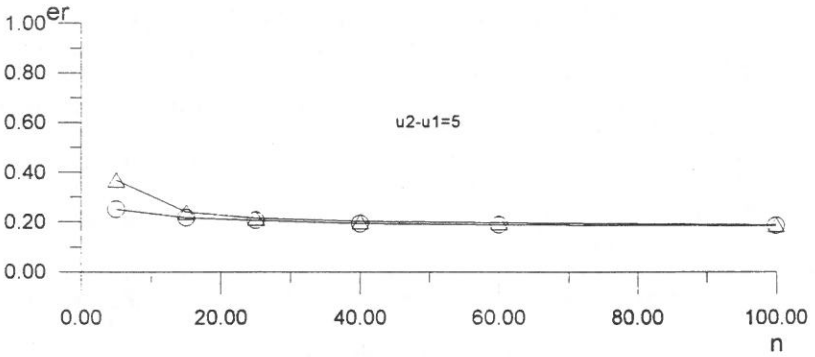

圖32 二母體分佈偏態爲左偏且變異相同。

註：△: Hausdorff 距離區別方法 $u2$-$u1$: 二母體期望值差

○: 核 (kernel) 區別方法 n: 樣本數 er: 失誤率

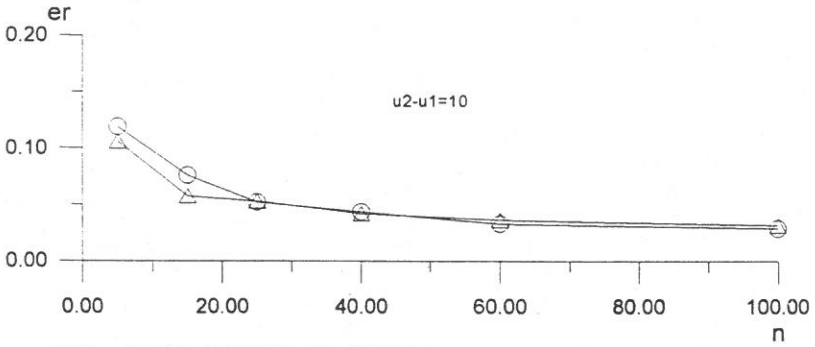

圖33 二母體分佈偏態爲左偏且變異相同。

註：△: Hausdorff 距離區別方法 $u2$-$u1$: 二母體期望值差

○: 核 (kernel) 區別方法 n: 樣本數 er: 失誤率

參考文獻

(1) T.W. Anderson, *An Introduction to Multivariate Statistical Analysis*, John Wiley: New York (1984).

(2) R.E. Bellman, *Adaptive Control Processes*, Princeton: Princeton University Press (1961).

(3) S. Cnatterjee and A. Narayanan, "A New Approch to Discrimination and Classification Using a Hausdorff Type Distance", *Austral. J. Statist.*, **34**(3), 391-406 (1992).

(4) L.P. Devroye and L. Györfi, *Nonparametric Density Estimation: The L_1 View*, New York: Wiley (1985).

(5) V.A. Epanechnikov, "Non-Parametric Estimation of a Multivariate Probability Density", *Theror. Prob. Appl.*, **14**, 153-158 (1969).
(6) R.A. Fisher, "The Use of Multiple Measurements in Taxonomic Problems", *Ann. Eugen.*. **7**, 179-188 (1936).
(7) E. Fix and J.L. Hodges, "Discriminatory Analysis-Nonparametric Discrimination: Consistency Properties", Report No. 4, Randolph Field, Texas: U.S. Air Force School of Aviation Medicine (Reprinted as pp. 261-279 of Agrawala, 1977) (1951).
(8) B. Flury and H. Riedwyl, *Multivariate Statistics: A Practical Approach*, London: Chapman and Hall (1988).
(9) M.P. Gessaman and P.H. Gessaman, "A Comparison of Some Multivariate Discrimination Procedures", *Journal of the Americ⁰n Statistical Association*, **67**, 468-472 (1972).
(10) M. Goldstein, "Comparison of Some Density Estimate Classification Procedures", *J. Amer. Statist. Assoc.*, **70**, 666-669 (1975).
(11) M. Goldstein and W.R. Dillon, *Discrete Discriminant Analysis*, Wiley: New York (1978).
(12) J.D.F. Habbema, J. Hermans and J. Remme, "Variables Kernel Density Estimation in Discriminant Analysis", Compstat 78, Ed., L.C.A. Corsten and J. Hermans, Publication Physica-Verlay, Vienna, 178-185 (1978).
(13) D.J. Hand, *Kernel Discriminant Analysis*, New York: Research Studies Press (1982).
(14) R.A. Johnson and D.W. Wichern, *Applied Multivariate Statistical Analysis*, 2nd ed., Prentice Hall, Engelwoods Cliffs: New Jersey (1988).
(15) M.G. Kendall and A. Stewart, *The Advanced Theory of Statistics*, Vol. 3, London: Griffin (1976).
(16) W.J. Krzanowski, "A Comparison Between Two Distance-Based Discriminant Principles", *Journal of Classification*, **4**, 73-84 (1987).
(17) K. Matusita. "On the Estimation by the Minimum Distance Method", *Ann. Inst. Stat. Math.*, Tokyo, Vol. V, pp. 59-65 (1954a).
(18) K. Matusita, "A Remark to 'On the Estimation by the Minimum Distance Method'", *Ann. Inst. Stat. Math.*, Tokyo, Vol. VI, p. 124 (1954b).
(19) K. Matusita, "Decision Rules, Based on the Distance, for Problems of Fit, Two Samples, and Estimation", *Ann. Math. Stat.*, **26**, 631-640 (1955).
(20) K. Matusita, "Decision Rule, Based on the Distance, for the Classfication Problem", *Ann. Inst. Statist. Math.*, **8**, 67-77 (1956).
(21) K. Matusita, *Classification Based on Distance in Multivariate Gaussian Cases Proceedings of the Fifth Berpeley Symposium on Mathematical Statistics and Probability*, Berkeley: University of California Press (1967).
(22) E. Parzen, "On Estimation of a Probability Density Function and Mode", *Ann. Math. Statist.*, **33**, 1065-1076 (1962).
(23) B.L.S. Prakasa Rao, *Nonparametric Functional Estimation*, Orlando, Florida: Academic Press (1983).
(24) G.A.F. Seber, *Multivariate Observation*, New York: John Wiley (1984).
(25) B.W. Silverman, *Density Estimation for Statistics and Data Analysis*, London: Chapman and Hall (1986).
(26) G.W. Stewart, "Collinearity and Least Squares Regression", *Statist. Sci.*, **2**, 68-100 (1987).

(27) J. Van Ness, "On the Dominance of Non-Parametric Bayes Rules Discriminant Algorithms in High Dimensions", *Pattern Recognition*, **12**, 355-368 (1980).
(28) J.W. Van Ness and C. Simpson, "On the Effects of Dimension in Discriminant Analysis", *Technometrics*, **18**, 175-187 (1976).
(29) J. Wolfowitz, "Estimation by the Minimum Distance Method", *Ann. Inst. Stat. Math.*, Tokyo, Vol. V, pp. 9-23 (1953).
(30) J. Wolfowitz, "Estimation by the Minimum Distance Method in Non-parametric Stochastic Difference Equations", *Ann. Math. Stat.*, **25**, 203-217 (1954).

A Comparison of the Kernel and Hausdorff Discriminant Analysis

CHIEN-T'UNG LIAO
Department of Mathematics
Fu Jen University
Taipei, Taiwan 24205, R.O.C.

YU-SHENG HSU
Department of Mathematics
National Central University
Chungli, Taiwan 32054, R.O.C.

ABSTRACT

The kernel and distance methods are two important methods in nonparametric discriminant analysis. The kernel method has many successful applications and good theoretical properties. The Hausdorff distance method is a new distance method that can be used even when the probability density function does not exist. The purpose of this paper is to find some properties of the Hausdorff distance method and compare its performance with the kernel method in terms of misclassification rates by simulations.

KERNEL AND DOUBLE KERNEL DISCRIMINANT ANALYSIS USING BOTH CONTINUOUS AND DISCRETE VARIABLES

SY-MIEN CHEN
Department of Mathematics
Fu Jen University
Taipei, Taiwan 24205, R.O.C.

YU-SHENG HSU
Department of Mathematics
National Central University
Chungli, Taiwan 32054, R.O.C.

ABSTRACT

In the discriminant analysis using both continuous and discrete (categorical) variables, most investigations were concentrated on the normal and binary distributions. The purpose of this research is to study the kernel and double kernel discriminant analyses using both arbitrary continuous and arbitrary discrete (categorical) variables.

Keywords and phrases: Bandwidth, Discrimination, Double Kernel Estimator, Kernel Estimator, Mean Square Error.

1. INTRODUCTION

In many fields such as psychology, medicine, soil science, medical diagnostic and family planning (see, for examples, Olkin and Tate[13], Chang and Afifi[2], Krzanowski[9], Wernecke[14], and Kumar and Sahai[12], respectively), statisticians must deal with random vectors (X, Y), where X and Y denote a continuous and a discrete (categorical or nominal) vectors, respectively. For instances, the continuous variables could be the soil ph, blood pressure, weight, total cholesterol, income and ages, etc.; the discrete variables could be the soil colour, presence or absence of a certain symptom (like depression, anxiety, or delusion, etc.), educations or occupations of wife and husband, etc..

To analyze such data, one may try to (1) categorize the continuous variables followed by analysis using standard methods for categorical data, (2) score the categorical variable and then use the standard methods for continuous data, or (3) analyze the two kinds of data separately and then attempt to synthesize the two sets of results. The drawbacks of these approaches are (1) loss information, (2) numerical score is subjective, and (3) ignore any association between the continuous and discrete variables, respectively. Therefore, another reasonable approach is required.

For simplicity, consider the case when both X and Y are one dimensional random variables. Clearly

$$f_{(X,Y)}(x, y)=f_{(X|Y)}(x|y)f_Y(y)=f_{(Y|X)}(y|x)f_X(x)$$

Hence, there are two approaches to analyze. We will consider the first one. Also, there are parametric, semi-parametric (logistic model, see Cox[3]) and nonparametric approaches. We will consider the last one. The other cases are still under investigation and will be reported later.

In the discriminant analysis using both continuous and discrete (categorical) variables, most investigations were concentrated on the normal and binary distributions (see Chang and Afifi[2], Cox[3], Krzanowski[7~11]). In practice, the distributions of the continuous and the discrete variables are rarely known. Therefore, the purpose of this research is to study the nonparametric discriminant analysis using both arbitrary continuous and arbitrary discrete (categorical) variables. Without specifying the parent distributions, we obtain wide range applications from the nonparametric methods. However, we inevitably lose some explicit results that could be derived only from the parametric methods.

The nonparametric discriminant analysis depends largely on the nonparametric density estimation. The density estimation of continuous or discrete variable has been studied extensively; but the mixture type variables case is relatively less explored. One possible nonparametric approach is to use the kernel estimator. But when the sample size is small, most of the kernel estimates are zero and hence can not be used. In order to improve this poor small sample behavior, the double kernel estimator has been introduced in Hsu[5] to smooth the kernel estimator

and still keep its large sample properties.

The purpose of this paper is to investigate the performances of the kernel and double kernel estimators in nonparametric discriminant analysis. In sections 2 and 3, we will first review some properties of the kernel and double kernel estimators in the framework of estimation theory. Section 4 consists of the performances of the kernel and double kernel estimators in discriminant analysis.

2. KERNEL ESTIMATION OF MIXTURE TYPE VARIABLES

Let X and Y denote a continuous and a discrete random variables respectively. Consider the kernel estimation of the joint density function $f(x, y)=f(x|y)f(y)$. Given a sample (X_1, Y_1), $\cdots$, (X_n, Y_n), the kernel estimator of $f(x, y)$ is defined as

$$f_n(x, y)=\frac{1}{nh_n}\sum_{i=1}^{n} K\left(\frac{x-X_i}{h_n}\right)I_{(y)}(Y_i) \tag{1}$$

where h_n is a sequence of positive constants converging to 0 and K is a symmetric density function.

For fixed kernel K, we want to find the optimal bandwidth h_n that minimizes the mean square error

$$E|f_n(x, y)-f(x, y)|^2. \tag{2}$$

The following results can be found in Hsu[6]. The mean square error is given by

$$\begin{aligned} E|f_n(x, y)-f(x, y)|^2=&\frac{1}{nh_n}f(x, y)\int K^2(s)ds \\ &+\frac{h_n^4}{4}\left[\frac{d^2f(x|y)}{dx^2}f(y)\int s^2K(s)ds\right]^2 \\ &+O\left(\frac{1}{n}\right)+O(h_n^6) \end{aligned} \tag{3}$$

Clearly, the mean square error converges to 0 provided that $h_n\to 0$ and $nh_n\to\infty$. The optimal bandwidth is given by

$$h_n=\left\{\frac{f(x,\ y)\int K^2(s)ds}{n\left[\frac{d^2f(x|y)}{dx^2}f(y)\int s^2K(s)ds\right]^2}\right\}^{1/5} \tag{4}$$

which minimizes the mean square error and the resulting mean square error

$$E|\hat{f}_n(x,\ y)-f(x,\ y)|^2=O(n^{-4/5}) \tag{5}$$

Based on the above results and assume $nh_n^5\to 0$, it is easy to find the following central limit theorem (see Hsu[5])

$$\mathcal{L}\{\sqrt{nh_n}[\hat{f}_n(x,\ y)-f(x,\ y)]\}\longrightarrow N\left[0,\ f(x,\ y)\int K^2(s)ds\right] \tag{6}$$

By Eq. (6) the optimal kernel function K can be chosen as the Epanechnikov[4] kernel which minimizes $\int K^2(s)ds$ under mild restriction on K.

Since h_n is a function of the unknown $f(x,\ y)$, $f(x|y)$, $f(y)$, it should and could be estimated by their consistent kernel estimators and the resulting kernel estimator will be consistent.

3. DOUBLE KERNEL ESTIMATION OF MIXTURE TYPE VARIABLES

Formula Eq. (1) can be written as

$$\begin{aligned}\hat{f}_n(x,\ y)&=\hat{f}_n(y|x)\hat{f}_n(x)\\&=\left[\frac{\sum_{i=1}^{n}K\left(\frac{x-X_i}{h_n}\right)I_{(y)}(Y_i)}{\sum_{i=1}^{n}K\left(\frac{x-X_i}{h_n}\right)}\right]\left[\frac{\sum_{i=1}^{n}K\left(\frac{x-X_i}{nh_n}\right)}{nh_n}\right].\end{aligned} \tag{7}$$

When the sample size is small, all the values of Y_i will not be equal to most values of y, then most values of $\hat{f}_n(y|x)$ and hence $\hat{f}_n(x,\ y)$ would be 0. Therefore, in Hsu[5] we use an Aitchison and Aitken[1] type kernel estimator $\hat{f}_{n\lambda}(x,\ y)$ to smooth it. Let Y has ℓ level, then $\hat{f}_{n\lambda}(y|x)$ is defined as

$$\hat{f}_{n\lambda}(y|x)=\lambda\hat{f}_n(y|x)+\frac{1-\lambda}{\ell-1}[1-\hat{f}_n(y|x)] \tag{8}$$

where $\frac{1}{\ell}\leq\lambda\leq 1$. Define

$$f_{n\lambda}(x,\ y)=f_{n\lambda}(y\,|x)f_n(x) \tag{9}$$

Since $f_{n\lambda}(x,\ y)$ is a function of the continuous kernel K and the discrete kernel λ, we call it a double kernel estimator.

Clearly,

$$f_{n\lambda}(x,\ y)=\frac{\lambda\ell-1}{\ell-1}\hat{f}_n(x,\ y)+\frac{1-\lambda}{\ell-1}\hat{f}_n(x) \tag{10}$$

For the optimal kernel K and the optimal bandwidth h_n, we want to find the best discrete kernel λ that minimizes the mean square error

$$\sum_y E[f_{n\lambda}(x,\ y)-f(x,\ y)]^2 \tag{11}$$

It is known (see Hsu[6]) that the optimal λ is given by

$$1-\lambda=\frac{A_n}{B_n} \tag{12}$$

where

$$\begin{aligned}A_n&=-\sum_y\left[\frac{f(x)-\ell f(x,\ y)}{\ell-1}\right]\left\{\frac{h_n^2}{2}\left[\frac{d^2f(x\,|y)}{dx^2}f(y)+f^{(2)}(x)\right]\int s^2K(s)ds\right\}\\&\quad+\sum_y\left[\frac{1}{nh_n}f(x,\ y)\int K^2(s)ds\right]+O\left(\frac{1}{n}\right)+O(h_n^4)\\&=O\left(\max\left\{h_n^2,\ \frac{1}{nh_n}\right\}\right)\end{aligned}$$

and

$$\begin{aligned}B_n&=\sum_y\left[\frac{f(x)-\ell f(x,\ y)}{\ell-1}\right]^2+\frac{\ell^2-2\ell}{(\ell-1)^2}\sum_y\left[\frac{1}{nh_n}f(x,\ y)\int K^2(s)ds\right]\\&\quad+\frac{1}{(\ell-1)^2}\frac{1}{nh_n}f(x)\int K^2(s)ds+O\left(\frac{1}{n}\right)+O(h_n^4)\\&=O(1)\end{aligned}$$

Assume $nh_n^3\to\infty$, then $\max\left\{h_n^2,\ \frac{1}{nh_n}\right\}=h_n^2$ for sufficiently large n and

$$1-\lambda=O(h_n^2) \tag{13}$$

and hence

$$\text{Var}\,\hat{f}_{n\lambda}(x, y)=O\left(\frac{1}{nh_n}\right) \tag{14}$$

$$[E\hat{f}_{n\lambda}(x, y)-f(x, y)]^2=O(h_n^4) \tag{15}$$

Therefore, the optimal λ and the resulting mean square error will be of order $O(n^{-1/5})$ and $O(n^{-4/5})$ respectively.

Since λ is a function of the unknown $f(x, y)$, $f(x|y)$, $f(x)$, it should and could be estimated by their consistent kernel estimators and the resulting double kernel estimator will be consistent.

4. APPLICATIONS IN DISCRIMINANT ANALYSIS

Let (X_{11}, Y_{11}), ···, (X_{m1}, Y_{m1}), and (X_{12}, Y_{12}), ···, (X_{n2}, Y_{n2}), denote two samples from two populations Π_1 and Π_2, respectively. Based on these two samples, the kernel estimators and double kernel estimators can be constructed and applied to classify any observation which comes from Π_1 or Π_2 with equal probability (the other cases can be discussed similarly). Moreover, assume the costs of misclssification are equal (the other cases can be discussed similarly). Then the goal of the discriminant analysis is to find a rule that minimizes the probability of misclassification.

When the densities $f_1(x, y)$ and $f_2(x, y)$ are known and the points that satisfies

$$f_1(x, y)=f_2(x, y) \tag{16}$$

receive probability 0, then the optimal discriminant rule that minimizes the probability of misclassification is given by: Classify (x, y) to Π_1 if $f_1(x, y)>f_2(x, y)$ and Π_2 otherwise (see Krzanowski[7]).

In practice, the densities are rarely known and must be estimated. We will consider the kernel and double kernel density estimations. For any fixed (x, y), if $f_1(x, y)>f_2(x, y)$, then the probability of misclassification is given by

$$
\begin{aligned}
&P\{f_{n_2}(x, y) > f_{m_1}(x, y)\} \\
&= P\{[\hat{f}_{n_2}(x, y) - f_2(x, y)] - \hat{f}_{m_1}(x, y) - f_1(x, y)] > f_1(x, y) - f_2(x, y)\} \\
&\leq P\{|[\hat{f}_{n_2}(x, y) - f_2(x, y)] - [\hat{f}_{m_1}(x, y) - f_1(x, y)]| > f_1(x, y) - f_2(x, y)\} \\
&\leq \frac{1}{[f_1(x, y) - f_2(x, y)]^2}\{E[\hat{f}_{m_1}(x, y) - f_1(x, y)]^2 + E[\hat{f}_{n_2}(x, y) - f_2(x, y)]^2 \\
&\quad + 2E|\hat{f}_{m_1}(x, y) - f_1(x, y)|E|\hat{f}_{n_2}(x, y) - f_2(x, y)|\} \\
&\to 0
\end{aligned}
$$

provided that the kernel and bandwidth are chosen properly according to section 2. Similar results holds for the case $f_2(x, y) > f_1(x, y)$. Therefore, we obtain the following theorem.

Theorem 4.1

Assume Eq. (16) holds with probability 0. The probability of misclassifying any point of the discriminant rules formed by the kernel estimators tend to 0 as sample sizes tend to ∞.

By a similar argument, we obtain the following theorem.

Theorem 4.2

Assume Eq. (16) holds with probability 0. The probability of misclassifying any point of the discriminant rules formed by the double kernel estimators tend to 0 as sample sizes tend to ∞.

5. ACKNOWLEDGEMENTS

This research was supported in part by research grants to the first author from the Fu Jen Catholic University SVD section.

REFERENCES

(1) J. Aitchison and C.G.G. Aitken, "Multivariate Binary Discrimination by the Kernel Method", *Biometrika*, **63**, 413-420 (1976).

(2) P.C. Chang and A.A. Afifi, "Classification Based on Dichotomous and Continuous Variables", *JASA*, **69**, 336-339 (1974).

(3) D.R. Cox, "The Analysis of Binary Multivariate Data", *Applied Statistics*, **21**, 113-120 (1972).

(4) V.A. Epanechnikov, "Nonparametric Estimation of a Multivariate Probability Density", *Theor. Prob. Appl.*, **14**, 153-158 (1969).

(5) Y.S. Hsu, "Double Kernel Joint Density Estimation of Mixture Type Variables", *Proceegings of the National Science Council, R.O.C. (A)*, **17**(6), 443-448 (1993).
(6) Y.S. Hsu, "Bandwidth and Kernel Selection of the Double Kernel Estimators", *Chinese J. Mathematics*, **23**, 225-233 (1995).
(7) W.J. Krzanowski, "Discrimination and Classification Using Both Binary and Continuous Variables", *JASA*, **70**, 782-790 (1975).
(8) W.J. Krzanowski, "Some Linear Transformations for Mixtures of Binary and Continuous Variables, with Particular Reference to Linear Discriminant Analysis", *Biometrika*, **66**, 33-39 (1979).
(9) W.J. Krzanowski, "Mixtures of Continuous and Categorical Variables in Discriminant Analysis", *Biometrics*, **36**, 493-499 (1980).
(10) W.J. Krzanowski, "Mixtures of Continuous and Categorical Variables in Discriminant Analysis: A Hypothesis-Testing Approach", *Biometrics*, **38**, 991-1002 (1982).
(11) W.J. Krzanowski, "The Location Model for Mixtures of Categorical and Continuous Variables", *J. of Classification*, **10**, 25-49 (1993).
(12) K. Kumar and A. Sahai, "Application of Discriminant Analysis to the Family Planning Data", *Biom. J.*, **35**, 869-875 (1993).
(13) I. Olkin and R.F. Tate, "Multivariate Correlation Model with Mixed Discrete and Continuous Variables", *Ann. Math. Stat.*, **32**, 448-465 (1961).
(14) K.D. Wernecke, "A Coupling Procedure for the discrimination of Mixed Data", *Biometrics*, 497-506 (1992).

含連續及離散變數之核區別分析及雙核區別分析

陳 思 勉
輔仁大學數學系

許 玉 生
中央大學數學系

摘 要

以往含連續及離散變數之無母數區別分析之研究，大都集中於常態及二項分布，本文則探討一般之連續及離散變數的核區別分析及雙核區別分析。

關鍵詞：窗距、區別分析、雙核估計值、核估計值、均槎。

THE CUBE OF EVERY CONNECTED GRAPH IS 1-EDGE FAULT-TOLERANT HAMILTONIAN

HONG-MIN SHAW
Department of Mathematics
Fu Jen Catholic University
Taipei, Taiwan 24205, R.O.C.

ABSTRACT

It is known that the cube of every connected graph is 1-hamiltonian. Here we show that it is also 1-edge fault-tolerant hamiltonian.

1. INTRODUCTION

Certain hamiltonian properties in powers of graphs have been studied for quite a while; see Lesniak-Foster[8] for a brief overview of the stretches of some basic results in this topic. In computer science, optimal fault-tolerant hamiltonian networks have gained a lot of studies recently due to their connection to network designs[6]. However it is usually difficult to verify that whether a given graph is fault-tolerant hamiltonian or not. Hence the author proposed a study of the sufficient conditions for a graph being k-edge fault-tolerant hamiltonian via the closure approach introduced by Bondy and Chvátal[1]. See Lin[9] for some basic results obtained by Lin.

Throughout this paper, a graph $G=(V, E)$ always means a finite simple graph of order $n=|V|\geq 3$. Undefined terminology or notation is referred to Bondy and Murty[2], Lesniak-Foster[8].

A hamiltonian graph G is called k-edge fault-tolerant hamiltonian (k-EFH in short), if after removing arbitrary k edges, say F, from G, $G-F$ remains hamiltonian. Clearly 0-EFH means simply hamiltonian. A hamiltonian graph G is called k-hamiltonian (in our sense, k-vertex fault-tolerant hamiltonian), if after removing arbitrary k vertices, say W, from G, $G-W$ remains hamiltonian.

Let $d_G(u, v)$ denote the distance between two vertices u, v in the graph G. The ℓ-th power of G, G^ℓ, is the graph with the same vertex-set as G and the edge-set $E(G^\ell)=\{uv \mid d_G(u, v)\leq \ell\}$.

For a connected graph G, it is known that G^3 is hamiltonian-connected[7,10] and 1-hamiltonian[4]; in this paper it will be shown that G^3 is also 1-EFH.

2. MAIN RESULT

We begin with the very first result in this topic which will be used in the proof of the main result.

Theorem 1 (**Sekanina; Karaganis**)

For any connected graph G of order $n\geq 2$, G^3 is hamiltonian-connected.

Next we state the main result of this paper.

Theorem 2

For any connected graph G of order $n\geq 4$, G^3 is 1-EFH.

Proof

Let T be a spanning tree of G. It is enough to show that T^3 is 1-EFH. Let $e=uv$ be an arbitrary edge of T^3, we show that T^3-e is hamiltonian. Let R be the unique path joining u with v in T and z be the vertex adjacent to u in R. Also let T_u and T_z be the subtrees of $T-uz$ containing u and z respectively.

Case 1: $T_u=\{u\}$ (Similarly for $T_z=\{z\}$ $(=\{v\})$)

Since $n\geq 4$, it is easy to verify that there exist two distinct vertices x, y in T_z-v with $d_T(u, x)\leq 3$ and $d_T(u, y)\leq 3$. By Theorem 1, T_z^3 is hamiltonian-connected. Thus there exists a hamiltonian (x, y)-path, say P, in T_z^3; and so $[uxPyu]$ is a hamiltonian cycle in T^3-e.

Case 2: $|T_u| \geq 2$

When $d_T(u, v) < 3$, it is easy to verify that there exist vertices x in $T_u - u$ and y in $T_z - v$ with $d_T(x, v) \leq 3$ and $d_T(y, u) \leq 3$. By Theorem 1, T_u^3 and T_z^3 are hamiltonian-connected. Thus there exist a homiltonian (x, u)-path, say P, in T_u^3 and a hamiltonian (y, v)-path, say Q, in T_z^3. Then $[uPxvQyu]$ is a hamiltonian cycle in $T^3 - e$.

When $d_T(u, v) = 3$, say $R = (u, z, y, v)$. Let x be a vertex in T_u adjacent to u. Again by Theorem 1, there exist a hamiltonian (x, u)-path, say P, in T_u^3 and a hamiltonian (y, z)-path, say Q, in T_z^3. Then $[uPxzQyu]$ is a hamiltonian cycle in $T^3 - e$.

Therefore the proof is completed.

□

3. QUESTIONS

For every 2-connected graph G, Fleischner[5] showed that G^2 is hamiltonian; and later it was shown[3] that G^2 is indeed hamiltonian-connected and 1-hamiltonian. We guess that G^2 is 1-EFH.

Notice that if T is a tree containing a vertex v so that some component of $T - v$ is a path of length 2, then $\delta(T^3) = 3$ and thus T^3 cannot be 2-EFH. However it is likely to be true that for any nonnegative integer k and any tree T of order $n \geq k+3$, T^{k+2} is k-EFH.

REFERENCES

(1) J.A. Bondy and V. Chvátal, "A Method in Graph Theory", *Disc. Math.*, **15**, 111-136 (1976).

(2) J.A. Bondy and U.S.R. Murty, *Graph Theory with Applications*, Macmillan, London, and Elsevier, New York (1976).

(3) G. Chartrand, A.M. Hobbs, H.A. Jung, S.F. Kapoor and C. St. J.A. Nash-Williams, "The Square of a Block is Hamiltonian Connected", *J. Combinat. Theory Ser. B*, **16**, 290-292 (1974).

(4) G. Chartrand and S.F. Kapoor, "The Cube of Every Connected Graph is 1-Hamiltonian", *J. Res. Nat. Bur. Stand.*, **73B**, 47-48 (1969).

(5) H. Fleischner, "The Square of Every Two-Connected Graph is Hamiltonian", *J. Combinat. Theory Ser. B*, **16**, 29-34 (1974).

(6) F. Harary and J.P. Hayes, "Edge Fault Tolerance in Graphs", *Networks*, **6**, 563-574 (1993).

(7) J.J. Karaganis, "On the Cube of a Graph", *Canad. Math. Bull.*, **11**, 295-296 (1968).
(8) L. Lesniak-Foster, "Some Recent Results in Hamiltonian Graphs", *J. Graph Theory*, **1**, 27-36 (1977).
(9) C. Lin, *On Edge Fault-Tolerant Hamiltonian Graphs*, Master Thesis, Fu Jen Catholic University (1995).
(10) M. Sekanian, "On an Ordering of the Vertices of a Connected Graph", *Publ. Fac. Sci. Univ. Brno*, **412**, 137-142 (1960).

任何連通圖的立方為1-盈邊漢米爾頓圖

蕭鴻銘
輔仁大學數學系

摘　　要

已知任何連通圖的立方為 1-盈點漢米爾頓圖，本文證其亦為 1-盈邊漢米爾頓圖。

SOME RESULTS ON ESTIMATION ALGERRAS IN NONLINEAR FILTERING THEORY

WEN-LIN CHIOU*
Department of Mathematics
Fu Jen University
Taipei, Taiwan 24205, R.O.C.

ABSTRACT

The idea of using estimation algebras to construct finite dimensional nonlinear filters was first proposed by Brockett and Mitter independently. It turns out that the concept of estimation algebra plays a crucial role in the investigation of finiti dimensional nonlinear filters. In his talk at the International Congress of Mathematicians in 1983, Brockett proposed to classify all finite-dimensional estimation algebras. Recently, Chen, Chiou, Leung and Yau have classified all finite-dimensional estimation algebras with maximal rank for state space dimension less than or equal to four. Rasoulian and Yau discussed four dimensional nonmaximal-rank estimation algebras for state space dimension two. Rasoulian and Yau have classified four dimensional estimation algebras for arbitrary state space dimension. In this paper we consider some filtering systems. In a special filtering system, we have similar results as Rasoulian and Yau's paper. Also we have classified all finite dimensional estimation algebras for state space dimension two. A more general filtering system is considered. We have classified all finite dimensional estimation algebras for state space dimension less than or equal to two, and all finite dimensional estimation algebras with maximal rank for state space dimension less than or equal to four. Therefore from the algebraic point of view, we have now understood generically some finite dimensional filters.

Key Words: Estimation algebras, Filtering systems, Finite dimensional nonlinear filters, Classification.

1. INTRODUCTION

The idea of using estimation algebras to construct finite dimensional nonlinear filters was first proposed in Brockett and Clark[5], Brockett[3]

* Funded by the NSC grant NSC 84-2121-M030-004.

and Mitter[14]. The concept of estimation algebras was proven to be an invaluable tool in the study of nonlinear filtering problems. In his famous talk at the International Congress of Mathematicians in 1983, Brockett[4] proposed to classify all finite dimensional estimation algebras. There were some interesting results in 1987 due to Wong[19] (cf. filtering system Eq. (1) below) under the assumptions that the observation $h(x)$ and drift term $f(x)$ are real analytic functions on $\boldsymbol{R}^n$, and f satisfies the following growth conditions: for any i, all the first, second and third order partial derivatives of f_i are bounded functions. Under all these conditions, Wong provides partial information towards the classification of finite dimensional estimation algebra. Namely he showed that if the estimation algebra is finite dimensional, then the degree of h in x is at most one and the estimation algebra has a basis consisting of one second degree differential operator, L_0 (cf. Eq. (5) below), first degree differential operators of the form

$$\sum_{i=1}^{n} \alpha_i \left(\frac{\partial}{\partial x_i} - f_i \right) + \sum_{i=1}^{n} \beta_i \frac{\partial \eta}{\partial x_i}$$

where α_i and β_i are constants and $\eta = -\frac{1}{2}\left(\sum_{i=1}^{n} \frac{\partial f_i}{\partial x_i} + \sum_{i=1}^{n} f_i^2 + \sum_{i=1}^{m} h_i^2 \right)$, and zero degree differential operators affine in x. In Tam, Wong and Yau[17] have introduced the concept of an estimation algebra with maximal rank of filtering system Eq. (4). Let n be the dimension of the state space. It turns out that all nontrivial finite dimensional estimation algebras are automatically exact with maximal rank if $n=1$. It follows from the works of Ocone[15], Tam, Wong and Yau[17], and Dong, Tam, Wong and Yau[13] that the finite dimensional estimation algebras are completely classified if $n=1$. In fact, Dong, Tam, Wong and Yau have classified all finite dimensional exact estimation algebras with maximal rank of arbitrary finite state space dimension for filtering system Eq. (4). For arbitrary finite dimensional state space, under the condition that the drift term is a linear vector field plus a gradient vector field, Yau[20] have classified all finite dimensional estimation algebras with maximal rank of filtering system Eq. (4). Chiou and Yau[9], and Chen, Leung and Yau[6] have classified all finite dimensional estimation algebras with maximal rank of filtering system Eq. (4) for $n=1$, 2, and $n=3$, 4 respectively. Chiou[8] considerd another filtering

system (cf. system Eq. (6)) and has similar results as (Chen et al.[6], Chiou and Yau[9], Dong et al.[13], Yau[20]) about classification theorems. Recently in Chen and Yau[7] have some structure results about finite-dimensional nonmaximal-rank estimation algebras for state space dimension two. In Rasoulian and Yau[16] have classified four dimensional estimation algebras for arbitrary state space dimension. As a striking result, they found 4-dimensional filters with arbitrary state space dimension such that the drift term is not the sum of a linear vector field and a gradient vectoor field. In this paper we consider some filtering systems. In a filtering system Eq. (6), we have similar results as in Rasolian and Yau[16]. We have classified all finite dimensional estimation algebras of filtering system Eqs. (4), (6) and (7) for $n=2$ (cf. §3 Main Theorems). Also we have classified all finite dimensional estimation algebras with maximal rank for $n\leq 4$. Therefore from the algebraic point of view, we have now understood generically some finite dimensional filters.

2. BASIC CONCEPTS

In this section, we will recall some basic concepts and results which we need for the next section. Consider a filtering problem based on the following signal observation model:

$$\left.\begin{aligned} dx(t)&=f[x(t)]dt+g[x(t)]dv(t), & x(0)&=x_0\\ dy(t)&=h[x(t)]dt+dw(t), & y(0)&=0 \end{aligned}\right\} \quad (1)$$

in which x, v, y and w are respectively $\boldsymbol{R}^n$, $\boldsymbol{R}^p$, $\boldsymbol{R}^m$ and $\boldsymbol{R}^m$ valued processes, and v and w have components which are independent, standard Brownian processes. We further assume that $n=p$, f, h are C^∞ smooth, and that g is an n by n C^∞ smooth matrix. We will refer to $x(t)$ as the state of the system at time t and to $y(t)$ as the observation at time t.

Let $\rho(t, x)$ denote the conditional density of the state given the observation $\{y(s): 0\leq s\leq t\}$. It is well known (see Davis[11], for example) that $\rho(t, x)$ is given by normalizing a function, $\sigma(t, x)$, which satisfies the following Duncan-Mortensen-Zakai equation (see Zakai[21], for

example):

$$d\sigma(t,\ x)=L_0\sigma(t,\ x)dt+\sum_{i=1}^{m}L_i\sigma(t,\ x)dy_i(t), \qquad \sigma(0,\ x)=\sigma_0 \quad (2)$$

where

$$L_0=\frac{1}{2}\sum_{i,j=1}^{n}\frac{\partial^2}{\partial x_i\partial x_j}(gg^t)_{ij}-\sum_{i=1}^{n}\frac{\partial}{\partial x_i}f_i-\frac{1}{2}\sum_{i=1}^{m}h_i^2$$

and for $i=1, \cdots, m$, L_i is the zero degree differential operator of multiplication by h_i. σ_0 is the probability density of the initial point x_0. In this paper, we will assume σ_0 is a C^∞ function.

Equation (2) is a stochastic partial differential equation. In real applications, we are interested in constructing state estimators from observed sample paths with some property of robustness. Davis[11] studied this problem and proposed some robust algorithms. In our case, his basic idea reduces to defining a new unnormalized density

$$\xi(t,\ x)=\exp\Big[-\sum_{i=1}^{m}h_i(x)y_i(t)\Big]\sigma(t,\ x)$$

It is easy to show that $\xi(t,\ x)$ satisfies the following time varying partial differential equation

$$\left.\begin{aligned}\frac{\partial\xi}{\partial t}(t,\ x)&=L_0\xi(t,\ x)+\sum_{i=1}^{m}y_i(t)[L_0,\ L_i]\xi(t,\ x)\\&\quad+\frac{1}{2}\sum_{i,j=1}^{m}y_i(t)y_j(t)\{[L_0,\ L_i],\ L_j\}\xi(t,\ x)\\\xi(0,\ x)&=\sigma_0\end{aligned}\right\} \quad (3)$$

where $[\cdot,\ \cdot]$ is the Lie bracket defined as:

Definition

If X and Y are differential operators, the Lie bracket of X and Y, $[X,\ Y]$, is defined by

$$[X,\ Y]\varphi=X(Y\varphi)-Y(X\varphi)$$

for any C^∞ function φ.

Recall that a real vector space $\mathcal{F}$, with an operation $\mathcal{F}\times\mathcal{F}\to\mathcal{F}$ denoted $(x,\ y)\mapsto[x,\ y]$ and called the Lie bracket of x and y, is called

a Lie algebra if the following axioms are satisfied:

(1) The Lie bracket operation is bilinear;

(2) $[x, x]=0$, for all $x\in\mathfrak{F}$;

(3) $\{x, [y, z]\}+\{y, [z, x]\}+\{z, [x, y]\}=0$, $(x, y, z\in\mathfrak{F})$.

Definition

The estimation algebra E of a filtering system Eq. (1) is defined to be the Lie algebra generated by $\{L_0, L_1, \cdots, L_m\}$ or $E=\langle L_0, L_1, L_m\rangle_{L.A.}$.

We further assume in system Eq. (1) that $g[x(t)]=o[x(t)]$ are orthogonal matrix as follows:

$$\left.\begin{aligned} dx(t)&=f[x(t)]dt+o[x(t)]dv(t), & x(0)&=x_0\\ dy(t)&=h[x(t)]dt+dw(t), & y(0)&=0 \end{aligned}\right\} \quad (4)$$

Here

$$\begin{aligned} L_0&=\frac{1}{2}\sum_{i=1}^{n}\frac{\partial^2}{\partial x_i^2}-\sum_{i=1}^{n}f_i\frac{\partial}{\partial x_i}-\sum_{i=1}^{n}\frac{\partial f_i}{\partial x_i}-\frac{1}{2}\sum_{i=1}^{m}h_i^2\\ &=\frac{1}{2}\left(\sum_{i=1}^{n}D_i^2-\eta\right) \end{aligned} \quad (5)$$

where

$$D_i=\frac{\partial}{\partial x_i}-f_i$$

and

$$\eta=\sum_{i=1}^{n}\frac{\partial f_i}{\partial x_i}+\sum_{i=1}^{n}f_i^2+\sum_{i=1}^{m}h_i^2$$

We also consider another filtering system, namely, in filtering system Eq. (1), we further assume that $g[x(t)]=G$ is a constant nonsingular n by n matrix.

$$\left.\begin{aligned} dx(t)&=f[x(t)]dt+Gdv(t), & x(0)&=x_0\\ dy(t)&=h[x(t)]dt+dw(t), & y(0)&=0 \end{aligned}\right\} \quad (6)$$

We need the following basic results for later discussion.

Theorem 1 (Ocone[15])

Let E be a finite dimensional estimation algebra of filtering system

Eqs. (4) and (6). If a function ξ is in E, then ξ is a polynomial of degree ≤ 2.

Theorem 2 (Yau[20])

Let $F(x_1, \cdots, x_n)$ be a polynomial on $\boldsymbol{R}^n$. Suppose that there exists a polynomial path $c: \boldsymbol{R} \to \boldsymbol{R}^n$ such that $\lim_{t\to\infty} \|c(t)\| = \infty$ and $\lim_{t\to\infty} F \circ c(t) = -\infty$. Then there is no C^∞ functions $f_1, f_2, \cdots, f_n$ on $\boldsymbol{R}^n$ satisfying the equation

$$\sum_{i=1}^{n} \frac{\partial f_i}{\partial x_i} + \sum_{i=1}^{n} f_i^2 = F$$

The following Theorem 3 was proven by Dong, Tam, Wong and Yau[13].

Theorem 3

There exist a sumooth vector field f on R^n satisfying $\sum_{i=1}^{n} \frac{\partial f_i}{\partial x_i} + \sum_{i=1}^{n} f_i^2 = \sum_{i=1}^{n} a_i x_1^2 - c$ if and only if $a_i \geq 0$, and $c \leq \sum_{i=1}^{n} \sqrt{a_i}$.

In Chiou and Yau[9], the following Proposition 1 was proven.

Proposition 1

Let $\tilde{x} = Rx$ be an orthogonal change of coordinate, i.e., R is an orthogonal matrix. Then

(1) $\tilde{f}(\tilde{x}) = Rf(x)$;

(2) $\tilde{L}_0 = L_0$;

(3) $(\tilde{\omega}_{ji}) = R(\omega_{\ell k})R^T$, where $\tilde{L}_0 = \frac{1}{2}\left[\sum_{i=1}^{n} \tilde{D}_i^2 - \tilde{\eta}(\tilde{x})\right]$, $\tilde{D}_i = \frac{\partial}{\partial \tilde{x}_i} - f_i$, $\tilde{h}(\tilde{x}) = h(x)$, $\tilde{\eta}(\tilde{x}) = \sum_{i=1}^{n} \frac{\partial \tilde{f}_i(\tilde{x})}{\partial \tilde{x}_i} + \tilde{f}(\tilde{x}) \cdot \tilde{f}(\tilde{x}) + \sum_{i=1}^{m} \tilde{h}_i^2(\tilde{x})$, and $\tilde{\omega}_{ji} = \frac{\partial \tilde{f}_i}{\partial \tilde{x}_j} - \frac{\partial \tilde{f}_j}{\partial \tilde{x}_i}$;

(4) $\tilde{E}$ is isomorphic to E as Lie algebra where $\tilde{E}$ is the Lie algebra generated by $\tilde{L}_0, \tilde{h}_1, \cdots, \tilde{h}_m$.

In Chiou[8], the following Proposition 2 were proven.

Proposition 2

Let $\tilde{x} = Rx$, where R is the inverse matrix of G. Then

(1) $\tilde{f}(\tilde{x})=Rf(x)$;

(2) $\tilde{L}=L_0$, where $\tilde{L}_0=\frac{1}{2}\sum_{i=1}^{n}\frac{\partial^2}{\partial\tilde{x}_i^2}-\sum_{i=1}^{n}\frac{\partial}{\partial\tilde{x}_i}\tilde{f}_i(\tilde{x})-\frac{1}{2}\sum_{i=1}^{m}\tilde{h}_i^2(\tilde{x})$, with $\tilde{h}(\tilde{x})=h(x)$;

(3) $\tilde{E}$ is isomorphic to E as Lie algebra where $\tilde{E}$ is the Lie algebra generated by $\tilde{L}_0$, $\tilde{h}_1$, $\cdots$, $\tilde{h}_m$.

In You[20], the following Proposition 3 and Theorem 4 were proven.

Proposition 3

$\frac{\partial f_j}{\partial x_i}-\frac{\partial f_i}{\partial x_j}=c_{ij}$ are constants for all i and j if and only if $(f_1, \cdots, f_n)=(\ell_1, \cdots, \ell_n)+\left(\frac{\partial\varphi}{\partial x_1}, \cdots, \frac{\partial\varphi}{\partial x_n}\right)$, where $\ell_1, \cdots, \ell_n$ are polynomials of degree one and φ is a C^∞ function. In particular, $c_{ij}=0$ if and only if f is a gradient field. In this case the estimation algebra is exact.

Theorem 4

Let E be a finite dimensional estimation algebra of filtering system Eq. (4) satisfying $\frac{\partial f_j}{\partial x_i}-\frac{\partial f_i}{\partial x_j}=c_{ij}$ where c_{ij} are constants for all $1\leq i, j\leq n$. Then $h_1, \cdots, h_m$ are polynomials of degree at most one.

A similar result as Theorem 4 was given by Chiou[8].

Theorem 5

Let $\tilde{x}=G^{-1}x$ and E be a finite dimensional estimation algebra of filtering system Eq. (6) satisfying

$$G^{-1}f(x)=[\ell_1(\tilde{x}), \cdots, \ell_n(\tilde{x})]^t+\left[\frac{\partial\psi(\tilde{x})}{\partial\tilde{x}_1}, \cdots, \frac{\partial\psi(\tilde{x})}{\partial\tilde{x}_n}\right]^t$$

where $\ell_1, \cdots, \ell_n$ are polynomials of degree one and ψ is a c^∞ function. Then $h_1, \cdots, h_m$ are polynomial of degree at most one.

In view of the above theorem, Chiou and Yau[9] and Chiou[8] introduced the following definition.

Definition

The estimation algebra E of a filtering problems Eqs. (4) and (6) is

said to be the estimation algebra with maximal rank if x_i+c_i is in E for all $1\leq i\leq n$ where c_i is a constant.

In this paper, we consider other cases, and give the following difinition.

Definition

The estimation algebra E of a filtering problems Eqs. (4) and (6) is said to be an estimation algebra without full rank or a nonmaximal-rank estimation algebra, if the dimension of vector space spanned by all those liner functions in E is less than n.

Suppose that the state space of the filtering system Eq. (4) is of dimension n. The following theorem is proven by Chiou and Yau[9] for $n=1$, 2, Chen, Leung and Yau[6] for $n=3$, 4.

Theorem 6

If E is a finite dimensional estimation algebra with maximal rank of filtering system Eq. (4), then the drift term f must be linear vector field plus gradient vector field and E is a real vector space of dimension $2n+2$ with basis given by 1, x_1, $\cdots$, x_n, D_1, $\cdots$, D_n and L_0, for $n\leq 4$.

A similar result as Theorem 6 was given by Chiou[8].

Theorem 7

Suppose that the state space of a filtering system Eq. (6) is of dimension n, $n\leq 4$. If E is a finite dimensional estimation algebra with maximal rank, then

$$G^{-1}f(x)=[\ell_1(\tilde{x}),\ \cdots,\ \ell_n(\tilde{x})]^t+\left(\frac{\partial\psi}{\partial\tilde{x}_1},\ \cdots,\ \frac{\partial\psi}{\partial\tilde{x}_n}\right)^t$$

where $\tilde{x}=G^{-1}x$ and ψ is C^∞ smooth. Therefore E is a real vector space of dimension $2n+2$ with basis given by 1, x_1, $\cdots$, x_n, $\frac{\partial}{\partial x_1}-f_1$, $\cdots$, $\frac{\partial}{\partial x_n}-f_n$, and L_0.

The following two classification theorems about nonmaximal-rank estimation algebras were proven by Rasoulian and Yau[16].

Theorem 8

Suppose that the state space of the filtering system Eq. (4) is of dimension two, then the 4-dimensional estimation algebra is isomorphic to a Lie algebra having the basis: 1, x_1, $D_1=\frac{\partial}{\partial x_1}-f_1(x_1, x_2)$ and $L_0=\frac{1}{2}\left(\sum_{i=1}^{2} D_i^2-\eta\right)$. Moreover $\omega_{12}=\frac{\partial f_2}{\partial x_1}-\frac{\partial f_1}{\partial x_2}=0$, $[L_0, x_1]=D_1$, $[D_1, x_1]=1$, $[L_0, D_1]=\frac{1}{2}\frac{\partial \eta}{\partial x_1}=ax_1+b$, where a, b, are constants. Also $\eta=ax_1^2+2bx_1+g(x_2)$, where $g(x_2)$ is in $C^\infty(R)$. In particular, f_1 and f_2 satisfy the equation

$$\frac{\partial f_1}{\partial x_1}+\frac{\partial f_2}{\partial x_2}+f_1^2+f_2^2=(a-1)x_1^2+2bx_1+g(x_2)$$

where $a\geq 1$.

Theorem 9

Suppose that the state space of the filtering system Eq. (4) is of dimension greater than two, then the 4-dimensional estimation algebra is isomorphic to a Lie algebra having the basis given by 1, x_1, $D_1=\frac{\partial}{\partial x_1}-f_1(x_1, \cdots, x_n)$ and $L_0=\frac{1}{2}\left(\sum_{i=1}^{n} D_i^2-\eta\right)$. Moreover $\omega_{12}=\omega_{13}=\cdots=\omega_{1n}=0$, $[L_0, x_1]=D_1$, $[D_1, x_1]=1$, $[L_0, D_1]=\frac{1}{2}\frac{\partial \eta}{\partial x_1}=ax_1+b$, where a, b, are constants. Also $\eta=ax_1^2+2bx_1+g(x_2, \cdots, x_n)$, where $g(x_2, \cdots, x_n)$ is in $C^\infty(R^{n-1})$. In particular, $f_1, \cdots, f_n$ satisfy the equation

$$\frac{\partial f_1}{\partial x_1}+\frac{\partial f_2}{\partial x_2}+f_1^2+f_2^2=(a-1)x_1^2+2bx_1+g(x_2, \cdots, x_n)$$

where $a\geq 1$.

The following four lemmas was proven by Chen and Yau[7].

Lemma 1

Suppose that the state space of the filtering system Eq. (4) is of dimension two. Let the estimation algebra is finite-dimensional. If $a(x)D_1+b(x)D_2+c(x)\in E$, then $a(x)=\beta_1 x_1 x_2+$linear function and $b(x)=\beta_2 x_1 x_2+$linear function, where β_1 and β_2 are constants.

Lemma 2

Suppose that the state space of the filtering system Eq. (4) is of dimension two. Let the estimation algebra is finite-dimensional. If $\xi \in E$ is a polynormial of degree two, then ω_{12} is a constant.

Lemma 3

Suppose that the state space of the filtering system Eq (4) is of dimension two. If the estimation algebra is finite-dimensional, then h_i is at most linear.

Lemma 4

Suppose that the state space of the filtering system Eq. (4) is of dimension two. If the estimation algebra is finite dimensional and $x_1 \in E$, then $\omega_{12}=\frac{\partial f_2}{\partial x_1}-\frac{\partial f_1}{\partial x_2}$ is constant.

3. MAIN THEOREMS

Two immediate results follow from by Theorem 8 and Theorem 9.

Theorem A

Suppose that the state space of the filtering system Eq. (6) is of dimension two, then the 4-dimensional estimation algebra is isomorphic to a Lie algebra having the basis: 1, x_1, $D_1=\frac{\partial}{\partial x_1}-f_1(x_1, x_2)$ and $L_0=\frac{1}{2}\left(\sum_{i=1}^{2} D_i^2-\eta\right)$. Moreover $\omega_{12}=\frac{\partial f_2}{\partial x_1}-\frac{\partial f_1}{\partial x_2}=0$, $[L_0, x_1]=D_1$, $[D_1, x_1]=1$, $[L_0, D_1]=\frac{1}{2}\frac{\partial \eta}{\partial x_1}=ax_1+b$, where a, b, are constant. Also $\eta=ax_1^2+2bx_1+g(x_2)$, where $g(x_2)$ is in $C^\infty(R)$. In particular, f_1 and f_2 satisfy the equation

$$\frac{\partial f_1}{\partial x_1}+\frac{\partial f_2}{\partial x_2}+f_1^2+f_2^2=(a-1)x_1^2+2bx_1+g(x_2)$$

where $a \geq 1$.

Theorem B

Suppose that the state space of the filtering system Eq. (6) is of dimension great than two, then the 4-dimensional estimation algebra is isomorphic to a Lie algebra having the basis given by 1, x_1, $D_1=\frac{\partial}{\partial x_1}-f_1(x_1, \cdots, x_n)$ and $L_0=\frac{1}{2}\left(\sum_{i=1}^{n} D_i^2-\eta\right)$. Moreover $\omega_{12}=\omega_{13}=\cdots=\omega_{1n}=0$, $[L_0, x_1]=D_1$, $[D_1, x_1]=1$, $[L_0, D_1]=\frac{1}{2}\frac{\partial \eta}{\partial x_1}=ax_1+b$, where a, b, are constants. Also $\eta=ax_1^2+2bx_1+g(x_2, x_n)$, where $g(x_2, x_n)$ is in $C^\infty(R^{-1})$. In particular, $f_1, \cdots, f_n$ satisfy the equation

$$\frac{\partial f_1}{\partial x_1}+\frac{\partial f_2}{\partial x_2}+f_1^2+f_2^2=(a-1)x_1^2+2bx_1+g(x_2, \cdots, x_n)$$

where $a\geq 1$.

The following Theorem C classifies all finite-dimensional estimation algebras, when the state spece is dimension two.

We need the following Corollary which follows from Theorem 2, and the proof is similar to Corollary in Tam, Wong and Yau[17].

Corollary

Let $F(x_1, \cdots, x_n)$ be a C^∞ function on $\boldsymbol{R}^n$, and a polynomial in $x_1, \cdots, x_k$, where $k\leq n$. Suppose that there exists a polynomial path c: $\boldsymbol{R}\to\boldsymbol{R}^k$ such that $\lim_{t\to\infty}\|c(t)\|=\infty$ and $\lim_{t\to\infty} F\circ c(t)=-\infty$, where $x_{k+1}, \cdots, x_n$ are fixed. Then there is no C^∞ functions $f_1, f_2, \cdots, f_n$ on $\boldsymbol{R}^n$ satisfying the equation

$$\sum_{i=1}^{n}\frac{\partial f_i}{\partial x_i}+\sum_{i=1}^{n} f_i^2=F$$

For convience, the following letters a, b, c, d, e and s denote constants, and the functions $u(x_2)$, $u_1(x_2)$, and $u(x_2)$ is in $C^\infty(R)$.

Theorem C

Suppose the state space is of dimension two. If the estimation algebra E of filtering system Eqs. (4) or (6) is finite-dimensional, then one of the following holds:

(i) E is a real space of dimension 6 with basis given by 1, x_1, x_2, $D_1=\frac{\partial}{\partial x_1}-f_1$, $D_2=\frac{\partial}{\partial x_2}-f_2$, and L_0.

(ii) E is a real space of dimension 4 which is isomorphic to the real vector space having the basis given by 1, x_1, D_1, and L_0.

(iii) E is a real vector space of dimension 2 with basis given by 1 and L_0.

(iv) E is a real vector space of dimension 1 with basis given by L_0.

Proof

By Proposition 2 and the proof of Theorem 7, we only need to prove the estimation algebra E in filtering system Eq. (4).

In view of Lemma 3, all the observation terms h_i $1\leq i\leq m$ are necessarily affine polynomials. So we have the following cases.

If all the h_i for $1\leq i\leq m$ are actually zero, then obviously we are in case (iv) above.

If all the h_i for $1\leq i\leq m$ are at most constants and one of them is nonzero, then $1\in E$, and

$$[L_0,\ 1]=\frac{1}{2}[D^2-\eta,\ 1]=0 \tag{7}$$

Therefore we are in case (iii) above.

If there is only one $h_i=ax_1+bx_2\in E$, where one of a and b is nonzero, and other h_j's are all constants. We may assume that $h_i=\frac{1}{\sqrt{1+c^2}}x_1+\frac{c}{\sqrt{1+c^2}}x_2$. Let $\tilde{x}_1=\frac{1}{\sqrt{1+c^2}}x_1+\frac{c}{\sqrt{1+c^2}}x_2$ and $\tilde{x}_2=\frac{1}{\sqrt{1+c^2}}x_1-\frac{c}{\sqrt{1+c^2}}x_2$, which is an orthogonal change of coordinates. By Proposition 1, in this case, we always can assume only one linear function $x_1+c\in E$. By Lemma 4, ω_{12} is a constant. Observe

$$[L_0,\ x_1]=\frac{1}{2}\left[\sum_{i=1}^{2}D_i^2-\eta,\ x_1\right]=D_1 \tag{8}$$

$$[D_1,\ x_1]=1 \tag{9}$$

$$Y_1=[L_0,\ D_1]=\left[\frac{1}{2}\left(\sum_{i=1}^{2}D_i^2-\eta\right),\ D_1\right]=\omega_{12}D_2+\frac{1}{2}\left[\frac{\partial\omega_{12}}{\partial x_2}-\frac{\partial\eta}{\partial x_1}\right]$$
$$=\omega_{12}D_2+\frac{1}{2}\frac{\partial\eta}{\partial x_1} \tag{10}$$

If $\omega_{12}=0$ the $\frac{\partial\eta}{\partial x_1}\in E$. This implies η is of the form

$ax_1^3+bx_1^2x_2+cx_1x_2^2+$lower degree polynormial terms$+u_1(x_2)$

by Theorem 1. Recall that

$$\frac{\partial f_1}{\partial x_1}+\frac{\partial f_2}{\partial x_2}+f_1^2+f_2^2=\eta-\sum_{i=1}^{m}h_i^2 \tag{11}$$

If η is a polynomial of degree 3, i.e., one of a, b, c is nonzero, then

$$\eta-\sum_{i=1}^{m}h_i^2=\eta-x_1^2+e \tag{12}$$

is also a polynomial of degree 3. According to Corollary, Eq. (11) has no C^∞ solution f. This leads to a contradiction. Therefore we have shown that $\frac{\partial\eta}{\partial x_1}$ is at most linear function. If $\frac{\partial\eta}{\partial x_1}=ax_1+bx_2+c$, where $b\neq0$. Then by Corollary and in view of Eqs. (11) and (12), there is no c^∞ solution f. This leads to a contradiction. By a similar argument for $\frac{\partial\eta}{\partial x_1}=$constant, we get a contradiction. Hence, $\frac{\partial\eta}{\partial x_1}=2ax_1+b$, for some non-zero constant a and constant b, or $\eta=ax_1^2+u(x_2)$.

By Theorem 2, we have $a>1$. In views of Eqs. (8), (9) and (10), under the assumption $\omega_{12}=0$, we are in the case (ii).

If $\omega_{12}=c\neq0$, observe

$$[Y_1,\ D_1]=\left[\omega_{12}D_2+\frac{1}{2}\left(\frac{\partial\omega_{12}}{\partial x_2}+\frac{\partial\eta}{\partial x_1}\right),\ D_1\right]$$
$$=\omega_{12}^2-\frac{1}{2}\frac{\partial^2\eta}{\partial x_1^2} \tag{13}$$

Then

$$\frac{\partial^2\eta}{\partial x_1^2}=ax_1^2+bx_1x_2+cx_2^2+dx_1+ex_2+s \tag{14}$$

$$[L_0, Y_1]=\left[L_0, \omega_{12}D_2+\frac{1}{2}\frac{\partial\eta}{\partial x_1}\right]$$
$$=\omega_{12}\left[\omega_{21}D_1+\frac{1}{2}\left(\frac{\partial\omega_{21}}{\partial x_1}+\frac{\partial\eta}{\partial x_2}\right)\right]$$
$$+\frac{1}{2}\frac{\partial^2\eta}{\partial x_1^2}D_1+\frac{1}{4}\frac{\partial^2\eta}{\partial x_1^2}+\frac{1}{2}\frac{\partial^2\eta}{\partial x_1\partial x_2}D_2+\frac{1}{4}\frac{\partial^2\eta}{\partial x_1\partial x_2} \quad (15)$$

Suppose $\deg\frac{\partial^2\eta}{\partial x_1^2}=2$. By Lemma 1, we have $a=c=0$ and hence $b\neq 0$

$$\frac{\partial^2\eta}{\partial x_1^2}=bx_1x_2+dx_1+ex_2+s$$

which means that

$$\eta=\frac{b}{6}x_1^3x_2+\frac{d}{6}x_1^3+\frac{e}{2}x_2x_1^2+\frac{s}{2}x_1^2+u_1(x_2)x_1+u_2(x_2)$$

Then

$$\frac{\partial^2\eta}{\partial x_1\partial x_2}=2bx_1^2+ex_1+u_1'(x_2)$$

Again, by Lemma 1, $b=0$. Hence,

$$\eta=\frac{d}{3}x_1^3+\frac{e}{2}x_2x_1^2+\frac{s}{2}x_1^2+u_1(x_2)x_1+u_2(x_2)$$

A contradiction occurs again if $d\neq 0$. Hence,

$$\frac{\partial^2\eta}{\partial x_1^2}=ex_2+s$$

If $e\neq 0$, then since x_1, $x_2\in E$, by Theorem 6, we are in case (i).

If $e=0$. Again from Eq. (12) we have Eq. (11) has no C^∞ solution f, this leads to a contradiction.

Finally if the vector space spanned by $h_1, \cdots, h_m$ contains x_1+a and x_2+b, by Theorem 6, we are in case (i).

At the end of this section, we consider a more general filtering system (15) containing filtering system Eqs. (4) and (6). Namely in filtering system (15), we further assume:

(i) $h_1, \cdots, h_m$ are analytic;

(ii) $g_1, \cdots, g_n$ are analytic vector field, where $g[x(t)]=\{g_1[x(t)], \cdots, g_n[x(t)]\}$;

(iii) The Lie Algebra A spanned by $g_1, \cdots, g_n$ is abelian and $A(x) \simeq R^n$, $\forall x \in R^n$.

Note

This filtering system was proposed by Collingwood[10].

Let $L_r = \sum_{i=1}^{n} r_i \frac{\partial}{\partial x_i}$.

Definition

The estimation algebra E of filtering system Eq. (7) is said to be estimation algebra with maximal rank, if there exists functions $r_1(x), \cdots, r_n(x) \in$ the vector space spanned by $h_1(x), \cdots, h_m(x)$ such that $L_{g_i}(r_j) = \delta_{ij}$, $1 \leq i, j \leq n$.

Theorem D

Let $n \leq 4$. Suppose the estimation algebra is a finite dimensional estimation algebra with maximal rank of filtering system Eq. (7). Then E is locally a real vector space of dimension $2n+2$ with basis given by $1, r_1, \cdots, r_n, L_{g_1} - f_1, \cdots, L_{g_n} - f_n$, and L_0, where $L_{g_i}(r_j) = \delta_{ij}$, $1 \leq i, j \leq n$.

Proof

Since $A(x) \simeq R^n$, $\forall x \in R^n$, and $[L_{g_i}, L_{g_j}] = 0$, for $1 \leq i, j \leq n$, we have $g_1(x), \cdots, g_n(x)$ are linearly independent vectors.

Hence for any fixed $x_0 \in R^n$, it is well-known, (see for example: Boothby[1]), that there is a diffeomorphism $F: U \to V$, where U is a neighborhood of x_0 and V is a neighborhood of the origin in R^n, which induces an isomorphism $F_*: T_x(U) \to T_{F(x)}(V)$ such that

$$F_*(L_{g_i})|_x(\xi) = \left.\frac{\partial \xi \circ F(x)}{\partial z_i}\right|_{z=F(x)} \tag{16}$$

for any analytic ξ at $z = F(x)$, and $x \in U$.

Locally, we represent the filtering system (15) by a system Eq. (4) with $g[x(t)] = I$. Moreover, in Brokett's paper[2], it is shown that the diffeomorphism F induces an isomorphism between the estimation algebra E of filtering system (15), and the estimation algebra $\tilde{E}$ of Eq. (4).

Therefore, $\tilde{E}$ is finite dimensional with state space $V \simeq R^n$. Since E is of maximal rank, there exist fuuctions $r_1(x)$, $\cdots$, $r_n(x) \in$ the vector space spanned by $h_1,(x)$, $\cdots$, $h_m(x)$ such that $L_{g_i}(r_j)=\delta_{ij}$, $1 \leq i, j \leq n$. From Eq. (16), we have that

$$\frac{\partial r_i \circ F^{-1}}{\partial z_j}(z)=\text{constant}, \qquad 1 \leq i, j \leq n$$

That is, z_1+c_1, $\cdots$, z_n+c_n are in $\tilde{E}$, where c_1, $\cdots$, c_n are constants, or $\tilde{E}$ is of maximal rank. By Theorem 6, $\tilde{E}$ is a real vector space having a basis 1, z_1, $\cdots$, z_n, $\frac{\partial}{\partial z_1}-\tilde{f}_1 \circ F^{-1}$, $\cdots$, $\frac{\partial}{\partial z_n}-\tilde{f}_n \circ F^{-1}$, and $\tilde{L}_0$. Hence, E is locally a vector space having a basis 1, $r_1(x)$, $\cdots$, $r_n(x)$, $L_{g_1}-f_1$, $\cdots$, $L_{g_n}-f_n$, and L_0, where $L_{g_i}(r_j)=\delta_{ij}$, $1 \leq i, j \leq n$.

Q. E. D.

Using a similar proof, we have the following classification theorems for $n=1$, 2.

Theorem E

Suppose that the state space of the filtering system (15) is of dimension one. If the estimation algebra E is finite dimensional, then either:

(i) E is locally a real vector space of dimension 4 with basis given by 1, $r(x)$, L_g-f and L_0.

(ii) E is locally a real vector space of dimension 2 with basis given by 1 and L_0.

(iii) E is locally a real vector space of dimension 1 with basis given by L_0.

Here $L_g[r(x)]=1$.

Theorem F

Suppose the state space is of dimension two. If the estimation algebra E of filtering system (15) is finite-dimensional, then one of the following holds:

(i) E is locally a real vector space of dimension 6 with basis given by 1, $r_1(x)$, $r_2(x)$, $L_{g_1}-f_1$, $L_{g_2}-f_2$ and L_0.

(ii) E is locally a real space of dimension 4 which is isomorphic to the real vector space having the basis given by 1, $r_1(x_1)$, $L_{g_1}-f_1$ and L_0.

(iii) E is locally a real vector space of dimension 2 with basis given by 1 and L_0.

(iv) E is locally a real vector space of dimension 1 with basis given by L_0.

Here $L_{g_i}[r_j(x)]=\delta_{ij}$, $1\leq i, j\leq 2$.

REFERENCES

(1) W.M. Boothby, "An Introduction to Differential Manifolds, and Riemannian Geometry", 2nd ed., Academic Press (1986).

(2) R.W. Brockett, "Classification and Equivalence in Esimation Theory", *Proceedings of the 18th IEEE Conference on Decision and Control*, Fort Lauderdale, FL, 172-175 (1979).

(3) R.W. Brockett, "Nonlinear Systems and Nonlinear Estimation Theory", in *The Mathematics of Filtering and Identification Applications*, M. Hazewinkel and J.S. Williems, eds., Reidel, Dordrecht, The Netherlands (1981).

(4) R.W. Brockett, "Nonlinear Control Theory and Differential Geometry", *Proceedings of the International Congress of Mathematicians*, 1357-1368 (1983).

(5) R.W. Brockett and J.M.C. Clark, "The Geometry of the Conditional Density Functions", in *Analysis and Optimization of Stochastic Systems*, O.L.R. Jacobs, et al., eds., Academic Press, New York (1979).

(6) J. Chen, C.-W. Leung and S.S.-T. Yau, "Finite Dimensional Filters with Nonlinear Drift, VIII: Classification of Finite Dimensional Estimation Algebras of Maximal Rank with State Space Dimension 4", (Preprint) (1993).

(7) J. Chen and S.S.-T. Yau, "Finite Dimensional Estimation Algebras of Nonmaximal Rank with State Space Dimension 2", (Preprint) (1995).

(8) W.-L. Chiou, "Estimation Algebras on Nonlinear Filtering Theory", *Proceedings of the International Conference on Control and Information* (1995).

(9) W.-L. Chiou and S.S.-T. Yau, "Finite Dimensional Filters with Nonlinear Drift, II: Brockett's Problem on Classification of Finite-Dimensional Estimation Algebras", *SIAM J. Control and Optimization*, **32**(1), 297-310, January (1994).

(10) P.C. Collingwood, "Some Remarks on Estimation Algebras", *Systems Control Lett.*, **7**, 217-224 (1986).

(11) M.H.A. Davis, "On a Multiplicative Functional Transformation Arising in Nonlinear Filtering Theory", *Z. Wahrsch. Verw. Gebiete*, **54**, 125-139 (1980).

(12) R.T. Dong, L.F. Tam, W.S. Wong and S.S.-T. Yau, "Filtering Systems with Finite Dimensional Estimation Algebras", (Preprint) (1993).

(13) R.T. Dong, L.F. Tam, W.S. Wong and S.S.-T. Yau, "Structure and Classification Theorems of Finite Dimensional Exact Estimation Algebras", *SIAM J. Control and Optimization*, **29**(4), 866-877 (1991).
(14) S.K. Mitter, "On the Analogy between Mathematical Problems on Nonlinear Filtering and Quantum Physics", *Richerche di Automatica*, **10**(2), 163-216 (1979).
(15) D.L. Ocone, "Finite Dimensional Estimation Algebras in Nonlinear Filtering Theory", in *The Mathematics of Filtering and Identification Applications*, M. Hazewinkeland and J.S. Williems, eds., Reidel, Dordrecht, The Netherlands (1981).
(16) A. Rasoulian and S.S.-T. Yau, "Recent Results on Classification of 4-Dimensional Estimation Algebras", *Proceedings of the International Conference on Control and Information* (1995).
(17) L.F. Tam, W.S. Wong and S.S.-T. Yau, "On a Necessary and Sufficient Condition for Finite Dimensionality of Estimation Algebras", *SIAM J. Control and Optimization*, **28**(1), 173-185 (1990).
(18) J. Wei and E. Norman, "On Global Representations of the Solutions of Linear Differential Equations as Product of Exponentials", *Proc. Amer. Math. Sock.*, **15**, 327-334 (1964).
(19) W.S. Wong, "Theorem on the Structure of Finite Dimensional Estimation Algebras", *Systems Control Lett.*, **19**, 117-124 (1987).
(20) S.S.-T. Yau, "Finite Dimensional Filters with Nonlinear Drift, I: A of Filters Including Both Kalman-Bucy Filters and Benes Filters", *Journal of Mathematical Systems, Estimation, and Control*, **4**(2), 181-203 (1994).
(21) M. Zakai, "On the Optimal Filtering of Diffusion Processes", *Z. Wahrsch. Verw. Gibe.*, **11**, 230-243 (1969).

在過濾理論上的一些結果估計代數

邱 文 齡
輔仁大學數學系

摘 要

Brockett 及 Mitter 分別提出利用估計代數構造有限維的非線性濾過。估計代數的概念扮演瞭解有限維非線性過濾的主要方法。在 1983 年 Brockett 提出將有限維估計代數分類。最近，Rasoulian 與 Yau 對任意維狀態空間下，已做 4 維有限維估計代數分類。在本篇論文中，我們考慮一些濾過系統。在一特殊濾過系統，我們有相同結果；同時我們在狀態空間維數是小於成等於 2，對於所有有限維估計代數予以分類。我們亦提出一濾過系統包含上述特殊濾過系統，在狀態空間維數是小於或等於 2，對於所有有限維估計代數予以分類；同時對在狀態空間維數是小於或等於 4，對於有限維具有最大秩的估計代數予以分類。

核多項式加速法及其它多項式加速法之研究

黃裕雄　張　康
輔仁大學數學研究所

摘　　要

本文提出用多項式加速法來加速基本迭代法以解大型線性系統 $Au=b$，其中 A 爲一個 n 乘 n 的對稱正定矩陣。出發點是去找一個實係數 m 次多項式 $P_m(x)$ 且 $P_m(1)=1$，使得第 m 次之誤差向量滿足 $\varepsilon^{(m)}=P_m(G)\varepsilon^{(0)}$，其中 G 爲基本迭代法中的迭代矩陣。如此的演算方式，僅涉及矩陣乘向量和向量的相加，所以，非常適合用向量電腦及平行電腦處理。

本文中我們用 Dirichlet 核，Féjer 核，和 Legendre 多項式來產生 $P_m(x)$，並架構出多項式加速法之演算公式，且與 Cheyshev 多項式加速法做比較。我們利用 VAX 4500 及 IBM ES 9000/860 來做數值實驗，其中後者爲向量電腦。

一、簡　　介

在科學研究中，常會遇到解大型稀疏線性系統

$$Ax=b \tag{1}$$

的問題。我們常考慮用迭代解法來求解，即：

$$\begin{cases} x^{(n+1)}=Gx^{(n)}+k, & n=0,1,2,\cdots \\ x^{(0)} \text{ 爲任意的起始猜測向量} \end{cases} \tag{2}$$

其中 $G=I-Q^{-1}A$，$k=Q^{-1}b$，而 Q 爲一個非奇異的 A 之分裂矩陣 (splitting matrix)，G 稱爲迭代矩陣 (iteration matrix)。

若 $(x^{(i)})$ 爲由公式 (2) 所求得的向量序列，則可考慮 $x^{(i)}$ 的線性組合

$$u^{(n)}=\sum_{i=0}^{n}\alpha_{n,i}x^{(i)}, \qquad n=0,1,\cdots \tag{3}$$

其中 $\sum_{i=0}^{n}\alpha_{n,i}=1$，$n=0,1,2,\cdots$ 這種產生向量序列 $(u^{(n)})$ 的方法稱爲基本迭代法的多項式加速法，因爲假設 $\bar{u}$ 爲公式 (1) 的眞確解，則：

$$x^{(i)}-\bar{u}=(Gx^{(i-1)}+k)-(G\bar{u}+k)=G^i(u^{(0)}-\bar{u})$$

於是

$$u^{(n)}-\bar{u}=\sum_{i=0}^{n}\alpha_{n,i}G^i(u^{(0)}-\bar{u})$$

故誤差向量 $\varepsilon^{(n)}=u^{(n)}-\bar{u}$ 滿足

$$\varepsilon^{(n)}=\sum_{i=0}^{n}\alpha_{n,i}G^i\varepsilon^{(0)}=P_n(G)\varepsilon^{(0)} \tag{4}$$

其中 $P_n(x)=\sum_{i=0}^{n}\alpha_{n,i}x^i$。由於公式 (4) 成立，故稱爲多項式加速法，$\alpha_{n,i}$ 的選取方法不同，則所得到的加速法也不同；常見的多項式加速法有 Chebyshev 加速法 (Chebyshev acceleration method)，及 Hestenes 與 Stiefel[5] 在 1952 提出的共軛梯度法 (conjugate gradient method，簡稱 CG 法)。

本篇論文的研究動機起源於 Jea 與 Yang[6] 所提的多項式算子法，我們發現 Féjer 核及 Dirichlet 核之振盪高度隨 n 變大而遞減很快，所以，希望能利用它建構多項式加速法，並且和其它的加速法做比較，以了解其效果。

二、Dirichlet 多項式加速法

Dirichlet 核定義如下：

$$\hat{D}_n(\theta)=\sum_{i=-n}^{n}\cos i\theta\,,\qquad \theta\in\mathcal{R}$$

於是

$$\hat{D}_n(\theta)=\begin{cases}\dfrac{\sin\left(n+\frac{1}{2}\right)\theta}{\sin\frac{\theta}{2}}\,, & \theta\neq 2j\pi\,,\ j\in\mathcal{Z}\\ 2n+1\,, & \theta=2j\pi\,,\ j\in\mathcal{Z}\end{cases} \tag{5}$$

故 $\lim_{n\to\infty}\lim_{\theta\to 0}\hat{D}_n(\theta)\to\infty$，而且當 $0<|\theta|\leq\pi$ 時，$\lim_{n\to\infty}\sup|\hat{D}_n(\theta)|<\infty$。令：

$$D_n(\theta)=\frac{\hat{D}_n(\theta)}{2n+1}=\begin{cases}\dfrac{1}{2n+1}\dfrac{\sin\left(n+\frac{1}{2}\right)\theta}{\sin\frac{\theta}{2}}\,, & \theta\neq 2j\pi\,,\ j\in\mathcal{Z}\\ 1\,, & \theta=2j\pi\,,\ j\in\mathcal{Z}\end{cases} \tag{6}$$

則對任意 n，$\lim_{\theta\to 0}D_n(\theta)=1$，而且當 $0<|\theta|\leq\pi$ 時，可得到 $\lim_{n\to\infty}D_n(\theta)=0$。

令 $T_{m+1}(x)=\cos((m+1)\cos^{-1}x)$ 爲 $m+1$ 次第一型 Chebyshev 多項式，而 $U_m(x)=\frac{1}{m+1}T'_{m+1}(x)$ 爲 m 次第二型 Chebyshev 多項式，則 $T_{m+1}(x)=2xT_m(x)-T_{m-1}(x)$ 且 $U_{m+1}(x)=2xU_m(x)-U_{m-1}(x)$。

令 $x=\frac{1-\cos\theta}{2}$，$\theta\in[0,\pi]$，則 x 介於 $[0,1]$ 之間。於是由公式(6)得：

$$\begin{aligned}D_{m+1}(\theta)&=\frac{\sin\left((m+1)+\frac{1}{2}\right)\theta}{[2(m+1)+1]\sin\frac{\theta}{2}}\\&=\frac{1}{2m+3}[2(1-x)U_m(1-2x)+T_{m+1}(1-2x)]\\&\equiv D_{m+1}(x)\end{aligned}\tag{7}$$

令 $\mathcal{D}_{m+1}(x)=D_{m+1}(1-x)$，由公式 (7) 及 $T_{m+1}(x)$ 和 $U_{m+1}(x)$ 之三項遞迴關係式可推導出：

$$\mathcal{D}_{m+1}(x)=\frac{2m+1}{2m+3}2(2x-1)\mathcal{D}_m(x)-\frac{2m-1}{2m+3}\mathcal{D}_{m-1}(x)\tag{8}$$

其中 $\mathcal{D}_0(x)=1$，$\mathcal{D}_1(x)=\frac{4x-1}{3}$。我們稱公式 (8) 所得之多項式爲 Dirichlet 多項式，因爲它們是從 Dirichlet 核建構出來的。

引理 1

對任意 $x>1$，$1=\mathcal{D}_0(x)<\mathcal{D}_1(x)<\cdots<\mathcal{D}_m(x)<\mathcal{D}_{m+1}(x)<\cdots$ 成立。

證 明

$\mathcal{D}_0(x)=1$，$\mathcal{D}_1(x)=\frac{4x-1}{3}>1$，明顯成立。我們用數學歸納法證明。假設 $\mathcal{D}_m(x)>\mathcal{D}_{m-1}(x)>1$ 成立，要證 $\mathcal{D}_{m+1}(x)>\mathcal{D}_m(x)$，i.e.，$\mathcal{D}_{m+1}(x)-\mathcal{D}_m(x)>0$

$$\begin{aligned}&\mathcal{D}_{m+1}(x)-\mathcal{D}_m(x)\\&=\frac{2(2x-1)(2m+1)-(2m+3)-(2m-1)}{2m+3}\mathcal{D}_m(x)+\frac{2m-1}{2m+3}[\mathcal{D}_m(x)-\mathcal{D}_{m-1}(x)]\\&>\frac{2(2x-1)(2m+1)-2(2m+1)}{m+1}\mathcal{D}_m(x)\\&=\frac{4(x-1)(2m+1)}{2m+3}\mathcal{D}_m(x)>\frac{4(2m+1)}{2m+3}(x-1)>x-1>0\end{aligned}$$

故

$$1=\mathcal{D}_0(x)<\mathcal{D}_1(x)<\cdots<\mathcal{D}_m(x)<\mathcal{D}_{m+1}(x)<\cdots,\qquad m=1,2,\cdots$$

□

由上式引理及其證明，還可以推導出下列定理：

定理 2

對任意 $x>1$，當 m 趨近於無窮大時，$\mathcal{D}_m(x)$ 趨近於無窮大。

定理 3

假設 n 是固定的正整數，d 是固定的實數，且 $d>1$。令：

$$H_n(w)=\frac{\mathcal{D}_n(w)}{\mathcal{D}_n(d)} \tag{9}$$

其中 $\mathcal{D}_n(x)$ 是 Dirichlet 多項式，則：

$$H_n(d)=1 \tag{10}$$

且

$$\max_{0\le w\le 1}|H_n(w)|=\frac{1}{\mathcal{D}_n(d)} \tag{11}$$

令 $S(G)$ 表示 G 矩陣之譜半徑 (spectral radius)，本文中討論可對稱化 (symmetrizable) 之基本迭代法的加速，且假設 $M(G)<1$。設 $M(G)$、$m(G)$ 分別爲 G 矩陣的最大及最小特徵值，x 爲任意實數，且 $m(G)\le x\le M(G)<1$，則將區間 $[m(G), M(G)]$ 映成到區間 $[0, 1]$ 之線性變換函數爲：

$$w(x)=\frac{x-m(G)}{M(G)-m(G)} \tag{12}$$

令 $d=\dfrac{1-m(G)}{M(G)-m(G)}$，則 $d>1$，於是 $H_n(w)=\dfrac{\mathcal{D}_n(w)}{\mathcal{D}_n(d)}=P_n(w[M(G)-m(G)]+m(G))$ 且 $\max\limits_{m(G)\le x\le M(G)}|P_n(x)|=\max\limits_{0\le w\le 1}|H_n(w)|$。於是可證明 Dirichlet 多項式加速法，必會收斂到精確解 $\bar{u}$。因爲由定理 3 得：

$$S(H_n(G))=\max\{|H_n(w)|, w\in[0, 1]\}=\frac{1}{\mathcal{D}_n(d)}$$

由定理 2，$\lim\limits_{n\to\infty}S(H_n(G))=\lim\limits_{n\to\infty}\dfrac{1}{\mathcal{D}_n(d)}=0$，又由公式 (4) 得 $\|\varepsilon^{(n)}\|\le\|H_n(G)\|\cdot\|\varepsilon^{(0)}\|=S(H_n(G))\|\varepsilon^{(0)}\|$，所以 $\lim\limits_{n\to\infty}\|\varepsilon^{(n)}\|=\lim\limits_{n\to\infty}\|u^{(n)}-\bar{u}\|=0$，故 $u^{(n)}$ 必會收斂到精確解 $\bar{u}$。

更一進步，我們可推導出 $P_{n+1}(x)$ 與 $P_n(x)$ 及 $P_{n-1}(x)$ 之遞迴關係，令 $w(x)=\dfrac{x-m(G)}{M(G)-m(G)}$，$z=\dfrac{1-m(G)}{M(G)-m(G)}$，$\sigma=\dfrac{1}{z}$，多項式 $P_{n+1}(x)=\dfrac{\mathcal{D}_{n+1}(w(x))}{\mathcal{D}_{n+1}(z)}$，則：

$$P_0(x)=1$$

$$P_1(x)=\gamma x+1-\gamma$$

其中 $\gamma=\dfrac{4}{4-M(G)-3m(G)}$。由公式 (8)

$$P_{n+1}(x)=\frac{(2n+1)(4z-1)}{2n+3}\frac{\mathcal{D}_n(z)}{\mathcal{D}_{n+1}(z)}(\gamma x+1-\gamma)P_n(x)$$
$$-\frac{2n+1}{2n+3}\frac{\mathcal{D}_n(z)}{\mathcal{D}_{n+1}(z)}P_n(x)-\frac{2n-1}{2n+3}\frac{\mathcal{D}_{n-1}(z)}{\mathcal{D}_{n+1}(z)}P_{n-1}(x) \qquad (13)$$

令

$$\rho_{n+1}=\frac{(2n+1)(4z-1)}{2n+3}\frac{\mathcal{D}_n(z)}{\mathcal{D}_{n+1}(z)} \qquad (14)$$

所以公式 (13) 可改寫爲：

$$P_{n+1}(x)=\rho_{n+1}(\gamma x+1-\gamma)P_n(x)+(1-\rho_{n+1})P_{n-1}(x)$$
$$+\frac{1}{4z-1}\rho_{n+1}[P_{n-1}(x)-P_n(x)] \qquad (15)$$

定義 $P_{-1}(x)=1$，及由公式 (14) 導出：

$$\rho_{n+1}=\left[\frac{4z-2}{4z-1}-\frac{1}{(4z-1)^2}\rho_n\right]^{-1}, \qquad n\geq 1 \qquad (16)$$

由公式 (4) 及公式 (16)，可以推導出迭代公式：

$$u^{(n+1)}=\rho_{n+1}\left(1-\frac{1}{4z-1}\right)u^{(n)}+\gamma\rho_{n+1}\delta^{(n)}$$
$$+\left[1-\left(1-\frac{1}{4z-1}\right)\rho_{n+1}\right]u^{(n-1)} \qquad (17)$$

其中 $\delta^{(n)}=Q^{-1}r^{(n)}=Q^{-1}(b-Au^{(n)})$ 爲擬餘向量 (pseudo-residual vector)。

綜合以上之推導，我們建構了 Dirichlet 多項式加速法，卽利用 Dirichlet 多項式來加速基本迭代法 (2) 之收斂，玆將其演算法列在下面：

清算法 4: Dirichlet 多項式加速法

(1) Input $M(G)$, $m(G)$

$u^{(0)}$ arbitray, $r^{(0)}=b-Au^{(0)}$

solve $Q\delta^{(0)}=r^{(0)}$

$u^{(1)}=u^{(0)}+\gamma\delta^{(0)}$, $\qquad \gamma=\dfrac{4}{4-M(G)-3m(G)}$

(2) $r^{(1)}=b-Au^{(1)}$

$$\rho_2=\left[\frac{4z-2}{4z-1}-\frac{1}{(4z-1)^2}\right]^{-1},\qquad z=\frac{1-m(G)}{M(G)-m(G)}$$

$k=1$

(3) Do until $\left(\frac{\|r^{(k)}\|}{\|r^{(0)}\|}\leq\varepsilon\right)$

solve $Q\delta^{(k)}=r^{(k)}$

$$u^{(k+1)}=\rho_{k+1}\left(1-\frac{1}{4z-1}\right)u^{(k)}+\gamma\rho_{k+1}\delta^{(k)}+\left[1-\left(1-\frac{1}{4z-1}\right)\rho_{k+1}\right]u^{(k-1)}$$

$$\rho_{k+2}=\left[\frac{4z-2}{4z-1}-\frac{1}{(4z-1)^2}\rho_{k+1}\right]^{-1}$$

$r^{(k+1)}=b-Au^{(k+1)}$

$k=k+1$

enddo

三、Féjer 多項式加速法

Féjer 核定義如下：

$$\hat{F}_n(\theta)=\frac{1}{n+1}\sum_{k=0}^{n}\hat{D}_k(\theta),\qquad \theta\in\mathcal{R}$$

於是

$$\hat{F}_n(\theta)=\begin{cases}\dfrac{1}{n+1}\left[\dfrac{\sin(n+1)\frac{\theta}{2}}{\sin\frac{\theta}{2}}\right]^2, & \theta\neq 2j\pi,\ j\in\mathcal{Z}\\ n+1, & \theta=2j\pi,\ j\in\mathcal{Z}\end{cases}\tag{18}$$

得到 $\lim\limits_{n\to\infty}\lim\limits_{\theta\to 0}\hat{F}_n(\theta)\to\infty$，而且當 $0<|\theta|\leq\pi$ 時，$\lim\limits_{n\to\infty}\hat{F}_n(\theta)=0$。令：

$$F_n(\theta)=\frac{\hat{F}_n(\theta)}{n+1}=\begin{cases}\dfrac{1}{(n+1)^2}\left[\dfrac{\sin(n+1)\frac{\theta}{2}}{\sin\frac{\theta}{2}}\right]^2, & \theta\neq 2j\pi,\ j\in\mathcal{Z}\\ 1, & \theta=2j\pi,\ j\in\mathcal{Z}\end{cases}\tag{19}$$

則對任意 n，$\lim_{\theta\to 0} F_n(\theta)=1$，而且當 $0<|\theta|\leq\pi$ 時，可得到 $\lim_{n\to\infty} F_n(\theta)=0$。

令 $x=\dfrac{1-\cos\theta}{2}$，$\theta\in[0,\pi]$，則 x 介於 $[0,1]$ 之間，於是由公式 (19)

$$F_m(\theta)=\frac{\sin^2(m+1)\dfrac{\theta}{2}}{(m+1)^2\sin^2\dfrac{\theta}{2}}=\frac{1-T_{m+1}(1-2x)}{2(m+1)^2x}\equiv F_m(x) \tag{20}$$

因爲 $1-T_{m+2}(1-2x)$ 是 $(m+2)$ 次多項式，且含有因式 x，所以 $F_{m+1}(x)$ 爲 Féjer 核所造出來的 $m+1$ 次多項式。令 $\mathfrak{F}_{m+1}(x)=F_{m+1}(1-x)$，由公式 (20) 及 $T_{m+2}(x)$ 之三項遞廻式可推導出：

$$\mathfrak{F}_{m+1}(x)=\frac{2(m+1)^2}{(m+2)^2}(2x-1)\mathfrak{F}_m(x)-\frac{m^2}{(m+2)^2}\mathfrak{F}_{m-1}(x)+\frac{2}{(m+2)^2} \tag{21}$$

其中 $\mathfrak{F}_0(x)=1$，$\mathfrak{F}_1(x)=x$。我們稱公式 (21) 之多項式爲 Féjer 多項式，因爲它們是從 Féjer 核建構出來的。類似於 Dirchlet 多項式加速法，我們可以證得下列定理：

引理 5

對任意 $x>1$，$1=\mathfrak{F}_0(x)<\mathfrak{F}_1(x)<\cdots<\mathfrak{F}_m(x)<\mathfrak{F}_{m+1}(x)<\cdots$ 成立。

定理 6

對任意 $x>1$，當 m 趨近於無窮大時，$\mathfrak{F}_m(x)$ 趨近於無窮大。

定理 7

假設 n 是固定的正整數，d 是固定的實數，且 $d>1$。令：

$$H_n(w)=\frac{\mathfrak{F}_n(w)}{\mathfrak{F}_n(d)} \tag{22}$$

其中 $\mathfrak{F}_n(w)$ 是 Féjer 多項式，則：

$$H_n(d)=1 \tag{23}$$

且

$$\max_{0\leq w\leq 1}|H_n(w)|=\frac{1}{\mathfrak{F}_n(d)} \tag{24}$$

假設一個可對稱化之基本迭代法 (2) 中 $M(G)<1$，則其 Féjer 多項式加速法，所產生之 $(u^{(n)})$ 向量序列，必會收斂到眞確解 $\bar{u}$。

爲了要建構出 Féjer 多項式加速法，我們推導如下：令 $w(x)=\frac{x-m(G)}{M(G)-m(G)}$，$z=\frac{1-m(G)}{M(G)-m(G)}$，$\sigma=\frac{1}{z}$，多項式 $P_n(x)=\frac{\mathcal{T}_n(w(x))}{\mathcal{T}_n(z)}$，則：

$$P_0(x)=1$$

$$P_1(x)=\gamma x+1-\gamma$$

其中 $\gamma=\frac{1}{1-m(G)}$。由公式 (21)

$$\begin{aligned}P_{n+1}(x)=&\frac{4(n+1)^2z}{(n+2)^2}\frac{\mathcal{T}_n(z)}{\mathcal{T}_{n+1}(z)}(\gamma x+1-\gamma)P_n(x)\\&-\frac{2(n+1)^2}{(n+2)^2}\frac{\mathcal{T}_n(z)}{\mathcal{T}_{n+1}(z)}P_n(x)-\frac{n^2}{(n+2)^2}\frac{\mathcal{T}_{n-1}(z)}{\mathcal{T}_{n+1}(z)}P_{n-1}(x)\\&+\frac{2}{(n+2)^2}\frac{1}{\mathcal{T}_{n+1}(z)}\end{aligned}\tag{25}$$

令

$$\rho_{n+1}=\frac{4(n+1)^2z}{(n+2)^2}\frac{\mathcal{T}_n(z)}{\mathcal{T}_{n+1}(z)}\tag{26}$$

所以公式 (25)，可改寫爲：

$$\begin{aligned}P_{n+1}(x)=&\rho_{n+1}(\gamma x+1-\gamma)P_n(x)+(1-\rho_{n+1})P_{n-1}(x)\\&+\frac{\rho_{n+1}}{2}\sigma[P_{n-1}(x)-P_n(x)]+\frac{\rho_{n+1}}{2(n+1)^2}\frac{1}{\mathcal{T}_n(z)}\sigma[1-P_{n-1}(x)]\end{aligned}\tag{27}$$

其中定義 $P_{-1}(x)=1$ 及由公式 (26) 導出：

$$\rho_{n+1}=\left[1-\frac{1}{2}\sigma-\frac{1}{16}\sigma^2\rho_n+\frac{1}{2(n+1)^2\mathcal{T}_n(z)}\sigma\right]^{-1},\qquad n\geq 1\tag{28}$$

由公式 (4) 及公式 (27)，可推導出迭代公式：

$$\begin{aligned}u^{(n+1)}=&\rho_{n+1}\left(1-\frac{1}{2}\sigma\right)u^{(n)}+\gamma\rho_{n+1}\delta^{(n)}\\&+\left[1-\rho_{n+1}\left(1-\frac{1}{2}\sigma\right)-\frac{\rho_{n+1}}{2(n+1)^2}\frac{\sigma}{\mathcal{T}_n(z)}\right]u^{(n-1)}\\&+\frac{\rho_{n+1}}{2(n+1)^2}\frac{\sigma}{\mathcal{T}_n(z)}u^{(0)}\end{aligned}\tag{29}$$

綜合以上之推導，我們建構了 Féjer 多項式加速法，來加速基本迭法 (2) 之收斂，茲將其演算法列在下面：

演算法 8: Féjer 多項式加速法

(1) Input $M(G)$, $m(G)$

$u^{(0)}$ arbitray, $r^{(0)}=b-Au^{(0)}$

solve $Q\delta^{(0)}=r^{(0)}$

$u^{(1)}=u^{(0)}+\gamma\delta^{(0)}$, $\qquad \gamma=\dfrac{1}{1-m(G)}$

(2) $r^{(1)}=b-Au^{(1)}$

$\rho_2=\left(1-\dfrac{1}{2}\sigma+\dfrac{3}{16}\sigma^2\right)^{-1}$, $\qquad \sigma=\dfrac{1}{z}$, $z=\dfrac{1-m(G)}{M(G)-m(G)}$

$k=1$

(3) Do until $\left(\dfrac{\|r^{(k)}\|}{\|r^{(0)}\|}\leq\varepsilon\right)$

$$u^{(k+1)}=\rho_{k+1}\left(1-\frac{1}{2}\sigma\right)u^{(k)}+\gamma\rho_{k+1}\delta^{(k)}$$
$$+\left[1-\rho_{k+1}\left(1-\frac{1}{2}\sigma\right)-\frac{\rho_{k+1}}{2(k+1)^2}\frac{\sigma}{\mathcal{F}_k}\right]u^{(k-1)}$$
$$+\frac{\rho_{k+1}}{2(k+1)^2}\frac{\sigma}{\mathcal{F}_k}u^{(0)}$$

solve $Q\delta^{(k)}=r^{(k)}$

$$\mathcal{F}_k=\begin{cases} z, & \text{if } k=1\\ \dfrac{8}{9}(2z-1)z+\dfrac{1}{9}, & \text{if } k=2\\ \dfrac{2k^2}{(k+1)^2}(2z-1)\mathcal{F}_{k-1}-\dfrac{(k-1)^2}{(k+1)^2}\mathcal{F}_{k-2}+\dfrac{2}{(k+1)^2}, & \text{if } k\geq 3\end{cases}$$

$$\rho_{k+2}=\left[1-\frac{1}{2}\sigma-\frac{1}{16}\rho_{k+1}\sigma^2+\frac{1}{2(k+2)^2}\frac{\sigma}{\mathcal{F}_{k+1}}\right]^{-1}$$

$r^{(k+1)}=b-Au^{(k+1)}$

$k=k+1$

enddo

四、Legendre 多項式加速法

Legendre 多項式是被 Legendre 介紹用在勢能 (potential) 理論上[15]，在牛頓勢能理論 (Newtonian theory of potential) 或庫侖勢能理論 (Coulomb potential) 中，它們是相關於距離的倒數之展開式。設 R 是任意兩點 a 和 b 的距離，γ 是 $\vec{a}$ 與 $\vec{b}$ 的夾角，則：

$$R=|\vec{a}-\vec{b}|=(|\vec{a}|^2+|\vec{b}|^2-2|\vec{a}||\vec{b}|\cos\gamma)^{1/2}$$

令 $\rho=\frac{|\vec{b}|}{|\vec{a}|}$，$x=\cos\gamma$，則 $\frac{1}{R}=\frac{1}{|\vec{a}|}(1-2x\rho+\rho^2)^{-1/2}=\frac{1}{|\vec{a}|}(1-2\rho\cos\gamma+\rho^2)^{-1/2}$。考慮函數 $\frac{1}{r}$ 的展開式[10]，其中：

$$\frac{1}{r}=(1-2\rho\cos\gamma+\rho^2)^{-1/2} \tag{30}$$

設 $|\rho|<1$，由二項展開式 (binomial expansion) 得：

$$\frac{1}{r}=(1-\rho e^{i\gamma})^{-1/2}(1-\rho e^{-i\gamma})^{-1/2}$$

$$=\sum_{n=0}^{\infty}(-1)^n\binom{-\frac{1}{2}}{n}\rho^n e^{in\gamma}\sum_{n=0}^{\infty}(-1)^n\binom{-\frac{1}{2}}{n}\rho^n e^{-in\gamma}$$

依柯西定律 (Cauchyś law)

$$\frac{1}{r}=\sum_{n=0}^{\infty}\rho^n\sum_{k=0}^{[n/2]}\binom{-\frac{1}{2}}{k}\binom{-\frac{1}{2}}{n-k}[(-1)^k(-1)^{n-k}e^{ik\gamma}e^{-i(n-k)\gamma}$$

$$+(-1)^k(-1)^{n-k}e^{-ik\gamma}e^{i(n-k)\gamma}]=\sum_{n=0}^{\infty}\rho^n\mathcal{L}_n(\cos\gamma) \tag{31}$$

其中

$$\mathcal{L}_n(\cos\gamma)=\frac{1\times3\times\cdots\times(2n-1)}{2\times4\times\cdots\times(2n)}2\cos\gamma+\frac{1\times3\times\cdots\times(2n-3)}{2\times4\times\cdots\times(2n-2)}$$

$$\times\frac{1}{2}2\cos(n-2)\gamma+\frac{1\times3\times\cdots\times(2n-5)}{2\times4\times\cdots\times(2n-4)}\frac{1\times3}{2\times4}2\cos(n-4)\gamma$$

$$+\cdots$$

令 $2|x|+|\rho|<1$，且 $\cos\gamma=x$，則：

$$(1-2\rho x+\rho^2)^{-1/2}=[1-2\rho(2x-\rho)]^{-1/2}$$
$$=1+\sum_{n=0}^{\infty}\rho^n\Big[\frac{1\times3\times\cdots\times(2n-1)}{n!}x^n$$
$$-\frac{1}{2}\frac{1\times3\times\cdots\times(2n-3)}{(n-1)!}\frac{n-1}{1}x^{n-2}$$
$$+\frac{1}{2^2}\frac{1\times3\times\cdots\times(2n-5)}{(n-2)!}\frac{(n-2)(n-3)}{1\times2}x^{n-4}-\cdots\Big]$$

上式與公式 (31) 比較，得：

$$\mathcal{L}_n(x)=\frac{1\times3\times\cdots\times(2n-1)}{n!}\Big[x^n-\frac{n(n-1)}{2(2n-1)}x^{n-2}$$
$$+\frac{n(n-1)(n-2)(n-3)}{2\times4\cdots(2n-3)(2n-1)}x^{n-4}+\cdots\Big] \tag{32}$$

我們稱公式 (32) 爲 Legendre 多項式。

若 $f(z)$ 在定義域內是解析的，且 $x\in z$，c 是在定域內，繞著 x 的一個正規 (regular)、簡單封閉曲線 (simple closed curve)，則：

$$f^{(n)}(x)=\frac{n!}{2\pi i}\oint_c\frac{f(t)}{(t-x)^{n+1}}dt \tag{33}$$

稱做 Cauchyś 積分公式 (Cauchyś integeral formula)。

令 $f(z)=(z^2-1)^n$，$n=0,1,2,\cdots$ 因爲 $f(z)$ 在平面上是處處可解析，而：

$$\mathcal{L}_n(x)=\frac{1}{2^n n!}\frac{d^n}{dx^n}(x^2-1)^n=\frac{1}{2^{n+1}\pi i}\oint_c\frac{(t^2-1)^n}{(t-x)^{n+1}}dt \tag{34}$$

考慮

$$\frac{d}{dt}\frac{(t^2-1)^{n+1}}{(t-x)^{n+1}}=2(n+1)t\frac{(t^2-1)^n}{(t-x)^{n+1}}-(n+1)\frac{(t^2-1)^{n+1}}{(t-x)^{n+2}}$$

上式沿著曲線 c 做積分，可得到：

$$0=2\oint_c t\frac{(t^2-1)^n}{(t-x)^{n+1}}dt-\oint_c\frac{(t^2-1)^{n+1}}{(t-x)^{n+2}}dt$$

因此

$$\mathcal{L}_{n+1}(x)=\frac{1}{2^{n+1}\pi i}\oint_c\frac{(t^2-1)^n}{(t-x)^n}dt+x\mathcal{L}_n(x) \tag{35}$$

由

$$\oint_c\frac{d}{dt}\Big[t\frac{(t^2-1)^n}{(t-x)^n}\Big]dt=0$$

得到：

$$\oint_c \frac{(t^2-1)^n}{(t-x)^n}dt+2n\oint_c t^2\frac{(t^2-1)^{n-1}}{(t-x)^n}dt-n\oint_c t\frac{(t^2-1)^n}{(t-x)^{n+1}}dt=0 \tag{36}$$

進而可推得：

$$(n+1)\oint_c \frac{(t^2-1)^n}{(t-x)^n}dt+2^n\pi i2n\mathcal{L}_{n-1}(x)-2^{n+1}\pi inx\mathcal{L}_n(x)=0$$

由上式及公式 (34) 得：

$$(n+1)\mathcal{L}_{n+1}(x)-(2n+1)x\mathcal{L}_n(x)+n\mathcal{L}_{n-1}(x)=0$$

導出 $\mathcal{L}_{n+1}(x)$ 之遞廻關係式：

$$\mathcal{L}_{n+1}(x)=\frac{2n+1}{n+1}x\mathcal{L}_n(x)-\frac{n}{n+1}\mathcal{L}_{n-1}(x) \tag{37}$$

要

$$\mathcal{L}_n(1)=1，\mathcal{L}_n(-1)=(-1)^n$$

設 $x\neq\pm1$，且令 c 是一個在 Cauchyś 積分公式裏的圓，若以 x 爲圓心，$|x^2-1|^{1/2}$ 爲半徑，且 $t=x+(x^2-1)^{1/2}e^{i\varphi}$ 其中 $-\pi\leq\varphi\leq\pi$，而 $(x^2-1)^{1/2}$ 爲 $\sqrt{x^2-1}$ 的分岐 (branch)，則

$$\mathcal{L}_n(x)=\frac{1}{2\pi i}\oint_c\frac{1}{2^n}\frac{(t^2-1)^n}{(t-x)^{n+1}}dt=\frac{1}{\pi}\int_0^\pi[x+(x^2-1)^{1/2}\cos\varphi]^n d\varphi \tag{38}$$

稱做 Laplaceś 公式，且 $-1<x<1$ 時，得 $|\mathcal{L}_n(x)|<1$。

同樣地，我們可以證明下列定理成立：

引理 9

對任意 $x>1$，$1=\mathcal{L}_0(x)<\mathcal{L}_1(x)<\cdots<\mathcal{L}_m(x)<\mathcal{L}_{m+1}(x)<\cdots$ 成立。

定理 10

對任意 $x>1$，當 m 趨近於無窮大時，$\mathcal{L}_m(x)$ 趨近於無窮大。

定理 11

假設 n 是固定正整數，d 是固定的實數，且 $d>1$。令：

$$H_n(w)=\frac{\mathcal{L}_n(w)}{\mathcal{L}_n(d)} \tag{39}$$

其中 $\mathcal{L}_n(w)$ 是 Legendre 多項式，則：

$$H_n(d)=1 \tag{40}$$

且

$$\max_{-1\le w\le 1}|H_n(w)|=\frac{1}{\mathcal{L}_n(d)} \tag{41}$$

設 $M(G)$，$m(G)$ 分別爲矩陣 G 的最大及最小特徵值，x 爲任意實數，且 $m(G)\le x\le M(G)<1$，則將區間 $[m(G)，M(G)]$ 映成到區間 $[-1，1]$ 之線性變換函數爲：

$$w=\frac{2x-M(G)-m(G)}{M(G)-m(G)} \tag{42}$$

令 $d=\dfrac{2-M(G)-m(G)}{M(G)-m(G)}$，則 $d>1$，於是：

$$H_n(w)=\frac{\mathcal{L}_n(w)}{\mathcal{L}_n(d)}=P_n\left(\frac{1}{2}w[M(G)-m(G)]+M(G)+m(G)\right)$$

且 $\max\limits_{m(G)\le x\le M(G)}|P_n(x)|=\max\limits_{-1\le w\le 1}|H_n(w)|$。於是可證明 Legendre 多項式加速法，必會收斂到眞確解 $\bar{u}$。

Legendre 加速法之推導可來自下列遞廻關係：令 $w(x)=\dfrac{2x-M(G)-m(G)}{M(G)-m(G)}$，$z=\dfrac{2-M(G)-m(G)}{M(G)-m(G)}$，$\sigma=\dfrac{1}{z}$，多項式 $P_n(x)=\dfrac{\mathcal{L}_n(w(x))}{\mathcal{L}_n(z)}$，則：

$$P_0(x)=1$$

$$P_1(x)=\gamma x+1-\gamma$$

其中 $\gamma=\dfrac{2}{2-M(G)-m(G)}$。由公式 (37)

$$P_{n+1}(x)=\frac{(2n+1)z}{n+1}\cdot\frac{\mathcal{L}_n(z)}{\mathcal{L}_{n+1}(z)}(\gamma x+1-\gamma)P_n(x)-\frac{n}{n+1}\cdot\frac{\mathcal{L}_{n-1}(z)}{\mathcal{L}_{n+1}(z)}P_{n-1}(x) \tag{43}$$

令

$$\rho_{n+1}=\frac{(2n+1)z}{n+1}\cdot\frac{\mathcal{L}_n(z)}{\mathcal{L}_{n+1}(z)} \tag{44}$$

所以公式 (43)，可改寫爲：

$$P_{n+1}(x)=\rho_{n+1}(\gamma x+1-\gamma)P_n(x)+\gamma\rho_{n+1}\delta^{(n)}+(1-\rho_{n+1})P_{n-1}(x) \tag{45}$$

其中 $\rho_1=1$，及由公式 (44) 導出：

$$\rho_{n+1}=\left(1-\frac{n^2}{4n^2-1}\rho_n\sigma^2\right)^{-1}, \qquad n\geq 1 \qquad (46)$$

由公式 (4) 及公式 (45)，可以推得迭代公式：

$$u^{(n+1)}=\rho_{n+1}u^{(n)}+\gamma\rho_{n+1}\delta^{(n)}+(1-\rho_{n+1})u^{(n-1)} \qquad (47)$$

綜合以上之推導，我們建構了 Legedre 多項式加速法，來加速基本迭法 (2) 之收斂，茲將其演算法列在下面：

演算法 12: Legendre 多項式加速法

(1) Input $M(G)$, $m(G)$

$u^{(0)}$ arbitray, $r^{(0)}=b-Au^{(0)}$

solve $Q\delta^{(0)}=r^{(0)}$

$u^{(1)}=u^{(0)}+\gamma\delta^{(0)}$, $\qquad \gamma=\dfrac{2}{2-M(G)-m(G)}$

(2) $r^{(1)}=b-Au^{(1)}$

$\rho_2=\left(1-\dfrac{1}{3}\sigma^2\right)^{-1}$, $\qquad \sigma=\dfrac{M(G)-m(G)}{2-M(G)-m(G)}$

$k=1$

(3) Do until $\left(\dfrac{\|r^{(k)}\|}{\|r^{(0)}\|}\leq\varepsilon\right)$

solve $Q\delta^{(k)}=r^{(k)}$

$u^{(k+1)}=\rho_{k+1}u^{(k)}+\gamma\rho_{k+1}\delta^{(k)}+(1-\rho_{k+1})u^{(k-1)}$

$\rho_{k+2}=\left[1-\dfrac{(k+1)^2}{4(k+1)^2-1}\ \rho_{k+1}\sigma^2\right]^{-1}$

$r^{(k+1)}=b-Au^{(k+1)}$

$k=k+1$

enddo

下面我們列出常用之 Chebyshev 加速法[4]的演算法，以做數值實驗之比較使用。

演算法 13: Cheyshev 多項式加速法

(1) Input $M(G)$, $m(G)$

$u^{(0)}$ arbitray, $r^{(0)}=b-Au^{(0)}$

solve $Q\delta^{(0)}=r^{(0)}$

$u^{(1)}=u^{(0)}+\gamma\delta^{(0)}$, $\qquad \gamma=\dfrac{2}{2-M(G)-m(G)}$

(2) $r^{(1)}=b-Au^{(1)}$

$\rho_2=\left(1-\dfrac{1}{3}\sigma^2\right)^{-1}$, $\qquad \sigma=\dfrac{M(G)-m(G)}{2-M(G)-m(G)}$

$k=1$

(3) Do until $\left(\dfrac{\|r^{(k)}\|}{\|r^{(0)}\|}\leq\varepsilon\right)$

solve $Q\delta^{(k)}=r^{(k)}$

$u^{(k+1)}=\rho_{k+1}u^{(k)}+\gamma\rho_{k+1}\delta^{(k)}+(1-\rho_{k+1})u^{(k-1)}$

$\rho_{k+2}=\left(1-\dfrac{1}{4}\rho_{k+1}\sigma^2\right)^{-1}$

$r^{(k+1)}=b-Au^{(k+1)}$

$k=k+1$

enddo

五、數值實驗

我們考慮下面這個在單位方塊上的 Dirchlet 問題：

$$\begin{cases}\nabla^2 u=-1, & 0<x<1,\ 0<y<1\\ u=0, & \text{on the boundary}\end{cases} \tag{48}$$

用五點中央差分法來離散化這個橢圓偏微分方程式，並且由 Varga[11] 及 Young[12]，可知其眞確解爲：

$$u(x,y)=\sum_{p,q=1}^{M-1}\alpha_{pq}\sin p\pi x\sin q\pi y \tag{49}$$

其中

$$\alpha_{pq}=\begin{cases} h^4\dfrac{\cot\dfrac{p\pi h}{2}\cot\dfrac{q\pi h}{2}}{\sin^2\dfrac{p\pi h}{2}+\sin^2\dfrac{q\pi h}{2}}, & \text{if } p,q \text{ are odd} \\ 0, & \text{otherwise} \end{cases}$$

而 $h=1/M$ 爲分割的網格長度。本文使用問題(48)經過五點中央差分法所求得的矩陣 A，乘上向量 $(1,1,\cdots,1)^T$ 所得到的向量 b 爲欲解之系統 $Au=b$。爲了更精確地比較結果，我們採用眞確停止判斷 (exact stopping test)，$\frac{\|\varepsilon^{(k)}\|_2}{\|\varepsilon^{(0)}\|_2}<\varepsilon=10^{-6}$ 且起始猜測值用 $u^{(0)}=(0,\cdots,0)^T$。所列的 cputime 是在眞確停止判斷下測量 20 次的平均值，單位爲秒。在以下的數值實驗中，矩陣的資料儲存方式是用非對稱對角線儲存格式 (nonsymmetric diagonal format)[9]，這種儲存法適合於大型稀疏矩陣的資料儲存，不但能節省儲存空間，而且利於向量演算。

首先考慮最簡單的 $Q=I$ 之 RF 基本迭代法，則迭代矩陣 $G=I-A$ 由表一得：

$$S(G)=S(I-A)=\max|\{-3+4\cos(\pi h),-3-4\cos(\pi h)\}|$$

$S(G)>1$，可知用 RF 基本迭代法解公式 (48) 會發散。而使用本文之多項式加速法後，卻可收斂到眞確解 $\bar{u}$。

表一 迭代矩陣 G 的最大特徵值 $M(G)$ 及最小特徵值 $m(G)$ 之理論值

Q	$M(G)$	$m(G)$
I	$-3+4\cos(\pi h)$	$-3-4\cos(\pi h)$
D	$\cos(\pi h)$	$-\cos(\pi h)$
$8I$	$\frac{1}{2}+\frac{1}{2}\cos(\pi h)$	$\frac{1}{2}-\frac{1}{2}\cos(\pi h)$

表二 $Q=I$ 時之迭代數

N	225	961	3,969	16,129
RF	24*	24*	24*	24*
RF-FJ	97	197	396	795
RF-DH	86	174	348	698
RF-LG	80	161	323	647

* 表示 overflow 在此迭代數時產生。

表三 $Q=D$ 時之迭代數

N	255	961	3,969	16,129
J	705	2,825	11,302	45,193
J-FJ	97	197	396	795
J-DH	86	174	348	698
J-LG	80	161	323	647

表四 $Q=8I$ 時之迭代數

N	225	961	3,969	16,129
$8I$	1,416	5,657	22,609	90,393
$8I$-FJ	97	197	396	795
$8I$-DH	86	174	348	698
$8I$-LG	80	161	323	647

表五 $h=\frac{1}{64}$，i.e.，$N=3{,}969$，$m_E=-M_E$，$M(G)=\cos\left(\frac{\pi}{64}\right)\approx 0.998795$ 之迭代數及 cputime，on IBM ES 9000

M_E	0.9983	0.9985	0.9987	0.998795	0.9988	0.9990	0.9992
J-FJ	551	498	434	396	394	288	377
	0.6825	0.6175	0.5280	0.4880	0.4840	0.3535	0.4615
J-DH	529	473	400	348	345	301	325
	0.6470	0.6785	0.4905	0.4265	0.4220	0.3780	0.3995
J-LG	518	459	383	323	319	325	361
	0.6725	0.5925	0.4980	0.4010	0.4205	0.4175	0.4680
J-CH	507	446	366	294	289	321	353
	0.6140	0.5375	0.4375	0.3595	0.3475	0.3865	0.4220

本文所提出的多項式加速法，需輸入迭代矩陣 G 的最大特徵值 $M(G)$ 及最小特徵值 $m(G)$。參見 Hageman and Young[4] 及 Young et al.[14] 可以求出如表一之值，如此我們將發現 $M(G)$ 與 $m(G)$ 有兩種關係：第一種情形 (Case I) 當 $Q=D$ 時，$m(G)=-M(G)$。第二種情形 (Case II) 當 $Q=I$ 或 $Q=8I$ 時，則 $m(G)<M(G)<1$。爲較客觀的討論特徵值對多項式加速法的影響，在 Case I 時我們選擇 $m_E=-M_E$，而 $M_E\leq M(G)$。在 Case II 時，我們固定 $m_E=m(G)$，而再選擇 $M_E<M(G)$ 做爲討論的依據。

表六 $h=\frac{1}{128}$，i.e.，$N=16{,}129$，$m_E=-M_E$，$M(G)=\cos\left(\frac{\pi}{128}\right)\approx 0.999699$ 之迭代數及 cputime，on IBM ES 9000

M_E		0.9992	0.9994	0.9996	0.999699	0.9997	0.9998	0.9999
J-FJ		1,672	1,402	1,053	795	791	756	894
		8.7125	6.8985	5.2945	4.1436	3.9555	3.7775	4.4785
J-DH		1,644	1,368	1,005	698	690	651	921
		8.4755	7.1570	5.2020	3.6825	3.6495	3.4490	4.9400
J-LG		1,631	1,351	981	648	638	722	994
		9.0675	7.1675	5.0895	3.4420	3.6195	3.9925	5.3695
J-CH		1,617	1,335	956	588	578	708	986
		7.9760	6.6410	4.6810	3.1550	2.8815	3.5085	4.8785

以下我們以 IBM ES 9000/860 的數值結果做爲說明，列 $h=\frac{1}{16}$、$\frac{1}{32}$、$\frac{1}{64}$ 與 $\frac{1}{128}$ 時，與不同的 Q 及不同的 M_E、m_E，對 FJ 法、DH 法、LG 法、CH 法收斂速率之影響。從理論上而言，若選擇估計值爲正確的特徵值時，則 DH 法、LG 法、CH 法，在預先條件化子 $Q=I$，$Q=D$，$Q=8I$ 是完全等價的，而數值結果也完全與理論符合。但若選擇的 $M_E\neq M(G)$ 其收斂情形就大大的不同了。

在整體上而言，若從特徵值的方向來看，高估 $M(G)$ 時（即 $M_E>M(G)$），FJ 法、DH 法、LG 法與 CH 法其收斂速率皆比低估 $M(G)$ 時（即 $M_E<M(G)$）好；在 $M_E\leq M(G)$ 時，$R(\mathrm{CH})>R(\mathrm{LG})>R(\mathrm{DH})>R(\mathrm{FJ})$（註：我們以 R（加速法）表示，該加速法之收斂速率），即 CH 法皆領先於 LG 法、DH 法、FJ 法；在 $M_E>M(G)$ 時，CH 法並不是處處皆領先的。

表七至表九爲各多項式加速法之 cputime 比值（以 $N=225$ 時，之 cputime 爲基準比值），我們發現，矩陣維度愈大時，IBM ES 9000 愈顯現優於 VAX 4500。

表七 FJ 法之 cputime 比值 (ratio)

N	961	3,969	16,129
VAX 4500	8.209125	91.787072	1,565.475285
IBM ES 9000	5.947368	51.368421	436.168421

表八 DH 法之 cputime 比值 (ratio)

N	961	3,969	16,129
VAX 4500	7.764706	90.441176	1,526.050420
IBM ES 9000	6.125000	53.312500	460.312500

表九 LG 法之 cputime 比值 (ratio)

N	961	3,969	16,129
VAX 4500	7.815945	86.205240	1,469.257642
IBM ES 9000	6.266666	53.466666	458.933333

六、結 論

本文提出以 Féjer 多項式加速法（簡稱 FJ 法），Dirichlet 多項式加速法（簡稱 DH 法）及 Legendre 多項式加速法（簡稱 LG 法），來加速基本迭代法 RF、Jacobi 及 $Q=8I$，用以解線性系統[1]，並與 Chebyshev 多項式加速法（簡稱 CH 法）做比較。這些多項式加速法的優點，在於程式設計方便簡單，且利於向量電腦的執行。而其向量序列 $(u^{(n)})$ 的每個分量皆爲線性獨立，所以，也非常適合用平行電腦來執行。

本文所提出的多項式加速法，需輸入迭代矩陣 G 的最大及最小特徵值，我們發現，用正確的特徵值時，當網格密度增加爲兩倍，FJ 法、DH 法、LG 法之迭代數也約略成爲兩倍，但未加速前之基本迭代法，卻成四倍增加。而 RF 基本迭代法完全發散無法求解。數值實驗顯示，LG 法的收斂速率優於 DH 法，而 DH 法的收斂速率又優於 FJ 法。另外，向量電腦的執行會比序列式電腦幫助大。當階數 N 足够大時，由 cputime 的比值可知，向量電腦 IBM ES 9000/860 之效率更加優於 VAX 4500。

整體來說，若不知 $M(G)$ 時，則高估 $M(G)$ 之收斂速率，皆大於低估 $M(G)$ 時。因此，值得更進一步探討各多項式加速法對特徵值的敏感度，及各種調適 (adaptive) 方法之運用及使用平行電腦來計算。

七、謝 誌

本文承蒙國科會研究計劃 NSC 83-0208-M030-018 的研究補助，得以順利完成，在此致上誠摯之謝意。

參考文獻

(1) E.W. Cheney, *Introduction to Approximation Theryy*, Chelsea Publising Company (1980).
(2) P.J. Davis, *Interpolation and Approximation*, Dover Publications, New York, N.Y. (1975).
(3) G.H. Golub and C.F. Van Loan, *Matrix Computation*, second edition, Johns Hopkins University Press, Baltimore (1989).
(4) L.A. Hageman and D.M. Young, *Applied Iterative Methods*, Academic Press, New York (1981).
(5) M.R. Hestenes and E.L. Stiefel, "Methods of Conjugate Gradients for Solving Linear Systems", *Nat. Bur. Std. J. Res.*, **49**, 409-436 (1952).
(6) K.C. Jea and C.T. Yang, "Polynomial Methods for Solving Large Sparse Linear Systems on Vector Computers", *Proceedings of the Conference on Highperformance Computing and Applications*, National Center for Highperformance Computing, 245-248 (1994).
(7) K.C. Jea and Wei-Cheng Chen, "Polynomial Preconditioners for Conjugate Methods", *Proceedings of the Workshop on Computational Sciences*, National Taiwan University, 53-57 (1994).
(8) D. Kincaid and W. Cheney, *Numerical Analysis*, Brooks/Cole Publishing Company, Pacific Grove, California (1991).
(9) T.C. Oppe, W.D. Joubert and D.R. Kincaid, "NSPCG User's Guide, Version 1.0", *Report CNA-216*, *Center for Numerical Analysis*, The University of Texas at Austin (1988).
(10) G. Sansone, *Othogonal Functions*, Revised Engilish Edition (1959).
(11) R.S. Varga, *Matrix Iterative Analysis*, Prentice-Hall, Englewood Cliffs, New Jersey (1962).
(12) D.M. Young, *Iterative Solution of Large Linear Systems*, Academic Press, New York (1971).
(13) D.M. Young and K.C. Jea, "Generalized Conjugate Graient Acceleration of Iterative Methods, Part II: The Nonsymmetrizable Case", *Report CNA-163*, *Center for Numerical Analysis*, The University of Texas at Austin (1981).
(14) D.M. Young, K.C. Jea and Linda J. Hayes, "Generalized Conjugate Graient Acceleration of Iterative Methods, Part I: The Symmetrizable Case", *Report CNA-162*, *Center for Numerical Analysis*, The University of Texas at Austin (1981).
(15) Z.X. Wang and D.R. Guo, *Special Functions*, World Scientific (1989).

On the Study of Polynomial Accelerations Constructed from Kernels

YU-HSIUNG HUANG AND KANG C. JEA
Graduate Institute of Mathematics
Fu Jen Catholic University
Taipei, Taiwan 24205, R.O.C.

ABSTRACT

In this paper, we study using three different type of polynomials to accelerate basic iterative methods for solving large sparse linear system $Au=b$, where A is an n by n spd matrix, and b is a given n-dimensional real vector.

The idea is to look for a polynomial of degree m, with $P_m(1)=1$, such that $\varepsilon^{(m)}=P_m(G)\varepsilon^{(0)}$ holds, where $\varepsilon^{(m)}$ is the mth error vector. Here, the matrix G is the iteration matrix. Such algorithms involve only matrix vector multiplications, and additions of vectors, so they are well suited for vector and parallel computers. Pylynomials used are generated from Féjer kernels, Dirichlet kernels, and Legendre polynomials. We derived the acceleration formulas and the algorithms for performing such methods. Some numerical results are given and we also compared them with the Chebyshev acceleration.

ON THE UNIQUENESS OF NONLINEAR APPROXIMATIONS

NANPING YANG
Department of Mathematics
Fu Jen Catholic University
Taipei, Taiwan 24205, R.O.C.

ABSTRACT

The uniqueness problem for best segmented approximation of continuous differentiable functions $C^1[0, 1]$ from a family of piecewise polynomials in the L_p norm, $p\geq 2$, is considered. Under appropriate hypothesis, we showed that there is an open and dense subset in $C^1[0, 1]$ such that each element in it has a unique best segmented L_p approimation.

1. INTRODUCTION

In this paper, we consider the uniqueness problem for best segmented approximation of continuous differentiable functions $C^1[0, 1]$ in the L_p norm, $p\geq 2$. In 1978, Barrow et al.[1] showed that for $f\in C^2[0, 1]$ with $f''>0$ on $[0, 1]$ and $\log f''$ is concave on $(0, 1)$, then f has a unique best approximation from S_k^2 in L_2 norm, where S_k^2 denotes the nonlinear family of all second order spline functions with at most k variable knots in $[0, 1]$. Later, Chow[2] extend the result to P_k^n, the nonlinear family of piecewise polynomial of degree n with at most k variable knots in $[0, 1]$. So the uniqueness property holds for both S_k^2 and P_k^n to a certain class of functions. However, these results are not true for general smooth functions f. Thus we study the uniqueness in a different aspect. Specifically, let P_k^n be approximating family for $f\in C^1[0, 1]$ with L_p norm, $p\geq 2$ and consider the topological size of $C^1[0, 1]$ functions which admit a unique best approximation. We found that the size of such a "uniqueness set" is open (in a C^1 topology) and dense in $C^1[0, 1]$. For notational simplicity, we only present the result for the case $k=1$.

Consider an open set $S=(0, 1)\times \boldsymbol{R}^{n+1}\times \boldsymbol{R}^{n+1}$. For $\xi\in(0, 1)$, $\boldsymbol{a}=(a_0, a_1, \cdots, a_n)\in \boldsymbol{R}^{n+1}$, $\boldsymbol{b}=(b_0, b_1, \cdots, b_n)\in \boldsymbol{R}^{n+1}$ and $\boldsymbol{x}=(\xi, \boldsymbol{a}, \boldsymbol{b})\in S$, define the parametrization map $A: S\to L_p[0, 1]$ by

$$A(\boldsymbol{x}, t)=\begin{cases} q_1(\boldsymbol{a}, t), & \text{if } 0\le t<\xi; \\ \frac{1}{2}[q_1(\boldsymbol{a}, t)+q_2(\boldsymbol{b}, t)], & \text{if } t=\xi; \\ q_2(\boldsymbol{b}, t), & \text{if } \xi<t\le 1, \end{cases} \tag{1}$$

where

$$q_1(\boldsymbol{a}, t)=\sum_{i=0}^{n} a_i t^i \quad \text{and} \quad q_2(\boldsymbol{b}, t)=\sum_{i=0}^{n} b_i t^i .$$

Then given $f\in C^1[0, 1]$, we seek an $\boldsymbol{x}_0\in S$ satisfying

$$\|A(\boldsymbol{x}_0)-f\|_p=\inf_{\boldsymbol{x}\in S}\|A(\boldsymbol{x})-f\|_p . \tag{2}$$

In other words, we attempt to minimize the functional

$$\begin{aligned} F(\boldsymbol{x}, f)&=\int_0^1 |A(\boldsymbol{x}, t)-f(t)|^p dt \\ &=\int_0^\xi |q_1(t)-f(t)|^p dt+\int_\xi^1 |q_2(t)-f(t)|^p dt . \end{aligned} \tag{3}$$

The $A(\boldsymbol{x}_0)$ in Eq. (2) is called a best segmented L_p approximation. For simplicity, we will simply say that $A(\boldsymbol{x}_0)$ is a best approximation. The knot ξ_0 in $\boldsymbol{x}_0$ is called an optimal knot. Sometimes we employ the convention $A(\boldsymbol{x})\leftrightarrow(\xi, q_1, q_2)$ meaning that $\boldsymbol{x}=(\xi, \boldsymbol{a}, \boldsymbol{b})$, $q_1(t)=q_1(\boldsymbol{a}, t)$, and $q_2(t)=q_2(\boldsymbol{b}, t)$.

2. EXISTENCE AND CHARACTERIZATION

The concept of approximative compactness as we introduce in the following is very useful toward the existence.

Definition 2.1

A subset M of a normed linear space X is called approximatively compact if for each $x\in X$ and each sequence $\{m_\nu\}$ in M with $\|m_\nu-x\|\to \inf_{m\in M}\|m-x\|$, there exists a subsequence $\{m_{\nu_j}\}$ and $m_0\in M$ such that $m_{\nu_j}\to m_0$ as $j\to\infty$ and $\|m_0-x\|=\inf_{m\in M}\|m-x\|$. The sequence $\{m_\nu\}$ is

called a minimizing sequence of x.

Theorem 2.2

$A(\bar{S})$ is approximatively compact.

Proof

Let $\{A(\boldsymbol{x}_\nu)\}$ be a minimizing sequence for $f\in C^1[0, 1]$. If $\xi_\nu\in(0, 1)$ for all ν, then the sequence of parameters $\{\boldsymbol{x}_\nu\}$ is a bounded infinite set in $\boldsymbol{R}^{2n+3}$. So there exists a point $\boldsymbol{x}_0\in\bar{S}$ such that $\boldsymbol{x}_\nu\to\boldsymbol{x}_0$ (by passing to a subsequence, if necessary). Assume first that $\xi_\nu\to\xi\in(0, 1)$. It easily follows that

$$\lim_{\nu\to\infty}\|A(\boldsymbol{x}_\nu)-f\|_p=\|A(\boldsymbol{x}_0)-f\|_p=\inf_{\boldsymbol{x}\in\bar{S}}\|A(\boldsymbol{x})-f\|_p\,.$$

New suppose that $\xi_\nu\to 0$ (The case $\xi_\nu\to 1$ is similar) and let $\{A(\boldsymbol{x}_\nu)\}$ be the minimizing sequence for $f\in C^1[0, 1]$. We note that $q_{1\nu}\in\Pi_n$ and $q_{2\nu}\in\Pi_n$ for all ν, where Π_n is the set of all polynomials of degree n. Since the sequence $\{q_{2\nu}\}$ is bounded in the L_p norm, there is a subsequence (also denoted by $q_{2\nu}$) such that

$$q_{2\nu}\to q_2, \qquad \text{as } \nu\to\infty$$

for some $q_2\in\Pi_n$. By the Minkowski's Inequality

$$\left(\int_0^{\xi_\nu}|q_{1\nu}-q_2|^p\right)^{1/p}\le\left(\int_0^{\xi_\nu}|q_{1\nu}-f|^p\right)^{1/p}+\left(\int_0^{\xi_\nu}|q_2-f|^p\right)^{1/p}.$$

From this we see that

$$\lim_{\nu\to\infty}\int_0^{\xi_\nu}(|q_{1\nu}-q_2|^p)^{1/p}=0$$

since $\xi_\nu\to 0$. Thus

$$\lim_{\nu\to\infty}\left(\int_0^{\xi_\nu}|q_{1\nu}-q_2|^p+\int_{\xi_\nu}^1|q_{2\nu}-q_2|^p\right)=0\,.$$

So the minimizing sequence $A(\boldsymbol{x}_\nu)$ converges to $A(\boldsymbol{x}_0)\in A(\bar{S})$, where $\boldsymbol{x}_0=(\xi_0, \boldsymbol{a}, \boldsymbol{b})$ with $\xi_0=0$ and $\boldsymbol{a}=\boldsymbol{0}$. The continuity of the map A in the L_p sense yields

$$\lim_{\nu\to\infty}\|A(\boldsymbol{x}_\nu)-f\|_p=\|q_2-f\|_p=\inf_{\boldsymbol{x}\in\bar{S}}\|A(\boldsymbol{x})-f\|_p$$

Theorem 2.3

Let $s\in\Pi_n$ be a best approximation to $f\in C^1[0, 1]$ in the L_p norm. If $f\notin\Pi_n$, then there always exists a point $\eta\in(0, 1)$ and that $q_1, q_2\in\Pi_n$ are best approximations to f on $[0, \eta]$ and $[\eta, 1]$, respectively in such a way that

$$\|q_1-f\|^p+\|q_2-f\|^p<\|s-f\|^p .$$

Proof

Suppose not. Then for all $t\in(0, 1)$ we have

$$\|q_1-f\|^p+\|q_2-f\|^p\geq\|s-f\|^p .$$

By hypothesis, $q_1, q_2\in\Pi_n$ are best approximations to f on $[0, t]$ and $[t, 1]$. Thus, on $[0, t]$,

$$\|q_1-f\|^p=\|s-f\|^p, \qquad \text{for all } t\in(0, 1).$$

By the characterization of L_p approximation

$$\int_0^t \operatorname{sgn}[s(y)-f(y)]|s(y)-f(y)|^{p-1}y^i dy=0, \qquad \text{for all } i=0, 1, \cdots, n .$$

In particular $(i=0)$,

$$\int_0^t \operatorname{sgn}[s(y)-f(y)]|s(y)-f(y)|^{p-1}dy=0 .$$

By taking the derivative with respect to t, we have

$$\operatorname{sgn}[s(t)-f(t)]|s(t)-f(t)|^{p-1}=0$$

and hence $f(t)=s(t)$ for all $t\in(0, 1)$. So $f(t)=s(t)$ for all $t\in[0, 1]$, a contradiction to the fact that $f\notin\Pi_n$.

Theorem 2.4

Let $f\in C^1[0, 1]\setminus A(S)$. Then the knot ξ being optimal implies that $\xi\in(0, 1)$.

Proof

If $\xi\notin(0, 1)$, then either $\xi=0$ or $\xi=1$. Let $s\in\Pi_n$ be a best approximation to f on $[0, 1]$. Since $f\notin A(S)$, there exists a $\eta\in(0, 1)$, a

polynomial $q_1 \in \Pi_n$ on $[0, \eta]$ and a polynomial $q_2 \in \Pi_n$ on $[\eta, 1]$ such that

$$\|q_1 - f\|^p + \|q_2 - f\|^p < \|s - f\|^p$$

by Theorem 2.3, which is a contradiction for ξ being an optimal knot.

The combination of Theorem 2.2 and Theorem 2.4 shows that best approximations to any $f \in C^1[0, 1]$ actually come from $A(S)$. Hence $A(S)$ is approximatively compact.

Now if $A(\boldsymbol{x})$ defined in Eq. (1) is a best approximation to $f \in C^1[0, 1]$, then

$$F'(\boldsymbol{x}, f, \boldsymbol{K}) = 0, \qquad \text{for all } \boldsymbol{K} \in \boldsymbol{R}^{2n+3}$$

where F is defined as in Eq. (3). In particular

$$\frac{\partial F}{\partial \xi} = |q_1(\xi) - f(\xi)|^p - |q_2(\xi) - f(\xi)|^p = 0$$

which implies that

$$|q_1(\xi) - f(\xi)| = |q_2(\xi) - f(\xi)|$$

So there are three types of best approximations to any function $f \in C^1[0, 1]$:

(1) $q_1(\xi) \neq q_2(\xi)$. In this case, we have $[q_1(\xi) - f(\xi)] = -[q_2(\xi) - f(\xi)]$ or $q_1(\xi) + q_2(\xi) = 2f(\xi)$.

(2) $q_1(\xi) = q_2(\xi)$ and $q_1(\xi) \neq f(\xi)$.

(3) $q_1(\xi) = q_2(\xi) = f(\xi)$.

For convenience, we shall consider subsets of $C^1[0, 1]$ according to the continuity properties of their best approximations listed above and denoted them by $C^*[0, 1]$, $C^{**}[0, 1]$ and $C^{***}[0, 1]$, respectively.

3. THE UNICITY

The unicity of best approximation is one of the basic questions in nonlinear approximation theory. It happens often that best approximations are, in general, not unique. Wolfe[4] presented this in strictly convex normed linear spaces. In the setting of nonlinear segmented best approximation introduced above, unicity cannot be guaranteed.

Example

Let $f(t)=t^2$, $t\in[-1, 1]$; then $f\in C^1[0, 1]$. For f to be approximated by step functions, we take $\boldsymbol{x}=\left(\xi, 1, -\frac{1}{3}\right)$ and

$$A(\boldsymbol{x}, t)=\begin{cases} 1, & \text{if } -1\leq t<\xi; \\ \frac{1}{3}, & \text{if } t=\xi; \\ -\frac{1}{3}, & \text{if } \xi<t\leq 1. \end{cases}$$

Then it is intended to minimize the functional

$$F(\boldsymbol{x}, f)=\int_{-1}^{\xi}(1-t^2)^2dt+\int_{\xi}^{1}\left(-\frac{1}{3}-t^2\right)^2dt.$$

The necessary condition of the minimization and straightforward computation show that $\xi=\frac{1}{\sqrt{3}}$ and $\xi=-\frac{1}{\sqrt{3}}$ are optimal knots for f.

So the unicity property we shall pursue is the one in topological sense. In what follows, the topology of $C^1[0, 1]$ is the standard one of uniform convergence of functions and their derivatives. The following is a standard result in approximation theory.

Theorem 3.1

Let M be an approximatively compact subset of a normed linear space E. Suppose $x\in E$ has $m\in M$ as its unique closest point in M and let $\{x_\nu\}$ be any sequence converging to x and $\{m_\nu\}$ be any corresponding sequence of closest points in M. Then $\|m_\nu-m\|\to 0$.

Proof

See Singer[3] (p. 388).

Definition 3.2

The element $A(\boldsymbol{x})\in A(S)$ is said to be normal if $\xi\in(0, 1)$ and A^{-1} exists in a neighborhood of $A(\boldsymbol{x})$ and is continuous.

Theorem 3.3

Suppose that $f\in C^*[0, 1]$ has a unique normal best approximation $A(\boldsymbol{x}_0)\leftrightarrow(\xi_0, q_1, q_2)$. Then there exists a neighborhood U of f such that $U\subseteq C^*[0, 1]$.

Proof

Suppose that the conclusion is false for some f satisfying the hypothesis of the theorem. Then there is a sequence $\{f_n\}\subset C^{**}[0, 1]\cup C^*[0, 1]$ such that $f_n\to f$ uniformly. Let $A(\boldsymbol{x}_n)\leftrightarrow(\xi_n, q_{1n}, q_{2n})$ be best approximations for f_n and apply Theorem 3.1 to get

$$A(\boldsymbol{x}_n)\to A(\boldsymbol{x}_0)\,.$$

Then by the normality of $A(\boldsymbol{x}_0)$ we have $\boldsymbol{x}_n\to\boldsymbol{x}_0$. Hence

$$(\xi_n, q_{1n}, q_{2n})\to(\xi_0, q_1, q_2)\,.$$

But each $A(\boldsymbol{x}_n)$ has the property that $q_{1n}(\xi_n)=q_{2n}(\xi_n)$, so

$$0=q_{1n}(\xi_n)=q_{2n}(\xi_n)\to q_1(\xi_0)-q_2(\xi_0)\neq 0$$

which is impossible.

Analogous to Theorem 3.3, we have.

Theorem 3.4

Suppose that $f\in C^{**}[0, 1]\backslash C^{***}[0, 1]$ has a unique normal best approximation $A(\boldsymbol{x}_0)\leftrightarrow(\xi_0, q_1, q_2)$. Then there exists a neighborhood U of f such that $U\subseteq C^{**}[0, 1]$.

Clearly, the necessary conditions to minimize Eq. (3) are

$$F'(\boldsymbol{x}, f, \boldsymbol{K})=0 \quad \text{and} \quad F''(\boldsymbol{x}, f, \boldsymbol{K}, \boldsymbol{K})\geq 0$$

for all $\boldsymbol{K}\in\boldsymbol{R}^{2n+3}$. We now do a further step to modify the second order derivative condition as follows.

Lemma 3.5

If $A(\boldsymbol{x})$ is a best approximation to f, then $B_1(\xi)\geq 0$, where

$$B_1(\xi)=\operatorname{sgn}[q_1(\xi)-f(\xi)]\,|q_1(\xi)-f(\xi)|^{p-1}[q_1'(\xi)-f'(\xi)]$$
$$-\operatorname{sgn}[q_2(\xi)-f(\xi)]\,|q_2(\xi)-f(\xi)|^{p-1}[q_2'(\xi)-f'(\xi)]\,.$$

Proof

A straightforward calculation yields

$$\frac{1}{p}F''(\boldsymbol{x},\ f,\ \boldsymbol{K},\ \boldsymbol{K})=K_0^2B_1(\xi)+K_0B_2(\xi)+(p-1)B_3(\xi)$$

where

$$\boldsymbol{K}=(K_0,\ K_{10},\ K_{11},\ \cdots,\ K_{1n},\ K_{20},\ K_{21},\ \cdots,\ K_{2n})$$

$$B_1(\xi)=\operatorname{sgn}[q_1(\xi)-f(\xi)]|q_1(\xi)-f(\xi)|^{p-1}[q_1'(\xi)-f'(\xi)]$$
$$-\operatorname{sgn}[q_2(\xi)-f(\xi)]|q_2(\xi)-f(\xi)|^{p-1}[q_2'(\xi)-f'(\xi)]$$

$$B_2(\xi)=\operatorname{sgn}[q_1(\xi)-f(\xi)]|q_1(\xi)-f(\xi)|^{p-1}\sum_{i=0}^{n}K_{1i}\xi^i$$
$$-\operatorname{sgn}[q_2(\xi)-f(\xi)]|q_2(\xi)-f(\xi)|^{p-1}\sum_{i=0}^{n}K_{2i}\xi^i$$

$$B_3(\xi)=\int_0^{\xi}|q_1(t)-f(t)|^{p-2}\left(\sum_{i=0}^{n}K_{1i}t^i\right)^2dt+\int_{\xi}^{1}|q_2(t)-f(t)|^{p-2}\left(\sum_{i=0}^{n}K_{2i}t^i\right)^2dt.$$

Now, consider the vector (1, 0, ···, 0). Then if $B_1(\xi)<0$ we have

$$\frac{1}{p}F''(\boldsymbol{x},\ f,\ \boldsymbol{K},\ \boldsymbol{K})=B_1(\xi)<0$$

which is a contradiction.

Lemma 3.6

If $f\in C^1[0,\ 1]$ has $A(\boldsymbol{x})\leftrightarrow(\xi,\ q_1,\ q_2)$ as a normal best approximation, then either

$$q_1'(\xi)-f'(\xi)\neq-[q_2'(\xi)-f'(\xi)],\qquad \text{if } q_1(\xi)+q_2(\xi)=2f(\xi),\tag{4}$$

or

$$q_1'(\xi)\neq q_2'(\xi),\qquad \text{if } q_1(\xi)=q_2(\xi) \text{ and } q_1(\xi)\neq f(\xi).\tag{5}$$

Proof

Suppose $f\in C^*[0,\ 1]$ but Eq. (4) fails. Then

$$\frac{1}{p}F''(\boldsymbol{x},\ f,\ \boldsymbol{K},\ \boldsymbol{K})=K_0B_2(\xi)+(p-1)B_3(\xi).$$

Pick $\boldsymbol{K}_1$ and $\boldsymbol{K}_2$ so that

$$\operatorname{sgn}[q_1(\xi)-f(\xi)]\sum_{i=0}^{n}K_{1i}\xi^i-\operatorname{sgn}[q_2(\xi)-f(\xi)]\sum_{i=0}^{n}K_{2i}\xi^i>0$$

and hence $B_2(\xi)>0$. For such a choice, $\|\boldsymbol{K}_1\|^2+\|\boldsymbol{K}_2\|^2\neq 0$; so we may assume

$$0<\|\boldsymbol{K}_1\|^2+\|\boldsymbol{K}_2\|^2<1$$

For $0<\epsilon<1$, let $\boldsymbol{K}_1(\epsilon)=\epsilon\boldsymbol{K}_1$, $\boldsymbol{K}_2(\epsilon)=\epsilon\boldsymbol{K}_2$, and

$$K_0(\epsilon)=-\sqrt{1-\epsilon\|\boldsymbol{K}_1\|^2-\epsilon\|\boldsymbol{K}_2\|^2}$$

Then $\boldsymbol{K}(\epsilon)=[K_0(\epsilon),\ \boldsymbol{K}_1(\epsilon),\ \boldsymbol{K}_2(\epsilon)]$ with $\|\boldsymbol{K}(\epsilon)\|=1$. Substituting $\boldsymbol{K}(\epsilon)$ for $\boldsymbol{K}$ in $B_2(\xi)$ and $B_3(\xi)$ to get $B_{2\epsilon}(\xi)$ and $B_{3\epsilon}(\xi)$. Observe that

$$\frac{K_0(\epsilon)B_{2\epsilon}(\xi)}{[\|\boldsymbol{K}_1(\epsilon)\|^2+\|\boldsymbol{K}_2(\epsilon)\|^2]^{1/2}}=\frac{K_0(\epsilon)\epsilon B_2(\xi)}{\epsilon(\|\boldsymbol{K}_1\|^2+\|\boldsymbol{K}_2\|^2)^{1/2}}=\frac{K_0(\epsilon)B_2(\xi)}{(\|\boldsymbol{K}_1\|^2+\|\boldsymbol{K}_2\|^2)^{1/2}}<0$$

for all $0<\epsilon<1$. However

$$\frac{B_{3\epsilon}(\xi)}{[\|\boldsymbol{K}_1(\epsilon)\|^2+\|\boldsymbol{K}_2(\epsilon)\|^2]^{1/2}}=\frac{\epsilon^2B_3(\xi)}{\epsilon(\|\boldsymbol{K}_1\|^2+\|\boldsymbol{K}_2\|^2)^{1/2}}\to 0,\qquad \text{as } \epsilon\to 0.$$

So for sufficiently small ϵ,

$$\frac{1}{p}F''[\boldsymbol{x},\ f,\ \boldsymbol{K}(\epsilon),\ \boldsymbol{K}(\epsilon)]<0$$

which is a contradiction. The same argument holds if Eq. (5) fails instead.

Remark

The combination of Lemma 3.5 and Lemma 3.6 says that $B_1(\xi)>0$ is a necessary condition for $A(\boldsymbol{x})$ being a best normal approximation to f.

Theorem 3.7

Let M be the collection of all $f\in C^*[0,\ 1]\cup C^{**}[0,\ 1]$ such that each $f\in M$ has a unique, normal best approximation from $A(S)$. Then M, in the $C^1[0,\ 1]$ topology, is an open subset of $C^*[0,\ 1]\cup C^{**}[0,\ 1]$.

Proof

We may assume $f\in C^*[0,\ 1]\cap M$. An analogous argument holds for $f\in C^{**}[0,\ 1]$. So suppose there is a sequence $f_\nu\to f$ such that each f_ν has two best approximations $A(\boldsymbol{x}_\nu)\leftrightarrow(\xi_\nu,\ q_{1\nu},\ q_{2\nu})$ and $A(\boldsymbol{y}_\nu)\leftrightarrow(\eta_\nu,\ s_{1\nu},\ s_{2\nu})$. Then, for sufficiently large ν

$$0=\frac{F(\boldsymbol{x}_\nu,\ f_\nu)-F(\boldsymbol{y}_\nu,\ f_\nu)-F'(\boldsymbol{y}_\nu,\ f_\nu,\ \boldsymbol{x}_\nu-\boldsymbol{y}_\nu)}{\|\boldsymbol{x}_\nu-\boldsymbol{y}_\nu\|^2}$$

$$=\frac{1}{2}F''\left(\boldsymbol{z}_\nu,\ f_\nu,\ \frac{\boldsymbol{x}_\nu-\boldsymbol{y}_\nu}{\|\boldsymbol{x}_\nu-\boldsymbol{y}_\nu\|},\ \frac{\boldsymbol{x}_\nu-\boldsymbol{y}_\nu}{\|\boldsymbol{x}_\nu-\boldsymbol{y}_\nu\|}\right),$$

where $\boldsymbol{z}_\nu=\theta_\nu\boldsymbol{x}_\nu+(1-\theta_\nu)\boldsymbol{y}_\nu$, $0<\theta_\nu<1$. Let

$$\omega_\nu=\theta_\nu\xi_\nu+(1-\theta_\nu)\eta_\nu$$

$$\phi_{i\nu}=\theta_\nu q_{i\nu}+(1-\theta_\nu)s_{i\nu},\qquad i=1,\ 2.$$

Then

$$\frac{1}{p}F''(\boldsymbol{z}_\nu,\ f,\ \boldsymbol{K}_\nu,\ \boldsymbol{K}_\nu)=K_{0\nu}^2B_{1\nu}(\omega_\nu)+K_{0\nu}B_{2\nu}(\omega_\nu)+(p-1)B_{3\nu}(\omega_\nu),$$

where

$$B_{1\nu}(\omega_\nu)=\operatorname{sgn}[\phi_{1\nu}(\omega_\nu)-f_\nu(\omega_\nu)]|\phi_{1\nu}(\omega_\nu)-f_\nu(\omega_\nu)|^{p-1}[q_1'(\omega_\nu)-f'(\omega_\nu)]$$
$$-\operatorname{sgn}[\phi_{2\nu}(\omega_\nu)-f_\nu(\omega_\nu)]|\phi_{2\nu}(\omega_\nu)-f_\nu(\omega_\nu)|^{p-1}[q_2'(\omega_\nu)-f'(\omega_\nu)]$$

$$B_{2\nu}(\omega_\nu)=\operatorname{sgn}[\phi_{1\nu}(\omega_\nu)-f_\nu(\omega_\nu)]|\phi_{1\nu}(\omega_\nu)-f_\nu(\omega_\nu)|^{p-1}Q_{1\nu}(\omega_\nu)$$
$$-\operatorname{sgn}[\phi_{2\nu}(\omega_\nu)-f_\nu(\omega_\nu)]|\phi_{2\nu}(\omega_\nu)-f_\nu(\omega_\nu)|^{p-1}Q_{2\nu}(\omega_\nu)$$

$$B_{3\nu}(\omega_\nu)=\int_0^{\omega_\nu}|\phi_{1\nu}(t)-f_\nu(t)|^{p-2}Q_{1\nu}^2(t)dt+\int_{\omega_\nu}^1|\phi_{2\nu}(t)-f_\nu(t)|^{p-2}Q_{2\nu}^2(t)dt,$$

and

$$Q_{i\nu}(t)=\frac{q_{i\nu}(t)-s_{i\nu}(t)}{\|\boldsymbol{x}_\nu-\boldsymbol{y}_\nu\|},\qquad i=1,\ 2.$$

Write $q_{i\nu}[\eta_\nu+(\xi_\nu-\eta_\nu);\ t]=q_{i\nu}(\xi_\nu;\ t)=q_{i\nu}(t)$, $q_{i\nu}(\eta_\nu;\ t)=s_{i\nu}(t)$ and note that

$$K_{0\nu}=\frac{\xi_\nu-\eta_\nu}{\|\boldsymbol{x}_\nu-\boldsymbol{y}_\nu\|}=\frac{\delta_\nu}{\|\boldsymbol{x}_\nu-\boldsymbol{y}_\nu\|}.$$

So

$$Q_{i\nu}(t)=K_{0\nu}\frac{q_{i\nu}(\eta_\nu+\delta_\nu;\ t)-q_{i\nu}(\eta_\nu;\ t)}{\delta_\nu},\qquad i=1,\ 2.$$

Let $\boldsymbol{x}=(\xi, \boldsymbol{a}, \boldsymbol{b})$. Then as $\nu\to\infty$, $\delta_\nu\to 0$ and $K_{0\nu}\to K_0$. Also $A(\boldsymbol{x}_\nu)\to A(\boldsymbol{x})$, $A(\boldsymbol{y}_\nu)\to A(\boldsymbol{x})$ by Theorem 3.1. By the normality of $A(\boldsymbol{x})$, $\boldsymbol{x}_\nu\to\boldsymbol{x}$ and $\boldsymbol{y}_\nu\to\boldsymbol{x}$. Therefore

$$\begin{aligned}\lim_{\nu\to\infty} Q_{1\nu}(t)&=\lim_{\nu\to\infty} K_{0\nu}\cdot\lim_{\nu\to\infty}\frac{1}{\delta_\nu}\left[\sum_{i=0}^{n} a_i(\eta_\nu+\delta_\nu)t^i-\sum_{i=0}^{n} a_i(\eta_\nu)t^i\right]\\&=K_0\sum_{i=0}^{n}\lim_{\nu\to\infty}\frac{a_i(\eta_\nu+\delta_\nu)-a_i(\eta_\nu)}{\delta_\nu}t^i\\&=K_0\sum_{i=0}^{n} a_i'(\xi)t^i\,.\end{aligned}$$

Similarly

$$\lim_{\nu\to\infty} Q_{2\nu}(t)=K_0\sum_{i=0}^{n} b_i'(\xi)t^i\,.$$

Recall the characterization of L_p best approximations,

$$E_j[a_i(\xi)]=\int_0^\xi \operatorname{sgn}[q_1(\xi;\ t)-f(\xi)]\,|q_1(\xi;\ t)-f(\xi)|^{p-1}t^j dt=0$$

for all $j=0, 1, \cdots, n$. Thus, for all j

$$\begin{aligned}E_j'[a_i(\xi)]&=\operatorname{sgn}[q_1(\xi;\ \xi)-f(\xi)]\,|q_1(\xi;\ \xi)|^{p-1}\xi^j\\&\quad+(p-1)\int_0^\xi |q_1(\xi;\ t)-f(\xi)|^{p-2}\left[\sum_{i=0}^{n} a_i'(\xi)t^i\right]t^j dt=0\end{aligned}$$

and hence

$$\begin{aligned}&\int_0^\xi |q_1(\xi;\ t)-f(\xi)|^{p-2}\left[\sum_{i=0}^{n} a(\xi)t^i\right]t^j dt\\&\quad=-\frac{1}{p-1}\operatorname{sgn}[q_1(\xi;\ \xi)-f(\xi)]\,|q_1(\xi;\ \xi)-f(\xi)|^{p-1}\xi^j\,.\end{aligned}$$

But

$$\begin{aligned}&\int_0^\xi |q_1(\xi;\ t)-f(\xi)|^{p-2}\left[\sum_{i=0}^{n} a_i'(\xi)t^i\right]t^j dt\\&=\left[\int_0^\xi |q_1(\xi;\ t)-f(\xi)|^{p-2}t^{j+i}dt\right]\cdot[a_0'(\xi),\ a_1'(\xi),\ \cdots,\ a_n'(\xi)]^T\\&=g_{ji}[a_0'(\xi),\ a_1'(\xi),\ \cdots,\ a_n'(\xi)]^T\,.\end{aligned}$$

So

$$\begin{aligned}A'(\xi)&=[a_0'(\xi),\ a_1'(\xi),\ \cdots,\ a_n'(\xi)]^T\\&=-\frac{1}{p-1}\operatorname{sgn}[q_1(\xi;\ \xi)-f(\xi)]\,|q_1(\xi;\ \xi)-f(\xi)|^{p-1}G^{-1}(0,\ \xi)\Xi\end{aligned}$$

where $G(0, \xi)$ is the matrix with entries g_{ji} and $\Xi=(1, \xi, \cdots, \xi^n)^T$.

Denote the inner product in R^{n+1} by $\langle \cdot, \cdot \rangle$ and define

$$\hat{P}_1(t)=\langle [G^{-1}(0, \xi)\Xi]^T, (1, t, \cdots, t^n)\rangle .$$

Then

$$\sum_{i=0}^{n} a_i'(\xi)t^i=-\frac{1}{p-1}\operatorname{sgn}[q_1(\xi;\ \xi)-f(\xi)]|q_1(\xi;\ \xi)-f(\xi)|^{p-1}\hat{P}_1(t)$$

Hence as $\nu\to\infty$

$$Q_{1\nu}(t)\to-\frac{K_0}{p-1}\operatorname{sgn}[q_1(\xi;\ \xi)-f(\xi)]|q_1(\xi;\ \xi)-f(\xi)|^{p-1}\hat{P}_1(t)$$

An analogous calculation yields

$$Q_{2\nu}(t)\to\frac{K_0}{p-1}\operatorname{sgn}[q_2(\xi;\ \xi)-f(\xi)]|q_2(\xi;\ \xi)-f(\xi)|^{p-1}\hat{P}_2(t), \qquad \text{as } \nu\to\infty$$

with

$$\hat{P}_2(t)=\langle [G^{-1}(\xi,\ 1)\Xi]^T, (1, t, \cdots, t^n)\rangle ,$$

where $G(\xi, 1)$ is the matrix with entries $\int_\xi^1 |q_2(\xi;\ t)-f(\xi)|^{p-2}t^{j+i}dt$. Note that

$$\phi_{i\nu}(\omega_\nu)\to q_i(\xi), \qquad i=1, 2, \text{ as } \nu\to\infty .$$

Thus

$$K_{0\nu}B_{2\nu}(\omega_\nu)\to-\frac{K_0^2}{p-1}|q_1(\xi;\ \xi)-f(\xi)|^{2(p-1)}\hat{P}_1(\xi)$$
$$-\frac{K_0^2}{p-1}|q_2(\xi;\ \xi)-f(\xi)|^{2(p-1)}\hat{P}_2(\xi)$$

Next, as $\nu\to\infty$

$$B_{3\nu}(\omega_\nu)\to K_0^2\int_0^\xi |q_1(t)-f(t)|^{p-2}\Big[\sum_{j=0}^{n} a_j'(\xi)t^j\Big]\Big[\sum_{i=0}^{n} a_i'(\xi)t^i\Big]dt$$
$$+K_0^2\int_\xi^1 |q_2(t)-f(t)|^{p-2}\Big[\sum_{j=0}^{n} b_j'(\xi)t^j\Big]\Big[\sum_{i=0}^{n} b_i'(\xi)t^i\Big]dt$$

Following a simple calculation we have

$$\int_0^\xi |q_1(t)-f(t)|^{p-2}\Big[\sum_{j=0}^{n} a_j'(\xi)t^j\Big]\Big[\sum_{i=0}^{n} a_i'(\xi)t^i\Big]dt$$
$$=\Big(\frac{1}{p-1}\Big)^2|q_1(\xi;\ \xi)-f(\xi)|^{2(p-1)}\hat{P}_1(\xi)$$

and

$$\int_{\xi}^{1}|q_2(t)-f(t)|^{p-2}\Big[\sum_{j=0}^{n}b_j'(\xi)t^j\Big]\Big[\sum_{i=0}^{n}b_i'(\xi)t^i\Big]dt$$
$$=\Big(\frac{1}{p-1}\Big)^2|q_2(\xi;\ \xi)-f(\xi)|^{2(p-1)}\hat{P}_2(\xi)$$

Consequently,

$$(p-1)B_{3\nu}(\omega_\nu)\to\frac{K_0^2}{p-1}|q_1(\xi;\ \xi)-f(\xi)|^{2(p-1)}\hat{P}_1(\xi)$$
$$+\frac{K_0^2}{p-1}|q_2(\xi;\ \xi)-f(\xi)|^{2(p-1)}\hat{P}_2(\xi).$$

Therefore as $\nu\to\infty$,

$$\frac{1}{p}F''(z_\nu, f_\nu, \boldsymbol{K}_\nu, \boldsymbol{K}_\nu)\to K_0^2\{\operatorname{sgn}[q_1(\xi)-f(\xi)]|q_1(\xi)-f(\xi)|^{p-1}[q_1'(\xi)-f'(\xi)]$$
$$-\operatorname{sgn}[q_2(\xi)-f(\xi)]|q_2(\xi)-f(\xi)|^{p-1}[q_2'(\xi)-f(\xi)]\}$$
$$=K_0^2B_1(\xi)>0,$$

a contradiction to the fact that $0=\frac{1}{2}F''(z_\nu, f_\nu, \boldsymbol{K}_\nu, \boldsymbol{K}_\nu)$ for all ν. So f_ν has only one best approximation for all ν sufficiently large.

Remark

In all proofs of topological properties the case $C^{***}[0, 1]$ can be ignored since it is nowhere dense in $C^1[0, 1]$. Indeed, for $f\in C^{***}[0, 1]$ having a unique best approximation (ξ, q_1, q_2), set

$$f_\lambda=f+\lambda g, \qquad \lambda\in\boldsymbol{R}$$

where $g\in C^1[0, 1]\backslash C^{***}[0, 1]$ has an optimal knot at ξ. Then ξ is also an optimal knot of f_λ. Assume $(\xi, q_{1\lambda}, q_{2\lambda})$ is a best approximation for f_λ. It follows from the characterization of L_p approximation to get $q_{1\lambda}(\xi)-f_\lambda(\xi)\neq 0$.

Theorem 3.8

Let M be defined as stated in Theorem 3.7, then M is dense in $C^*[0, 1]\cup C^{**}[0, 1]$.

Proof

Given $f \in C^*[0, 1] \cup C^{**}[0, 1]$, set

$f_\nu = f - \lambda_\nu h$, with $\lambda_\nu > 0$ and $\lambda_\nu \to 0$, as $\nu \to \infty$.

Then for sufficiently large ν, f_ν has a unique best approximation. Indeed, if ξ_ν and ζ_ν are optimal for f_ν, then by following lemma

$\xi_\nu \to \xi$ and $\zeta_\nu \to \xi$, as $\nu \to \infty$

where ξ is one of the optimal knots of f. Repeat the proof of Theorem 3.7, a contradiction will be obtained.

In the proof of the above theorem, we used the following lemma which we state as follows.

Lemma 3.9

Suppose that $f \in C^*[0, 1] \cup C^{**}[0, 1]$ has a best approximation $A(\boldsymbol{x}) = (\xi, q_1, q_2)$. Set

$f_\nu = f - \lambda_\nu h$, with $\lambda_\nu > 0$ and $\lambda_\nu \to 0$ as $\nu \to \infty$.

If ξ_ν is an optimal knot for f_ν, then $\xi_\nu \to \xi$ as $\nu \to \infty$.

In light of the remark prior to Theorem 3.8, we summarize the main result as follows.

Theorem 3.10

There is an open and dense subset M in $C^1[0, 1]$ such that each element in M has a unique best approximation using the L_p norm, $p \geq 2$.

4. ACKNOWLEDGEMENTS

The author wishes to thank the supporting fund of this research from Fu Jen Catholic University SVD section.

REFERENCES

(1) D.J. Barrow, C.K. Chui, P.W. Smith and J.D. Ward, "Unicity of Best Mean Approximation by Second Order Splines with Variable Knots", *Math. Comp.*, **32**, 1131-1143 (1978).

(2) J, Chow, "On the Uniqueness of Best $L_2[0, 1]$ Approximation by Piecewise Polynomials with Variable Breakpoints", *Math. Comp.*, **39**, 571-589 (1982).
(3) I. Singer, *Best Approximation in Normed Linear Spaces by Elements of Linear Subspaces*, Springer-Verlag, New York (1970).
(4) J.M. Wolfe, "On the Unicity of Nonlinear Approximation in Smooth Spaces", *J. Approx. Theory*, **12**, 165-181 (1974).
(5) J.M. Wolfe, "Differentiability of Nonlinear Best Approximation Operators in a Real Inner Product Space", *J. Approx. Theory*, **16**, 341-346 (1976).

非線性逼近之唯一性

楊南屏
輔仁大學數學系

摘　要

本文考慮應用 L_p 範數，$p \geq 2$ 從分段多項式的集合對可微分且連續的函數 $C^1[0, 1]$ 作最佳區段逼近的唯一性問題。在適當假設下證得在 $C^1[0, 1]$ 中存在一開且綢密的子集，此一集合的每個元素均有唯一之 L_p 最佳區段逼近。

TEMPERATURE DEPENDENT RAMAN SCATTERING IN $KTiOPO_4$ AND $KTiOAsO_4$ SINGLE CRYSTALS

CHI-SHUN TU, A. R. GUO[+], RUIWU TAO[+], R. S. KATIYAR[+], RUYAN GUO[++] AND A. S. BHALLA[++]

Department of Physics
Fu Jen Catholic University
Taipei, Taiwan 24205, R.O.C.

(*Accepted by J. of Appl. Physis*)

ABSTRACT

The longitudinal (LO) and transverse (TO) A_1 vibrational modes have been measured between 30-1,200 cm^{-1} as a function of temperature (30-1,240 K) for both $KTiOPO_4$ (KTP) and $KTiOAsO_4$ (KTA). KTP and KTA exhibit an obviously different Raman spectra in the frequency region 400-650 cm^{-1} (with respect to KTA). This middle-frequency difference is attributed to the substitution ions in XO_4 group (X=P or As) modifing the force constant of crystal. The relative intensities of the low frequency bands increase dramatically with increasing temperature due to high mobility of K^+ ion. There is no typical soft-mode like behavior in the measured frequency range. A higher symmetric structure taking place above T_c has been confirmed by the disappearance of the A_{1g}(LO) stretching modes of TiO_6 group. Comparison of each frequency belonging to the symmetry A_1, A_2, B_1 and B_2 measured along the [110] phonon direction shows complex difference. The vibrational frequencies of various symmetries were also obtained.

Key Words: Raman scattering, $KTiOPO_4$, $KTiOAsO_4$, Phase transition and Ferroelectric phase.

1. INTRODUCTION

Potassium titanyl phosphate $KTiOPO_4$ and potassium titanyl arsenate $KTiOAsO_4$ belong to the family of the nonlinear optical crystals with

[+] Present address: Department of Physics, University of Puerto Rico, P.O. Box 23343 San Juan, Puerto Rico 00931-3343.
[++] Present address: Material Research Laboratory, The Pennsylvania State University Park, Pennsylvania 16802.

the general formula $M^{+}TiOX^{5+}O_4$, where M={K, Rb, Tl, Cs} and X={P or As}[1~20]. Potassium titanyl phosphate KTP is the most famous one of this type of materials[9~20]. The high damage threshold, large nonlinearity and broad angular acceptance have made KTP the industried material for frequency doubling of the Nd-based laser near 1 μm[5~7]. The ion-exchange properties also make KTP one of the best candidates for many waveguide applications, including phase matched frequency doubling of infrared diode lasers and integrated electro-optic modulators. From dielectric measurements, KTP is shown as a superionic conductor with high mobility of K^{+} ions, markedly at high temperature[2,19]. By high-pressure nonpolarized Raman study at room temperature, Kourouklis et al. reported that there are two pressure induced phase transitions in KTP from ferroelectric to an antiferroelectric phase near 5.5 GPa and then to a paraelectric one near 10 GPa[15]. Especially, the A_1 mode near 56 cm^{-1} was found to exhibit a soft mode-like behavior. However, Furusawa et al. recently measured the Raman spectra of KTP as a function of temperature (300-1,100 K) and suggested that there is no apparent evidence of soft mode near 56 cm^{-1}[10]. It was concluded that KTP would not be undertaking a displacive-type phase transition.

At room temperature, both KTP and KTA have orthorhombic structure with noncentrosymmetric point group C_{2v}(mm2) and space group $Pna2_1$ (Z=8). The lattice parameters of KTP and KTA are a_o=12.814 Å, b_o=6.404 Å, c_o=10.616 Å and a_o=13.103 Å, b_o=6.558 Å, c_o=10.746 Å, respectively[4,6]. Structural studies of the solid solution imply that the high temperature point group symmetry is D_{2h}(mmm) with space group Pnma. The dielectric anomalies indicate that both KTP and KTA have a second-order structural transition from ferroelectric to paraelectric phase at T_c~1,200 K and T_c~1,150 K, respectively[6,19]. Crystal framework is constructed by three dimensional chains which are made from corner-linked TiO_6 octahedral and XO_4 (X=P or As) tetrahedral[9]. Four oxygen ions of the TiO_6 belong to the XO_4 groups and the two remaining which do not belong to XO_4 tetrahedral groups link the TiO_6 groups. The distortion of the TiO_6 octahedral in which the Ti^{+} ions are displaced from the centers of the octahedral results in four medium-length Ti-O bonds, one long-length Ti-O bond and one short-length Ti-O bond. This framework forms the channels along the

c-axis and K^+ ion is located at structural voids[9].

It is believed that KTA should have similar attractive properties as KTP and can compensate the applications of KTP such as the extension of frequency doubling. To our knowledge, there is no prior polarized Raman spectroscopic study on KTP and KTA in a wide temperature range crossing over phase transition point. We have therefore carried out polarized Raman spectroscopy with various geometries. The aim of the present paper is to study the various interatomic vibrational modes over a wide frequency range, to comprehend the character of potassium motion inside the crystals, and to provide a better understanding of their non-linear optical properties for both crystals.

2. EXPERIMENTAL PROCEDURE

KTP and KTA single crystals were being grown using a tungstate flux by a process described previously in Ballman et al.[21]. The crystals were oriented by X-ray and were cut into rectangular shape having (100), (010) and (001) faces. The average dimensions of specimens are $5.0\times3.0\times1.5\,mm^3$ and $3.0\times3.0\times1.5\,mm^3$ for KTP and KTA, respectively. All sample surfaces for measurements were polished to be optically smooth. The green light with $\lambda=514.5$ nm from an Argon ion laser was used as an excitation source of Raman scattering. In order to avoid sample heating, the power on the sample was kept at $\sim$30 mW. A triple grating monochromator (ISA Model T64000) equipped with a liquid nitrogen cooled CCD (coupled charge device) detector was used. The subtractive mode operation was chosen with a resolution $0.5\,cm^{-1}$. The backscattering spectra were measured from geometries $Z(YY)\bar{Z}$ and $X(ZZ)\bar{X}$. Here X, Y and Z correspond to the crystal a-, b- and c-axes, respectively. The vibrations from scattering configurations $Z(YY)\bar{Z}$ and $X(YY)\bar{X}$ are associated with A_1(LO) and A_1(TO) modes, respectively. The spectra of symmetries A_1, A_2, B_1 and B_2 observed under the general $X(\alpha\beta)Y$ scattering configuration also have been measured at room temperature.

A high-temperature furnace made by Marshall Co. was used an Eurotherm temperature controller. The sample was heated from room temperature up to $\sim$1,240 K (for KTP) and $\sim$1,180 K (for KTA) in steps.

For low temperature (<300 K) measurements, a modified Cryogenic Tech. Closed-cycle Refrigerator Model 20 was used with a LakeShore DRC-84C temperature controller. The data were collected automatically using a microcomputer interfaced to the Raman equipment. The error of temperature reading was controlled to better than ±1.0 K by a feed back from the calibrated thermocouples placed near the sample. The incident beam was refocused for each temperature to optimize the signal. Since black-body radiation becomes apparently stronger and superimposes with the Raman components above ~1,070 K, the measured Raman spectra for temperatures above 1,070 K was subtracted by the background due to black-body radiation. Results were found to be reproducible for both KTP and KTA compounds.

In order to determine the position and half-width of various vibrational mode, the damped harmonic oscilator model with spectral response function (for Stokes scattering), i.e.[22]

$$S(\omega)=\frac{\chi_o\Gamma\omega\omega_o^2}{(\omega^2-\omega_o^2)^2+\Gamma^2\omega^2}\cdot\frac{1}{1-\exp\left(-\frac{\hbar\omega}{kT}\right)} \qquad (1)$$

was used. Where, ω_o and Γ correspond to the mode frequency and half-width, respectively. χ_o is susceptibility constant (in arbitrary units). k is Boltzmann's constant and T is absolute temperature.

3. RESULTS AND DISCUSSION

By a factor group analysis for the KTP-type structure (which contains eight molecular units of KTiOPO$_4$ in a primitive unit cell); at zero wavevector, the vibrational modes in the C_{2v}(mm2) orthorhombic symmetry can be decomposed into the following irreducible representations[23]:

$$\Gamma_{vib}=47A_1(IR,\ R)+48A_2(R)+47B_1(IR,\ R)+47B_2(IR,\ R) \qquad (2)$$

The symmetry species A_1, B_1 and B_2 are infrared active with dipole moments oriented along the z, x and y directions, respectively[24]. All four representations are Raman active[24]. We shall now discuss the important features that were observed in Raman spectra as a function of temperature.

(1) Longitudinal (LO) A_1 modes

Actual temperature dependent A_1(LO) Raman modes of KTP and KTA in the frequency range 30-1,150 cm^{-1} from scattering configuration $Z(YY)\bar{Z}$ are shown in Figs. 1(a) and 1(b), respectively. Both compounds exhibit an unusually high scattering efficiency in this geometry. This fact is also observed in the RTP and is related to the non-linear properties[18]. In KTP, the main part of the scattering intensity arises from the Raman components at frequencies near 210, 380, 490 and 770 cm^{-1}. Similarly, the peaks located near 350, 480, 730 and 820 cm^{-1} are the main contribution of the scattering intensity in KTA. Beside the region 400-650 cm^{-1}, frequency shifts and half-widths of both KTP

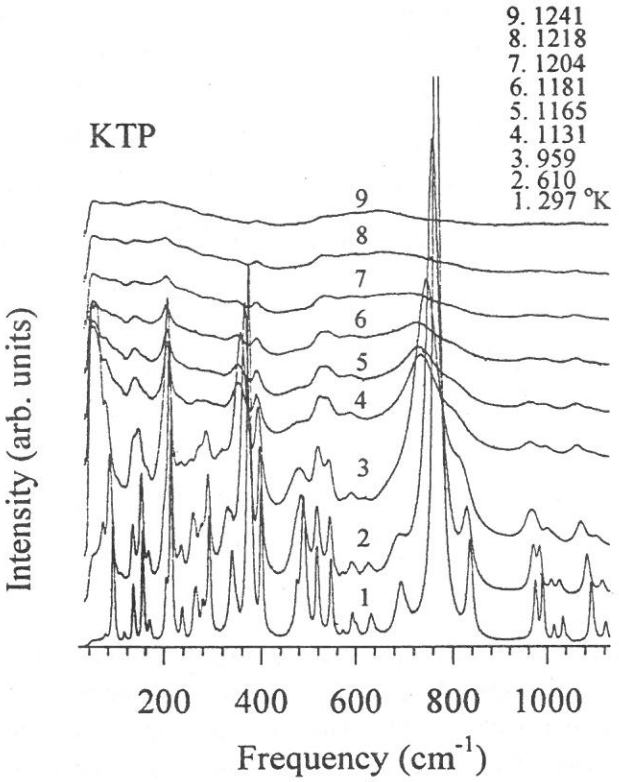

Fig. 1(a). Temperature dependence of Raman spectra of KTP measured from the $Z(YY)\bar{Z}$ geometry between 30 to 1,150 cm^{-1}. Here, the longitudinal A_1 modes are observed.

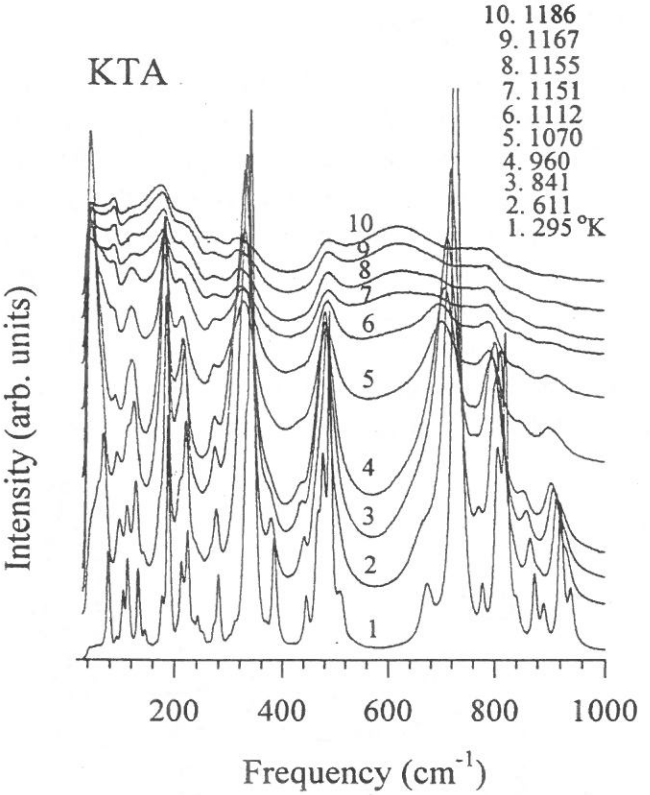

Fig. 1(b). Temperature dependence of Raman spectra of KTA measured from the $Z(YY)\bar{Z}$ geometry between 30 to 1,150 cm^{-1}. Here, the longitudsnal A_1 modes are observed.

and KTA display a similar pattern with all corresponding Raman active modes of KTA shifting to lower frequencies due to the heavier cesium atom.

What are the origins of the vibrational modes in KTP and KTA? According to the crystallographic investigations, the vibrational modes of a perfect 'isolated' TiO_6 octahedron can be decomposed into two pure bond streching vibrations of symmetry $A_{1g}(\nu_1)$ and $E_g(\nu_2)$, two interbond angle bending vibrations ν_5 and ν_6 of symmetry F_{2g} and F_{2u}, respectively, and two vibrations ν_3 and ν_4, considered as combinations of stretching and bending, both of F_{1u} symmetry. The g modes are Raman active and only the F_{1u} are infrared active, the F_{2u} being silent[9]. With the

lowering of the symmetry inside the KTP and KTA crystals, all selection rules for a 'isolated' TiO_6 group are broken and all these vibrations can become active. The symmetries and relative ion displacements related to these motions were given in Kugel et al.[9].

The $\nu_1(A_{1g})$ mode, a symmetic Ti-O stretching mode is expected to have the strongest intensity of the high-frequency vibrations. This was confirmed in many substances containing MO_6 groups such as $SnNbO_4$, $BiNbO_4$ and $LaCuO_4$[25,26]. In our cases, the intense and broad bands near 770 cm^{-1} (in KTP) and 730 cm^{-1} (in KTA) are related to the $\nu_1(A_{1g})$ stretching modes. The $\nu_2(E_g)$ vibration is expected to occurs at a lower frequency as compared to $\nu_1(A_{1g})$. The peaks observed near 690 cm^{-1} (in KTP) and 670 cm^{-1} (in KTA), most likely correspond to the $\nu_2(E_g)$ stretching modes. However, the $\nu_3(F_{1u})$ stretching mode involving a Ti-O anti-phase motion is expected to have a similar frequency as the $\nu_2(E_g)$ vibration. The vibrational modes $\nu_4(F_{1u})$, $\nu_5(F_{2g})$ and $\nu_6(F_{2u})$ were predicated to occur at much lower frequencies[9]. After all, it is difficult to distinguish those vibrations in both KTP and KTA due to the severely superimposed Raman components in the low frequency range.

The internal vibrations of a free 'PO_4' tetrahedron have been calculated as a non-degenerate $A_1(\nu_1)$ mode, a doubly degenerate $E(\nu_2)$ mode and two triply degenerate $F_2(\nu_3)$ and $F_2(\nu_4)$ modes. The frequencies of the ν_1, ν_2, ν_3 and ν_4 fundamental modes calculated by Herzberg[27] are 363, 515, 980 and 1,082 cm^{-1}, respectively, and are 420, 5.5, 938 and 1,017 cm^{-1} obtained by Farmer[28]. The symmetries and relative ion displacements associated with these motions can be found in Kugel et al.[9]. One can expect that the similar vibrational modes should be observed in the AsO_4 group with lower frequencies due to arsenic atom mass. Apparently, the intense peaks near 380 cm^{-1} (in KTP) and 350 cm^{-1} (in KTA) are related to the $\nu_2(E)$ modes. The peaks located near 500 cm^{-1} in both KTP and KTA can be assign to the $\nu_4(F_2)$ modes. The splitting character observed in both $\nu_2(E)$ and $\nu_4(F_2)$ modes is attributed to the slight deformation of the PO_4 (or AsO_4) tetrahedral which breaks the energy degenercy[4]. Those modes located above 800 cm^{-1} are reasonably related to the $\nu_1(A_1)$ and $\nu_3(F_2)$ high-frequency vibrations. The peaks below $\sim$200 cm^{-1} and some low-intensity components up to $\sim$400 cm^{-1} mainly belong to the external lattice vibrations

lattice vibrations involving the K^+ ion motion, TiO_6 and AsO_4 groups, and are consequently influenced by substitution of various ion. The fact that the difference between KTP and KTA are observed in the frequency range 400-650 cm^{-1} can be explained by that the various substitution ions (in XO_4 group) modify the force constant of crystal with different ways.

The temperature dependences of four selected modes for each compound are plotted in Figs. 2(a) and 2(b). The two higher frequency modes correspond to the $\nu_1(A_{1g})$ stretching mode of TiO_6 group and the $\nu_2(E)$ vibration of PO_4 (or AsO_4) group. All four components show an obvious softening with increasing temperature. In the region of 30-1,150 K, the reductions of the $\nu_1(A_{1g})$ modes of TiO_6 group are about 36 cm^{-1} (4.7%) in KTP and 31 cm^{-1} (4.2%) in KTA. The $\nu_2(E)$ vibrations

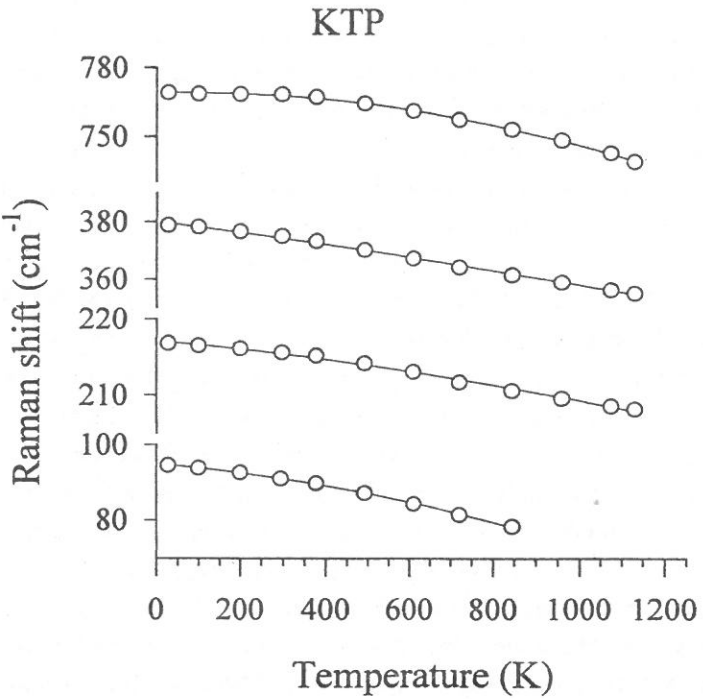

Fig. 2(a). Frequency vs. temperature variations of four selected A_1(LO) modes for KTP measured from the $Z(YY)\bar{Z}$ geometry. The solid lines are guides to the eye.

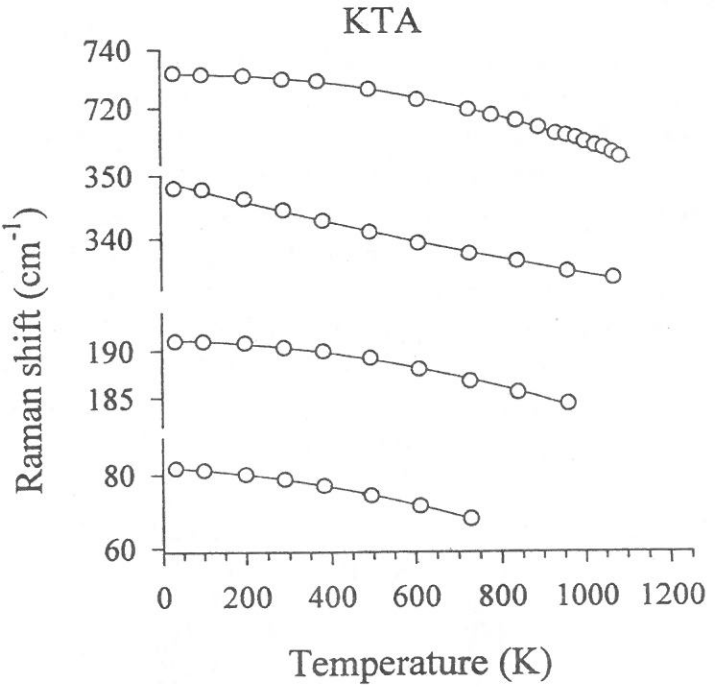

Fig. 2(b). Frequency vs. temperature variations of four selected A_1(LO) modes for KTA measured from the $Z(YY)\bar{Z}$ geometry. The solid lines are guides to the eye.

of PO_4 (or AsO_4) group reduce about 27 cm^{-1} (7.1%) in KTP and 16 cm^{-1} (4.6%) in KTA. Clearly, the typical soft mode behavior doesn't occur in both LO modes.

Another important feature is that the relative scattering intensity of low frequency bands (below 100 cm^{-1}) increases dramatically with increasing temperature. This anomaly can be understood as resulting of high ionic conductivity due to the high mobility of the K^+ ion. One can notice that the $\nu_1(A_{1g})$ modes of TiO_6 group (near 770 cm^{-1} in KTP and 730 cm^{-1} in KTA) gradually decreases and eventually disappears around $T_c \sim 1{,}200$ K and $T_c \sim 1{,}150$ K, respectively. This phenomena confirms a higher symmetric structure taking place at T_c.

(2) Transverse (TO) A_1 modes

Actual temperature dependent TO Raman spectra of KTP and KTA at frequency range 30-1,150 cm^{-1} from scattering configuration $X(ZZ)\bar{X}$ are shown in Figs. 3(a) and 3(b), respectively. KTP and KTA crystals exhibit several apparently different bands at frequencies between 400-650 cm^{-1}. Beside this region, both KTP and KTA display a similar Raman spectra with all corresponding Raman active modes of KTA shifting to lower frequencies due to the heavier arsenic atom. The middle-frequency difference between KTP and KTA could be understood as results of various XO_4 groups (X=P and As) and consequent influences in TiO_6 group. In KTP, the main part of the scattering intensity arises from the frequencies near 220, 270 and 690 cm^{-1}.

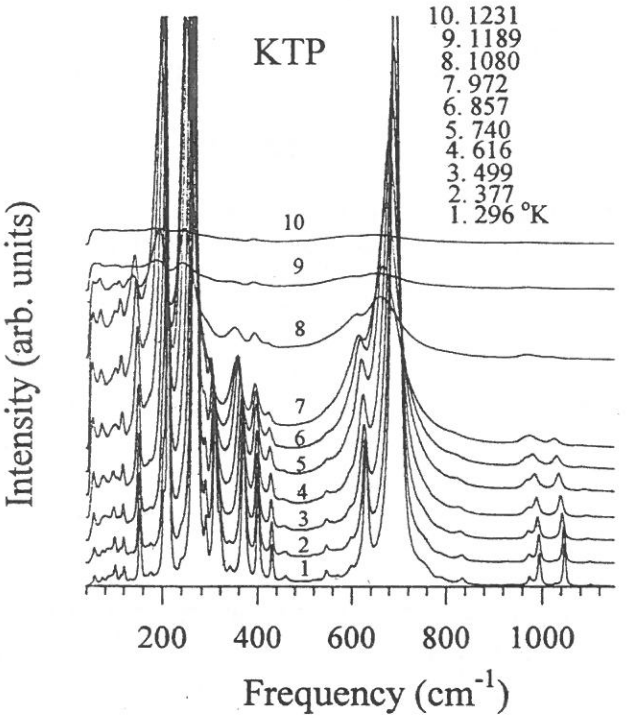

Fig. 3(a). Temperature dependence of Raman spectra of KTP measured from the $X(ZZ)\bar{X}$ geometry between 30 to 1,150 cm^{-1}. Here, the transverse A_1 modes are observed.

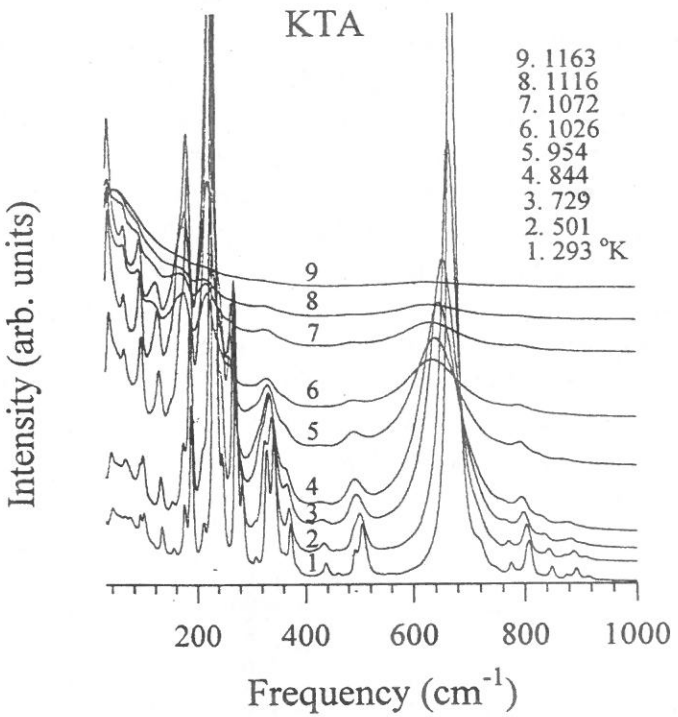

Fig. 3(b). Temperature dependence of Raman spectra of KTA measured from the $X(ZZ)\bar{X}$ geometry between 30 to 1,150 cm^{-1}. Here, the transverse A_1 modes are observed.

Similarly, the peaks located around 230, 270, 370 and 730 cm^{-1} are the main contribution of the scattering intensity in KTA.

The relative scattering intensity at frequencies below 100 cm^{-1} in KTA is evidently stronger than one in KTP. It indicates that the ionic mobility of ptassium ion in KTA is higher than in KTP. One important feature is that the relative scattering intensity of low frequency modes increases dramatically with increasing temperature and reaches a rough saturation near 1,200 and 1,150 K for KTP and KTA, respectively. It is consistent with the results from the LO modes and confirms a structural transition taking place at ~1,200 and ~1,150 K in KTP and KTA, respectively.

Do any TO soft modes exist in the low frequency region? The spectra below 170 cm^{-1} are enlarged in Figs. 4(a) and 4(b) for both KTP and KTA. Obviously, a strong background exists in KTA and the average half-width of the bands in KTA also shows larger magnitude. It implies that the potassium ion has larger mobility inside KTA crystal. The temperature dependences of four selected TO modes for each compound are plotted in Figs. 5(a) and 5(b). Both $\nu_1(A_{1g})$ stretching modes of TiO_6 group (near 695 cm^{-1} in KTP and 675 cm^{-1} in KTA) and the vibration located below 270 cm^{-1} exhibit obvious softening as temperature increases. The reductions of $\nu_1(A_{1g})$ modes of TiO_6 group are about 24 cm^{-1} (3.5%) in KTP and 34 cm^{-1} (5.0%) in KTA from 300 to 800 K. Obviously, the typical soft-mode behavior isn't observed for the TO modes in the measured frequency range.

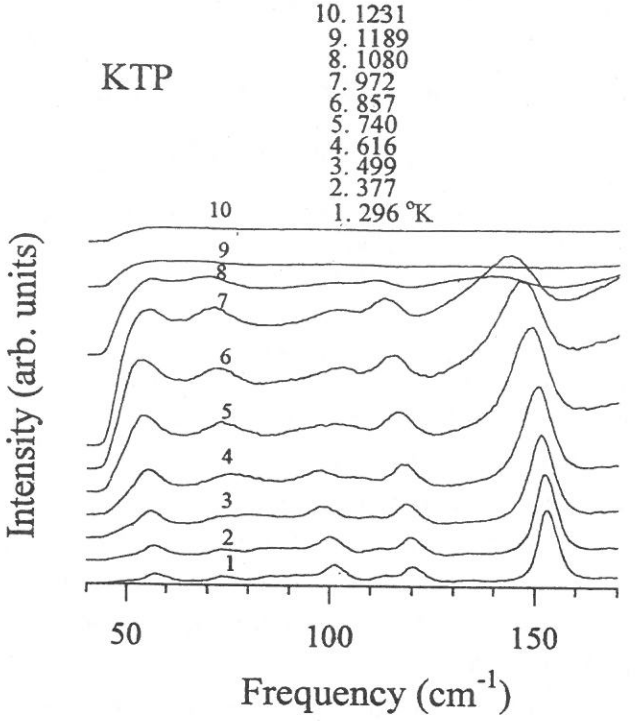

Fig. 4(a). Temperature dependence of Raman spectra of KTP measured from the $X(ZZ)\bar{X}$ geometry between 30 t0 170 cm^{-1}.

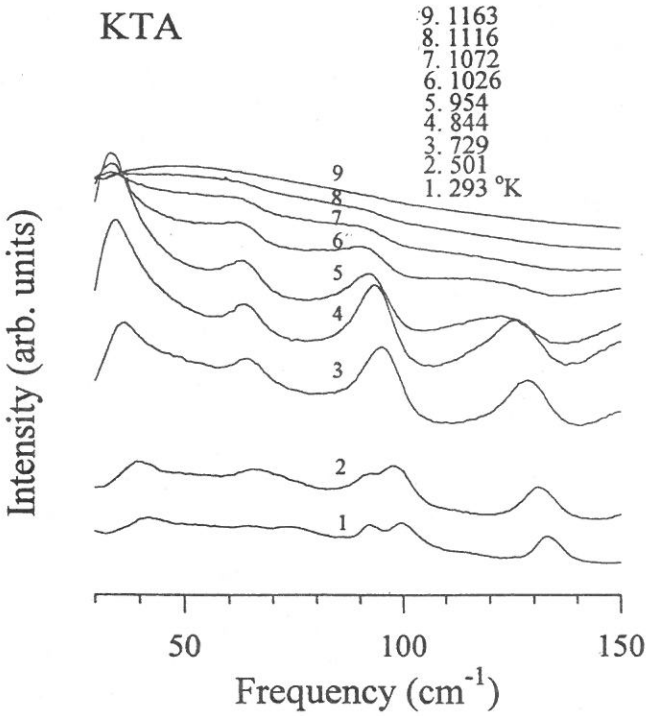

Fig. 4(b). Temperature dependence of Raman spectra of KTA measured from the $X(ZZ)\bar{X}$ geometry between 30 to 170 cm^{-1}.

(3) Comparison of various symmetry species

The Raman spectra of the A_1, A_2, B_1 and B_2 symmetries measured along the [110] phonon propagation direction at room temperature are given in Figs. 6(a) and 6(b) for both KTP and KTA. All four spectra of the A_1, A_2, B_1 and B_2 symmetries from KTP and KTA show complicated pattern with very different frequencies. It implies that the high optical anisotropy exists inside both crystals. In KTP, at room temperature, 32 A_1, 48 A_2, 45 B_1 and 43 B_2 modes have been identified as against 37 A_1, 42 A_2, 44 B_1 and 44 B_2 modes KTA. By using Eq. (1) to fit the spectra, the vibrational frequencies of various symmetries were also obtained and listed in Table 1 for both KTP and KTA.

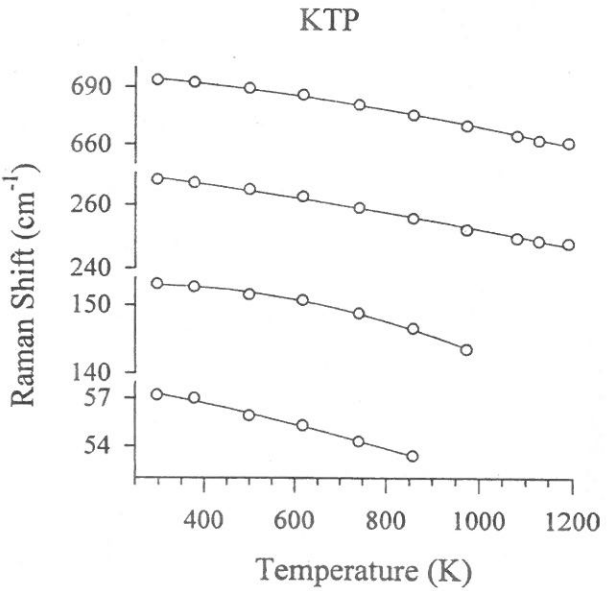

Fig. 5(a). Frequency vs. temperature variations of four selected A_1(TO) modes for KTP. The solid lines are guides to the eye.

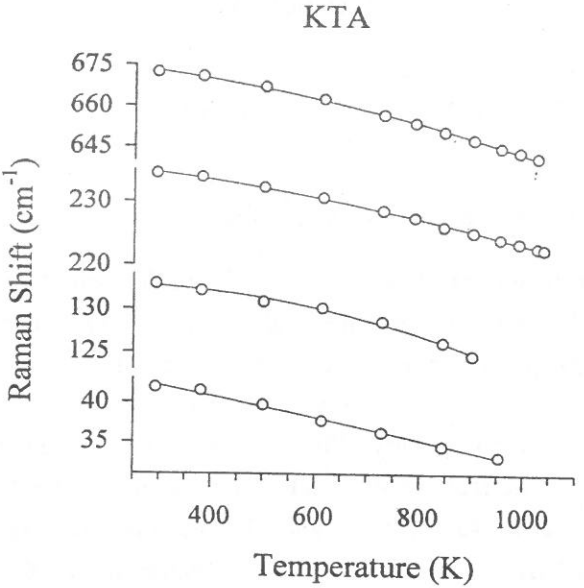

Fig. 5(b). Frequency vs. temperature variations of four selected A_1(TO) modes for KTA. The solid lines are guides to the eye.

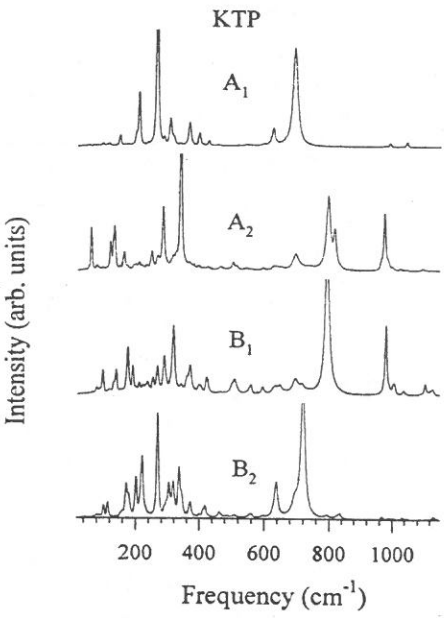

Fig. 6(a). Reman components of A_1 $X(ZZ)Y$, A_2 $X(YX)Y$, B_1 $X(ZX)Y$ and B_2 $X(YZ)Y$ symmetries for KTP measured at room temperature.

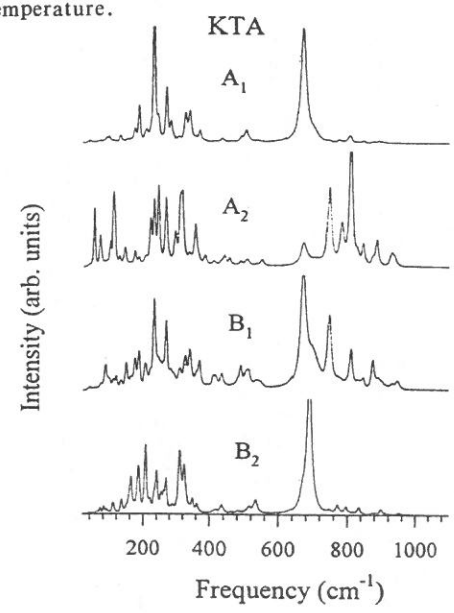

Fig. 6(b). Raman components of A_1 $X(ZZ)Y$, A_2 $X(YX)Y$, B_1 $X(ZX)Y$ and B_2 $X(YZ)Y$ symmetries for KTA measured at room temperature.

Table 1. The vibrational frequencies of A_1, A_2, B_1 and B_2 symmetries observed along the [110] phone direction at room temperature. The unit of frequency is cm^{-1}

A_1 $X(ZZ)Y$		A_2 $X(YX)Y$		B_1 $X(ZX)Y$		B_2 $X(YZ)Y$	
KTP	KTA	KTP	KTA	KTP	KTA	KTP	KTA
56.7	41.3	65.5	53.9	67.3	40.6	70.2	40.8
74.1	54.8	84.8	72.0	82.0	53.3	81.3	51.3
86.5	64.3	100.6	101.2	90.9	73.0	90.3	62.8
101.3	72.6	110.7	111.5	101.0	87.8	102.0	70.9
112.9	91.9	123.9	116.1	119.0	98.7	114.5	82.0
120.5	99.5	132.2	131.1	133.7	110.6	156.3	91.3
153.2	111.5	136.7	146.6	141.3	119.6	171.4	110.7
176.5	132.9	151.0	161.8	159.6	133.5	179.3	135.8
202.8	156.3	165.2	164.9	176.4	150.3	201.5	160.2
212.1	175.1	177.9	175.9	192.3	163.8	220.6	164.5
228.6	188.4	195.3	188.2	204.9	175.6	236.3	186.4
267.4	209.3	201.7	206.9	211.3	187.8	268.7	207.8
289.8	233.8	211.7	222.6	222.9	207.0	289.8	222.2
308.3	247.0	223.1	233.7	230.0	220.8	295.6	233.8
319.4	271.0	233.6	246.9	237.9	234.0	304.0	240.9
340.0	285.7	250.3	270.0	253.5	250.0	317.9	254.1
369.2	305.0	268.4	297.8	268.2	270.1	336.1	261.5
400.1	328.3	285.9	312.6	289.8	290.6	344.7	269.6
429.6	341.7	315 9	319.3	318.4	310.6	371.1	289.4
461.6	359.3	325.3	340.2	340.4	327.3	399.3	311.4
545.5	371.2	341.3	358.7	360.8	342.1	411.4	325.1
569.5	414.0	370.6	386.8	371.7	360.9	418.6	349.1
596.6	435.8	381.3	410.9	398.0	370.7	429.8	362.8
627.7	463.0	398.1	415.0	405.5	411.2	463.0	411.9
693.0	490.0	412.2	433.7	424.6	418.5	487.5	419.4
832.0	504.5	428.5	442.4	504.8	434.5	507.5	433.6
935.0	538.0	468.0	457.7	510.5	479.7	555.0	437.4
973.5	664.9	504.6	489.2	555.1	489.5	561.8	463.5
992.5	696.9	516.1	504.9	559.7	505.3	595.6	482.8
1,024.8	732.9	536.5	510.4	595.6	512.9	637.9	513.9
1,045.9	768.9	544.8	534.0	634.3	532.0	694.3	533.8
1,098.4	799.7	557.9	551.5	649.9	545.0	718.8	669.4
	840.8	597.0	672.1	674.5	668.7	790.3	687.8
	868.8	629.0	744.9	695.2	697.3	821.9	745.3
	885.3	638.0	780.1	716.8	744.1	833.6	767.6
	899.1	651.8	806.9	793.7	783.1	966.6	776.5
	940.0	696.1	828.2	980.5	806.0	990.4	792.4
		743.3	843.8	1,003.5	825.0	1,003.6	813.7
		796.7	872.0	1,008.4	843.0	1,031.6	831.2
		817.5	883.6	1,036.5	871.6	1,045.6	870.6
		964.6	925.9	1,046.0	886.0	1,092.2	879.9
		975.2	934.3	1,088.1	895.0	1,112.2	895.6
		984.7		1,105.0	926.9	1,131.1	907.4
		1,002.0		1,121.4	943.5		948.9
		1,026.7		1,129.1			
		1,044.9					
		1,096.3					
		1,121.6					

4. CONCLUSIONS

KTP and KTA crystals exhibit an apparently different Raman spectra for their LO and TO modes in the frequency range 400-650 cm^{-1}. The substitution ions in XO_4 group (X=P or As) modifing the force constant of crystal play an important role for the difference between KTP and KTA in the middle-frequency region. The relative intensity of low frequency bands shows to increases with increasing temperature. This anomaly is attributed to the change of K^+ ion mobility. A softening behavior has been observed on several LO and TO modes as increasing temperature. However, there is no typical soft-mode like behavior in the measured frequency range. A higher symmetric structure taking place above T_c has been confirmed by the disappearance of the LO (A_{1g}) stretching modes of TiO_6 group. Comparison of each frequency belonging to the symmetry A_1, A_2, B_1 and B_2 measured along the [110] phonon direction shows complex difference.

5. ACKNOWLEDGEMENT

This work was supported by DOE Grant DE-FC02-94ER75764, ARO Grant DAAH04-93-2-0008, and EPSCOR-NSF.

REFERENCES

(1) G. Marnier, B. Boulanger and B. Menaert, *J. Phys.: Condens. Matter*, **1**, 5509 (1989).
(2) G.M. Loiacono, D.N. Loiacono and R.A. Stolzenberger, *J. of Crystal Growth*, **131**, 323 (1993).
(3) G.M. Loiacono, *Appl. Phys. Lett.*, **64**, 2457 (1994).
(4) I. Tordjman, R. Masse and J.C. Guitel, *Z. F. Kristallographie*, **139**, 103 (1974).
(5) L.K. Cheng, L.-T. Cheng, J.D. Bierlein, F.C. Zumsteg and A.A. Ballman, *Appl. Phys. Lett.*, **62**, 346 (1993).
(6) J.D. Bierlein, H. Vanherzeele and A.A. Ballman, *Appl. Phys. Lett.*, **54**, 783 (1989).
(7) G.M. Loiacono, D.N. Loiacono, J.J. Zola, R.A. Stolzenberger, T. McGee and R.G. Norwood, *Appl. Phys. Lett.*, **61**, 895 (1992).
(8) R. Farhi, P. Moch and R.V. Pisarev, *Phase Tansitions*, **33**, 65 (1991).
(9) G.E. Kugel, F. Brehat, B. Wyncke, M.D. Fontana, G. Marnier, C. Carabatos and J. Mangin, *J. Phys. C.: Solid State Phys.*, **21**, 5565 (1988).

(10) S. Furusawa, H. Hayasi, Y. Ishibashi, A. Miyamoto and T. Sasaki, *J. of the Phys. Soc. of Japan*, **60**, 2470 (1991).
(11) V.D. Kugel, G. Rosenman, N. Angert, E. Yaschin and M. Roth, *J. Appl. Phys.*, **76**, 4823 (1994).
(12) L.K. Cheng, L.T. Cheng and J.D. Bierlein, *Appl. Phys. Lett.*, **64**, 1321 (1994).
(13) F.C. Zumsteg, J.D. Bierlein and T.E. Gier, *J. of Appl. Phys.*, **47**, 4980 (1976).
(14) H. Li and X. Wang, *Ferroelectric Lett.*, **17**, 91 (1994).
(15) G.A. Kourouklis, A. Jayaraman and A.A. Ballman, *Solid State Commun.*, **62**, 379 (1987).
(16) L.T. Cheng, L.K. Cheng, J.D. Bierlein and F.C. Zumsteg, *Appl. Phys. Lett.*, **63**, 2618 (1993).
(17) J.C. Jacco, *Matt. Res. Bull.*, **21**, 1189 (1986).
(18) G.E. Kugel, B. Mohamadou and G. Marnier, *Ferroelectrics*, **107**, 115 (1990).
(19) V.K. Yanovskii and V.I. Voronkova, *Phys. State Sol. (a)*, **93**, 665 (1980).
(20) Y.V. Shaldin and R. Poprawski, *Ferroelectrics*, **106**, 399 (1990).
(21) A.A. Ballman, H. Brown, D.H. Olson and C.E. Rice, *J. Cryst. Growth*, **75**, 390 (1986).
(22) J.F. Ryan, R.S. Katiyar and W. Taylor, *Effet Raman Et Théorie*, **C2**, 49 (1971).
(23) D.L. Rousseau, R.P. Bauman and S.P.S. Porto, *J. of Raman Spectroscopy*, **10**, 253 (1981).
(24) G. Turrell, *Infrared and Raman Spectra of Crystals*, Academic Press (1972).
(25) P. Ayyub, M.S. Multani, V.R. Palkar and R. Viyayarahavan, *Phys. Rev. B*, **34**, 8137 (1986).
(26) S. Sugai, *Phys. Rev. B*, **35**, 3621 (1987).
(27) G. Herzberg, *Infrared and Raman Spectra of Polyatomic Molecules*, (Van Nostrand, New York, 1975).
(28) V.C. Farmer, *The Infrared Spectra of Minerals*, London, Mineralogical Soc. (1974).

$KTiOPO_4$ 和 $KTiOAsO_4$ 單晶之溫度相依的拉曼散射研究

杜繼舜
輔仁大學物理系

摘　要

在溫度範圍 (30-1,240 K) 和頻率範圍 (30-1,200 cm^{-1}) 的拉曼散射實驗已完成測量及初步分析。高溫的鐵電相變也被證實。

THE SIZE EFFECT OF SUBSTITUENTS IN SOLID-STATE PHOTODIMERIZATION OF CHALCONE DERIVATIVES

JUNG-NAN CHEN
Department of Chemistry
Fu Jen University
Taipei, Taiwan 24205, R.O.C.

ABSTRACT

The photochemistry of a series of 4,4′-diacyloxychalcone in solid state were studied. A significant size effect of the acyl groups on the solid photodimerization reactivity and products distribution was found. All possible (2+2) photodimers with the same skeleton of 4,4′-dihydroxychalcone but different in acyl groups were synthesized and studied. The selectivity is explained in turns of the size effect.

Key Words: Photodimerization, Chalcones, 4,4′-Diacyloxychalcones.

1. INTRODUCTION

Chalcone (1, 3-diphenyl-2-propene-1-one, I) may undergo (2+2) photodimerization in solid state, polymerization or *cis-trans* isomerization in liquid or solution under the irradiation of UV light[1~3]. The derivatives of chalcones are increasingly important in materials technology. 4, 4′-Diglycidyl-chalcone (DGE-chalcone) for example is a dual functional epoxy resins and is widely used as photoresist[4,5].

In our studies of epoxy resin, the synthesis of 4, 4′-dihydroxychalcone (I_a) photodimers is required. Not all the chalcones can undergo (2+2) photodimerization. 4, 4′-Dihydroxychalcone (I_a), for example, can proceed polymerization in solid state or in solution. According to Schmidt et al.[6~8], the solid photodimerization is governed by the crystal arrangement of molecules. The separation of double bounds between the nearest molecules in solid must be in the range of 3.5~4.2 Å. Since no study on (2+2) photodimers with the same skeleton of chalcones was reported so far. Extensive study of (2+2) photodimers of 4, 4′-

dihydroxychalcone and the study of the structure are attractive. The size effect of the substituent on the molecular arrangement in a unit cell of crystals is quite well known. Thus, a series of the ester derivatives of 4,4′-dihydroxychalcone with acyl group of various sizes have been synthesized as starting materials to vary the size effect on reactivities of chalcones and product distribution.

2. RESULT AND DISCUSSION

Basically solid state photodimerization of chalcones may have four different kinds of stereoisomers: syn-head-to-head (syn H-H, II), anti-head-to-head (anti H-H, III), syn-head-to-tail (syn H-T, IV) and anti-head-to-tail (anti H-T, V) (Scheme 1). Several different carboxylic esters ($I_b \sim I_f$) were obtained from 4,4′-dihydroxychalcone. We found that the size change can affect solid photodimerization both in reactivity and products distribution. Through this method we can obtain all photodimers of 4,4′-dihydroxychalcone.

Scheme 1

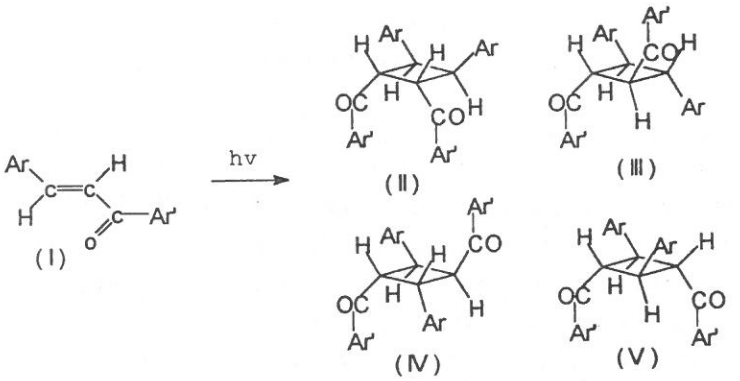

(I) Ar= C_6H_5- Ar'= C_6H_5-

(Ia) Ar= 4-HOC_6H_5- Ar'= 4-HOC_6H_5-

(Ib) Ar= 4-$CH_3COOC_6H_4$- Ar'=4-$CH_3COOC_6H_4$-

(Ic) Ar= 4-$CH_3CH_2COOC_6H_4$- Ar'=4-$CH_3CH_2COOC_6H_4$-

(Id) Ar= 4-$CH_3CH_2CH_2COOC_6H_4$- Ar'=4-$CH_3CH_2CH_2COOC_6H_4$-

(Ie) Ar= 4-$(CH_3)_2CHCOOC_6H_4$- Ar'=4-$(CH_3)_2CHCOOC_6H_4$-

(If) Ar= 4-$C_6H_5COOC_6H_4$- Ar'=4-$C_6H_5COOC_6H_4$-

Table 1 lists the results of these chalcones after UV light irradiation. The ester derivatives with different acyl groups showed various reactivites and products distribution of photodimerization. Under UV irradiation 4,4′-diacetoxychalcone (I_b) yield stereospecific dimerization product, syn H-T IV_b. Similary 4,4′-dipropionoxychalcone (I_c) produced a mixture os syn H-T IV_c, anti H-H III_c and syn H-H II_c as the trace products. 4,4′-Dibutyroxychalcone (I_d) produced a different mixture of syn H-T IV_d, syn H-H II_d and anti H-T V_d as trace products. 4,4′-Diisobutyroxychalcone (I_e) is a photosensitive compound. It dimerizes readily to give a highly stereoselective product syn H-T IV_e in greater than 99% yield. The solid of 4,4′-dibenzoxychalcone (I_f) was photostable and no reaction was observed after prolonged irradiation.

Table 1. Products distribution of solid photodimerization of 4,4′-diacyloxychalcones

Reagent*	Irradiation time	Product (Yield)
I_b	10 days	IV_b (70%)
I_c	30 days	II_c (trace)
		III_c (3%)
		IV_c (27%)
I_d	30 days	II_d (16%)
		IV_d (20%)
		V_d (4%)
I_e	2 days	III_e (trace)
		IV_e (>99%)
I_f	10 days	NR

* I_b: Ar=Ar′=4-$CH_3COOC_6H_4$- I_e: Ar=Ar′=4-$CH_3CHCOOC_6H_4$-CH_3
I_c: Ar=Ar′=4-$CH_3CH_2COOC_6H_4$- I_f: Ar=Ar′=4-$C_6H_5COOC_6H_4$-
I_d: Ar=Ar′=4-$CH_3CH_2CH_2COOC_6H_4$-

The couformations of cyclobuane have been discussed[9]. The conformations of these photodimers are depicted in Scheme 2; Syn H-H dimer as VI and VII, anti H-H dimer as VIII, syn H-H dimer as IX and X, and anti H-T dimer as XI. Table 2 lists of all the ^1H NMR data of the hydrogens on the cyclobutane of dimeric products. All of them show characteristic signals around 3.8~5.2 ppm. Dimer of anti

Scheme 2

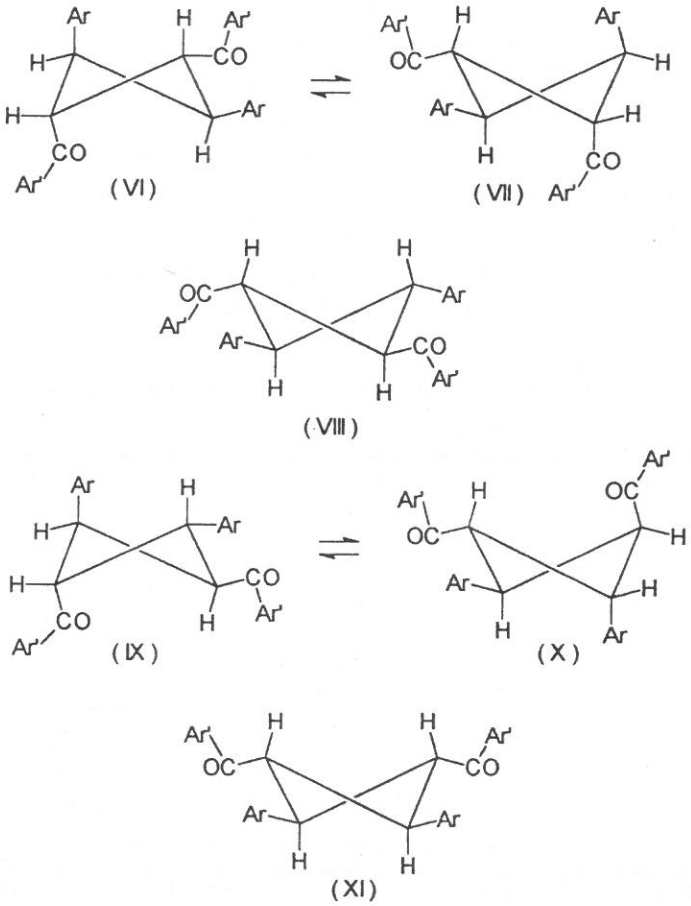

H-T as V shows a A_2X_2 pattern, and all the others are of AA'BB' patterns. V_d has the major conformation as XI. All protons on the cyclobutane ring are in the axial-like position and the phenyl or benzoyl groups are in the equatorial-like position. In this case the protons α to the benzoyl groups are in the position shielded by benzene rings. Therefore the protons on the cyclobutane ring α to benzoyl groups of V_d show signals on higher field. Dimer of anti H-H as III_c have the major conformation as VIII which is similar to the conformation as XI.

Table 2. The ^1H NMR datas of hydrogens on cyclobutane of dimer products

Dimer	Proton NMR data (δ, DMSO-d_6)
IV_b	4.8~5.0 (4H, *m*)
III_c	4.58 (2H, *d*, J=9.0 Hz), 3.90 (2H, *d*, J=9.0 Hz)
IV_c	4.8~5.0 (4H, *m*)
II_d	5.12 (2H, *d*, J=5.3 Hz), 4.29 (2H, *d*, J=5.3 Hz)
IV_d	4.8~5.0 (4H, *m*)
V_d	4.55 (2H, *t*, J=9.0 Hz), 3.89 (2H, *t*, J=9.0 Hz)
IV_e	5.0~4.8 (4H, *m*)

All protons on cyclobutane ring must be in the axial-like position while all phenyl and benzoyl groups are in equatorial-like position. Those protons are all in the shielded region of the benzene ring. So they show the signals of a higher field also. Furthermore the dihedral angle of the neighboring protons are nearly equal for XI and VIII, such that they have similar coupling constants (J=~9 Hz). The protons on the cyclobutane ring of III_c show AA'BB' patterns with $J_{AB'}$=~0 Hz and $J_{A'B}$=~0 Hz. So they show two doublet with J=9 Hz. The conformations of syn H-H as II_d are in rapid equilibrium between VI and VII. Both phenyl and benzoyl groups are too crowded to be in axial-like position. In this case the protons on the cyclobutane ring are not shielded by the benzene ring; Their NMR signals are in normal distribution. Protons α to benzoyl groups are in lower field (~5.1 ppm) and benzylic to phenyl groups are in higher field (~4.3 ppm). All of them belong to AA'BB' patterns. Since $J_{AB'}\simeq 0$ Hz, $J_{A'B}\simeq 0$ Hz and their dihedral angle are not the same as that of in XI and VIII, two doublets with $J\simeq$5.3 Hz are observed. The conformations of syn H-T as IV_b are in rapid equilibrium between IX and X. Like II_d, the protons on cyclobutane ring are not shielded by benzene ring. However these protons are in the position of $\alpha\gamma$ and $\beta\beta$ to benzoyl groups. Therefore the difference of their chemical shift are small (~4.95 and ~4.89 ppm) and $J_{AB}\neq J_{AB'}\neq 0$ Hz (or $J_{trans}\neq J_{cis}\neq 0$ Hz). So they show signals in typical AA'BB' patterns with multiplets at 4.92 ppm. These types of NMR signals of photodimer of chalcones have been reported by us[10,11].

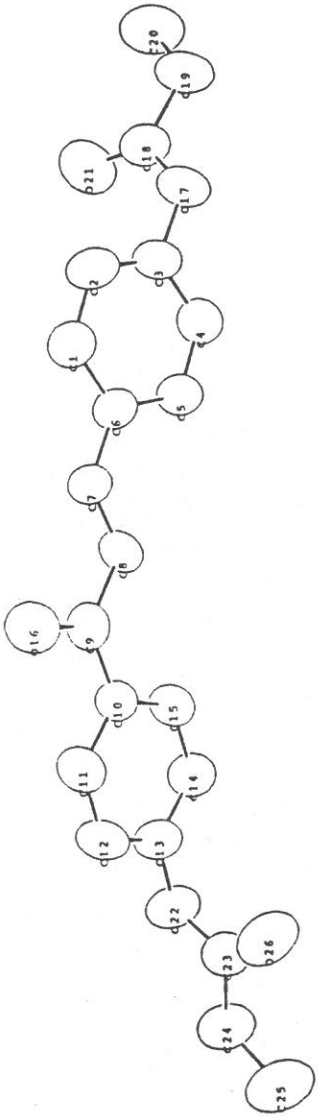

Fig. 1. Molecular structure of 4,4′-dipropionoxychalcone (H atoms omitted).

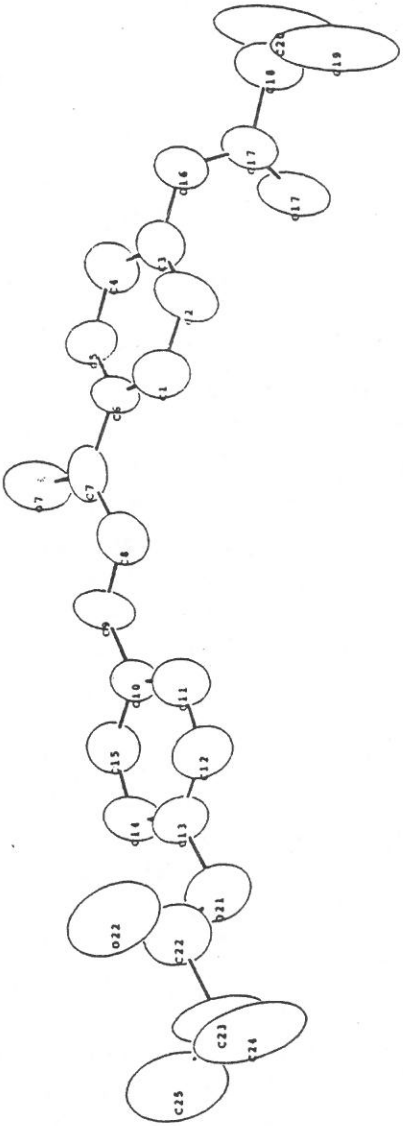

Fig. 2. Molecular structure of 4,4′-diisobutyroxychalcone (H atoms omitted).

The stereo-structure of 4,4′-dipropionoxychalcone (I_c) and 4,4′-diisobutyroxychalcone (I_e) in crystal have been studied by X-ray diffraction as shown in Figs. 1 and 2. Their atomic positional parameters are list in Tables 3 and 4. Their crystal data are list in Table 5. The molecular arrangement in the unit cell of I_c and I_e are shown in Figs. 3 and 4. The relative atomic positional parameters of carbon-carbon double bonds in the unit cell of I_c and I_e are list in Tables 6 and 7.

Table 3. Fractional atomic coordinates, with standard deviations in parenthesis, for 4,4′-dipropionoxychalcone (I_c)

	X	*Y*	*Z*	Beq
C1	0.2075 (4)	0.2253 (5)	0.13725 (7)	5.73 (11)
C2	0.3250 (4)	0.1562 (5)	0.16372 (7)	6.37 (24)
C3	0.4393 (4)	0.0742 (4)	0.16044 (7)	5.31 (21)
C4	0.5008 (4)	0.0612 (4)	0.13212 (7)	5.09 (20)
C5	0.4451 (4)	0.1300 (5)	0.10600 (7)	4.89 (19)
C6	0.3283 (3)	0.2151 (4)	0.10808 (7)	4.49 (18)
C7	0.2620 (4)	0.2872 (4)	0.08188 (7)	4.92 (19)
C8	0.3069 (3)	0.2972 (4)	0.05274 (7)	4.44 (18)
C9	0.2279 (3)	0.3775 (4)	0.02852 (7)	4.51 (18)
C10	0.2788 (3)	0.4031 (4)	−0.00368 (7)	4.08 (17)
C11	0.1977 (3)	0.4802 (5)	−0.02492 (8)	5.40 (20)
C12	0.2401 (4)	0.5138 (5)	−0.05471 (7)	5.74 (21)
C13	0.3645 (3)	0.4687 (4)	−0.06319 (7)	4.91 (19)
C14	0.4451 (4)	0.3923 (5)	−0.04327 (7)	5.45 (20)
C15	0.4032 (3)	0.3590 (4)	−0.01322 (7)	5.00 (19)
O16	0.11809 (24)	0.4280 (3)	0.03521 (5)	6.62 (16)
O17	0.4913 (3)	−0.0090 (3)	0.18581 (5)	7.04 (16)
C18	0.5483 (4)	0.0678 (5)	0.20940 (7)	6.10 (24)
C19	0.5996 (5)	−0.0444 (5)	0.23276 (8)	7.7 (3)
C20	0.6786 (5)	0.0271 (6)	0.25767 (9)	9.3 (3)
O21	0.5561 (3)	0.2075 (3)	0.21014 (6)	8.95 (19)
O22	0.4102 (3)	0.5141 (3)	−0.09246 (5)	6.23 (15)
C23	0.3865 (4)	0.6232 (4)	−0.11678 (8)	5.49 (21)
C24	0.4246 (4)	0.4990 (5)	−0.14636 (8)	6.98 (25)
C25	0.3963 (5)	0.4122 (6)	−0.17466 (9)	9.8 (3)
O26	0.3376 (3)	0.2959 (3)	−0.11415 (6)	9.04 (19)

Table 4. Fractional atomic coordinates, with standard deviations in parenthesis, for 4,4′-diisobutyroxychalcone (I_c)

	X	Y	Z	Beq
C1	0.7142 (7)	0.243 (5)	0.2074 (13)	5.7 (15)
C2	0.6886 (8)	0.312 (6)	0.2520 (18)	8.3 (21)
C3	0.6618 (7)	0.167 (5)	0.2651 (14)	5.9 (16)
C4	0.6600 (7)	−0.045 (6)	0.2350 (17)	7.0 (19)
C5	0.6840 (7)	−0.109 (6)	0.1882 (15)	6.9 (17)
C6	0.7114 (6)	0.036 (5)	0.1751 (12)	5.2 (15)
C7	0.7384 (7)	−0.044 (5)	0.1276 (15)	6.1 (16)
O7	0.7382 (6)	−0.245 (4)	0.1092 (12)	9.8 (14)
C8	0.7642 (7)	0.116 (5)	0.0999 (16)	6.8 (18)
C9	0.7844 (7)	0.044 (6)	0.0487 (13)	6.2 (17)
C10	0.8123 (6)	0.188 (5)	0.0188 (12)	4.6 (15)
C11	0.8221 (8)	0.403 (5)	0.0428 (16)	7.3 (18)
C12	0.8499 (8)	0.517 (6)	0.0180 (15)	7.0 (18)
C13	0.8668 (7)	0.427 (5)	−0.0345 (15)	6.9 (18)
C14	0.8587 (8)	0.215 (6)	−0.0597 (17)	7.9 (19)
C15	0.8299 (8)	0.098 (5)	−0.0335 (15)	6.7 (17)
O16	0.6377 (5)	0.230 (4)	0.3137 (9)	8.0 (12)
C17	0.6093 (8)	0.350 (6)	0.2886 (16)	8.9 (21)
O17	0.6038 (6)	0.409 (6)	0.2249 (11)	13.3 (19)
C18	0.5842 (9)	0.406 (8)	0.3399 (17)	11.4 (27)
C19	0.5834 (14)	0.638 (11)	0.3567 (25)	19.7 (44)
C20	0.5508 (14)	0.339 (11)	0.329 (3)	21.4 (49)
C21	0.8902 (5)	0.567 (4)	−0.0715 (12)	9.5 (14)
C22	0.9237 (9)	0.555 (8)	−0.0486 (22)	11.8 (28)
O23	0.9362 (7)	0.439 (8)	−0.0043 (18)	19.3 (29)
C24	0.9458 (12)	0.689 (8)	−0.099 (3)	17.4 (39)
C25	0.9636 (13)	0.871 (10)	−0.063 (3)	18.7 (43)
C26	0.9689 (13)	0.565 (11)	−0.1406 (21)	16.9 (42)

The separation of carbon-carbon double bonds between the nearest molecules of I_c is 4.29 Å exceeding the upper limit of 4.2 Å. Thus I_c photodimerized slowly. The orientation of double bonds are not parallel to each other. Therefore I_c gives mixed products of syn H-T and anti H-H dimers. The separation of double bonds between the nearest

Table 5. Crystal data for I_c and I_e

Compound	I_c	I_e
Formula	$C_{21}O_5H_{20}$	$C_{23}O_5H_{24}$
Fw	352.39	380.44
Space group	Pbca	C2/c
a, Å	10.2399 (9)	37.142 (13)
b, Å	8.4575 (6)	5.9373 (14)
c, Å	442.873 (3)	18.885 (5)
β, deg		95.52 (3)
V, A	3,713.0 (5)	4,145.3 (20)
Z	8	8
D (calcd), g•cm^{-3}	1.261	1.219
λ, Å	1.54056	0.70930
F(000)	1,487.83	1,743.80
Temperature	298 K	298 K
μ (mm^{-1})	0.70	0.03
$2\theta_{max}$	119.9	45.0
Octants (h, k, ℓ)	0~11, 0~9, 0~48	−40~39, 0~6, 0~21
No. of unique reflns	2,760	2,717
No. of obs. reflns	1,905 ($>2\sigma$)	850 ($>2\sigma$)
No. of variables	235	254
R(F)	0.063	0.089
Rw(F)	0.049	0.087
S	3.11	1.39

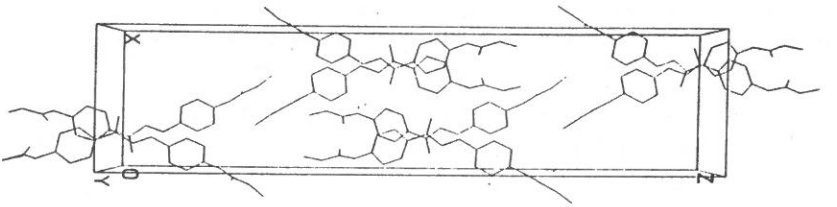

Fig. 3. Molecular arrangement in the unit cell of 4,4′-dipropionoxychalcone.

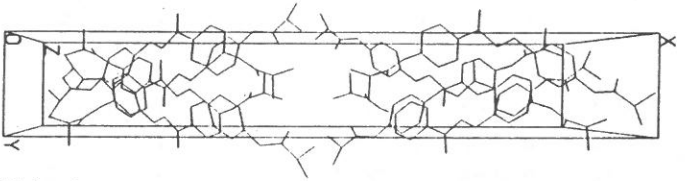

Fig. 4. Molecular arrangement in the unit cell of 4,4′-diisobutyroxychalcone.

Table 6. The relative atomic positions of carbon-carbon double bonds in a unit cell of 4, 4′-dipropinoxychalcone (I_c)

	Orginal	Atomic	Position	0.26204	0.28720	0.08188	
C7	0.26204	0.28720	0.08188	X	Y	Z	
	0.73796	0.71280	0.91812	$-X$	$-Y$	$-Z$	(1, 1, 1)
	0.23796	0.78720	0.08188	$\frac{1}{2}-X$	$\frac{1}{2}+Y$	Z	
	0.76204	0.21280	0.91812	$\frac{1}{2}+X$	$\frac{1}{2}-Y$	$-Z$	(0, 0, 1)
	0.26204	0.21280	0.58188	X	$\frac{1}{2}-Y$	$\frac{1}{2}+Z$	
	0.73796	0.78720	0.41812	$-X$	$\frac{1}{2}+Y$	$\frac{1}{2}-Z$	(1, 0, 0)
	0.23796	0.71280	0.58188	$\frac{1}{2}-X$	$-Y$	$\frac{1}{2}+Z$	(0, 1, 0)
	0.76204	0.28720	0.41812	$\frac{1}{2}+X$	Y	$\frac{1}{2}-Z$	
	Orginal	Atomic	Position	0.30695	0.29723	0.05274	
C8	0.30695	0.29723	0.05274	X	Y	Z	
	0.69305	0.70277	0.94726	$-X$	$-Y$	$-Z$	(1, 1, 1)
	0.19305	0.79723	0.05274	$\frac{1}{2}-X$	$\frac{1}{2}+Y$	Z	
	0.80695	0.20277	0.94726	$\frac{1}{2}+X$	$\frac{1}{2}-Y$	$-Z$	(0, 0, 1)
	0.30695	0.20277	0.55274	X	$\frac{1}{2}-Y$	$\frac{1}{2}+Z$	
	0.69305	0.79723	0.44726	$-X$	$\frac{1}{2}+Y$	$\frac{1}{2}-Z$	(1, 0, 0)
	0.19305	0.70277	0.55274	$\frac{1}{2}-X$	$-Y$	$\frac{1}{2}+Z$	(0, 1, 0)
	0.80695	0.29723	0.44726	$\frac{1}{2}+X$	Y	$\frac{1}{2}-Z$	

Table 7. The relative atomic positions of carbon-carbon double bonds in a unit cell of 4, 4′-diisobutyroxychalcone (I_e)

	Orginal	Atomic	Position	−0.07952	0.26801	0.32892	
C8	0.92048	0.26801	0.32892	X	Y	Z	(1, 0, 0)
	0.42048	0.23199	0.67108	$\frac{1}{2}+X$	$\frac{1}{2}-Y$	$-Z$	(0, 0, 1)
	0.07952	0.76801	0.17108	$-X$	$\frac{1}{2}+Y$	$\frac{1}{2}-Z$	
	0.57952	0.73199	0.82892	$\frac{1}{2}-X$	$-Y$	$\frac{1}{2}+Z$	(0, 1, 0)
	Orginal	Atomic	Position	−0.03986	0.19916	0.29062	
C9	0.96014	0.19916	0.29062	X	Y	Z	(1, 0, 0)
	0.46014	0.30084	0.70938	$\frac{1}{2}+X$	$\frac{1}{2}-Y$	$-Z$	(0, 0, 1)
	0.03986	0.69916	0.20938	$-X$	$\frac{1}{2}+Y$	$\frac{1}{2}-Z$	
	0.53986	0.80084	0.79062	$\frac{1}{2}-X$	$-Y$	$\frac{1}{2}+Z$	(0, 1, 0)

molecules of I_a is 3.89 Å and parallel to each other. The distance is within the limit of 4.2 Å. The orientation arrangement of molecules is in centrosymmetric way. So it gives the photodimer of syn H-T after UV irradiation in solid state. These X-ray data along with the result of photodimerization confirm the conclusions of Schmidt's proposal. Although various methods of recrystallizing I_b, I_d and I_f had been tried, no single crystal of good quality was obtained.

By changing the size of the acyl group of 4,4′-diacyloxychalcones, all four possible photodimers of 4,4′-dihydroxychalcone skeleton are obtained in the solid state photolysis. Hydrogens on the cyclobutane ring show characteristic NMR signals for all photodimers, which can be very useful for the identifcation of the photodimerization products of other chalcones. However, most 4,4′-diacyloxychalcones photodimerized slowly except I_e, with syn H-T dimer as the major product. How to increase the quantum yield of photodimerization and how to control the products distribution are quite interesting. Further works are in progress.

3. EXPERIMENTAL SECTION

Melting points are uncorrected. NMR spectra were obtained on a Bruker AC-300 (300 MHz) NMR spectrometer. IR spectra were measured on a Perkin-Elmer 983 IR spectrophotometer. Mass spectra were obtained on a Jeol JMS-D100 Mass spectrometer. UV spectra were measured on Shimadzu UV-160 UV-Vis spectrophotometer. A UVP Blak-ray Ultraviolet Lamp Model B-100 AP was used as the UV light source for photoreaction.

(1) 4,4′-Dihydroxychalcone (I_a)

To a mixture of 4-hydroxybenzaldehyde (12.2 g, 0.1 mol) and 4′-hydroxyacetophenone)13.6 g, 0.1 mol) in ethanol (50 ml) was added KOH solution (70 g, 40%) slowly. The reaction mixture was kept at 50°C for 20 hr. Then the mixture was poured into ice cold water (500 ml) and neutralized with HCl (0.1 N) with vigorous stirring. The yellow powder was collected and recrystalized from THF to get I_a (19.2 g, 80%);

mp. 203~206°C; UV λ_{max} 340.4 nm (ε 29,600); IR (cm^{-1}) 3,476, 3,099, 1,638, 1,602, 1,549, 1,506, 1,447, 1,345, 1,277, 1,226, 1,167, 1,050, 992, 824, 754, 682; ^1H NMR (DMSO-d_6) δ 10.39 (1H, *s*), 10.07 (1H, *s*) 8.02 (2H, *d*, J=8.6 Hz), 7.69 (2H, *d*, J=8.6 Hz), 7.69 (1H, *d*, J=15.4 Hz), 7.61 (1H, *d*, J=15.4 Hz), 6.89 (2H, *d*, J=8.6 Hz), 6.82 (2H, *d*, J=8.6 Hz); ^{13}C NMR (DMSO-d_6) δ 187.5, 162.1, 160.0, 131.4, 131.2, 130.8, 130.6, 129.7, 126.2, 116.3, 115.8, 115.3.

(2) General procedure for the preparation of 4, 4′-diacyloxychalcones (I_b~I_f)

All 4, 4′-diacyloxychalcones were prepared by mixing equimolar ratio of 4, 4′-dihydroxychalcone and the corresponding acyl chloride in pyridine. The mixture was then washed with water and HCl (0.1 N) to remove pyridinium chloride and excess pyridine. The products were recrystalized from ethanol.

(3) 4, 4′-Diacetoxychalcone (I_b)

Pale yellow crystal: mp. 124~125°C: UV λ_{max} 314.0 nm (ε 22,400); IR (cm^{-1}) 3,040, 2,950, 1,750, 1,663, 1,609, 1,596, 1,579, 1,500, 1,413, 1,378, 1,331, 1,300, 1,226, 1,165, 1,110, 1,033, 1,013, 983, 955, 850, 817, 765, 751, 712, 687, 650; ^1H NMR (DMSO-d_6) δ 8.22 (2H, *d*, J=8.6 Hz), 7.94 (2H, *d*, J=8.5 Hz), 7.93 (1H, *d*, J=15.6 Hz), 7.75 (1H, *d*, J=15.6 Hz), 7.33 (2H, *d*, J=8.6 Hz), 7.27 (2H, *d*, J=8.5 Hz), 2.30 (3H, *s*), 2.28 (3H, *s*); ^{13}C NMR (DMSO-d_6) δ 188.4, 168.9, 168.8, 154.1, 152.2, 135.1, 132.3, 130.5, 130.4, 129.8, 122.6, 122.4, 122.1.

(4) 4, 4′-Dipropionoxychalcone (I_c)

Pale yellow crystal: mp. 112~113°C; UV λ_{max} 314.8 nm (ε 22,600); IR (cm^{-1}) 3,040, 2,950, 1,752, 1,656, 1,605, 1,594, 1,577, 1,500, 1,459, 1.414, 1,357, 1,335, 1,301, 1,289, 1,214, 1,167, 1,150, 1,079, 1,035, 1,014, 984, 942, 903, 839, 809, 761, 713; ^1H NMR (DMSO-d_6) δ 8.23 (2H, *d*, J=8.6 Hz), 7.95 (2H, *d*, J=8.6 Hz), 7.94 (1H, *d*, J=15.6 Hz), 7.75 (1H, *d*, J=15.6 Hz), 7.33 (2H, *d*, J=8.6 Hz), 7.23 (2H, *d*, J=8.6 Hz), 2.6~2.7 (4H, *m*), 1.1~1.7 (6H, *m*); ^{13}C NMR (DMSO-d_6) δ 188.0, 172.3, 172.1, 154.2, 152.2, 135.0, 132.2, 130.4, 129.7, 122.5, 122.4, 122.0, 121.8, 27.1, 26.9, 8.85, 8.46.

(5) **4, 4′-Dibutyroxychalcone (I_d)**

Pale yellow crystal: mp. 117~118°C; UV λ_{max} 313.2 nm (ε 23,800); IR (cm^{-1}) 3,050, 2,958, 2,871, 1,743, 1,655, 1,599, 1,575, 1,500, 1,459, 1,412, 1,378, 1,364, 1,327, 1,304, 1,279, 1,214, 1,171, 1,145, 1,100, 1,077, 1,026, 1,015, 986, 951, 924, 876, 831, 821, 754; ^{1}H NMR (DMSO-d_6) δ 8.22 (2H, *d*, *J*=8.6 Hz), 7.95 (2H, d, *J*=8.5 Hz), 7.93 (1H, *d*, *J*=15.6 Hz), 7.75 (1H, *d*, *J*=15.6 Hz), 7.33 (2H, *d*, *J*=8.6 Hz), 7.23 (2H, *d*, *J*=8.5 Hz), 2.5~2.7 (4H, *m*), 1.6~1.7 (4H, *m*), 0.9~1.0 (6H, *m*); ^{13}C NMR (DMSO-d_6) δ 188.0, 171.4, 171.3, 154.2, 152.3, 143.1, 135.1, 132.3, 130.2, 130.1, 122.3, 122.2, 122.0, 35.3, 178.8, 13.3.

(6) **4, 4′-Diisobutyroxychlcone (I_e)**

Pale yellow crystal: mp. 165~168°C; UV λ_{max} 313.2 nm (ε 23,200); IR (cm^{-1}) 3,050, 2,971, 2,357, 1,750, 1,656, 1,605, 1,596, 1,578, 1,500, 1,465, 1,415, 1,383, 1,212, 1,181, 1,166, 1,128, 1,028, 1,012, 984, 882, 859, 806; ^{1}H NMR (DMSO-d_6) δ 8.23 (2H, *d*, *J*=8.6 Hz), 7.95 (2H, *d*, *J*=8.7 Hz), 7.94 (1H, *d*, *J*=15.6 Hz), 7.75 (1H, *d*, *J*=15.6 Hz), 7.23 (2H, *d*, *J*=8.6 Hz), 7.21 (2H, *d*, *J*=8.7 Hz), 2.9~2.8 (2H, *m*), 1.3~1.2 (12H, *m*); ^{13}C NMR (DMSO-d_6) δ 188.0, 174.8, 174.5, 154.5, 154.3, 143.1, 135.1, 132.3, 130.3, 130.1, 122.2, 122.1, 121.5, 33.4, 33.3, 18.5.

(7) **4, 4′-Dibenzoyloxychalcone (I_f)**

Yellow crystal: mp. 184~186°C; UV λ_{max} 316.0 nm (ε 22,800); IR (cm^{-1}) 3,080, 1,732, 1,662, 1,605, 1,580, 1,500, 1,449, 1,412, 1,332, 1,265, 1,212, 1,196, 1,181, 1,165, 1,080, 1,065, 1,024, 989, 881, 863, 806, 701; ^{1}H NMR (DMSO-d_6) δ 8.31 (2H, *d*, *J*=8.7 Hz), 8.17 (2H, *d*, *J*=7.2 Hz), 8.15 (2H, *d*, *J*=7.2 Hz), 8.04 (2H, *d*, *J*=8.7 Hz), 8.02 (1H, *d*, *J*=15.6 Hz), 7.81 (1H, *d*, *J*=15.6 Hz), 7.77 (2H, *t*, *J*=7.2 Hz), 7.63 (2H, *t*, *J*=7.2 Hz), 7.62 (2H, *t*, *J*=7.2 Hz), 7.52 (2H, *d*, *J*=8.7 Hz), 7.42 (2H, *d*, *J*=8.7 Hz); ^{13}C NMR (DMSO-d_6) δ 188.0, 164.3, 164.1, 154.2, 152.4, 143.1, 135.3, 134.2, 134.1, 132.5, 130.2, 130.1, 129.8, 129.7, 128.9, 128.7, 128.6, 122.4, 122.3, 122.1.

(8) General procedure for solid photodimerization

4, 4′-Diacyloxychalcone (0.1 mol) was added to a 500 ml Pyrex flask, which was rotated by a spinner. Then the UV lamp was turned on. After 1 hr, 2 hr, 4 hr, 8 hr, 24 hr, 2 days, 5 days, 10 days, 20 days and 30 days, Sample (a few mgs) was withdrawn and monitored by NMR. The results are presented in Table 1 and the procedure for the isolation of dimers described below.

(9) Syn H-T photodimer of 4, 4′-diacetoxychalcone (IV_b)

After the unreacted 4, 4′-diacetoxychalcone was extracted with boiling acetone. The resulting white powder was recrystalized from chloroform to get white crystal IV_b; mp. 254~256°C; UV λ_{max} 257 nm (ε 19,600); IR (cm^{-1}) 3,050, 1,744, 1,670, 1,596, 1,502, 1,407, 1,368, 1,311, 1,260, 1,216 1,202, 1,166, 1,104, 1,049, 913, 854, 799, 701; ^1H NMR (DMSO-d_6) δ 7.83 (4H, *d*, J=8.5 Hz), 7.30 (4H, *d*, J=8.4 Hz), 7.13 (4H, *d*, J=8.5 Hz), 6.84 (4H, *d*, J=8.4 Hz), 5.0~4.8 (4H, *m*), 2.26 (6H, *s*), 2.17 (6H, *s*); ^{13}C NMR (DMSO-d_6) δ 197.3, 168.8, 168.5, 153.8, 148.9, 136.5, 133.8, 129.7, 129.0, 121.7, 121.0, 49.4, 40.9, 20.8, 20.7; MS (70 eV) *m/e* (%) 649 (M^+, 5), 325 (30), 307 (48), 289 (20), 154 (100), 136 (65), 107 (20); *Anal. Calcd* for $C_{38}H_{32}O_{10}$: C, 70.36, H, 4.97. *Found*: C, 70.50, H, 4.99.

(10) Syn H-T photodimer of 4, 4′-dipropionoxychalcone (IV_c)

After the unreacted 4, 4′-dipropionoxychalcone was extracted with boiling *n*-hexane. The resulting white powder was recrystalized from chloroform to get white crystal IV_c; mp. 222~224°C; UV λ_{max} 258 nm (ε 19,600); IR (cm^{-1}) 3,050, 2,980, 1,758, 1,666, 1,597, 1,502, 1,459, 1,411, 1,352, 1,314, 1,352, 1,314, 1,261, 1,203, 1,166, 1,140, 1,076, 1,015, 982, 892, 837; ^1H NMR (DMSO-d_6) δ 7.85 (4H, *d*, J=8.7 Hz), 7.31 (4H, *d*, J=8.6 Hz), 7.14 (4H, *d*, J=8.7 Hz), 6.85 (4H, *d*, J=8.6 Hz), 5.0~4.8 (4H, *m*), 2.5~2.7 (8H, *m*), 1.2~1.0 (12H, *m*); ^{13}C NMR (DMSO-d_6) δ 197.4, 172.3, 172.0, 154.0, 149.0, 136.5, 133.7, 129.8, 129.1, 121.7, 121.1, 49.5, 41.0, 26.9, 26.8, 8.75, 8.70; MS (70 eV) *m/e* (%) 704 (M^+, 5), 527 (10), 353 (10), 352 (10), 296 (50), 240 (100), 121 (35); *Anal. Calcd* for $C_{42}H_{40}O_{10}$: C, 71.76, H, 5.65. *Found*: C, 71.58, H. 5.82.

(11) Anti H-H photodimer of 4, 4′-dipropionoxychalcone (III_c)

The residue of mother liquid of IV_c was fractional recrystalized from ethanol—*n*-hexane (1:1) to get tiny needle crystal III_c: mp. 105~107°C; UV λ_{max} 257 nm (ε 18,900); IR (cm^{-1}) 3,050, 2,981, 1,758, 1,662, 1,596, 1,502, 1,459, 1,412, 1,350, 1,210, 1,165, 1,140, 1,076, 1,014, 982, 851, 759; ^1H NMR (DMSO-d_6) δ 7.82 (4H, *d*, *J*=8.7 Hz), 7.37 (4H, *d*, *J*=8.5 Hz), 7.12 (4H, *d*, *J*=8.7 Hz), 7.07 (4H, *d*, *J*=8.5 Hz), 4.58 (2H, *d*, *J*=9.0 Hz), 3.90 (2H, *d*, *J*=9.0 Hz), 2.6~2.5 (8H, *m*), 1.2~1.0 (12H, *m*); ^{13}C NMR (DMSO-d_6) δ 197.1, 172.4, 171.9, 154.5, 149.5, 138.3, 132.7, 130.1, 128.2, 121.9, 47.2, 46.4, 26.8, 8.72, 8.58; MS (70 eV) *m/e* (%) 705 (M^++1, 40), ς27 (10), 381 (85), 353 (45), 325 (40), 296 (45), 269 (20), 240 (30), 212 (20), 177 (20), 154 (40), 136 (35), 121 (100), 57 (35); *Anal. Calcd* for $C_{40}H_{40}O_{10}$: C, 71.58, H, 5.72. *Found*: C, 71.64, 5.58.

(12) Syn H-T photodimer of 4, 4′-dibutyroxychalcone (IV_d)

After the unreacted 4, 4′-dibutyroxychalcone was extracted with boiling *n*-hexane. The resulting white powder was recrystalized from chloroform to get white crystal IV_d; mp. 117~118°C; UV λ_{max} 257 nm (ε 19,200); IR (cm^{-1}) 3,050, 2,967, 1,756, 1,663, 1,596, 1,502, 1,459, 1,410, 1,357, 1,301, 1,260, 1,237, 1,202, 1,166, 1,147, 1,077, 1,047, 1,018, 985 920, 846; ^1H NMR (DMSO-d_6) δ 7.84 (4H, *d*, *J*=8.7 Hz), 7.30 (4H, *d*, *J*=8.5 Hz), 7.12 (4H, *d*, *J*=8.7 Hz), 6.84 (4H, *d*, *J*=8.5 Hz), 5.0~5.4 (4H, *m*), 2.6~2.4 (8H, *m*), 1.66~1.58 (8H, *m*), 1.0~0.8 (12H, *m*); ^{13}C NMR (DMSO-d_6) δ 197.3, 171.3, 171.0, 153.8, 148.9, 136.4, 133.7, 129.7, 129.0, 121.6, 121.0, 49.4, 41.2, 35.2, 35.1, 17.7, 13.3; MS (70 eV) *m/e* (%) 761 (M^++1, 5), 569 (10), 380 (35), 310 (95), 240 (100), 70 (35); *Anal. Calcd* for $C_{46}H_{48}O_{10}$: C, 72.61, H, 6.36. *Found*: C, 72.66, H, 6.21.

(13) Syn H-H photodimer of 4, 4′-dibutyroxychalcone (II_d)

The residue of mother liquid of IV_d was fractional recrystalized in ethanol—benzene (1:1) to get tiny needle crystal II_d: mp. 158~159°C; UV λ_{max} 253 nm (ε 19,100); IR (cm^{-1}) 3,050, 2,965, 1,756, 1,677, 1,597, 1,503, 1,411, 1,356, 1,208, 1,165, 1,097, 925, 865; ^1H NMR (DMSO-d_6) δ 7.91 (4H, *d*, *J*=8.4 Hz), 7.23 (4H, *d*, *J*=8.1 Hz), 7.19 (4H, *d*, *J*=8.4 Hz), 6.90 (4H, *d*, *J*=8.1 Hz), 5.12 (2H, *d*, *J*=5.4 Hz), 4.29 (2H, *d*, *J*=5.4 Hz),

2.6~2.4 (8H, *m*), 1.7~1.5 (8H, *m*) 1.0~0.8 (12H, *m*); ^{13}C NMR (DMSO-d_6) δ 196.8, 171.1, 170.8, 153.7, 148.4, 136.0, 132.7, 129.2, 128.3, 121.7, 120.7, 47.2, 43.5, 35.0, 17.5, 17.4, 12.5, 12.4; MS (70 eV) *m/e* (%) 761 (M^++1, 50), 569 (45), 409 (55), 381 (30), 339 (40), 310 (32), 269 (25), 240 (30), 191 (18), 175 (20), 121 (100), 71 (25); *Anal. Calcd* for $C_{46}H_{48}O_{10}$: C, 72.61, H, 6.36. *Found*: C, 72.69, H, 6.23.

(14) Anti H-T photodimer of 4, 4′-dibutyroxychalcone (V_d)

The residue of mother liquid of II_d was fractional recrystalized from ethanol—*n*-hexane (1:1) to get tiny needle crystal V_d: mp. 142~143°C; UV λ_{max} 260 nm (ε 18,700); IR (cm^{-1}) 3,050, 2,965, 1,750, 1,670, 1,600, 1,500, 1,400, 1,350, 1,200, 1,160, 1,090, 925, 865, 790; ^{1}H NMR (DMSO-d_6) δ 7.66 (4H, *d*, *J*=8.2 Hz), 7.50 (4H, *d*, *J*=8.0 Hz), 7.06 (4H, *d*, *J*=8.2 Hz), 7.03 (4H, *d*, *J*=8.0 Hz), 4.55 (2H, *t*, *J*=9.0 Hz), 3.89 (2H, *t*, *J*=9.0 Hz), 2.6~2.4 (8H, *m*), 1.7~1.5 (8H, *m*), 1.0~0.9 (12H, *m*); ^{13}C NMR (DMSO-d_6) δ 197.1, 171.5, 171.0, 154.3, 149.5, 137.9, 132.8, 130.1, 128.8, 121.8, 121.7, 51.8, 35.19, 17.74, 17.61, 13.20; MS (70 eV) *m/e* (%) 760 (M^+, 35), 742 (35), 569 (45), 554 (45), 381 (35), 310 (100), 240 (95), 191 (20), 70 (35); *Anal. Calcd* for $C_{46}H_{48}O_{10}$: C, 72.61, H, 6.36. *Found*: C, 72.28, H, 6.30.

(15) Syn H-T photodimer of 4, 4′-diisobutyroxychalcone (IV_e)

The product, resulted from 4, 4′-diisobutyroxychalcone upon irriadiation with UV light for 2 days was recrystalized in benzene—*n*-hexane (1:1) to get while crystal IV_e: mp. 255~257°C; UV λ_{max} 258.6 nm (ε 19,300); IR (cm^{-1}) 3,050, 2,937, 1,757, 1,664, 1,597, 1,501, 1,466, 1,409, 1,383, 1,302, 1,258, 1,235, 1,201, 1,168, 1,122, 1,104, 1,043, 1,015, 986, 916, 870, 809; ^{1}H NMR (DMSO-d_6) δ 7.85 (4H, *d*, *J*=8.7 Hz), 7.31 (4H, *d*, *J*=8.6 Hz), 7.13 (4H, *d*, *J*=8.7 Hz), 6.84 (4H, *d*, *J*=8.6 Hz), 5.0~4.8 (4H, *m*), 2.78 (2H, hept, *J*=6.9 Hz), 2.71 (2H, hept, *J*=6.9 Hz), 1.21 (12H, *d*, *J*=6.9 Hz), 1.16 (12H, *d*, *J*=6.9 Hz); ^{13}C NMR (DMSO-d_6) δ 197.3, 174.6, 174.3, 154.0, 149.2, 136.4, 133.7, 129.7, 129.0, 121.6, 120.9, 52.0, 42,4, 28.9, 8.82; MS (70 eV) *m/e* (%) 760 (M^+, 5), 569 (10), 380 (65), 310 (100), 240 (43), 70 (48); *Anal. Calcd* for $C_{46}H_{48}O_{10}$: C, 72.61, H, 6.36. *Found*: C, 72.80, H, 6.44.

4. ACKNOWLEDGEMENT

We are indebted to the National Science Council of the Republic of China for financial support of this research. We are also grateful to Professor Yu Wang, Department of Chemistry, National Taiwan University, for helpful X-ray data collection.

REFERENCES

(1) H. Stobbe and A. Hensel, *Ber.*, **59**, 2260 (1926).
(2) A. Mustafa, *Chem. Rev.*, **51**, 1 (1952).
(3) V. Ramamurthy, *Tetrahedron*, **42**, 5753 (1986).
(4) S.P. Panda, *J. Appl. Polym. Sci.*, **18**, 2317 (1974).
(5) S.A. Zahir, *J. Appl. Polym. Sci.*, **23**, 1355 (1979).
(6) M.D. Cohn and G.M.J. Schmidt, *J. Chem. Soc.*, 1996 (1964).
(7) M.D. Cohn, G.M.J. Schmidt and F.I. Sonntag, *J. Chem. Soc.*, 2000 (1964).
(8) G.M.J. Schmidt, *J. Chem. Soc.*, 2014 (1964).
(9) A.C. Legon, *Chem. Rev.*, **80**, 231 (1980).
(10) Jung-Nan Chen and Jen-Yeh Wun, International Symposium on Inorganic and Organic Chemistry, Taipei Taiwan, Abstract No. 0-20, November 20 (1992).
(11) In our other series of studies on nitrochalcones, 3′-nitrochalcone was found to undergo stereospecific photodimerization to get syn H-T photodimer. The syn H-T photodimer of 3′-nitrochalcone shows a strong solvent effect on NMR signals. The protons on the cyclobutane ring of the photodimer of 3′-nitrochalcone show typical AA′BB′ multiplets at 5.05 ppm in DMSO-d_6 and show two peaks (doublet of doublet) at 5.06 and 4.77 ppm with J_{AB}=10.8 Hz and $J_{AB'}$=6.9 Hz in $CDCl_3$. This phenomenon does not happen in the case of syn H-T photodimers of 4,4′-diacyloxychalcones. However it is a good evidence for structural determination of syn H-T photodimers of chalcones ($J_{trans} \neq J_{cis} \neq 0$ Hz).

取代基大小改變對查克酮衍生物光偶合反應之影響

陳 榮 男
輔仁大學化學系

摘 要

我們以不同大小的醯氧基之 4,4′-二醯氧基查克酮 (4,4′-diacyloxychalcones) 爲材料，進行這類查克酮衍生物之固態照光 (2+2) 偶合反應研究。改變這些醯氧基後，我們發現這些 4,4′-二氫氧基查克酮 (4,4′-dihydroxychalcone) 的二元酮衍生物，它們在固態照光偶合反應方面，無論是反應活性或產物分配，都有明顯變化。我們也以 4,4′-二丙醯氧基查克酮和 4,4′-二異丁醯氧基查克酮的 X-ray 結構分析，來解說兩者之間反應活性和產物分配的異同。

SYNTHESIS OF NOVEL CHARGED THERMOTROPIC LIQUID CRYSTALS

WIN-LONG CHIA*, RONG-CHUNG CHEN,
YU-KOON SHAW AND CHUN-NAN CHEN
Department of Chemistry
Fu Jen Catholic University
Taipei, Taiwan 24205, R.O.C.

HONG-CHEU LIN*
Institute of Chemistry
Academia Sinica
Taipei, Taiwan, R.O.C.

ABSTRACT

Three new series of charged thermotropic mesogens, *trans*-4-(*p'*-alkoxystyryl)-1-methylpyridinium iodide [$(C_nH_{2n+1}OC_6H_4CH{=}CHC_5H_4NCH_3)^+I^-$] (abbreviated as $PSOC_n$), *trans*-4-(*p'*-alkoxystyryl)-1,3-dimethylpyridinium iodide (abbreviated as $LSOC_n$), and *trans*-4-(*p'*-alkoxystyryl)-3-ethyl-1-methylpyridinium iodide (abbreviated as $CSOC_n$), are synthesized for all homologues between methoxy ($n=1$) and tetradecanoxy ($n=14$) and those of $n=16$, 18. Excellent yields are usually obtained.

1. INTRODUCTION

Liquid crystalline (mesogenic) compounds are well known to be differentitated into thermotropic, which change phases on heating, and lyotropic, which usually contain charged molecules and undergo phase changes on addition of solvents. Unfortunately, charged thermotropic liquid crystalline compounds are rarely studied up to now[1]. Introduction of charges into thermotropic liquid crystals may be potentially desired because certain properties such as colour, paramagnetism and electrical conductivity may be conveniently generated in these charged molecules. Molecular properties such as polarizability or hyperpolarizability can also be enhanced by the introduction of charges into thermotropic liquid crystals, and this could result in enhanced refractive indices and large non-linear optical coefficients[2].

In this paper we wish to report the synthesis of three new series of charged mesogens: *trans*-4-(*p'*-alkoxystyryl)-1-methylpyridinium iodides of general formula $[(C_nH_{2n+1}OC_6H_4CH{=}CHC_5H_4NCH_3)^+I^-]$ (abbreviated to $PSOC_n$, where *n* denotes the number of carbon atoms in the terminal alkyl chain), *trans*-4-(*p'*-alkoxystyryl)-1, 3-dimethylpyridinium iodide (abbreviated as $LSOC_n$) and *trans*-4-(*p'*-alkoxystyryl)-3-ethyl-1-methylpyridinium iodide (abbreviated as $CSOC_n$).

2. RESULTS AND DISCUSSION

Preparation of *trans*-4-(*p'*-alkoxystyryl)-1-methylpyridinium iodides and its 3-methyl and 3-ethyl analogues were done by condensation reactions between various 4-alkoxybenzaldehydes with pyridine methiodide using piperidine as the catalyst in which pyridine methiodide can be prepared by reacting pyridine with methyl iodide under methanol reflux (Scheme 1). This type of reactions can be proceeded in an one-pot and mild conditions[3]. Yields of these reactions were found to be excellent (83~96%, see Tables 1~3). Trans isomers were found to be

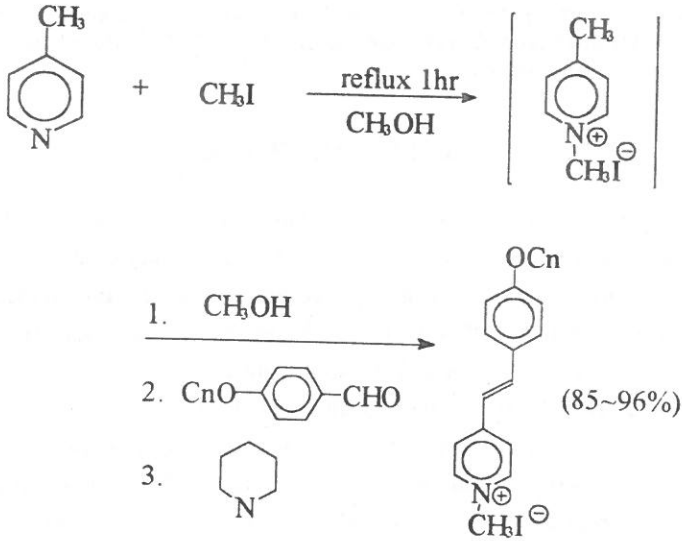

Scheme 1

Table 1. Physical properties of 4-(*p'*-alkoxystyryl)-1-methylpyridinium iodide

Compound	Yield	^{1}H NMR	IR	Mass
$PSOC_1$	92	3.80 (*s*, 3H), 4.22 (*s*, 3H), 7.36 (*d*, 1H, *J*=16 Hz), 7.71 (*d*, 2H, *J*=8.7 Hz), 7.79 (*d*, 1H, *J*=16 Hz), 8.15 (*d*, 2H, *J*=6.7 Hz), 8.79 (*d*, 2H, *J*=6.7 Hz)	1,605, 1,186	226 (100), 353 (5)
$PSOC_2$	87	1.31 (*t*, 3H, *J*=6 Hz), 4.06 (*q*, 2H, *J*=6.1 Hz), 4.22 (*s*, 3H), 7.01 (*d*, 2H, *J*=8.4 Hz), 7.35 (*d*, 1H, *J*=16 Hz), 7.69 (*d*, 2H, *J*=8.4 Hz), 7.97 (*d*, 1H, *J*=16 Hz), 8.16 (*d*, 2H, *J*=6.3 Hz), 8.80 (*d*, 2H, *J*=6.3 Hz)	1,608, 1,188	240 (100), 367 (4)
$PSOC_3$	86	0.96 (*t*, 3H, *J*=6 Hz), 1.72 (*m*, 2H), 3.97 (*t*, 2H, *J*=7 Hz), 4.22 (*s*, 3H), 7.02 (*d*, 2H, *J*=9 Hz), 7.35 (*d*, 1H, *J*=16 Hz), 7.69 (*d*, 2H, *J*=9 Hz), 7.96 (*d*, 1H, *J*=16 Hz), 8.15 (*d*, 2H, *J*=6 Hz), 8.90 (*d*, 2H, *J*=6 Hz)	1,591, 1,175	254 (100), 381 (1)
$PSOC_4$	86	0.91 (*t*, 3H, *J*=6 Hz), 1.41 (*m*, 2H), 1.68 (*m*, 2H), 4.01 (*t*, 2H, *J*=7 Hz), 4.22 (*s*, 3H), 7.02 (*d*, 2H, *J*=9 Hz), 7.35 (*d*, 1H, *J*=16 Hz), 7.68 (*d*, 2H, *J*=9 Hz), 7.96 (*d*, 1H, *J*=16 Hz), 8.20 (*d*, 2H, *J*=6 Hz), 8.90 (*d*, 2H, *J*=6 Hz)	1,598, 2,970, 1,181	268 (100), 395 (2)
$PSOC_5$	90	0.87 (*t*, 3H, *J*=6 Hz), 3.39 (*m*, 2H), 1.70 (*m*, 2H), 4.00 (*t*, 2H, *J*=6 Hz), 4.22 (*s*, 3H), 7.01 (*d*, 2H, *J*=9 Hz), 7.35 (*d*, 1H, *J*=16 Hz), 7.68 (*d*, 2H, *J*=9 Hz), 7.96 (*d*, 1H, *J*=16 Hz), 8.16 (*d*, 2H, *J*=6 Hz), 8.90 (*d*, 2H, *J*=6 Hz)	2,980, 1,604, 1,185	282 (100), 409 (2)
$PSOC_6$	88	0.86 (*d*, 2H, *J*=6 Hz), 1.30 *m*, 3H), 1.37 (*m*, 2H), 1.70 (*p*, 2H, *J*=6 Hz), 4.01 (*d*, 2H, *J*=6 Hz), 4.22 (*s*, 3H), 7.03 (*d*, 2H, *J*=9 Hz), 7.35 (*d*, 1H, *J*=16 Hz), 7.68 (*d*, 2H, *J*=9 Hz), 7.96 (*d*, 1H, *J*=16 Hz), 8.14 (*d*, 2H, *J*=6 Hz), 8.80 (*d*, 2H, *J*=6 Hz)	2,960, 1,594, 1,173	296 (100), 423 (2)
$PSOC_7$	83.9	0.84 (*t*, 3H, *J*=6 Hz), 1.29 (*m*, 8H), 1.67 (*p*, 2H, *J*=6 Hz), 4.00 (*t*, 2H, *J*=7 Hz), 4.22 (*s*, 2H), 7.01 (*d*, 2H, *J*=9 Hz), 7.35 (*d*, 1H, *J*=16 Hz), 8.16 (*d*, 2H, *J*=6 Hz), 8.80 (*d*, 2H, *J*=6 Hz)	2,944, 1,594, 1,172	310 (100), 437 (2)
$PSOC_8$	85.2	0.84 (*t*, 2H), 1.30 (*m*, 10H), 1.70 (*p*, 2H, *J*=6 Hz), 4.00 (*t*, 2H, *J*=6 Hz), 4.22 (*s*, 3H), 7.02 (*d*, 2H, *J*=9 Hz), 7.35 (*d*, 1H, *J*=16 Hz), 7.68 (*d*, 2H, *J*=9 Hz), 7.96 (*d*, 1H, *J*=16 Hz), 8.15 (*d*, 2H, *J*=6 Hz), 8.80 (*d*, 2H, *J*=6 Hz)	2,942, 1,593, 1,174	324 (100), 451 (1)

Table 1. Physical properties of 4-(*p'*-alkoxystyryl)-1-methylpyridinium iodide (Continued)

Compound	Yield	^{1}H NMR	IR	Mass
$PSOC_9$	83.5	0.88 (*t*, 3H, *J*=6 Hz), 1.35 (*m*, 12H), 1.81 (*p*, 2H, *J*=6 Hz), 3.98 (*t*, 2H, *J*=6 Hz), 4.48 (*s*, 3H), 6.91 (*d*, 2H, *J*=9 Hz), 7.00 (*d*, 1H, *J*=15.6 Hz), 7.59 (*d*, 2H, *J*=9 Hz), 7.65 (*d*, 1H, *J*=15.6 Hz), 7.96 (*s*, 2H), 8.93 (*s*, 2H)	2,955, 1,594, 1,170	338 (100), 465 (7)
$PSOC_{10}$	82.7	0.87 (*t*, 3H, *J*=6 Hz), 1.27 (*m*, 14H), 1.79 (*p*, 2H, *J*=6 Hz), 3.98 (*t*, 2H, *J*=6 Hz), 4.48 (*s*, 3H), 6.91 (*d*, 2H, *J*=9 Hz), 7.00 (*d*, 1H, *J*=15.6 Hz), 7.58 (*d*, 2H, *J*=9 Hz), 7.65 (*d*, 1H, *J*=15.6 Hz), 7.96 (*d*, 2H, *J*=6 Hz), 8.97 (*s*, 2H)	1,939, 1,597, 1,177	352 (100), 479 (6)
$PSOC_{11}$	86.4	0.87 (*t*, 3H, *J*=6 Hz), 1.26 (*m*, 14H), 1.45 (*m*, 2H), 3.98 (*t*, 3H, *J*=6 Hz), 4.52 (*s*, 3H), 6.91 (*d*, 2H, *J*=9 Hz), 6.99 (*d*, 1H, *J*=15.6 Hz), 7.58 (*d*, 2H, *J*=9 Hz), 7.65 (*d*, 1H, *J*=15.6 Hz), 7.94 (*d*, 2H, *J*=6 Hz), 9.00 (*d*, 2H, *J*=6 Hz)	2,939, 1,592, 1,172	366 (100), 493 (1)
$PSOC_{12}$	87.1	0.87 (*t*, 3H, *J*=6 Hz), 1.26 (*m*, 14H), 1.45 (*m*, 2H), 1.81 (*m*, 2H), 3.98 (*t*, 2H, *J*=7 Hz), 4.51 (*s*, 3H), 6.92 (*d*, 2H, *J*=9 Hz), 6.98 (*d*, 1H, *J*=15.6 Hz), 7.57 (*d*, 2H, *J*=9 Hz), 7.66 (*d*, 1H, *J*=15.6 Hz), 7.94 (*d*, 2H, *J*=6 Hz), 8.97 (*d*, 2H, *J*=6 Hz)	2,954, 1,595, 1,171	380 (100), 507 (2)
$PSOC_{13}$	89.4	0.87 (*t*, 3H, *J*=6 Hz), 1.26 (*m*, 16H), 1.45 (*m*, 2H), 1.80 (*p*, 2H, *J*=6 Hz), 4.00 (*t*, 2H, *J*=6 Hz), 4.56 (*s*, 3H), 6.95 (overlap, 3H), 7.57 (*d*, 2H, *J*=9 Hz), 7.68 (*d*, 1H, *J*=15.6 Hz), 7.92 (*d*, 2H, *J*=6 Hz), 9.05 (*s*, 2H)	2,936, 1,595, 1,171	394 (100), 521 (1)
$PSOC_{14}$	92.8	0.87 (*t*, 3H, *J*=6 Hz), 1.26 (*m*, 20H), 1.45 (*m*, 2H), 1.79 (*p*, 2H, *J*=6 Hz), 3.99 (*t*, 2H, *J*=6 Hz), 4.55 (*s*, 3H), 6.94 (overlap, 3H), 7.57 (*d*, 2H, *J*=6 Hz), 7.63 (*d*, 1H, *J*=15.6 Hz), 7.92 (*d*, 2H, *J*=6 Hz), 9.05 (*s*, 2H)	2,936, 1,595, 1,172	408 (100), 535 (1)
$PSOC_{16}$	91.3	0.87 (*t*, 3H, *J*=6 Hz), 1.26 (*m*, 24H), 1.45 (*m*, 2H), 1.80 (*p*, 2H, *J*=6 Hz), 4.00 (*t*, 2H, *J*=6 Hz), 4.57 (*s*, 3H), 6.95 (overlap, 3H), 7.57 (*d*, 2H, *J*=9 Hz), 7.63 (*d*, 1H, *J*=15.6 Hz), 7.90 (*d*, 2H, *J*=6 Hz), 9.07 (*s*, 2H)	2,960, 1,594, 1,173	436 (100), 563 (1)
$PSOC_{18}$	91.6	0.87 (*t*, 3H, *J*=6 Hz), 1.26 (*m*, 28H), 1.46 (*m*, 2H), 1.80 (*p*, 2H, *J*=6 Hz), 4.00 (*t*, 2H, *J*=6 Hz), 4.58 (*s*, 3H), 6.93 (*d*, 2H, *J*=9 Hz), 6.97 (*d*, 2H, *J*=15.6 Hz), 7.90 (*d*, 2H, *J*=6 Hz), 9.11 (*s*, 2H)	2,932, 1.592, 1,172	464 (100), 591 (2)

Table 2. Physical properties of 3-methyl-4-(*p'*-alkoxystyryl)-1-methylpyridinium iodide

Compound	Yield	^{1}H NMR	IR	Mass
$LSOC_1$	83.5	2.52 (*s*, 3H), 3.82 (*s*, 3H), 4.20 (*s*, 3H), 7.04 (*d*, 2H, *J*=9 Hz), 7.32 (*d*, 1H, *J*=16 Hz), 7.78 (*d*, 2H, *J*=8.8 Hz), 7.89 (*d*, 1H, *J*=16 Hz), 8.32 (*d*, 1H, *J*=7 Hz), 8.68 (*d*, 1H, *J*=7 Hz), 8.76 (*s*, 1H)	3,025, 1,643, 1,598	240 (100), 367 (1)
$LSOC_2$	92.0	1.34 (*t*, 3H, *J*=7 Hz), 2.50 (*s*, 3H), 4.09 (*q*, 2H, *J*=7 Hz), 4.19 (*s*, 3H), 7.02 (*d*, 2H, *J*=9 Hz), 7.31 (*d*, 1H, *J*=6 Hz), 7.77 (*d*, 2H, *J*=8.8 Hz), 7.90 (*d*, 1H, *J*=16 Hz), 8.32 (*d*, 1H, *J*=7 Hz), 8.68 (*d*, 1H, *J*=7 Hz), 8.75 (*s*, 1H)	3,025, 1,638, 1,598	254 (100), 381 (1)
$LSOC_3$	87.1	0.97 (*t*, 3H, *J*=7 Hz), 2.31 (*m*, 2H), 2.50 (*s*, 3H), 3.98 (*t*, 2H, *J*=7 Hz), 4.19 (*s*, 3H), 7.02 (*d*, 2H, *J*=9 Hz), 7.31 (*d*, 1H, *J*=16 Hz), 7.77 (*d*, 2H, *J*=8.8 Hz), 7.90 (*d*, 1H, *J*=16 Hz), 8.33 (*d*, 1H, *J*=7 Hz), 8.68 (*d*, 1H, *J*=7 Hz), 8.76 (*s*, 1H)	3,023, 1,642, 1,601	268 (100), 395 (1)
$LSOC_4$	83.6	0.93 (*t*, 3H, *J*=7 Hz), 1.44 (*m*, 2H), 1.70 (*m*, 2H), 2.50 (*s*, 3H), 4.03 (2H, *J*=7 Hz), 4.19 (*s*, 3H), 7.02 (*d*, 2H, *J*=9 Hz), 7.31 (*d*, 1H, *J*=16 Hz), 7.77 (*d*, 2H, *J*=8.8 Hz), 7.90 (*d*, 1H, *J*=16 Hz), 8.32 (*d*, 1H, *J*=7 Hz), 8.68 (*d*, 1H, *J*=7 Hz), 8.75 (*s*, 1H)	2,950, 1,642, 161	282 (100), 409 (1)
$LSOC_5$	86.0	0.88 (*t*, 3H, *J*=7 Hz), 1.35 (*m*, 4H), 1.71 (*m*, 2H), 2.50 (*s*, 3H), 4.01 (*t*, 2H, *J*=7 Hz), 4.19 (*s*, 3H), 7.02 (*d*, 2H, *J*=9 Hz), 7.31 (*d*, 1H, *J*=16 Hz), 7.77 (*d*, 2H, *J*=8.8 Hz), 7.90 (*d*, 1H, *J*=16 Hz), 8.33 (*d*, 1H, *J*=7 Hz), 8.68 (*d*, 1H, *J*=7 Hz), 8.76 (*s*, 1H)	2,950, 1,640, 1,593	296 (100), 423 (1)
$LSOC_6$	83.7	0.87 (*t*, 3H, *J*=7 Hz), 1.30 (*m*, 6H), 1.70 (*m*, 2H), 2.51 (*s*, 3H), 4.02 (*t*, 2H, *J*=7 Hz), 4.19 (*s*, 3H), 7.02 (*d*, 2H, *J*=9 Hz), 7.31 (*d*, 1H, *J*=16 Hz), 7.77 (*d*, 2H, *J*=8.8 Hz), 7.89 (*d*, 1H, *J*=16 Hz), 8.32 (*d*, 1H, *J*=7 Hz), 8.68 (*d*, 1H, *J*=7 Hz), 8.75 (*s*, 1H)	2,964, 1,641, 1,599	310 (100), 437 (1)
$LSOC_7$	83.2	0.86 (*t*, 3H, *J*=7 Hz), 1.33 (*m*, 8H), 1.70 (*m*, 2H), 2.51 (*s*, 3H), 4.02 (*t*, 2H, *J*=7 Hz), 4.19 (*s*, 3H), 7.02 (*d*, 2H, *J*=9 Hz), 7.31 (*d*, 1H, *J*=16 Hz), 7.77 (*d*, 2H, *J*=8.8 Hz), 7.89 (*d*, 1H, *J*=16 Hz), 8.32 (*d*, 1H, *J*=7 Hz), 8.68 (*d*, 1H, *J*=7 Hz), 8.75 (*s*, 1H)	2,935, 1,644, 1.601	324 (100), 451 (1)
$LSOC_8$	83.3	0.86 (*t*, 3H, *J*=7 Hz), 1.32 (*m*, 10H), 1.71 (*m*, 2H), 2.50 (*s*, 3H), 4.03 (*t*, 2H, *J*=7 Hz), 4.19 (*s*, 3H), 7.02 (*d*, 2H, *J*=9 Hz), 7.31 (*d*, 1H, *J*=16 Hz), 7.77 (*d*, 2H, *J*=8.8 Hz), 7.89 (*d*, 1H, *J*=16 Hz), 8.32 (*d*, 1H, *J*=7 Hz), 8.68 (*d*, 1H, *J*=7 Hz), 8.75 (*s*, 1H)	2,941, 1,642, 1,601	338 (100), 465 (1)

Table 2. Physical properties of 3-methyl-4-(*p'*-alkoxystyryl)-1-methylpyridinium iodide (Continued)

Compound	Yield	^{1}H NMR	IR	Mass
$LSOC_9$	85.2	0.84 (*t*, 3H, *J*=6 Hz), 1.24 (*m*, 12H), 1.71 (*m*, 2H), 2.51 (*s*, 3H), 4.01 (*t*, 2H, *J*=7 Hz), 4.19 (*s*, 3H), 7.02 (*d*, 2H, *J*=9 Hz), 7.31 (*d*, 1H, *J*=16 Hz), 7.77 (*d*, 2H, *J*=8.8 Hz), 7.89 (*d*, 1H, *J*=16 Hz), 8.31 (*d*, 1H, *J*=7 Hz), 8.68 (d, 1H, *J*=7 Hz), 8.75 (*s*, 1H)	2,923, 1,643, 1,600	352 (100), 479 (1)
$LSOC_{10}$	83.41	0.84 (*t*, 3H, *J*=6 Hz), 1.24 (*m*, 14H), 1.71 (*m*, 2H), 2.51 (*s*, 3H), 4.01 (*t*, 2H, *J*=7 Hz), 4.19 (*s*, 3H), 7.02 (*d*, 2H, *J*=9 Hz), 7.31 (*d*, 1H, *J*=16 Hz), 7.77 (*d*, 2H, *J*=8.8 Hz), 7.89 (*d*, 1H, *J*=16 Hz), 8.31 (*d*, 1H, *J*=7 Hz), 8.68 (*d*, 1H, *J*=7 Hz), 8.75 (*s*, 1H)	2,922, 1,642, 1,957	366 (100), 493 (1)
$LSOC_{11}$	85.8	0.83 (*t*, 3H, *J*=6 Hz), 1.22 (*m*, 16H), 1.73 (*m*, 2H), 2.51 (*s*, 3H), 3.92 (*t*, 2H, *J*=7 Hz), 4.41 (*s*, 3H), 6.86 (*d*, 2H, *J*=9 Hz), 6.97 (*d*, 1H, *J*=16 Hz), 7.56 (*d*, 2H, *J*=8.8 Hz), 7.62 (*d*, 1H, *J*=16 Hz), 8.15 (*d*, 1H, *J*=7 Hz), 8.79 (*d*, 1H, *J*=7 Hz), 8.92 (*s*, 1H)	2,921, 1,642, 1,599	380 (100), 507 (1)
$LSOC_{12}$	88.8	0.85 (*t*, 3H, *J*=6 Hz), 1.34 (*m*, 18H), 1.75 (*m*, 2H), 2.54 (*s*, 3H), 3.95 (*t*, 2H, *J*=7 Hz), 4.45 (*s*, 3H), 6.89 (*d*, 2H, *J*=9 Hz), 7.00 (*d*, 1H, *J*=16 Hz), 7.58 (*d*, 2H, *J*=8.8 Hz), 7.63 (*d*, 1H, *J*=16 Hz), 8.16 (*d*, 1H, *J*=7 Hz), 8.82 (*d*, 1H, *J*=7 Hz), 8.98 (*s*, 1H)	2,923, 1,638, 1,599	394 (100), 521 (1)
$LSOC_{13}$	85.3	0.85 (*t*, 3H, *J*=6 Hz), 1.24 (*m*, 20H), 1.75 (*m*, 2H), 2.54 (*s*, 3H), 3.95 (*t*, 2H, *J*=7 Hz), 4.45 (*s*, 3H), 6.89 (*d*, 2H, *J*=9 Hz), 7.00 (*d*, 1H, *J*=16 Hz), 7.58 (*d*, 2H, *J*=8.8 Hz), 7.64 (*d*, 1H, *J*=16 Hz), 8.16 (*d*, 1H, *J*=7 Hz), 8.83 (*d*, 1H, *J*=7 Hz), 8.96 (*s*, 1H)	2,922, 1,644, 1,600	408 (100), 535 (2)
$LSOC_{14}$	91.5	0.87 (*t*, 3H, *J*=6 Hz), 1.34 (*m*, 22H), 1.77 (*m*, 2H), 2.57 (*s*, 3H), 3.99 (*t*, 2H, *J*=7 Hz), 4.49 (*s*, 3H), 6.92 (*d*, 2H, *J*=9 Hz), 7.02 (*d*, 1H, *J*=16 Hz), 7.59 (*d*, 2H, *J*=8.8 Hz), 7.63 (*d*, 1H, *J*=16 Hz), 8.14 (*d*, 1H, *J*=7 Hz), 8.86 (*d*, 1H, *J*=7 Hz), 8.97 (*s*, 1H)	2,921, 1,637, 1,598	422 (100), 549 (2)
$LSOC_{16}$	96.2	0.87 (*t*, 3H, *J*=6 Hz), 1.28 (*m*, 26H), 1.77 (*m*, 2H), 2.59 (*s*, 3H), 4.00 (*t*, 2H, *J*=7 Hz), 4.50 (*s*, 3H), 6.93 (*d*, 2H, *J*=9 Hz), 7.04 (*d*, 1H, *J*=16 Hz), 7.57 (*d*, 2H, *J*=8.8 Hz), 7.62 (*d*, 1H, *J*=16 Hz), 8.12 (*d*, 1H, *J*=7 Hz), 8.86 (*d*, 1H, *J*=7 Hz), 8.93 (*s*, 1H)	2,921, 1,641, 1,512	450 (100), 577 (1)
$LSOC_{18}$	88.9	0.87 (*t*, 3H, *J*=6 Hz), 1.29 (*m*, 30H), 1.79 (*m*, 2H), 2.59 (*s*, 3H), 4.01 (*t*, 2H, *J*=7 Hz), 4.50 (*s*, 3H), 6.94 (*d*, 2H, *J*=9 Hz), 7.04 (*d*, 1H, *J*=16 Hz), 7.57 (*d*, 2H, *J*=8.8 Hz), 7.62 (*d*, 1H, *J*=16 Hz), 8.12 (*d*, 1H, *J*=7 Hz), 8.82 (*d*, 1H, *J*=7 Hz), 8.92 (*s*, 1H)	2,921, 1,657, 1,597	478 (100), 605 (1)

Table 3. Physical properties of 3-ethyl-4-(*p'*-alkoxystyryl)-1-methylpyridinium iodide

Compound	Yield	^{1}H NMR	Mass
$CSOC_1$	96	1.22 (*t*, 3H, *J*=7 Hz), 2.97 (*q*, 2H, *J*=7 Hz), 3.81 (*s*, 3H), 4.22 (*s*, 3H), 7.03 (*d*, 2H, *J*=9 Hz), 7.35 (*d*, 1H, *J*=16 Hz), 7.78 (*d*, 2H, *J*=8.8 Hz), 7.90 (*d*, 1H, *J*=16 Hz), 8.35 (*d*, 1H, *J*=7 Hz), 8.69 (*d*, 1H, *J*=7 Hz), 8.74 (*s*, 1H)	254 (100), 381 (0.4)
$CSOC_2$	95	1.22 (*t*, 3H, *J*=7 Hz), 1.32 (*t*, 3H, *J*=7 Hz), 2.93 (*q*, 2H, *J*=7 Hz), 4.07 (*q*, 2H, *J*=7 Hz), 4.22 (*s*, 3H), 7.00 (*d*, 2H, *J*=9 Hz), 7.33 (*d*, 1H, *J*=16 Hz), 7.77 (*d*, 2H, *J*=8.8 Hz), 7.90 (*d*, 1H, *J*=16 Hz), 8.35 (*d*, 1H, *J*=7 Hz), 8.69 (*d*, 1H, *J*=7 Hz), 8.74 (*s*, 1H)	268 (100), 395 (0.4)
$CSOC_3$	89	0.97 (*t*, 3H, *J*=7 Hz), 1.22 (*t*, 3H, *J*=7 Hz), 1.73 (*m*, 2H), 2.96 (*q*, 2H, *J*=7 Hz), 3.98 (*q*, 2H, *J*=7 Hz), 4.21 (*s*, 3H), 7.01 (*d*, 2H, *J*=9 Hz), 7.35 (*d*, 1H, *J*=16 Hz), 7.78 (*d*, 2H, *J*=8.8 Hz), 7.89 (*d*, 1H, *J*=16 Hz), 8.33 (*d*, 1H, *J*=7 Hz), 8.69 (*d*, 1H, *J*=7 Hz), 8.72 (*s*, 1H)	282 (100), 409 (0.4)
$CSOC_4$	85.8	0.92 (*t*, 3H, *J*=7 Hz), 1.22 (*t*, 3H, *J*=7 Hz), 1.41 (*m*, 2H), 1.70 (*m*, 2H), 2.96 (*q*, 2H, *J*=7 Hz), 4.02 (*q*, 2H, *J*=7 Hz), 4.22 (*s*, 3H), 7.01 (*d*, 2H, *J*=9 Hz), 7.34 (*d*, 1H, *J*=16 Hz), 7.77 (*d*, 2H, *J*=8.8 Hz), 7.90 (*d*, 1H, *J*=16 Hz), 8.34 (*d*, 1H, *J*=7 Hz), 8.69 (*d*, 1H, *J*=7 Hz), 8.73 (*s*, 1H)	296 (100), 423 (0.4)
$CSOC_5$	90.2	0.89 (*t*, 3H, *J*=7 Hz), 1.22 (*t*, 3H, *J*=7 Hz), 1.35 (*m*, 4H), 1.72 (*m*, 2H), 2.95 (*q*, 2H, *J*=7 Hz), 4.02 (*q*, 2H, *J*=7 Hz), 4.22 (*s*, 3H), 7.01 (*d*, 2H, *J*=9 Hz), 7.34 (*d*, 1H, *J*=16 Hz), 7.77 (*d*, 2H, *J*=8.8 Hz), 7.90 (*d*, 1H, *J*=16 Hz), 8.34 (*d*, 1H, *J*=7 Hz), 8.69 (*d*, 1H, *J*=7 Hz), 8.73 (*s*, 1H)	310 (100), 437 (0.4)
$CSOC_6$	87.8	0.89 (*t*, 3H, *J*=7 Hz), 1.22 (*t*, 3H, *J*=7 Hz), 1.32 (*m*, 6H), 1.72 (*m*, 2H), 2.95 (*q*, 2H, *J*=7 Hz), 4.02 (*q*, 2H, *J*=7 Hz), 4.21 (*s*, 3H), 7.01 (*d*, 2H, *J*=9 Hz), 7.34 (*d*, 1H, *J*=16 Hz), 7.77 (*d*, 2H, *J*=8.8 Hz), 7.89 (*d*, 1H, *J*=16 Hz), 8.33 (*d*, 1H, *J*=7 Hz), 8.86 (*d*, 1H, *J*=7 Hz), 8.72 (*s*, 1H)	324 (100), 451 (0.5)
$CSOC_7$	88.9	0.85 (*t*, 3H, *J*=7 Hz), 1.22 (*t*, 3H, *J*=7 Hz), 1.31 (*m*, 8H), 1.71 (*m*, 2H), 2.95 (*q*, 2H, *J*=7 Hz), 4.02 (*q*, 2H, *J*=7 Hz), 4.21 (*s*, 3H), 7.01 (*d*, 2H, *J*=9 Hz), 7.34 (*d*, 1H, *J*=16 Hz) 7.77 (*d*, 2H, *J*=8.8 Hz), 7.89 (*d*, 1H, *J*=16 Hz), 8.33 (*d*, 1H, *J*=7 Hz), 8.69 (*d*, 1H, *J*=7 Hz), 8.72 (s, 1H)	338 (100), 465 (0.5)
$CSOC_8$	86.4	0.85 (*t*, 3H, *J*=7 Hz), 1.22 (*t*, 3H, *J*=7 Hz), 1.31 (*m*, 10H), 1.71 (*m*, 2H), 2.95 (*q*, 2H, *J*=7 Hz), 4.02 (*q*, 2H, *J*=7 Hz), 4.21 (*s*, 3H), 7.01 (*d*, 2H, *J*=9 Hz), 7.34 (*d*, 1H, *J*=16 Hz), 7.77 (*d*, 2H, *J*=8.8 Hz), 7.89 (*d*, 1H, *J*=16 Hz), 8.33 (*d*, 1H, *J*=7 Hz), 8.69 (*d*, 1H, *J*=7 Hz), 8.72 (*s*, 1H)	352 (100), 479 (0.5)

Table 3. Physical properties of 3-ethyl-4-(*p'*-alkoxystyryl)-1-methylpyridinium iodide (Continued)

Compound	Yield	^{1}H NMR	Mass
$CSOC_9$	85.7	0.84 (*t*, 3H, *J*=7 Hz), 1.23 (*m*, 15H), 1.70 (*m*, 2H), 2.95 (*q*, 2H, *J*=7 Hz), 4.00 (*q*, 2H, *J*=7 Hz), 4.22 (*s*, 3H), 7.01 (*d*, 2H, *J*=9 Hz), 7.34 (*d*, 1H, *J*=16 Hz), 7.77 (*d*, 2H, *J*=8.8 Hz), 7.87 (*d*, 1H, *J*=16 Hz), 8.34 (*d*, 1H, *J*=7 Hz), 8.69 (*d*, 1H, *J*=7 Hz), 8.73 (*s*, 1H)	366 (100), 493 (0.5)
$CSOC_{10}$	84.6	0.84 (*t*, 3H, *J*=7 Hz), 1.22 (*m*, 17H), 1.70 (*m*, 2H), 2.95 (*q*, 2H, *J*=7 Hz), 4.00 (*q*, 2H, *J*=7 Hz), 4.22 (*s*, 3H), 7.01 (*d*, 2H, *J*=9 Hz), 7.35 (*d*, 1H, *J*=16 Hz), 7.77 (*d*, 2H, *J*=8.8 Hz), 7.87 (*d*, 1H, *J*=16 Hz), 8.34 (*d*, 1H, *J*=7 Hz), 8.69 (*d*, 1H, *J*=7 Hz), 8.73 (*s*, 1H)	380 (100), 507 (0.5)
$CSOC_{11}$	86.1	0.84 (*t*, 3H, *J*=7 Hz), 1.22 (*m*, 19H), 1.71 (*m*, 2H), 2.95 (*q*, 2H, *J*=7 Hz), 4.02 (*q*, 2H, *J*=7 Hz), 4.21 (*s*, 3H), 7.01 (*d*, 2H, *J*=9 Hz), 7.35 (*d*, 1H, *J*=16 Hz), 7.77 (*d*, 2H, *J*=8.8 Hz), 7.87 (*d*, 1H, *J*=16 Hz), 8.33 (*d*, 1H, *J*=7 Hz), 8.68 (*d*, 1H, *J*=7 Hz), 8.72 (*s*, 1H)	394 (100), 521 (0.3)
$CSOC_{12}$	87.5	0.84 (*t*, 3H, *J*=7 Hz), 1.22 (*m*, 21H), 1.71 (*m*, 2H), 2.95 (*q*, 2H, *J*=7 Hz), 4.02 (*q*, 2H, *J*=7 Hz), 4.21 (*s*, 3H), 7.01 (*d*, 2H, *J*=9 Hz), 7.35 (*d*, 1H, *J*=16 Hz), 7.77 (*d*, 2H, *J*=8.8 Hz), 7.89 (*d*, 1H, *J*=16 Hz), 8.33 (*d*, 1H, *J*=7 Hz), 8.69 (*d*, 1H, *J*=7 Hz), 8.72 (*s*, 1H)	408 (100), 535 (0.3)
$CSOC_{13}$	88.8	0.83 (*t*, 3H, *J*=7 Hz), 1.22 (*m*, 23H), 1.71 (*m*, 2H), 2.95 (*q*, 2H, *J*=7 Hz), 4.00 (*q*, 2H, *J*=7 Hz), 4.21 (*s*, 3H), 7.01 (*d*, 2H, *J*=9 Hz), 7.35 (*d*, 1H, *J*=16 Hz), 7.77 (*d*, 2H, *J*=8.8 Hz), 7.89 (*d*, 1H, *J*=16 Hz), 8.34 (*d*, 1H, *J*=7 Hz), 8.69 (*d*, 1H, *J*=7 Hz), 8.72 (*s*, 1H)	422 (100), 549 (0.3)
$CSOC_{14}$	95.7	0.83 (*t*, 3H, *J*=7 Hz), 1.22 (*m*, 25H), 1.71 (*m*, 2H), 2.95 (*q*, 2H, *J*=7 Hz), 4.01 (*q*, 2H, *J*=7 Hz), 4.21 (*s*, 3H), 7.01 (*d*, 2H, *J*=9 Hz), 7.35 (*d*, 1H, *J*=16 Hz), 7.77 (*d*, 2H, *J*=8.8 Hz), 7.89 (*d*, 1H, *J*=16 Hz), 8.34 (*d*, 1H, *J*=7 Hz), 8.69 (*d*, 1H, *J*=7 Hz), 8.72 (*s*, 1H)	436 (100), 563 (0.3)
$CSOC_{16}$	94.8	0.87 (*t*, 3H, *J*=7 Hz), 1.25 (*m*, 29H), 1.76 (*m*, 2H), 2.95 (*q*, 2H, *J*=7 Hz), 3.98 (*q*, 2H, *J*=7 Hz), 4.53 (*s*, 3H), 6.92 (*d*, 2H, *J*=9 Hz), 7.06 (*d*, 1H, *J*=16 Hz), 7.57 (*d*, 2H, *J*=8.8 Hz), 7.63 (*d*, 1H, *J*=16 Hz), 8.17 (*d*, 1H, *J*=7 Hz), 8.88 (*d*, 1H, *J*=7 Hz), 8.91 (*s*, 1H)	464 (100), 591 (0.2)
$CSOC_{18}$	90.3	0.87 (*t*, 3H, *J*=7 Hz), 1.25 (*m*, 33H), 1.76 (*m*, 2H), 2.95 (*q*, 2H, *J*=7 Hz), 3.99 (*q*, 2H, *J*=7 Hz), 4.53 (*s*, 3H), 6.93 (*d*, 2H, *J*=9 Hz), 7.05 (*d*, 1H, *J*=16 Hz), 7.57 (*d*, 2H, *J*=8.8 Hz), 7.63 (*d*, 1H, *J*=16 Hz), 8.15 (*d*, 1H, *J*=7 Hz), 8.85 (*d*, 1H, *J*=7 Hz), 8.91 (*s*, 1H)	492 (100), 619 (0.3)

only products in all of our reactions which could be easily identified by ^{1}H NMR. However, prevention of light exposure to these products is mandatory in all preparation and purification processes. Otherwise, *cis*-isomers are usually encountered. Since these charged liquid crystalline materials are mesogenic in nature, melting points of these materials are not easily identified. Preliminary thermal scanning on one of these compounds showed that several phase region were observed (see Fig. 1). Detailed thermal properties analysis and mesophases identification will be discussed in a paper elsewhere.

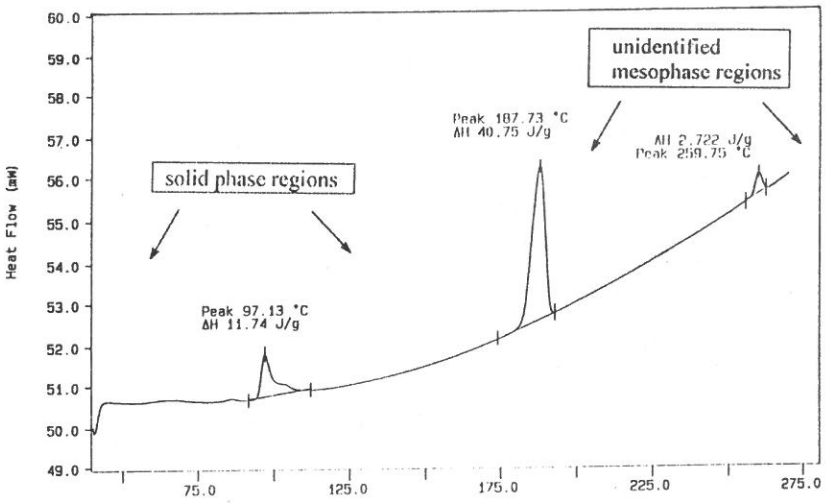

Fig. 1. Differential therml scanning calorimetry of *trans*-4-(*p'*-octyloxtstyryl)-1-methylpyridinium iodides ($PSOC_8$).

Higher alkane numbers of 4-alkoxybenzaldehydes are not commercially available and have to be prepared in lab. Preparation of these 4-alkoxybenzadehydes can be done by reacting 4-formyl-phenol with various alkyl bromides under basic conditions (Scheme 2). Since excess residue of alkyl bromides were found to be reacted with piperidine in the next step, isolation of these 4-alkoxybenzadehydes were found to be required. Yields of them were only fair (50%). Precise stoichiometric equivalent of bases were found to be required to get higher yields of products. Side reactions such as nucleophilic attack by hydroxide to form alcohols and nucleophilic attacks by alkoxides to form ethers would occur when excess bases were used (Scheme 3).

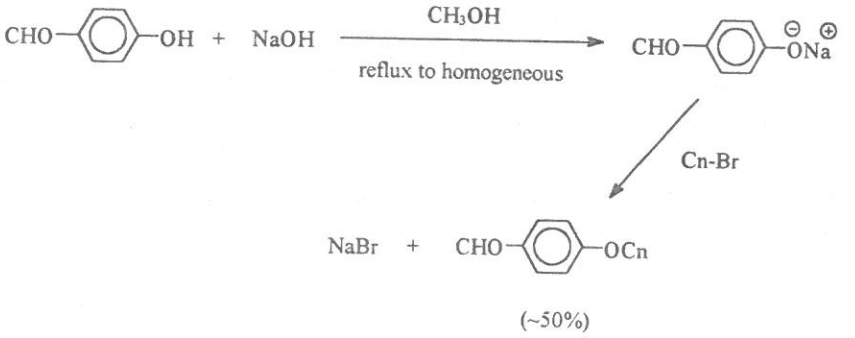

Scheme 2

Side Reactions :

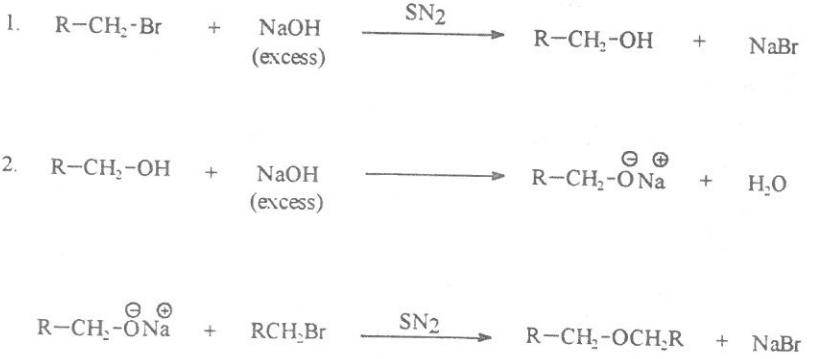

Scheme 3

3. EXPERIMENTAL

Substituted methoxy to decanoxy aryl aldehydes, 4-picoline, 3,4-lutidine, and colidine (aldrich) were used as received. Methanol was dried over calcium chloride. ^{1}H NMR spectra were recorded on a Bruker AM-300 spectrometer. The MS spectra were obtained by using a Joel Jms Sx/Sx 102A system at 70 eV, infrared spectra were recorded by Beckman instrument. Differential thermal scanning calorimetry was done on Perkin-Elmer DSC-7 with a scan rate at 10°C/min under nirogen atmosphere.

4. GENERAL PROCEDURE

(1) Synthesis of higher alkane number of 4-alkoxybenzaldehydes

To a round bottom flask were added 4-hydroxybenzaldehyde (10 mmol), 25 ml methanol, and sodium hydroxide (12 mmol). The solution was then heated to reflux until a homogeneous phase was obtained. After cooling to room temperature, alkyl bromide (12 mmol) was then added to the flask. Solution was again heated to reflux and left for overnight. The reaction was worked up by extraction with methylene chloride and 5% sodium hydroxide aqueous solution. The organic layer was neutralized by 5% hydrochloric acid aqueous solution and dried over magnesium sulfate. After rotovap off the solvent, crude yields (~50%) of 4-alkoxybenzaldehydes were obtained. The 4-alkoxybenzaldehyde was further purified by running through a liquid chromatograph column before it was used for next reaction.

(2) Synthesis of $PSOC_n$, $LSOC_n$ or $CSOC_n$

To a round bottom flask were added 4-picoline (or 3, 4-lutidine or colidine) (4.48 mmol) and methyl iodide (0.5 ml, 8.03 mmol). The mixture was stirred under 2 ml of methanol reflux for one hour. After cooling to room temperature, another 5 ml of methanol was added, followed by the aryl aldehyde (1.5~2.0 eq) and about 1 ml of piperidine (0.5 eq). The resulting solution was heated to reflux with stirring for another three hours. After the solution was cooled to zero degree C, 20~30 ml of ethyl ether was then added to precipitate the products. After filtration under reduced pressure, the crude products of 3-methyl-4′-substituted-4-styrylpyridine methiodide were isolated. Crude yields of products were about 83~98%. Recrystallization was done in CH_3OH/CH_2Cl_2 (1:3).

5. ACKNOWLEDGEMENT

We thank the National Science Council of the Republic of China for financial support NSC 83-0208-M030-020 and NSC 84-2113-M001-016.

REFERENCES

(1) D.W. Bruce, David A. Dunmur, Elena Lalinde, Peter M. Maitlis and Peter Styring, *Nature*, **323**, 791 (1986).
(2) (a) D.W. Bruce, David A. Dunmur, Peter M. Maitlis, Michael M. Manterfield and Robert Orr, *J. Chem. Mater.*, **1**, 255 (1991).
(b) D.W. Bruce, Clive Bertram, David A. Dunmur, Susan E. Hunt, Peter M. Maitlis and Mark McCann, *J. Chem. Soc. Chem. Commun.*, p. 69 (1991).
(3) (a) A.P. Philips, *J. Org. Chem.*, **14**, 302 (1949).
(b) Win-Long Chia, Chun-Nan Chen and Huey-Jiuan Sheu, *Mater. Res. Bull.*, in print (1995).
(c) Win-Long Chia and Chun-Nan Chen, *Fu Jen Studies*, **28**, 37 (1994).

新的帶電荷熱向型液晶的合成

賈文隆　陳榮鐘　蕭玉焜　陳俊男
輔仁大學化學系
林宏洲
中央研究院化學所

摘　要

已合成三個新的系列且帶電荷的熱向型液晶：反-4-(對-烷氧苯乙烯基)-1-甲基-碘化比啶鹽 [$(C_nH_{2n+1}OC_6H_4CH{=}CHC_5H_4NCH_3{}^+I^-$] (縮寫爲 $PSOC_n$)、反-4-(對-烷氧苯乙烯基)-1, 3-二甲基-碘化比啶鹽 (縮寫爲 $LSOC_n$) 及反-4-(對-烷氧苯乙烯基)-1-甲基-3-乙基-碘化比啶鹽 (縮寫爲 $CSOC_n$)，這包括同類物從碳一 ($n=1$) 至碳十四 ($n=14$) 及另外的碳十六和碳十八。產率通常極佳。

REALIZATION OF NEW MUTUALLY COUPLED CIRCUIT USING CCIIs

YUNG-CHANG YIN
Department of Electronic Engineering
Fu Jen Catholic University
Taipei, Taiwan 24205, R.O.C.

ABSTRACT

A new method for realizing mutually coupled circuits using current conveyors (CCIIs) as active elements is proposed. The realized circuits are composed of very few CCIIs, resistors and grounded capacitors. On the other hand, the values of a primary reciprocal self-inductance, a secondary reciprocal self-inductance and a mutual reciprocal inductance can be tuned by resistors or capacitors. The circuits include only grounded capacitors which are suitable for integrated circuit implementation.

1. INTRODUCTION

Several methods for realizing mutually coupled circuits using active elements have been published[1~6]. Many of them mentioned the tunable values of self-inductors and mutually inductor used eight Operational Transconductance Amplifiers (OTAs) or current conveyors (CCIIs). However, there is no circuit which can be tuned the values of a primary reciprocal self-inductance (Γ_{11}), a secondary reciprocal self-inductance (Γ_{22}) and a mutual reciprocal inductance (Γ_{12}). In this paper, we propose a new method for simulating the mutually coupled using few current conveyors (CCIIs) as active elements. Three reciprocal inductances (Γ_{11}, Γ_{22} and Γ_{12}) in the circuits can be adjusted to the desired values by three resistors; meanwhile, employing of grounded capacitors is suitable for integrated circuit fabrication.

2. CIRCUIT CONFIGURATIONS

A mutually coupled circuit and its equivalent circuit are shown in Figs. 1(a) and 1(b). The Y-matrix is given by

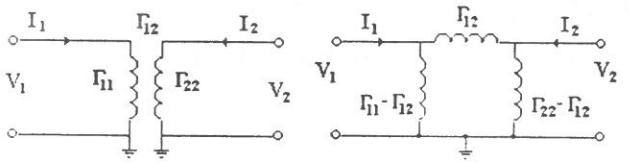

(a) Mutually coupled circuit (b) Equivalent circuit

Fig. 1. Mutually coupled circuit.

$$\begin{bmatrix} I_1 \\ I_2 \end{bmatrix} = \begin{bmatrix} \frac{\Gamma_{11}}{s} & \frac{\Gamma_{12}}{s} \\ \frac{\Gamma_{12}}{s} & \frac{\Gamma_{22}}{s} \end{bmatrix} \begin{bmatrix} V_1 \\ V_2 \end{bmatrix} \tag{1}$$

where $\Gamma_{12}=-K\sqrt{\Gamma_{11}\Gamma_{22}}$, K is a coefficient of coupling. A grounded inductor is shown in Fig. 2[7]. The reciprocal inductance is given below:

$$\Gamma=\frac{GG_a}{sC} \tag{2}$$

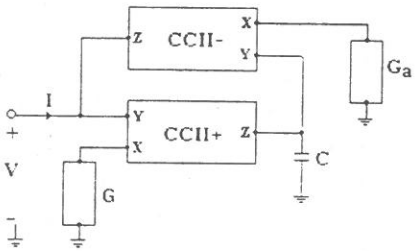

Fig. 2. Grounded inductor of Eq. (2).

From the circuit shown in Fig. 3, the following reciprocal inductance matrix with $K>0$ is obtained:

$$\Gamma=\begin{bmatrix} \frac{G(G_a+G_b)}{C} & \frac{-GG_b}{C} \\ \frac{-GG_b}{C} & \frac{G(G_b+G_c)}{C} \end{bmatrix} \tag{3}$$

where C is capacitance, and G, G_a, G_b and G_c are conductances.

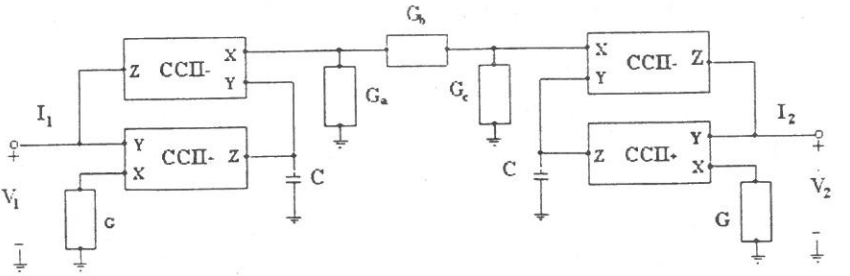

Fig. 3. CCII circuit of Eq. (3).

It is obvious that the values of Γ_{11} and Γ_{22} can be adjusted independently by tuning the values of G_a and G_c, respectively. Moreover, we can simultaneously vary the three reciprocal inductances Γ_{11}, Γ_{22} and Γ_{12} by adjusting the values of conductor G_b, G or grounded capacitor C. If the value of G_b is negative, the coefficient of coupling K is negative. We may use the well-know Generalized Impedance Converter (GIC) circuit to achieve the object. Figure 4 shows the circuit with the following reciprocal inductance matrix:

$$\Gamma=\begin{pmatrix} \dfrac{G(G_a-G_b)}{C} & \dfrac{GG_b}{C} \\ \dfrac{GG_b}{C} & \dfrac{G(G_c-G_b)}{C} \end{pmatrix} \tag{4}$$

By adjusting the two conductors G_a and G_c, we can independently tune the reciprocal inductances Γ_{11} and Γ_{22}. Moreover, by adjusting the values of conductors G, G_b, or capacitor C, we can simultaneously vary the values of Γ_{11}, Γ_{22} and Γ_{12}.

It should be noted that the circuits shown in Figs. 3 and 4 include only grounded capacitors, which are suitable for integrated circuit implementation.

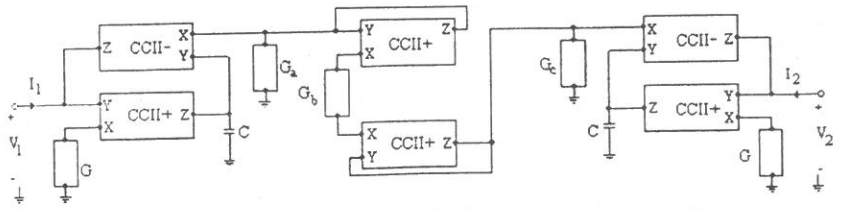

Fig. 4. CCII circuit of Eq. (4).

3. EXPERIMENTAL RESULTS

To verify the theoretical prediction, we built the mutually coupled circuit of Fig. 3 with $G=G_a=G_b=G_c=10^{-3}$ siemens, $K=0.5$ and $C=1\,\mu$F as well as Fig. 4 with $G=1$ m siemens, $G_a=G_c=2$ m siemens, $K=-1$ and $C=1\,\mu$F. We constructed the coupled tuned circuit shown in Fig. 5 with $R_1=R_2=1\,k\Omega$, $C_1=C_2=1\,\mu$F for Fig. 3 and $C_1=C_2=10\,\mu$F for Fig. 4. The operational amplifier (AD 844) was chosen as CCII. The measured values were found by Hewlett Packard network/spectrum analyzed 4195A. The measured frequency responses of the coupled tuned circuit Figs. 3 and 4 are shown in Figs. 6 and 7 in order. They agree with the theoretical analysis well.

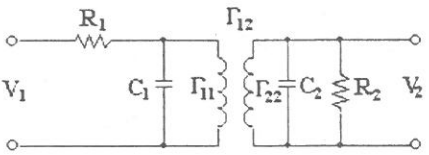

Fig. 5. Coupled tuned circuit.

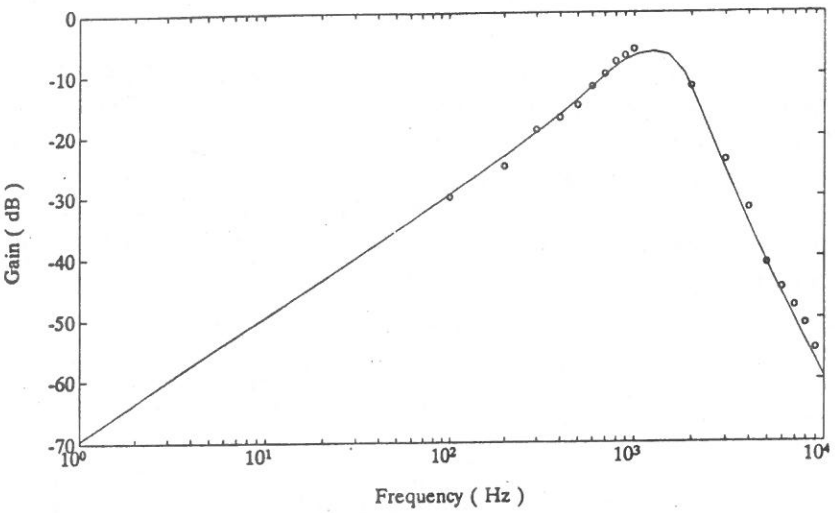

Fig. 6. Frequency response of a mutually coupled circuit with $K=0.5$. Solid curves: Ideal response, "○" Measured response

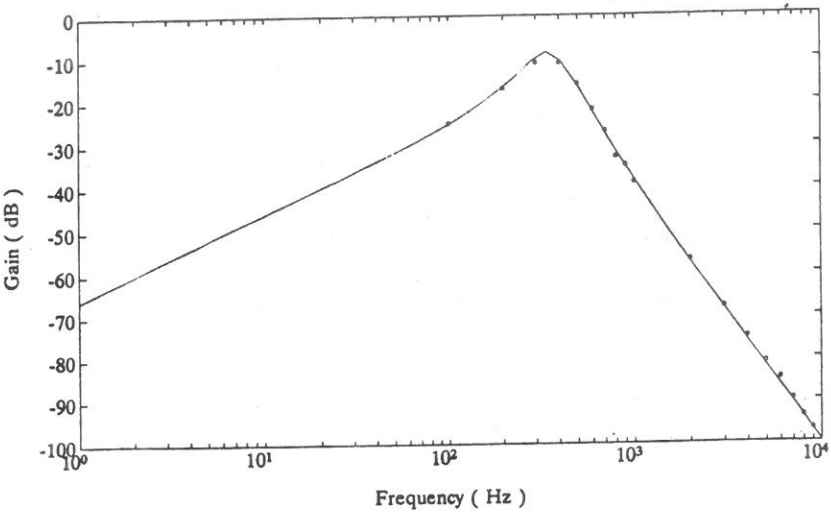

Fig. 7. Frequency response of a mutually coupled circuit with $K=-1$. Solid curves: Ideal response, "*" Measured response

4. CONCLUSION

We have proposed a new method for realizing mutually coupled circuit using few CCIIs as active elements. Three reciprocal inductances (Γ_{11}, Γ_{22} and Γ_{12}) in the circuit can be tuned independently by resistors, and the circuits are suitable for integrated circuit implementation owing to the use of grounded capacitors.

5. ACKNOWLEDGEMENT

The another wishes to thank the financial support of Societas Verbi Divini. The another is also grateful to Dr. Chun-Li Hou for his constructive suggestions, and Mr. Yue-Cheng Liu and Mr. Han-De Guan for their experimental assistance.

REFERENCES

(1) M.E. Van Valkenburg, "Analog Filter Design", CBS College Publishing (1982).

(2) G.S. Moschytz, "Linear Integrated Networks: Fundamentals", Van Nostand Reinbold (1974).
(3) M. Higashimura and Y. Fukui, "Realization of New Mutually Coupled Circuits Using Mutators", *Int. J. Electron.*, **58**(3), 477-485 (1985).
(4) M. Higashimura and Y. Fukui, "Electronically Tunable OTA-C Mutually Coupled Circuits", *Electron. Lett.*, **27**, 1251-1252 (1991).
(5) M. Higashimura and Y. Fukui, "RC Avtive Realization of Mutually Coupled Circuit", *IEEE ISCAS*, **6**, 1343-1346 (1991).
(6) M. Higashimura, "A Realization of Mutually Coupled Circuit Using CCIIs", *IEICE Transactions*, **74**, 3924-3926 (1991).
(7) C.L. Hou, R.D. Chen, Y.P. Wu and P.C. Hu, "Realization of Grounded and Floating Immittance Function Simulators Using Current Conveyors", *Int. J. Electron.*, **74**(6), 917-923 (1993).

使用電流傳輸器合成具有互感耦合電路

鄞 永 昌
輔仁大學電子工程系

摘 要

本文提出一個嶄新的使用第二代電流傳輸器合成具有互感耦合的電路。此互感耦合電路僅使用少量的第二代電流傳輸器，電阻以及接地電容。另一方面自感及互感的電感值可單獨經由電阻或電容調整得之。由於此電路僅含接地電容，所以此電路適合製成積體電路。

論孟稱舜《嬌紅記》傳奇的情節結構藝術

謝錦桂毓
輔仁大學理工外語民生學院文史哲共同科

摘　　要

本文以晚明孟稱舜"嬌紅記"傳奇爲對象，分析其情節結構藝術，以呈現其主題。除說明本劇戲劇衝突集前代愛情劇之大成，並指出本劇思想超越前代，在文學史上居於承先啓後之地位。

一、前　　言

孟稱舜是晚明劇壇的重要作家，《嬌紅記》是明末劇壇一部具有承先啓後意義的重要傳奇劇作，但長期的戲曲研究，卻沒有給予應有的重視。直到近年來狀況才有了改變，研究的文章日漸增多，討論的內容也日漸深化。

《嬌紅記》的主題，一般論者的看法是：「男女青年爭取婚姻自由」[1]，「反映了人性自覺的普遍覺醒」[2]，「歌頌其愛情和反抗鬪爭精神，揭露封建婚姻制度的罪惡。……將理想寄託於理想化的虛幻世界中」[3]。或說「通過出色感人的戲劇情節，展示了歷史的必然要求——進步的社會理想和人的正常生活要求——和這個要求實際上不可能實現——雖出現實現歷史必然要求的可能性，但舊勢力過於強大，所以還不能實現——之間的悲劇性衝突」[4]。這些論述雖已指出《嬌紅記》主題思想的方向，但對主題的實質內涵和具體的呈現方式，則說解得不够清楚。我們認爲《嬌紅記》的主題是：「通過申嬌自擇且以同心子爲標準的愛情，來歌頌至情，並反映傳統制度及價值體系造成的悲劇，傳達那個時代的精神面貌。」因爲上述論者所下的主題，放在前此之任何愛情劇中，幾乎都可以適用，而《嬌紅記》之特別，正在於申嬌愛情的內涵所傳達的思想超越前代，且其愛情承受的壓力也比以前愛情劇深重。當然，多數論者陳述主題雖不够具體，但在文章中則或深或淺地論述到了，因此我們在此不再討論主題思想究竟是什麼，而重在作品如何透過情節結構表達該主題。

《嬌紅記》的情節結構，一般論文不是沒有討論，就是沒有以「情節結構」爲討論重點。只有蕭善因很明確地指出「嬌娘自擇良配的過程，即申嬌確立愛情的過程是構成全劇的一條主線，還有一條次線是王父的勢利和帥子的間阻所造成的愛情悲劇。……兩條線交織，構成雙線條的戲劇衝突」[5]。另外葉小帆也稍微

點到：「在情節安排和結構布局上，運用了一悲一喜，悲喜相錯的對比方式。」[6]蕭善因的說法雖然明確，但仍不够具體；本文要做的工作，就是明確畫出情節結構線，並從探討情節結構中，說明≪嬌紅記≫的主題。

評論中國戲曲，消極方面要避免偏執一隅、牽強附會，積極方面則要具體而完備[7]。若僅就戲曲結構論，也當包括關目布置與排場處理。就傳統戲劇言，其美學基礎建基在詩歌、音樂、舞蹈上，所以排場處理比關目布置更重要。這個特色造成傳統戲劇關目一般都不精彩，直接影響主題的開掘與深刻，也影響戲曲研究中忽視情節結構藝術的現象。本文一者篇幅所限，再者不求具體完備，也不避一隅之譏，僅談≪嬌紅記≫之情節結構，並藉以呈現主題。其他問題且待來日，還請方家包涵指正。

二、分析的原則

爲了呈現≪嬌紅記≫的主題，我們理出的情節結構是：以申嬌爭取戀愛婚姻自由爲主軸，其間所遭遇的愛情內部問題（如面對愛情的思考、互相試探了解、自身性格的發展、……），和外在壓力的問題（婚姻制度、傳統觀念的束縛、……），交織衝突，推衍至最後的結局。

根據結構線，我們畫出的結構圖是：按照戲劇情節自身的進展繪出起伏有據的情節結構線，標示情節發展的樞紐點；再循戲劇情節的發展、轉折，劃分爲七大階段，並依據各階段所集中體現的思想內容訂定其階段標目。我們將「愛情內部」和「外在壓力」以一條結構線表示，是因爲這兩方面的內容表面上看來各有其領域，然而放在本劇的戲劇情境中考量，則實是互爲因果、密不可分的，所以我們不用雙線結構的方式，而期望能將「愛情內部的發展」和「外在壓力造成的衝突推移」以及「此二方面互動形成的波瀾起伏」融滙在單一主線中表示；爲了能較明確地標示，圖中用實線代表愛情內部的發展，用虛線代表外在壓力的推移。

最後，在結構線下方，掛上劇本原先所列的齣別，以便查考。至於第八齣＜番獷＞、十一齣＜防番＞、十三齣＜遣召＞則併入十六齣＜城守＞所呈現的戰爭背景中討論；而第五齣＜訪麗＞、十九齣＜歸圖＞、三十齣＜玩圖＞、三十四齣＜客請＞、四十四齣＜演喜＞等塑造帥公子性格的情節，也將放在四十二齣＜帥媾＞時一併討論。由於戲曲特有的分折分齣形式，可以自由穿插、安排各方面情節同時進展，而呈現渲染氣氛和佈局巧妙的藝術效果，但我們在探究情節結構總體概念時，爲了避免頭緒紛亂，說解不易，則不宜黏滯於劇本原先的齣別次第，呆板地按齣討論。因此我們做如上的安排，把握情節結構大綱，進行本文的探討。

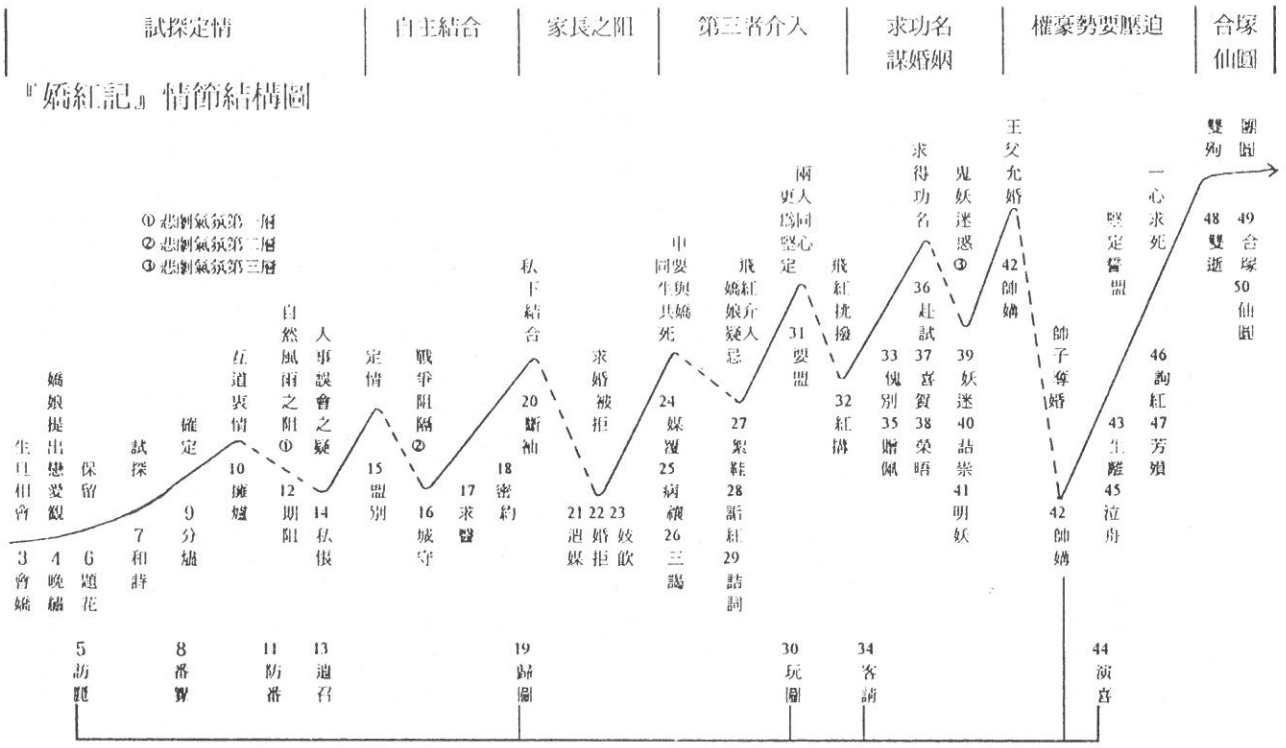
試探定情
自主結合
家長之阻
第三者介入
求功名
姻婚謀
權豪勢要壓迫
合塚
仙圓
『嬌紅記』情節結構圖
生旦相會
3會嬌
保留
6道花
試探
7和詩
娘提出戀愛觀
4晚磵
紅道衷情
10擁嫂
確定
9分磵
①悲劇氣氛第一層
②悲劇氣氛第二層
③悲劇氣氛第三層
自然風雨之阻①
12期阻
人事誤會之疑
14私振
定情
15盟別
戰爭阻隔②
16城守
17求聲
私下結合
20斷袖
18密約
求婚被拒
21迫媒
22婚拒
23妓飲
申要與生共嬌死
24媒覆
25病疲
26三謁
飛紅介入疑忌
27絮鞋
28詐紅
29詰詞
兩人同心堅定
31要盟
飛紅挑撿
32紅搆
求得功名
33傀別
35贈佩
36赴試
37喜賀
38榮晤
鬼妖迷惑③
39妖迷
40詰崇
41明妖
王父允婚
42帥媾
帥子奪婚
42帥媾
堅定誓盟
43生離
45泣舟
一心求死
46詢紅
47芳殞
48雙逝
團圓
雙列
49合塚
50仙圓
5訪聞
8番訝
11防番
13追召
19歸圖
30玩圖
34客請
44演喜

圖 1 「嬌紅記」情節結構圖。

三、嬌紅記的情節結構與主題呈現

「嬌紅記」情節結構圖（如圖 1）。

曲線走勢即情節之進展；曲線走勢間落差的大小，即申嬌愛情所受壓力之大小。大體二人情愈堅，曲線越高，而足以摧毀其愛情的，掉到二人彼此確定前，造成干擾卻未必能摧毀愛情的則落差較小。

下面我們就分段探討情節結構，並在討論過程中逐步說明主題。

1. 申嬌試探定情

這個階段是男女主人公相識、相戀到定情的過程。重點是一開始嬌娘提出明確的戀愛觀，以及從申嬌確定愛情之前所經過的一連串試驗中，初步顯示了≪嬌紅記≫與衆不同的主題思想。

首先，在申嬌初會的描寫上，作者讓他們在家筵上以表兄妹的身份相會，兩人的表現是「偷晴兩下頻來往」「乍相逢早已私相傍」（＜會嬌＞），乍看之下，似乎與一般才子佳人劇「一見鍾情」的俗套沒什麼兩樣；但是，作者的用心之處，正在於「一見鍾情」這個場面之前之後的舖敍。

「一見鍾情」之前的舖敍，主要是針對申純。他一出場就是個「科場不利」「失志功名」的景況。對當時年輕的文人而言，「婚」「宦」就是他們勾勒人生未來藍圖的兩大方向；申純對仕途已是意興闌珊，但是對戀愛婚姻則還抱著熱烈期待。看他初到舅家就熱切地問候尚未謀面的表妹：「百一姐今庚十幾了？」（＜會嬌＞，下同）、「聞得聰慧異常。」、「可曾許聘了麼？」、「不知要許甚樣人家？」、「小甥禮合請見。」這樣的表現，接續後面一見嬌娘就心動神馳的情節，不就顯得自然而然、順理成章嗎？所以「一見鍾情」這個情節正是延續前情用以體現申純與一般才子對待愛情的不同態度：他是有心而且期待的。他的欣喜若狂也不應視同爲一般才子的輕狂。

「一見鍾情」之後的舖敍則主要是針對嬌娘。在嬌娘初見申純的場面上，我們只看到一個少女對「神清玉朗」的異性流露出傾慕之心，還看不到她的思想內涵。作者高明的筆觸在呈現了乍逢可意少年的正常反應之後，立刻讓這個少女將戀愛婚姻的深刻思想呈現在讀者面前。我們看到，嬌娘對愛情的想法，不是只停留在「一見鍾情」而已，而是引發她更嚴肅的思考，進一步提出自己對戀愛婚姻的主張。

所以，在所謂「一見鍾情」的情節中實已滲入「歌頌至情」的主題思想，作者是緊扣著這個主題，用前舖後敍的結構方式，來設計「生旦相會」的情節的；我們在討論這個情節時，應放回整個作品中探究，不應把它抽離出來單獨探討，而得出一見鍾情是落入俗套的結論。

其次，我們要探究嬌娘的戀愛觀。前面我們談過，在初見申純激起傾心的漣漪之後，嬌娘並沒有像一般少女那樣立即墜入愛的漩渦，反而是更引發她深刻的思考。她從自身窒悶的生長環境積壓出來的愁緒，思考到掌握當時女子一生幸福的關鍵——婚姻問題，清清楚楚地看到「若乃紅顏失配，抱恨難言」（＜晚繡＞）這種婚姻不自由造成的不幸現實。所以，她明白地表示：對於關乎自己一生幸福的戀愛婚姻問題，她要自己做主，而不是讓父母、媒妁、門第、……等等外在力量替她做決定！因此她提出她戀愛觀中第一個重點：「自擇良配。」那麼，擇配標準又是什麼呢？她提出她戀愛觀第二個重點：以「同心子」爲擇偶標準。嬌娘指出她不要「富貴子弟」、「薄倖才子」，這種考慮實已跨越了以「名」、「利」爲考量的社會價值觀的範疇，也超越了一般才子佳人淺薄的愛情認知領域；這種超越是很值得注意的。審視《嬌紅記》以前的愛情劇，男女青年從服從父母之命、媒妁之言，到開始覺醒要自己選擇對象，這是一大進步。但他們對對象內涵的認識，仍停留在男有才（取功名的本事）、女有貌的層次，再進一步也只到「才貌雙全」的愛情憧憬和幻想；《嬌紅記》選擇對象的思想，卻已從外在的功名富貴，進到才貌雙全，還深化到對內涵的要求！至於所謂內涵，即「同心子」的具體內容，這裏嬌娘只說出要能「死共穴、生同舍」，亦即對愛情要有能「生死與共」的堅定與執著；其他具體內涵則是一點一滴地在申嬌戀情發展的過程中逐漸體現出來，最後才能總結地予以說明。但是，嬌娘提出的戀愛觀，在整個情節結構中是起著領頭的作用，回應前面「歌頌至情」的主題思想，引導全劇情節結構的進展。

接下來，就要探討試探定情階段中戀情開展的過程。嬌娘和申純並不是從一見傾心直接跨到兩情相悅，甚至乾柴烈火的階段；在這中間，他們還經歷過一段互相試探考驗的過程。我們要從嬌娘對申純態度的變化探究她的內心思想，並從這個過程檢視申純何以會是嬌娘的「同心子」。

我們可以看到嬌娘自遇申生是「心上眷眷」（＜晚繡＞）、滿腹情思，但她面對申生時卻是「似眞似假，如迎如拒」（＜題花＞），作者通過一連串的科介「旦見生驚介」「旦不答低頭介」「旦轉看花介」「旦看、低嘆不語介」「旦袖詩欲行介」「旦徐步下」（以上＜題花＞）卻不發一語的表現，傳遞嬌娘態度上的保留，這時候她心中還是擔心「倘相如，未必果心兒如我」（＜和詩＞）；但申純面對嬌娘各種反應：不管是故做冷淡，或是一語不發，甚至嚴詞以拒，他始終沒有打退堂鼓，就此罷手；這表明他不是一時興趣來挑逗嬌娘，他是認眞在追求兩情相悅的。這種表現讓嬌娘安心不少，她的試探得到了確定：「申生、申生，你的衷腸，我已盡知。」（＜分燼＞）於是才有接下來＜擁爐＞互道衷情的情節，嬌娘確定申純是她的「同心子」；由此，我們可以看出「同心子」第一個具體內容：兩人都很重視愛情，對待愛情的態度都是有心而且眞誠。

確定彼此感情之後，作者接連安排了兩個逆流壓抑愛情之路的順暢：自然風雨之阻、人事誤會之疑。就情節布局言，這使情節呈現波瀾起伏的效果；就呈現思想內容言，自然風雨之阻是營造悲劇氣氛的第一層渲染。因爲風雨本身就是悲涼的意象，而自然界要風雨又是人力所無法影響、改變的。這種悲涼又無奈的意象正是作者在申嬌戀情剛發展起來的時候，舖下第一層悲劇氣氛而淡淡地籠罩全局。

再看人事誤會之疑，則呈現了嬌娘自身性格的侷限，這也是造就悲劇的根源之一。嬌娘只因申生醉中不應，就推想到「他敢無情對我，故此推託睡著了」(<私悵>)！這是久桎傳統婚姻制度下初戀女子正常的心理反應。如果以今來律古，則可以看出嬌娘性格中遇事不去探究解決，卻自怨自艾、歸諸宿命的消極習慣。我們同情這種文化情境中不能自覺也無能爲力的狀況，但就劇本論，這種致命的性格反應，在往後情節每一次重要轉折處，就凸顯男女主角對自己未來無力掌控的沈滯拖沓感，而把自己的人生託給所謂命運的安排，只能隨外在形勢的轉變浮沈其中了。也許正因爲有許多無奈，申嬌的愛情才顯得更悲涼。在寫法上，嬌娘私悵而歸的情節，運用了獨行花徑、風搖竹影等意象來烘托她自憐自嘆的情境，這種藝術技巧影響後來≪紅樓夢≫。黛玉訪寶玉吃了閉門羹的情節，與<私悵>一齣相較，頗有神似形化之妙。

越過風雨與誤會兩次逆流之後，愛情之浪衝得更高了，申嬌二人眞正誓海盟山地定下情衷，這一試探定情階段就到此完成了。

2. 私下自主結合

申嬌剛達到兩情相悅的階段，隨卽又因戰事造成分離。從<番鬻>、<防番>、<遣召>一直到<盟別>、<城守>，作者蘊釀了一系列戰爭氣氛，並讓這個事件造成了男女主角不得不分離的情況。我們認爲這個情節是營造悲劇氣氛的第二層渲染。前面提到自然風雨是人力不可及的，而此戰爭雖屬人爲，但人禍與天災一樣，不是一般百姓可以預料、防範、改變的，這種無可奈何不得不分的景況，正是作者延續第一層渲染，著力營造的第二層悲劇氣氛，略顯沈重地舖下往後劇情的陰影。

這個階段最重要的情節就是申嬌私下自己結合了。值得注意的是，他們的結合是有前段複雜而深刻的試探定情爲基礎的，他們不是一見鍾情後就直接受情慾支配。正因爲經過前面那一連串彼此確定的過程，他們的結合便有更深刻的內蘊意義：互相認定了，就自己作主。這個舉動不能單純以情慾的驅動來解釋，它更深刻的意義在於：體現不屈從制度成規的自主精神。就在這裏，申嬌結合體現≪嬌紅記≫思想的卓越。也因此，結合後嬌娘所憂不是像前此劇作的女子，擔心發生性關係後男子負心，因爲嬌娘與申生有相當程度的情感基礎；她擔憂的是事

被人知，這就體現了嬌娘另一個性格侷限：她雖有深刻的思想和相當程度的自覺精神，但其高度還不足以衝破她心中築起的禮教陰霾。這也同時表示，那個時代雖可孕育出如此見解的思想，卻沒有讓這種思想繼續成長的土壤。

3. 家長之阻

結合之後，嬌娘要申生遣媒說婚。我們看到，嬌娘有先進的戀愛觀，卻仍循著腐朽不堪的謀婚方式求合，這眞是「以封建的方式追求其不容的東西，這無異於陸行乘舟」[8]。申家求婚被拒，是申嬌愛情進展以來首次正式遭遇社會壓力的打擊，這個部份體現的是父母之命、門第觀念的問題。

我們在這個階段主要要探討在婚拒事件中申嬌性格的反應和發展。首先看嬌娘。她那種歸諸宿命消極習性的性格反應，在王父拒媒這個情節上表露無遺，她只能在禮教下壓抑自己，並等待命運的恩賜，而絕沒有勇氣站出來爲自己說句話，這又是她思想先進而行動卻保守傳統的又一證明。值得注意的是申純並未因婚拒而心灰意冷、放棄這段感情，相反的，他更堅定執著地說出「拼今世呵、定要和你生同衾死同墓」（<媒覆>），這已經符合嬌娘一開始提出的「生死與共」的同心子」內涵了。這個階段愛情剛曝光卽受到打壓，但這個打壓卻更激發了申嬌愛情的高度和堅定度。

4. 第三者介入

這一階段是更深入體現愛情內部另一層次的問題：第三者介入的問題。飛紅身份雖是侍婢，但她不再是只跟在小姐身邊爲劇情服務的概念化人物了。她有自己的思想、意志，對自己她沒有低人一等的觀念，所以對小姐的態度不卑下；對不合理之處，她也勇於頂嘴，「難道女人家不是人哪？」（<詬紅>）她身上是有個體自覺意識的。事實上對她心儀的人也有追求幸福的自覺行動；這樣一個人物就具有成爲愛情事件中第三者的資格。必須注意到：傳統愛情劇的第三者幾乎都是挾帶門第權勢意義，來壓迫自主愛情的，如《西廂記》的鄭恆，本劇的帥公子；但是本劇的作者卻注意到屬於愛情內部另一層次的第三者問題，他把飛紅提昇到與申、嬌同等的地位——同爲有追求愛情的權利的個體。提出這個問題，標示著戲曲史中愛情問題廣度的拓展。

在這個事件中，嬌娘顯得敏感而悲憤，這是與她「同心子」思想一貫相通的，因爲她要求一對一的專情，所以不容許申生有與她定情又同時和別人調情的情況出現。這裏又呈現了「同心子」的另一具體內涵：要求男女都能有一對一的專情。

申生一開始時會和飛紅等侍婢調情胡鬧，這是當時男子的習性，因爲長期在男尊女卑、一夫多妻制度的浸淫下，嬌娘雖是她唯一付出愛情的對象，但對別的

丫頭他仍免除不了這種輕薄習性。當嬌娘秉持一貫的戀愛觀而責怨他時，才促使他反省，而更清楚認知感情專一的意義，改掉薄行浮浪之病，這表示他是可以教育的。在申純身上我們確實看到了《紅樓夢》裏賈寶玉的雛形，事實上，申純的反思與認知，已跨越了傳統男尊女卑、一夫多妻的觀念範疇，走向互相尊重、對等的現代戀愛觀了。

5. 求功名謀婚姻

由於紅搆導致申嬌第三度分離，這是延續上個階段第三者問題的；但接下來嬌娘勸申純去應試求中，以重遣求婚，則邁入另一階段。嬌娘的舉動是延續前面思想的，可以說她對社會制度還是抱持著幻想，而且期盼能將自己的愛情納入社會體系之內，相容並存、兩全其美。她這種想法放回那個時代情境中看，其實正是前此愛情劇所有的才子佳人共同的期盼。他們是從人性的角度出發，看到人類自然天性的需求——渴望自由戀愛，但是當自然需求與長久以來既定的制度格式相觝觸時，他們思的並不是如何衝出這個依存成習的結構，而是如何在這個架構下尋求生存發展的空間。在嬌娘之前的才子佳人找到了利用求得功名來解決婚姻問題的途徑，於是嬌娘也踩著前輩的足跡，朝著這個方向進行。然而，特別的是申生對待功名的態度，如果說嬌娘的期盼功名是歷史情境的延續，那麼申純的無心於功名則是一種時代精神的發展了。他這種明確地把愛情放在功名之上的表現，的確是種人性的覺醒。他不再盲從於制度安排好的路線，而表達了自己的想法和需求。功名對他沒什麼意義，愛情才是他執著想望的；這也就是他一旦考取之後，仍然一心往見嬌娘的具體內涵。他不再是「有了功名，就不怕沒好姻緣」這傳統制度、觀念下奴性難除的文人，而是體現了相當的進步意義。

在本階段插入「鬼妖迷惑」的情節，可以說是作者營造悲劇氣氛的第三層渲染。本來一般愛情劇的進程是「金榜題名時」就是「洞房花燭夜」了；但本劇作者在申純取得功名與王父許婚之間，插入了這樣一個情節，不單只是在藝術效果上製造跌宕起伏，更是要延續前面的悲劇氣氛，做更濃重的渲染。鬼魂世界是人力無法掌控了解的虛渺境界，這種陰氣森森、隱憂重重的舖敍，預示了劇情發展的漸臻晦暗。也可以說，鬼魂是另一形態的第三者，又來介入申嬌之間。作者筆端歌頌至情的範圍，已從男女主角的有情，擴展到丫環侍婢普通人等的有情，更觸及到鬼妖自然界亦是有情。嬌娘在此事件中的反應也是有成長的，她聽聞申生房中有另一女子，感受申生對她態度的隔閡，這次她沒有一下子就自怨自嘆，驟起疑懼，反而是對申生積極相詢，這表現他們感情的長進、有一定默契和信賴度。我們看到申嬌愛情一步步穩定成長，這爲後來他們的雙殉提供堅實合理的基礎。

王父允婚的動作，道道地地呈現了傳統觀念中，婚姻和功名的臍帶關係；有了功名、就可以使自由意志的愛情和門第觀念、父母之命這兩種互相矛盾的事實，妥協共存，這也就是傳統愛情劇畫下句點的時刻；但《嬌紅記》卻走出了這個假相，繼續走向下一個階段。

6. 權豪勢要壓迫

剛剛取得妥協的情況，立即被更高層次的社會壓力破壞了。我們看看破壞申嬌愛情的這個帥公子的形象：他是個典型的「花花太歲」（＜訪麗＞），正是嬌娘所摒棄的那類「氣勢村沙」「性情惡劣」的「豪富子弟」（＜晚繡＞）。他和申純比較，外貌相當，才學則無，又兼品質低劣，對嬌娘更沒有申純那種至誠尊重可言，只有垂涎其美色，想佔爲己有的卑劣思想。這樣一個人何以能取代申純已幾乎坐穩的王家嬌婿的位置呢？歸究其因，竟然是在其社會地位的高下上。帥公子雖無功名，卻挾父威權而打敗了有功名但官小位低的申純。這樣的一個事實，確實體現了「取得功名、改換門庭，可以解決愛情與門第的矛盾，但不能解決大魚吃小魚的矛盾」[9]。作者清楚指出這個現象，與以前愛情劇相較，他的思想和對制度弊端的剖析，是有所提昇的。

嬌娘面對婚變打擊時，她一貫的宿命消極反應又表現出來了。她對自己認定的愛情，執著無悔；但她就是沒有辦法拿犧牲性命的勇氣去爲自己表白爭取。當飛紅問她：「小姐既然誓志不回，當初老爺改許帥家之時，何不明言所以？」她卻回答：「我自那日已只辦的一死。……況我與申生私遇，此事怎向爹跟前說的也呵一」（＜芳殞＞）嬌娘身上的束縛侷限，也正是那個時代的侷限，這表示那個時代雖已可以產生如此高度思想內容的愛情，卻仍沒有辦法打破格局，重建新的局面。

但是，嬌娘對愛情的執著堅定，的確呈現了耀眼的精神光輝。當飛紅的人性自覺抵抗不了社會壓力，轉而成爲家長的說客，前來勸慰嬌娘回心轉意時，嬌娘卻不爲所動。我們要從三個層次來看她的精神高度：第一是她對帥公子的不屑一顧：嬌娘並非對帥公子有何成見才對他不屑，而是在她心中只有一個申純，所以「那人便美煞，與我何干」（＜芳殞＞）？。她不是拿二人相比才厭惡帥子，而是她一開始即選擇了申生，帥子連存在她心中的機會都沒有，更無從比較起。第二是她對申純的信賴：飛紅以孝道勸她，以申生他幸哄她，她只是一句話：「相從數年，申生心事，我豈不知？」「我固知申生非負心者。」（＜芳殞＞）這種堅定的信任和深刻的相知相惜，又豈是一般愛情劇淺薄的男歡女愛所能望其項背的！第三是她對自己感情的堅定執著：當飛紅勸她說「倘你果有不幸，難道申生當眞休了不成？那時你則飲恨於荒塚黃泉之下，他卻追歡於瑤臺華席之中，悔也悔不迭了」。她卻一點不遲疑地說：「我甘心一死渾無二。」（＜芳殞＞）她堅持於她

所認定的，即使必須犧牲生命去成就它也在所不惜；而且這種執著是不考量任何外在因素的轉變的，她是對自己的心意負責。經過了以上三個層次的剖析，眞可以說嬌娘的愛情內容確實達到了前所未有的思想高度了。

比起嬌娘一往直前的堅決，申純在面對婚變打擊時顯然有過一時的軟弱和動搖。前面說過，嬌娘身上那種宿命消極的性格，也是一直存在申純身上的。對帥子奪婚事件，申純會有與現實妥協的想法，而說出勸嬌娘「勉事新君」(＜生離＞)、「暫從別氏」(＜泣舟＞)這樣的話來；但是，就像前面第三者介入階段一樣，受到嬌娘光潔精神的影響感召，申純的思想感情有再提昇的可能。當他得知嬌娘殉亡時，他也一心要隨之於地下，即使別人拿一貫的禮教大帽子——孝義禮法——扣到他頭上，他也明白表現他殉情的堅決，這種殉情已不是盲從，而是經過思考後堅定執著於自擇的愛情之路的表現。和≪孔雀東南飛≫裏同是殉情的焦仲卿比較，申純的選擇死亡顯然有更清醒的認知，和更深刻的內涵意義，這個結局完全是他自己決定的，這就是所謂自覺的表現。

申嬌之死對制度禮法是一大打擊。傳統禮法要求的內容如：遵從父命，克守孝道，受制於一切社會道德規範；而自擇愛情的內容卻是：要求人能正常面對與生俱來的愛情生活。情和理的衝突下，申嬌選擇了情，他們雖未獲得實質上的勝利，但他們精神上卻戰勝了理；而固執於理的一方，則不論在實質或精神方面，都是慘敗的。這在相當程度上凸顯了作者歌頌至情，批判傳統與社會的思想精神。所以在本階段，申嬌遭受的打擊雖是如此之大，在情節結構線上他們的愛情之浪卻也衝到最高，呈現極高層次的精神光輝。

7. 合塚仙圓

按照戲劇情節的總體架構來看，本劇情節發展到第六階段實已完成，但在悲劇後面又加了＜合塚＞、＜仙圓＞。這個問題比較複雜。

一般的說，它可以彌補人類心靈的缺憾。在現實中無法完成的事，搬到另一個世界去搬演，這種造成精神勝利的浪漫手法所在都有，不贅。

從戲曲發展的角度看，宋及元初悲劇創作勃興，經元代後期的轉換，明代已全然化爲大團圓，到晚明時期，又漸漸向悲劇回復，而明末清初已是悲劇迭現了。本劇舊作新編，正處於悲劇復現已顯徵兆的晚明時期，所以主體實是悲劇，卻沒有脫離大團圓的氛圍，而帶個團圓的尾巴是可以理解的。

從劇本本身看，作者安排的團圓其實並無喜氣，反多悲涼與省思。首先，王父「負恨於死者，有愧於生人」(＜仙圓＞，以下引文不注明者皆同)，其合塚之舉，即因女兒之死而有悔悟。這無疑是否定社會禮法，而肯定申、嬌自我追尋的眞情。與前此愛情劇青年男女最後大體都要納入以家長爲代表的社會價值體系比較，顯有進步。其次，申、嬌死後，「朝暮相隨」，雖說「地下之樂，不減人間」

，但並未超越凡情，反而重遊舊地，不忘情於昔日的歡洽與哀傷；尤其嬌娘仍眷念老父與幼弟。成了天仙，也難遣愁懷，這就更顯其悲。如與人間親人墳前悲吊比對，則劇本的悲劇情調是前後一致的。再次，申、嬌復歸仙班，東華帝君的證詞說：「王嬌憐才誓死，化石之節何慚；申純踐約捐生，抱柱之貞奚愧。慕色牽情，雖有乖於常法；秉志守義，亦夙重於仙家。」並交代兼掌世上姻緣之事，「舉凡佳人才子，量其應否，悉與如願，勿使錯配，有負生成。」作者在劇尾藉男女主角高唱：「辨取眞情種，終須有天長地久。」「死生交，鸞鳳友，一點眞誠永不負。則願普天下有情人做夫妻呵，一一的皆如心所求。」這些話考慮禮法是虛，顧念眞情是實，顯見作者從頭到尾立場都一致。所以這種團圓的寫法實是延續悲劇主題，藉地下天上團圓批判現實，說明人間不能實現眞情，只有死才能完成，傳達了更深一層的悲涼感。第四，作者對這種悲劇，心情是沈重的。他說：「世間只有心難化，地上無如情久長」，「只有恩情最難朽」，甚至用「一川水東流」形容這「鴛鴦塚，千載錦江頭」的長恨。作者無力面對現實，也提不出其他的解決方式，只好看作是命運的捉弄，歸諸「老天之定數」（<合塚>），若以今律古，說成是作者受時代思想的局限也無不可，而就劇作言，這個局限卻正好證成本劇的「悲」，一種表面的團圓中滲透的人生面臨困境時無可如何的悲情。我們可說，作者是以出世的筆墨，作入世的文章。

四、結　　論

如果說文學的歷史就是民族心靈的歷史，那麼，《嬌紅記》就是我們民族心靈歷史中重要的組成部份。它的內容、結構既有繼承，也有開拓，是承先啓後的重要作品。

內容上，《嬌紅記》超越前代的地方主要有：把元明戲曲愛情劇「郎才女貌」、「才貌雙全」等著重外在條件的情況往前推進到要求內在心靈的契合；愛情不再從屬於功名；侍婢捲入主人的愛情糾葛，宣稱自己也有做人的權利；阻礙愛情的最大力量變成權豪勢要而非家長；功名不再能主導解決愛情困境。因此，《嬌紅記》寫的是傳統愛情戲碼，思想卻更深刻，尤其人性的自覺，更能撥動心弦，顯出它在人類心靈歷史的地位和意義。這對往後的作品如《長生殿》、《紅樓夢》是有啓示意義的。

好的內容理當有好的載體，才能相得益彰。《嬌紅記》的情結構適時承擔了這個任務。它可說集前代愛情劇衝突之大成。作品先寫申、嬌了解、試探、佯怒嬌嗔等兒女糾紛，這是說明主人公內心情理的衝突；次寫天降暴雨、申生熟睡，兩次誤了約會，這是偶然因素造成的衝突；再寫申父兩次促歸造成的離別和王父拒婚造成的痛苦，這是家長造成的衝突；四寫飛紅介入和鬼妖迷惑造成申、嬌誤會，這是第三者介入造成的衝突；末寫帥府逼婚，導致申、嬌殉情，這是權豪勢

要造成的衝突。這些衝突環環相扣、前後相連，使情節曲折跌宕，使申、嬌愛情受到更多、更重的考驗，也使他們的愛情理想更爲堅定、明亮。其中二、四項在製造誤會的舊形式下有了新的內容，而第五項則是前所未有，它開拓了空間，使申、嬌愛情承受了更深重的壓力，從而也提升了作品的思想意義。

這樣一部作品是近年來才受到重視的。筆者在翻閱相關論著時，感到一些重點雖經研究者出，總覺不是很完整。作者如何藉情節結構具體呈現主題，至今尚未有專文，故不揣鄙陋，定了個很窄的題目，希望能落實到作品上面，更清晰的說明≪嬌紅記≫的特點，做爲文學史思考的基礎。

參考文獻

(1) 王季思等，「「節義鴛鴦塚嬌紅記」後記」，中國十大古典悲劇集，第 495 頁。
(2) 蕭作銘，「時代的浩歌——孟稱舜劇作思想內容淺析」，武漢大學學報，第六期，第 114 頁 (1985)。
(3) (a) 蕭善因、張全太，「一部承先啓後的愛情悲劇——「嬌紅記」和元代四大愛情劇的比較分析」，中華戲曲第二輯，第 261-264 頁。
(b) 葉小帆，「「羅密歐與朱麗葉」和「嬌紅記」比較初探」，見葉小帆比較文學論文集，第 111-117 頁 (1984)。
(c) 歐陽光，「孟稱舜和他的「嬌紅記」」，古代戲曲論叢，中山大學學報哲學社會科學論叢第一輯，第 149-153 頁。
(d) 高義龍，「「嬌紅記」賞析」，中國古典名劇鑑賞辭典，第 683 頁。
(4) (a) 朱穎輝，「孟稱舜「嬌紅記」的悲劇美」，戲曲研究第九輯，第 143-152 頁。
(b) 歐陽光，「孟稱舜和他的「嬌紅記」」，古代戲曲論叢，中山大學學報哲學社會科學論叢第一輯，第 149-153 頁。
(5) 蕭善因、張全太，「一部承先啓後的愛情悲劇——「嬌紅記」和元代四大愛情劇的比較分析」，中華戲曲第二輯，第 255 頁。
(6) 葉小帆，「「羅密歐與朱麗葉」和「嬌紅記」比較初探」，見葉小帆比較文學論文集，第 117 頁 (1984)。
(7) 曾永義，「評論欣賞中國古典戲劇的態度與方法」，見中國古典戲劇的認識與欣賞，正中書局，第 299-323 頁 (1991)。
(8) 「嬌紅記賞析」，中國古代十大悲劇賞析，北京廣播學院，第 985 頁。
(9) 蕭善因、張全太，「一部承先啓後的愛情悲劇——「嬌紅記」和元代四大愛情劇的比較分析」，中華戲曲第二輯，第 262 頁。

The Art of Plot Arrangement in Meng Cheng-Shun's Lyrical Drama Chiao Hung Chi

CHIN-KUEI-YU HSIEH
Department of General Subject in Chinese, History, and Philosophy
Colleges of Science and Engineering, Foreign Languages, Human Ecology,
Fu Jen Catholic University,
Taipei, Taiwan 24205, R.O.C.

ABSTRACT

This paper deals with Meng Cheng-Shun's Chiao Hung Chi, a lyrical drama written during the late Ming period. The purpose of the study is to analyze the arrangement of plots in Chiao Hung Chi in order to present its theme. The author concludes that this lyrical drama is an epitome of dramatic conflicts found in former romantic plays. Furthermore, the thoughts demonstrated in the lyrical drama have proved to transcend those described in any work of the same kind that has ever been written before. Therefore, Chiao Hung Chi may be said to serve as a link between past and future in the history of Chinese literature.

ABSTRACTS OF PAPERS BY FACULTY MEMBERS OF THE COLLEGE OF SCIENCE AND ENGINEERING THAT APPEARED IN OTHER REFEREED JOURNALS DURING THE 1995 ACADEMIC YEAR

The Asymptotic Distribution of the Process Capability Index C_{pmk}

SY-MIEN CHEN (陳思勉) AND NAI-FENG HSU

Communications in Statistics: Theory and Methods,
Volume 24, Issue 5, pp. 1279-1291 (SCI) (1995)

The main result of this paper is that under some regularity conditions, the distribution of an estimator of the process capability index C_{pmk} is asymptotically normal.

A Stydy on Economic $\bar{X}$-Control Charts

陳思勉　湯翠玲

第四屆南區統計研討會論文集，第 493-505 頁 (1995)

本篇論文的研究重點是想突破多重模型中，關於非隨機因素（assignable causes）發生情形的獨立性。在以往的研究中，我們不難發現在各種多重模型中，常有不符合實際狀況的情形出現；往往一方面假設其彼此的發生是無關的、互不影響的，但在分析時卻又因模型分析上的困難，常多加製肘的添加一些甚爲勉強的理由加以限制。

在本文中，我們嘗試在完全不加以限制非隨機因素發生的條件下，找出解決的方法。結果令人頗爲滿意。甚至由原先的二重非隨機因素模型，更推廣至多重非隨機因素模型的一般式，其亦有完善圓滿的結果。

Estimation Algebras on Nonlinear Filtering Theory

WEN-LIN CHIOU (邱文齡)

Proceedings of the International Conference on
Control and Information, pp. 367-370 (1995)

The idea of using estimation algebras to construct finite dimensional nonlinear filters was first proposed by Brockett and Mitter independently. It turns out that the concept of estimation algebra plays a crucial role in the investigation of finite dimensional nonlinear filters. In his talk at the International Congress of Mathematicians in 1983, Brockett proposed to classify all finite-dimensional estimation algebras. In this paper we consider some filtering systems. In a special filtering system: (1) We have some structure results. (2) For any arbitrary finite dimensional state space, under the condition that the drift term is a linear vector field plus a gradient vector field, we classify all finite dimensional estimation algebras with maximal rank. (3) We classify all finite dimensional estimation algebras with maximal rank if the dimension of the state space is less than or equal to three. A more general filtering system is considered. The above three results can be 'used' locally. Therefore from the algebraic point of view, we have now understood generically some finite dimensional filters.

多成份鹵化物玻璃的拉曼散射

JIUNN-DER YANG AND LUU-GEN HWA (華魯根)

Chinese Journal of Materials Science, **26**(4), 319-322 (1994)

以氟化鋯 (ZrF_4) 和／或氟化鉿 (HfF_4) 爲基質的多成份氟化玻璃，展現從紫外光區到中紅外光區的極高透明度，爲了瞭解影響比玻璃對紅外光透明度的原因，我們應用偏極化拉曼散射來研究玻璃的結構，試圖從拉曼散射光譜的譜峰位置來證實玻璃結構中各種原子的振動模態，比較氟化玻璃，與其相似成份的氟化物晶體的拉曼頻率位移，可得到玻璃基本結構中各原子的配位數大小。此外，低頻拉曼散射與玻璃無序性結構的關係，將被簡單的討論。

Temperature and Frequency Dependence of Multiphonon Absorption in Halide Glasses

SIN-YI KO AND LUU-GEN HWA (華魯根)

Chinese Journal of Materials Science, 27(1), 67-70 (1995)

The halide glasses based on ZrF_4 or/and HfF_4 heavy metals exhibit high transparency over the frequency range from the near UV to the mid IR. This makes them the promising infrared transmitting materials. In order to understand their infrared properties, the temperature and frequency dependence measurement of multiphonon edge absorption in 2 multicomponent halide glasses were performed. The results show the IR edge is featureless with weak structure, and the multiphonon absorption coefficients decrease exponentially with increasing frequency. The results will be discussed in terms of intrinsic multiphonon absorption theory.

Studied of the Hydrated Surface Layer on Heavy-Metal Fluoride Glasses by IR Spectroscopy

FU-FA HSAO AND LUU-GEN HWA (華魯根)

Proceedings of 1995 Conference of the Chinese Society for Material Sciences, Vol. II, p. 20 (1995)

The Fluoride Glasses based on ZrF_4 or/and HfF_4 heavy metal exhibit high transparency over the frequency range from the near UV to the mid IR (6-7 μm). This property makes them possible candidate for a wide variety of application ranging from laser windows to infrared fiber optics. We studied the attack of liquid water on the surface layer of two commercial available ZBLAN (ZrF_4-BaF_2-LaF_3-AlF_3-NaF) Heavy-Metal Fluoride Glasses by IR spectroscopy. IR absorption measurments were performed as a function of time and temperature for ZBLAN glasses. Two IR peaks were observed at 3,440 and 1,640 cm^{-1} respectively.

The relationship between the absorbance and immersion time will be discussed in light of diffusion theory and the develpment of the absorption peaks is related to a surface layer formation on these glasses.

The Structural Investigation of Heavy-Metal Fluoride Glasses by Vibrational Spectroscopy

PI-LIN WANG AND LUU-GEN HWA (華魯根)

Proceedings of 1995 Conference of the Chinese Society for Material Sciences, Vol. II, p. 22 (1995)

The Heavy-Metal Fluoride glasses exhibit high transparency from the mid-IR to the near UV. The property makes them possible candidate for a wide variety of applications ranging from laser window to infrared fiber optics. The structural investigations of Heavy-Metal Fluoride glasses by vibrational spectroscopy (Infrared Reflectivity Multiphonon edge absorption and Polarized Raman Scattering measurements) were performed. From our study, we are able to understand the fundamental vibrational characteristics of these glasses and the primary mechanisms influencing their infrared transparency. The LO-TO vibrational pairs splitting were also observed for these glasses by IR reflection measurement at different incident angle. The results will be discussed in light of short and/or intermediate range order.

Aqueous Coprecipitation Synthesis of $Nd_{1.85}Ce_{0.15}CuO_{4-y}$ Superconductors

Y. D. YAO, J. K. WU, K. T. WU (吳坤東),
Y. Y. CHEN, C. TIEN AND D. S. HUNG

Physica C, pp. 235-240, 553-554 (1994)

An aqueous coprecipitation synthesis process has been developed to preparing high quality *N*-type NdCeCuO superconductors. Due to the intimate mixture of coprecipitates was treated at the atomic level; with proper controlling the pH value of the solutions, the superconducting properties of the final homogeneous fine-grain-size NdCeCuO superconductors are much better than that prepared by solid state reaction technique.

Magnetoresistance Study in Cr-Co Superlattices and Films

Y. D. YAO, Y. LIOU, J. C. A. HUANG, S. Y. LIAO, C. H. LEE, K. T. WU (吳坤東), Y. Y. CHEN, C. L. LU AND W. T. YANG

Chinese J. Phys., **32**, 863-869 (1994)

The magnetoresistance (MR) of $(Co/Cr)_{70}$ superlattice with *hcp*-Co layers and *bcc*-Cr layers on both MgO and Al_2O_3 substrates with Mo as a buffer layer, and the anisotropy magnetoresistance (AMR) of the single-crystal *hcp*-Co, *fcc*-Co, as well as the CoCr alloy thin films have been studied at 10 and 295 K, respectively. The MR of Co/Cr multilayers has been observed to increase by a factor of 3.8 with replacing its substract MgO (100) by Al_2O_3 $(1\bar{1}02)$ only. The AMR of Co films has been found to decrease rapidly by the buffer layer as well as the alloying effect between Co and Cr.

Influence of Crystal Structure on the Magnetoresistance of Co/Cr Multilayers

Y. LIOU, J. C. A. HUANG, Y. D. YAO, C. H. LEE, K. T. WU (吳坤東), C. L. LU, S. Y. LIAO, Y. Y. CHEN, N. T. LIANG, W. T. YANG, C. Y. AND B. C. HU

J. Appl. Phys., **76**, 6516-6518 (1994)

Epitaxial Co/Cr multilayers, and single-crystal Co thin films etc. have been grown on MgO and Al_2O_3 substrates with Cr and Mo as buffer layers by molecular beam epitaxy technique. From the structure and magnetoresistance studies, we have found that the ferromagnetic anisotropy of resistance (AMR) is strongly influenced by the buffer layer, but with negligible effect due to the variation of the structure of Co films. The AMR of Co film on Cr buffer layer is quite small (0.1%); however, the MR of Co/Cr multilayers is almost one order larger than the AMR of Co film on Cr buffer layer. An enhancement factor of 4 for the MR in Co/Cr multilayers by the interface roughness has been observed. This suggests that the effect due to the spin dependent scattering at the interfacial regions of the superlattice is larger than that due to the spin dependent scattering in the ferromagnetic layers for the MR in the Co/Cr multilayer system.

Effect of the Waue-Shear Interaction on Gravity Wave Activity in the Lower and Middle Atmosphere

F. S. KUO AND H. Y. LUE (呂秀鏞)

J. Atmos. Terr. Phys., 56(9), 1147-1155 (1994)

Observaional results of the wave activities and the vertical wave number spectra of the horizontal wind fluctuations and the temperature/density fluctuations in the lower and middle atmosphere obtained by various groups using different instruments at different locations are reviewed and summarized. Then, we use a simple analytic model of wave shear interaction to explain the wave-energy dissipation observed in the stratosphere/lower mesosphete, the east west anisotropy of the wave propagation, and the deceleration of the zonal mean flow, in summer and in winter in the middle mesosphere, the annual variation in the upper troposphere/stratospher/lower mesosphere, and the semi-annual variation in the middle mesosphere. We also point out that the saturation spectra observed in the middle mesosphere and the winter troposphere are caused by wave motions in the strong background wind shear and the low stability temperature profile, and that the saturation spectrum is universally $N^2/2m^3$ (where N is the Brunt-Väisälä frequency and m is the vertical wave number).

Regio- and Stereocontrolled Synthesis and Diels-Alder Reactions of (*Z*)-2-(Phenylthio)-1-(trimethylsilyl)-1, 3-butadiene

SHANG-SHING P. CHOU (周善行) AND MAO-HSUN CHAO

Tetrahedron Letters, 36(48), 8825-8828 (1995)

The title compound was prepared from 3-phenylthio-2-sulfolene by (1) deprotonation with butyllithium followed by treatment with chlorotrimethylsilane; (2) isomerization to the 3-sulfolene analog by deprotonation and quenching with acid at low temperature; (3) thermal desulfonylation. The Diels-Alder reaction of the title diene was also studied.

Stereoselective Synthesis and Diels-Alder Reactions of (*Z*)- and (*E*)-1, 2-Bis(phenylthio)-1, 3-butadiene

SHANG-SHING P. CHOU (周善行), DER-JEN SUN AND HAI-PING TAI

Journal of the Chinese Chemical Society, **42**, 809-814 (1995)

Bromination of 3-phenylthio-2-sulfolene (2) with *N*-bromosuccinimide gave 2-bromo-3-phenylthio-2-sulfolene (3) which was converted mainly was converted mainly to 2, 3-bis(phenylthio)-2-sulfolene (4) by treatment with sodium phenylthiolate. Thermal desulfonylation of 4 at different temperatures in the presence of a base (DBU) yielded stereoselectively the (*Z*)- and (*E*)-1, 2-bis(phenylthio)-1, 3-butadiene (6). These two geometric isomers could be thermally interconverted. The Diels-Alder reactions of 6 were also investigated. Only the (*Z*)-diene **6a** could undergo the Diels-Alder reaction; the (*E*)-diene **6b** was *in situ* converted to the *Z* isomer before undergoing the Diels-Alder reaction. The reaction of **6a** with *N*-phenylmaleimide gave the cycloaddition product 7 with complete *endo* selectivity, but under daylight or during chromatography it readily underwent a thioallylic rearrangement to yield 8 wihe inversion of configuration. The cycloaddition of **6a** with methyl acrylate proceeded regiospecifically, but generating a mixture of *endo* and *exo* isomers. The *endo/exo* ratio could be increased by using $ZnCl_2$ as the catalyst.

Regioselectivity of Ene Reaction: Dimerization of 8-Chlorobicyclo[5.1.0]oct-1(8)-ene

GON-ANN LEE (李國安), CHAUR-SHENQ SHIAU, CHI-SHENG CHEN AND JAY CHEN

Journal of Organic Chemistry, **60**, 3565-3567 (1995)

2-Chlorinated 1,3-fused bicyclic cyclopropene, 8-chlorobicyclo[5.1.0]oct-1(8)-one (6) is synthesized and isolated from the dehalogenation of the 1-bromo-8, 8-dichlorobicyclo[5.1.0]octane (7) derived from cycloheptene.

Compound **6** undergoes ene reaction to form two dimers, 8-chloro-7-(8-chlorobicyclo[5.1.0]oct-1-yl)bicyclo[5.1.0]oct-1(8)-one (**9**) and 8-chloro-7-(8-chlorobicyclo[5.1.0]oct-8-yl)-bicyclo[5.1.0]oct-1(8)-one (**10**) (ratio 1:30). The compound **9** rearranges to vinyl carbene followed by intramolecular carbene insertion to generate cyclic allene which isomerized to 2-chloro-4-(8-chlorobicyclo[5.1.0]oct-1-yl)cycloocta-1, 3-diene (**12**).

Characterization of a Polypyrrole Microsensor for Nitrate and Nitrite Ions

JONG-RU RAU, SHOW-CHUNG CHEN (陳壽椿)
AND HSIN-WEI SUN

Electrochimica Acta, **39**(18), 2773-2779 (1994)

Affinities of polypyrrole for nitrite and nitrate ions can be exploited for use in ion sensing.Using modern microsensor fabrication technique this has led to the development of a highly stable, sensitive and fast-response sensor for nitrate and nitrite ion. Despite its poor differentiation between these two ions and despite cationic interferences from heavy metals present in high concentrations, it promises reliable monitoring of nitrate or nitrite ion in a well-defined environment.

Structure and Thermodynamics of 7-Azaindole Hydrogen-Bonded Complexes

PI-TAI CHOU, CHING-YEN WEI,
CHEN-PIN CHANG (張鎮平) AND MENG-SHIN KUO

J. Phys. Chem., **99**, 11994-12000 (1995)

The thermodnamics of a variety of 7-azaindole (7AI) hydrogen-bonded complexes in the ground state have been studied on the basis of absorption spectroscopy in combination with *ab inttio* calculations at 6-31G* level. The results indicate that the strength of hydrogen bonding significantly affects the ground-state electronic configuration of 7AI in both normal and tautomer forms. The enthalpy, ΔH, of the association reactions was calculated to be −14.2, −11.3 and −9.2 kcal/mol for the

1:1 acetic acid/7AI complex, 7AI dimer, and methanol/7AI complex, respectively. These values are in fair agreement with the experimental results of −12.3, −9.5 and −6.3 kcal/mol. Calculations also show a stronger hydrogen-bonding effect in the tautomer complex forms than in their respective normal forms. Relative energy levels of excited-state double proton transfer are discussed on the basis of ground-state thermodynamics in combination with the spectroscopic data.

Acid Catalysis of Excited-State Double-Proton Transfer in 7-Azaindole

CHEN-PIN CHANG (張鎮平), WEN-CHI HWANG,
MENG-SHIN KUO, PI-TAI CHOU AND JOHN H. CLEMENTS

J. Phys. Chem., **98**, 8801-8805 (1994)

The acid-catalyzed excited-state double-proton transfer (ESDPT) in 7-azaindole has been studied. In carboxylic acids and phosphoric acids, the formation of a 1:1 cyclic hydrogen bonded acid/7-azaindole complex was observed with a remarkably large association constant of $>1.0\times10^{4}\ M^{-1}$. In contrast to alcohol-catalyzed ESDPT, in which the slow ESDPT dynamics involve a large amplitude of solvent reorganization, the rate of acid catalyzed ESDPT is much greater than the decay rate ($\sim1.0\times10^{9}\ s^{-1}$) of the normal emission, resulting in a unique tautomer emission. The highly efficient acid-catalyzed ESDPT in 7-azaindole points to the biological application of 7-azaindole as a suitable acid derivative probe in a hydrophobic environment such as in the cell membrane.

Study of Droplet Configuration of Polymer Dispersed Liquid Crystal Films

SUNG-CHANG PENG, JIUNN-WEN YU
AND SUNG-NUNG LEE (李選能)

IUPAC International Symposium on Functional and High Performance Polymers, Taipei, Preprints, pp. 357-358 (1994)

Polymer dispersed liquid-crystal (PDLC) composites have been the

subject of many researchers during the last several years due in part to their usefulness in making displays. In a PDLC composite, a liquid crystal (LC) mixture with positive dielectric anisotropy is dispersed in an isotropic polymer matrix in the form of droplets of micrometer or submicrometer sizes. Such a PDLC composite can be cast into a thin film that has a translucent appearance if there is a mismatch between the refractive index of the LC droplets and that of the polymer matrix. Under an applied voltage, the films change to an optically transparent state provided the ordinary refractive index of LC droplets matches the refractive index of the polymer. The refractive index of the LC is controlled by the molecular alignment in the LC droplets. The present study tries to establish the correlations between the molecular alignment, droplet size and dielectric behaviors. Study the effect of the LC fraction and the domain size of the PDLC film on the dielectric properties, as well as on its switching voltage.

New Aspect on Di-μ-[bis(diphenylphosphino)methane]-dichlorotrigold (I) Chloride, Including Its Crystal and Molecular Structure

IVAN J. B. LIN (林志彪), J. M. HWANG, DA-FA FENG, M. C. CHENG AND YU WANG

Inorganic Chemistry, **33**, 3467 (1994)

The reaction of $HAuCl_4 \cdot 4H_2O$ with dppm ($PPh_2CH_2PPh_2$) in ethanol produces $[Au_3(dppm)_2Cl_2]Cl$, **3**. This compound equilibrates with $Au_2(dppm)Cl_2$, **1**, and $Au_2(dppm)_2Cl_2$, **2**, in solution. ^{31}P NMR studies at various temperatures suggest that the exchange rate between compounds **1** and **3** is faster than that between compounds **2** and **3**. The free chloride anion in **3** is responsible for these exchanges. The strong emission of **3** in solid is attributed to the short Au···Au distances. Crystal structure data for compound **3**·EtOH: space group $C2/c$, with $a=14.184(3)$Å, $b=18.556(6)$Å, $c=20.597(6)$Å, $\beta=97.56(2)°$, $Z=4$, and $V=5{,}285(3)$Å^3.

Electronic-Relaxation Dynamics in Solution

P. J. ROSSKY, B. J. SCHWARTZ
AND WEN SHYAN SHEU (許文賢)
Ultrafast Phenomena IX, **60**, 53-57 (1994)

Results obtained via quantum molecular dynamics simulation with electronic transitions are presented for the systems of a hydrated excited state halide ion and the hydrated electron. The ability to simultaneously describe the molecular processes and directly evaluate the ultrafast spectral observables is shown to provide a unique window on the underlying microscopic processes.

Graft Copolymer Networks of Polyurethane and Epoxy Structures, I: Dynamic Mechanical Properties

PO-HOU SUNG (宋博厚) AND WEN-GUEY WU
Eur. Polym. J., **30**(8), 905-909 (1994)

The dynamic mechanical properties of polyurethane (PU) grafted epoxy polymer networks have been investigated. The glass transition region is successfully broadened on variation of the degree of phase separation. The tensile strength initially increases with increasing PU content and reaches its maximum value when the PU/epoxy ratio is about 20/80.

7-Azaindole-Assisted Lactam-Lactim Tautomerization via Excited-State Double Proton Transfer

PI-TAI CHOU, CHING-YEN WEI,
CHEN-PIN CHANG (張鎮平) AND CHIENG-HWA CHIU
J. Am. Chem. Soc., **117**, 7259-7260 (1995)

The photophysics of 7-azaindole (7AI) have been studied extensively since Taylor et al. first reported the excited-state double proton transfer

(ESDPT) in the 7AI dimer. The current topic of ESDPT in a variety of 7AI hydrogen-bonded complexes has important applications for probing both solvation dynamics and biological systems. The ESDPT reaction in 7AI hydrogen-bonded systems can be classified into two categories. The acid, alcohol, and water assisted ESDPT in 7AI can be specified as a catalytic process since the molecular structure of the guest species (e. g., acetic acid in the acetic acid/7AI complex) remains unchanged. On the other hand, adiabatic ESDPT in the 7AI dimer results in a $7AI^{T*}/7AI^{T}$ form consistin of an excited and an unexcited proton-transfer tautomer (* represents the excited state). Since both host and guest molecules change their structures, the ESDPT is a noncatalytic process in which 7AI in the dimeric form acts not as a catalyst but rather as a reactant. The latter case is important from a chemistry perspective. In the acetic acid catalyzed ESDPT reaction, the $7AI^{k}\rightarrow 7AI^{T*}$ tautomerization has been estimated to be ~13 kcal/mol exothermic. Since the noncatalytic type of ESDPT requires simultaneous tautomerization for both 7AI and its guest molecule, this process, from the energy viewpoint, provides ~13 kcal/mol excess.

黑面琵鷺之生態研究（一）

顏仁德　廖光正　陳立楨　劉靜榆
曾彥學　王　穎　陳擎霞　張宏明
J. JONKER　E. P. R. POORTER

83 年生態研究第號，第 9 號，第 38-57 頁 (1990)

本研究之目的在於了解黑面琵鷺渡冬區之狀況，調查方式休息區、覓食區及新浮沙洲三區進行。經 83 年 1 至 6 月調查結果休息區共發現魚類 26 種、昆蟲類 8 目 18 科 31 種、鳥類 4 目 12 科 26 種；蟹類 5 科 19 種；軟體動物 8 科 10 種；常見植物有土牛膝等 6 種。覓食區方面共發現魚類 23 種、哺乳類 2 種、兩棲類 1 種、昆蟲類 5 目 6 科 15 種、鳥類 7 目 14 科 31 種；蟹類 4 科 15 種；軟體動物 8 科 10 種；植物有土牛膝、五節芒等 162 種，新浮崙沙洲共發現魚類 24 種、哺乳類 2 種、昆蟲類 7 目 11 科 16 種、鳥類 3 目 6 科 13 種；蟹類 3 科 15 種；軟體動物 7 科 8 種；常見植物有白茅等 5 種。

比較黑面琵鷺棲息區、鄰近覓食區及可能替代棲地之結果，有關臺南縣政府所擬保護區設置替代方案之新浮崙沙洲，與黑面琵鷺原棲地環境差異極大，底棲動物雖類似，但族群數量則顯著的差異，且新浮崙沙洲區之漲退潮差明顯的較堤內之浮覆洲爲大，又因其面積逐潮縮減，作爲替代區可能缺少足够之安全距離。

德基水庫集水區自然生態動植物種源調查計畫（二）——武陵地區生態種源庫之調查

陳 擎 霞

中華民國自然生態保育協會，第 1-66 頁 (1994)

武陵四秀爲大雪山的精華地帶，亦爲七家灣溪的集水區。其由東北向西南成矩狀的環抱，以喀拉業山、詩崙山、桃山、池有山、品田山、雪山北峰、雪山東峰。依其山塊之形狀、高度、斷崖、山麓階層來推斷，其爲板塊運動時所形成的疊狀山地。加上四周的雪山、南湖大山所擁有明顯冰斗、冰谷的地形與桃山頂西南面下的羊伏石而得知，武陵四秀曾爲冰河的遺跡。故七家灣溪中能發現到冰河期的孑遺生物櫻花鉤吻鮭。在此環境中，其生態資源自彌足珍貴，但由於人爲的開發，果園、菜園逐漸蠶食其原生植被分布地。經調查結果發現該地區擁有 101 科 383 種植種，稀有種有 10 科，野生種有 17 目 46 科 113 種，其中哺乳類 18 種、鳥類 66 種、兩棲爬蟲類 5 科、蝶類 24 種。

德基水庫集水區自然生態動植物種源調查計畫（三）——大雪山地區生態種源庫之調查

陳 擎 霞

中華民國自然生態保育協會，第 1-44 頁 (1995)

大雪山山系以北屬苗栗縣泰安鄉，以南爲臺中縣和平鄉，該山系亦爲志樂溪與大雪溪之分界，也是大雪溪向志樂溪搶水的區域，有多處相當典型的塌陷地形。本區海拔雖高，但因受雪山山系及雪山與大霸尖山之間的稜脊屏障，多數的山頂除高山箭竹外都有大片的喬木森林生長，植被茂密而完整；且因路遠而山勢陡峻，甚少人跡，因而提供能適應高海拔地區的野生動物，良好之棲息場所，區內常可見中、大型動物活動的痕跡。根據調查結果顯示該地區擁有 71 科 154 屬 207 種植物，野生動物有 9 目 21 科 41 種，其中哺乳動物 5 目 9 科 11 種，鳥類 4 目 12 科 30 種，特有種有 14 種，保育類野生動物共 19 種。

無尾港水鳥保護區基礎調查——植被狀況、人文社會調查及地理資訊蒐集計畫

陳 瑩 霞

宜蘭縣政長委託中華民國野鳥學會研究，第 1-88 頁 (1993)

無尾港水鳥保護區位於宜蘭縣蘇澳鎮內，於民國八十二年九月二十四日正式公告成立。其爲一狹長河道淤積之沒口河，東西太平洋、西界岳明國小、南至澳仔角涯邊、北抵新城溪，面積爲 1,016,194 公頃。涵蓋河流、湖泊、沼澤、旱田、沙灘、防風林及山丘樹林等複雜之生態環境。其間植種豐富、植生變化多、植被分佈適當、隱遮性高，再加上水質除鐵質含量較高外，無污染可言。故每年吸引大批候鳥在此停息，是北部地區鳥類的天堂，亦爲臺灣十二大濕地之一。此地區若加以勢當規劃，則能達到生態保育、自然教育、戶外休閒遊憩欣賞等功能。

Cellular Thiols as a Determinant of Responsiveness to Menadione in Cardiomyocytes

WONG-FANG TZENG (曾婉芳), TZEON-JYE CHIOU, CHIN-PENG WANG, JIA-LUEN LEE AND YEE-HSIUNG CHEN

J. Mol. Cell. Cardiol., **26**, 889-897 (1994)

The role of intracellular thiols in menadione-mediated toxicity was studied in neonatal rat cardiomyocytes. The sensitivity of cardiomyocytes to menadione was greater than that of skeletal muscle cells and 3T3 fibroblasts. Before cell degeneration, menadione induced marked depletion of intracellular thiols and an increase of oxidized glutathione. The sensitivity of these cells to menadione correlated with the level of depletion of intracellular thiols. After incubation of cardiomyocytes with menadione, glutathione reductase activity was inhibited and lipid peroxidation was increased. Both dicumarol (an inhibitor of DT-diaphorase) and diethyldithiocarbamate (an inhibitor of superoxide dismutase) enhanced the capacity of menadione to induce cellular damage and to cause depletion of intracellular glutathione. Decreasing intracellular glutathione by pretreatment of cells with *N*-ethylmaleimide or buthionine sulphoximine also increased menadione-induced cell degeneration. Preincubation with cysteine or dithiothreitol suppressed

the capacity of menadione to damage the cells. Menadione-induced lipid peroxidation was also suppressed by the same treatment. These results show that the oxidative stress induced by menadione in cardiomyocytes results in the depletion of glutathion and protein thiols. Both DT-diaphorase and superoxide dismutase can protect cells from the toxicity of menadione. Cellular thiols are determinants of the responsiveness to menadione.

Methods for Preventing Precipitation of Copper from Copper Based Bactericidal Compostitions Containing Iron

M. N. SCHROTH, Y.-A. LEE (李永安) AND D. M. CHONG

United States Patent, **5**, 385, 934 (1995)

Disclosed herein are copper based fungicidal and bactericidal compositions having enhnaced activity against fungi and bacteria, methods of using such compositions as well as methods for increasing the effectiveness of the copper based fungicidal and/or bactericidal compounds employed in such compositions. An aggregation inhibiting salt is included within these compositions to prevent aggregate and/or sediment formation upon the addition of Fe^{3+} to the composition.

Genes Involved in Quinate Metabolism are Specific to the DNA Homology Group 6 of *Xanthomonas campestris*

Y.-A. LEE (李永安), C.-H. LI AND P. P. YU

Plant Pathol. Bull., **3**, 237 (1994)

Genes involved in quinate metabolism (QM) were cloned from a strain C5 of *X. c.* pv. *juglandis*, which is a member of DNA homology group 6 of *Xanthomonas campestris*. The genes were located on a 4.2 kb *Kpn* I-*Eco* RV fragment, pQM 38, which conferred quinate metabolism capacity to *X. c.* pv. *celebensis*, which is negative on succinate-quinate (SQ) medium test. Tn3-Spice insertional analyses further located QM genes on a length of about 3.0 kb within pQM 38.

A 0.7 kb *Sal* I-*Pst* I fragment internal to QM genes was used as a probe to hybridize against total genomic DNA from 43 pathovars of *X. campestris*. The fragment hybridized only to total genomic DNA from the four pathovars of DNA homology group 6, i.e., *X. c.* pv. *celebensis*, *X. c.* pv. *corylina*, *X. c.* pv. *juglandis*, and *X. c.* pv. *pruni*, and from *X. c.* pv. *carotae*, which belongs to DNA homology group 5, but is most closely related to DNA homology group 6. This 0.7 kb fragment was also used as a probe to hybridize *Bam* HI or *Sal* I-digested total genomic DNAs from four pathovars of DNA homology group 6 and *X. c.* pv. *carotae*. Restriction fragment length polymorphism (RFLP) was found when total genomic DNAs were digested with *Bam* HI, but all four pathovars of the group 6 contain a 5.7 kb band, which is not found in *X. c.* pv. *carotae*. No RFLP was found when digested with *Sal* I. Accordingly, quinate metabolism is the first group 6-specific property both phenotypically and genotypically.

Isolation of Specific Probes for Plant Pathogenic Bacteria by a DNA Subtractive Hybridization

C.-C. WANG AND Y.-A. LEE (李永安)

Plant Pathol. Bull., 3, 236 (1994)

The subtractive hybridization method developed by Kunkel et al. was modified to isolate specific probes against plant pathogenic bacteria, such as *Xanthomonas campestris* pv. *campestris*, and *Erwina carotovora* subsp. *carotovora*. The specificity of cloned probes was first tested by dot-blotting against genomic DNAs isolated from 43 different pathovars of *X. campestris*, or from 6 different species of *Erwinia*, and then by colony hybridization against saprophytic bacteria isolated from leaf surfaces of cabbages, and soil samples from cabbage cultivation areas in Young-Ming mountain. The results showed that the modified method could rapidly and specifically isolate a probe for bacteria. The probes isolated by the method can be used for epidemiological studies and for understanding the functions specific to each plant pathogenic bacteria.

A Repetitive Sequence Widely Distributed in the Pathovars of *Xanthomonas camppestris* Shows Locational Variation within the Strains of *X. c.* pv. Campestris

S.-P. CHU AND Y.-A. LEE (李永安)

Plant Pathol. Bull., **3**, 237 (1994)

A repetitive sequence was found inside the 1.7 kb *Sma* I fragment cloned from *Xanthomonas campestris* pv. *juglandis*. The sequence had at least 6 copies in the bacterial genome determined by Southern hybridization using two internal fragments separated by a single restriction enzyme site as probes. Through hybridization tests, homologous sequences were detected in several pathovars of *X. campestris*, such as *X. c.* pv. *campestris*, *X. c.* pv. *oryzae*, *X. c.* pv. *oryzicola*, *X. c.* pv. *cassiae*, *X. c.* pv. *khayae*, *X. c.* pv. *lespedezae*, and some other pathovars, but not found in *X. c.* pv. *phaseoli*, *X. c.* pv. *physalidis*, and *X. c.* pv. *vesicatoria*. A 0.5 kb *Ava* II internal fragment of repetitive sequence was chosen as a probe to determine the repetitive patterns in the several strains of *X. c.* pv. *campestris* isolated from cabbages in the cultivation areas of Young-Ming mountain. The highly locational variation of repetitive sequence was found within the strains of *X. c.* pv. *campestris*. The same phenomenon also occurred within the strains of *X. c.* pv. *juglandis*. The results indicated that the repetitive sequence were widely distributed in the pathovars, and may cause genomic variation in each pathovar.

Molecular Cloning and Expression of the Coat Protein Genes of Cf, A Filamentous Bacteriophage of *Xanthomonas campestris* pv. *citri*

MEI-KWEI YANG (楊美桂), HUEI-MEI HUANG, YEN-CHUN YANG AND WEI-CHIH SU

Bot. Bull. Acad. Sin., **36**, 207-214 (1995)

Particles of the filamentous bacteriophage cf contain a major coat

protein, the B protein with a molecular weight of approximately 6,000 daltons. In addition, a minor coat protein, the A protein, has a molecular weight of about 50,000 daltons was also identified on sodium dodecyl sulfate-containing polyacrylamide gels. A 3.3 Kbp *Hind* II fragment derived from cf genome was cloned into the expression plasmid pG 308N, a *E. coli* plasmid which carries pL promoter. The recombinant plasmid pG 33 and a series of deletion derivatives of pG 33 were constructed and transformed into *E. coli* DG 116 for expression of phage cf genes. The genes code for A and B proteins of cf were found to be located on the 2.0 Kbp *Eco* RI-*Hinc* II fragment. The complete nucleotide sequences of the 2.0 Kbp *Eco* RI-*Hinc* II insert were determined. The deduced amino acid sequence corresponds to a 62-amino-acid-residue polypeptide that has a calculated Mr of 6,070 was identified by SDS/PAGE and immunoblotting as the B protein. Another open reading frame (ORF 419) downstream of the B protein gene (ORF 62) was found and shown to code for a polypeptide of 419 amino acids with a calculated Mr of 44,676 that exhibit considerable identity to the A protein. The presence of promoter regions was examined upstream of these two ORFs and the apparent capability to activate the expression of these genes was also shown.

The Hysteresis Effect of Magnetizing Branch on Torque Pulsations of an Induction Machine with Nonsinusoidal Excitation

YUANG-SHUNG LEE (李永勳) AND KOU-CHENG HSU (徐國政)

Proceedings of the IASTED International Conference,
Colombo, Sri Lanka, pp. 127-130 (1995)

A dynamic model that includes saturation and hysteresis of the magnetizing branch is proposed for multiple winding machine. A novel describing function is used to trace the nonlinearity of core magnetization characteristics of an induction machine. Steady state and transient analysis are presented to show the significant influence of the magnetizing branch nonlinearity on torque fluctuation of an induction machine with pulse width modulation (PWM) inverter excitation. The

configuration scheme under investigation bases on multiple stator winding sets with a multiple terminal inverter motor driving system for different displacement angles between the stator winding sets. Simulation results and Fast-Fourier-Transform (FFT) analysis demonstrate that not only can the torque fluctuation amplitude be reduced, but the system dynamic performance is also improved through a multiple terminal inverter feeding to a multiple winding induction machine with proper winding displacement angle.

Shaft Torsional Oscillation of Induction Machine Including Saturation and Hysteresis of Magnetizing Branch with an Inertia Load

YUANG-SHUNG LEE (李永勳) and KOU-CHENG HSU (徐國政)

Proceedings of 1995 International Conference on Energy Management and Power Delivery (EMPD 1995), The West in Stamford and West in Plaza, Sigapore, pp. 134-139 (1995)

This paper describes the torsional oscillation phenomenon occurring in a multiple winding induction machine. It includes the effects of nonlinearity and component interactions between driver and inertia load through mass spring coupling system under starting transient disturbance. The model fidelity is evaluated from the foreseen torsional torque of the motor driving system by several excitation sources. Steady state and transient analysis are presented to show the significant influence of the magnetizing branch nonlinearity on the torque oscillation for an induction machine with sinusoidal or pulse width modulation (PWM) inverter excitation to drive inertia load. Simulation results and Fast-Fourier-Transform (FFT) analysis demonstrate that not only can the torsional oscillation amplitude be reduced, but the system dynamic performance is also improved through a multiple terminal inverter feeding with proper displacement angle between stator winding sets. In addition, starting process analysis shows that the torsional oscillation components can be substantially reduced by the selected starting methods with proper switching coordination. The risk of premature component failure due to the excess of the designed limit for dynamic torsional stresses can also be deminished.

Least Squares Order-Recursive Lattice Smoothers

JENQ-TAY YUAN (袁正泰) AND JOHN A. STULLER

IEEE Transactions on Signal Processing, 43(5), 1058-1067 (1995)

Conventional least squares order-recursive lattice (LSORL) filters use present and past data values to estimate the present value of a signal. This paper introduces LSORL smoothers which use past, present and future data for that purpose. Except for an overall delay needed for physical realization, LSORL smoothers can substantially outperform LSORL filters while retaining all the advantages of an order-recursive structure.

A Universal Active Filter with Transfer Admittance and Transfer Current Ratio Using Single OTA

CHUN-LI HOU, YUNG-CHANG YIN (鄞永昌)
AND PANG-CHIA CHEN

Journal of the Chinese Institute of Electrical Engineering,
2(2), 131-137 (1995)

A universal configuration for the current-mode first-order and biquadratic filters using an OTA are suggested. The proposed current-mode OTA filters can be easily cascaded with transfer current ratio filters or any load impedances. Since current is the output of an OTA, the transfer admittance and the transfer current ratio are very important. This paper gives one circuit of the same biquadratic type (i.e., lowpass, highpass, bandpass, and bandstop) for the two transfer functions mentioned above. For allpass filter, it is impossible to use the same value components to get two first-order allpass transfer functions at the same time. All the capacitors are grounded.

Least Squares Lattice Smoothers for Adaptive Equaalization

JENQ-TAY YUAN (袁正泰) AND JOHN A. STULLER

Proceedings of International Conference on Telecommunications
(ICT 1995), Nusa Dua, Bali, Indonesia, pp. 55-60 (1995)

This paper introduces least squares order-recursive lattice (LSORL)

smoothers for adaptive equalization. The LSORL smoothers use past, present and future received data sequence to estimate the present value of the transmitted data sequence. Except for an overall delay needed for physical realization, LSORL smoothers can substantially outperform conventional LSORL filters in adaptive equalization while retaining all the advantages of an order-recursive structure.

Efficient Implementation of Binary Morphological Image Processing

BRIAN K. LIEN (連國珍)

Optical Engineering, **33**(11), 3733-3738 (1994)

Morphological image processing is an important tool for a broad range of problems in image processing. A 512-entry table lookup method is used for real-time implementation. But it is not efficient to transfer this method directly into software. The author proposes a fast software implementation technique, in which a 256-entry lookup table containing neighborhood information is built and a dynamic table lookup process is applied to reduce the number of logical matching operations and the number of accesses of the neighboring pixels. In this proposed method only the foreground pixels, which are pixels on the object, are processed. Among the foreground pixels, only at the starting pixel of each "run" of 1's is it necessary to read the eight neighboring pixels. For the other pixels, it is necessary to read only three neighbors. This method shows a significant improvement in timesaving. In addition, for systems supporting fast access to consecutive address memory, the author proposes another implementation, which treats the image as a contiguous block of memory. Thus advantage is taken of RAM technology.

Part Segmentation from Stereo

LIANG-HUA CHEN (陳良華), WEI-CHUNG LI AND HONG-YUAN MARK LIAO

International Journal of Imaging Systems and Technology, **5**, 206-219 (1994)

This article addresses the problem of segmenting objects into parts

using stereo images. There are three components in the part segmentation process: surface segmentation, region grouping, and volumetric models (superquadrics) recovery/segmentation. The rurface segmentation process segments the image into a set of regions such that each region represents a smooth surface. The region grouping process merges the segmented regions into parts. Finally the process of volumetric models recovery/segmentation recovers the part model and segments that part into smaller parts if necessary. Because we use both surface and volumetric models to drive the part segmentation process, we can capture geometric properties of the object, and the application domain of our approach is broader than that of previous approaches. The performance of the proposed system is demonstrated with real images and synthetic images. Experimental results show that the system is stable and capable of handling a variety of objects.

A Bar-Code Recognition System Using Backpropagation Neural Networks

HONG-YUAN LIAO, SHU-JEN LIU,
LIANG-HUA CHEN (陳良華) AND HSIAO-RONG TYAN
Engng. Applic. of Artif. Intell., 8(1), 81-90 (1995)

In this paper, a bar-code recognition system using neural networks is proposed. It is well known that in many stores laser bar-code readers are used at check-out counters. However, there is a major constraint when this tool is used. That is, unlike traditional camera-based picturing, the distance between the laser reader (sensor) and the target object is close to zero when the reader is applied. This may result in inconvenience in store automation because the human operator has to manipulate either the sensor or the objects, or both. For the purpose of in-store automation, the human operator needs to be removed from the the process, i.e., a robot with visual capability is required to play an important role in such a system. This paper proposes a camera-based bar-code recognition system using backpropagation neural networks. The ultimate goal of this approach is to use a camera instead of a laser reader so that in-store automation can be achieved.

There are a number of steps involved in the proposed system. The first step the system has to perform is to locate the position and orientation of the bar code in the acquired image. Secondly, the proposed system has to segment the bar code. Finally, a trained backpropagation neural network is used to perform the bar-code recognition task. Experiments have been conduced to corrobrate the efficiency of the proposed method.

臺灣地區有關「韓國獨立運動」史料及研究概況

林 楠 法

韓國獨立運動研究國際學術會議論文滙編，第 96-119 頁 (1995)

韓國對獨立運動的重視正如中國對辛亥革命的重視一樣，不但彙集許多史料，且有許多專書研究，更召開許多次學術研討會，其研究成果亦爲國際所肯定。然由於韓國臨時政府在中國成立，許多獨立運動之資料散居中國各地，許多相關史料陸續被整理出來，韓國學者雖努力赴各地蒐集，仍有未盡之處。歷史研究者最需要的是史料、臺灣地區學者對韓國獨立運動，自胡春惠教授選寫『韓國獨立運動在中國』之後，有部份論文以此爲研究，而且國史館、中國國民黨中央黨史委員會、中央研究院近代史研究所朱家驊檔案等所藏之韓國獨立運動資料暨其他相關之回憶錄具有參考價值，本文分別加以介紹，並將臺灣地區出版（包括臺灣學者或在臺灣地區發表及出版的論著）之史料彙編及研究概況作簡單的評述，以爲研究韓國獨立運動之學者參酌。